Report of the Evaluation of Maximum Earthquake and Site Ground Motion Parameters Associated with the Offshore Zone of Deformation San Onofre Nuclear Generating Station

PREPARED FOR

SOUTHERN CALIFORNIA EDISON
P.O. BOX 800
ROSEMEAD, CALIFORNIA 91770

JUNE 1979

Woodward-Clyde Consultants

Report of the Evaluation of Maximum Earthquake and Site Ground Motion Parameters Associated with the Offshore Zone of Deformation San Onofre Nuclear Generating Station

PREPARED FOR

SOUTHERN CALIFORNIA EDISON
P.O. BOX 800
ROSEMEAD, CALIFORNIA 91770

JUNE 1979

Woodward-Clyde Consultants

TABLE OF CONTENTS

TABLE OF CONTENTS (Cont'd)

REPORT OF THE EVALUATION OF MAXIMUM EARTHQUAKE AND SITE GROUND MOTION PARAMETERS ASSOCIATED WITH THE OFFSHORE ZONE OF DEFORMATION SAN ONOFRE NUCLEAR GENERATING STATION

0.0 SUMMARY

Detailed geologic, seismologic and earthquake engineering analyses and reviews have been completed for the San Onofre site to estimate the maximum earthquake magnitude that may be associated with the hypothesized offshore zone of deformation (OZD) (Figure 1), and the maximum ground motions that may be instrumentally recorded at the site during the maximum earthquake.

The PSAR and FSAR for SONGS Units 2 and 3 have presented extensive data regarding the geology, seismicity, and response characteristics of the site. Although no earthquake magnitude was estimated for the controlling earthquake source, a conservatively large earthquake was postulated for a fault 8 kilometers (5 miles) offshore from the site. As a result of these earlier studies, the Atomic Energy Commission (AEC) and its consultants agreed to a 2/3g design basis earthquake (DBE) and the spectral shape documented in their 20 October 1972 Safety Evaluation Report (SER).

Certain geologic models and assumptions have been defined by either the applicant or by the regulatory agency in the past and are important when estimating earthquake magnitudes. Based on the USGS and NOAA reports appended to the SER, the AEC concluded that the Newport-Inglewood zone of deformation (NIZD), the South Coast Offshore zone of deformation (SCOZD), and the Rose Canyon fault zone (RCFZ) cannot be disassociated and that they form a

linear zone of deformation hypothesized to extend 240 kilometers (145 miles) from the Santa Monica Mountains south to Baja California. This zone, referred to as the hypothesized offshore zone of deformation (OZD) is about 8 kilometers (5 miles) west of the SONGS site. It was assumed to be capable of an earthquake having a magnitude commensurate with the length of the zone. The AEC further concluded that the hypothesized OZD, as described in the SER, would be the source of the DBE, and that the ground motions at the site from that earthquake would be accommodated in design by the 2/3g DBE and the spectral shape proposed in Section 2.5.2.6 of the FSAR.

The applicant concurs that the 2/3g DBE and spectral shape will accommodate potential effects of earthquake shaking at the site. The applicant suggests, however, that the hypothesized OZD is composed of three structural entities from north to south: the NIZD, the SCOZD, and the RCFZ. Interpretation of geologic data indicates that the hypothesized OZD is not continuous and, therefore, not capable of large earthquakes. A conservative approach was taken when evaluating site ground motions, in that the hypothesized OZD was considered as a whole, and capable of generating significant earthquake shaking at the site. This approach led to the development of the 2/3g DBE and spectral shape documented in Section 2.5.2.6 of the FSAR.

It is the purpose of the present study to estimate the maximum potential earthquake magnitude on the hypothesized OZD, to estimate the associated maximum instrumentally recorded ground motion values and to compare these values with the design basis parameters. The approach taken in this study is to model the hypothesized OZD according to the characteristics of the known-capable NIZD to the north.

This study concluded that the maximum magnitude associated with the NIZD is estimated to be M 6-1/2. This conclusion is based on

an analysis of the geologic and seismologic environment of the hypothesized OZD and its similarity to other southern California faults, and on an empirical relationship between fault slip rate and earthquake magnitude. The conservatism of the above estimated maximum magnitude for the hypothesized OZD is demonstrated by the lower seismicity, the lower degree of deformation, and the lower stress environment of the hypothesized OZD compared to the NIZD. Given the estimated maximum earthquake magnitude of 6-1/2, the known local soil conditions at the San Onofre site, and the regional tectonic setting, 56 earthquake records were selected to correspond closely to the conditions of the estimated maximum earthquake and analyzed to develop instrumental mean (average) and 84th-percentile response spectra. A comparison between the computed 84th-percentile spectrum and the design spectrum shows that the design spectrum exceeds the instrumental spectrum at all periods.

1.0 INTRODUCTION

1.1 Purpose

The purposes of this study were to estimate the magnitude of maximum earthquake that the hypothesized OZD may be capable of generating, to provide the rationale for that estimate, and to evaluate the level of conservatism of the DBE 2/3g spectrum.

1.2 Terminology and Locations

Various names have been applied to geologic features discussed in the PSAR, FSAR and the AEC Safety Evaluation Report for the SONGS site. The terminology selected for this report (Figure 1) is consistent with that used in the FSAR. It also reflects the applicants' interpretation of the nature of the geologic features.

A zone of deformation, hypothesized by the AEC (USGS letter of July 1972) to extend from the Santa Monica Mountains south to Baja, California, will be referred to as the hypothesized offshore zone of deformation (OZD). Geologic interpretation of this hypothesized OZD indicates that it consists of three structural entities in Miocene and younger rocks, each of which consists of various faults and folds.

The most northerly portion of the hypothesized OZD has been called by various investigators and review committees the Newport-Inglewood fault, the Newport-Inglewood fault zone, the Newport-Inglewood zone of deformation, the Newport-Inglewood structural zone, and the Newport-Inglewood zone of folds and faults. This structural trend does not consist of a single fault trace or zone of faults; it is most accurately described as a zone of en echelon faults and folds not having demonstrable continuity. Therefore, in this report, it will be designated the Newport-Inglewood zone of deformation (NIZD).

South of the NIZD, the hypothesized OZD passes approximately 8 kilometers (5 miles) seaward of the SONGS site and consists of several faults and gentle folds. This portion of the hypothesized OZD has been referred to as a disturbed zone of Fault "A", the South Coast Offshore fault, and South Coast Offshore fault system. This segment of the hypothesized OZD, which occurs in Tertiary-age and younger rocks, is a series of broad folds and short, discontinuous breaks extending from near Laguna Beach southeasterly to near Oceanside. This segment will be referred to as the South Coast Offshore zone of deformation (SCOZD) in this report.

At the southern end of the hypothesized OZD, a zone of onshore faults and offshore folds and faults has been called the Rose Canyon fault zone (RCFZ) and this name will be used in this report. The RCFZ extends from offshore near Oceanside to onshore in San Diego; it is not known farther south than San Diego Bay.

The region investigated includes the major tectonic elements in southwestern California and extends from the San Andreas fault zone on the east to the San Clemente fault on the west, and from the Santa Monica-San Gabriel Mountains on the north to northern Baja California on the south.

1.3 Organization of the Report

This report has been organized to provide a succinct description of the analyses and data used to evaluate the maximum earthquake and the associated ground-motion spectra for the SONGS site. Some of the detailed technical discussions and data bases are presented in appendices attached to this summary report. Section 1 introduces the study and Section 2 describes the methods used. Section 3 discusses the geologic, tectonic, and seismologic setting of the site. Section 4 presents the derivation of the maximum earthquake postulated on the hypothesized OZD. Section 5 translates the maximum earthquake on

the hypothesized OZD to calculated instrumental response spectra at the site and presents a comparison of those spectra with the current design spectra. Section 6 presents conclusions regarding the conservatism of the present design spectral values. The appendices are presented in a sequence similar to that of the report.

2.0 METHOD OF STUDY

The method of study followed the four steps diagrammed on Table 1. The first three steps correspond with the three major technical elements defining: (1) the seismic-tectonic model for the hypothesized OZD; (2) the maximum earthquake that may be associated with the hypothesized OZD; and (3) the maximum instrumental ground motion parameters for the SONGS site associated with the maximum earthquake. The fourth step was a comparison of the instrumental ground motion parameters with the DBE of the SONGS site.

2.1 Selection of a Tectonic Model for the Hypothesized OZD

The three segments of the hypothesized OZD have been evaluated by various techniques including conventional field mapping (RCFZ and NIZD), offshore geophysics (SCOZD and RCFZ), and subsurface exploration by the oil industry (NIZD). There are several geologic features common to each area: typically northwest-trending en echelon fault segments; northwest- to west-trending folds associated with or lying between the en echelon faults; and numerous smaller second-order faults intersecting the primary faults and generally trending in a north-south direction. These features taken together are suggestive of predominant wrench faulting (Harding, 1973). However, as discussed in Section 3.2, there appear to be some differences in the amount and style of faulting between the segments with the degree of deformation becoming less pronounced from north to south. Because of the many similarities in structural style that exist among the three areas of the hypothesized OZD and because of the extensive and high quality data regarding the style and amount of deformation along the NIZD, the NIZD was selected as a model for the purpose of characterizing the hypothesized OZD. Of the three segments of the hypothesized OZD, the NIZD has by far the highest levels of both historical and recorded seismic activity. It has produced two damaging earthquakes, one in Inglewood in 1920, having an estimated magnitude of 4.9, and the other in Long Beach in 1933,

having a recorded magnitude of 6.3. For these reasons, the NIZD is considered a conservative model for the hypothesized OZD.

2.2 Estimation of the Maximum Earthquake

Evaluation of the hypothesized OZD does not lend itself to conventional analyses of maximum earthquake magnitudes. Conventional methods of estimating earthquake magnitudes include the use of empirical relationships between length of surface rupture or amount of surface displacement per event and earthquake magnitude. Because the hypothesized OZD is not a through-going fault, information on fault lengths and displacement is questionable and difficult to verify along its length. Conventional methods involving fault length-magnitude relationships are therefore not directly applicable. Fault-length data are available for short segments of the NIZD based on extensive well drilling along the zone; however, the offshore geophysical interpretations are not of sufficient quality to estimate fault lengths with certainty. Similarly, the displacement-per-event relationship cannot be applied to the hypothesized OZD because surface traces or escarpments for evaluating displacement histories are not present along most of the zone. In addition, exploration along the few prominent scarps on the NIZD has not exposed surface or Holocene displacements. Therefore, a method for estimating earthquake magnitude was developed that is based on comparing the degree of fault activity utilizing slip rate data on the hypothesized OZD with that of similar faults in the southern California region. By correlating this level of activity with the maximum earthquakes associated with those faults an estimate can be made of the maximum earthquake that may be associated with the hypothesized OZD.

Many geologists and seismologists (for example, Albee and Smith, 1966; Slemmons, 1977; Cluff, 1978) recognize that a wide variation exists among faults in terms of the degree of fault

activity, that is, slip rate, size and recurrence interval of earthquakes, and amount of slip per event. This is true not only for faults in different tectonic environments, but also for different faults within the same tectonic environment. According to Slemmons (1977) and Cluff (1978) faults having higher degrees of activity present a greater earthquake hazard than faults having lower degrees of activity. Therefore, the method used to estimate the maximum earthquake magnitude associated with the hypothesized OZD relied on evaluating long-term geologic slip rates and historical seismicity to characterize the degree of activity along the hypothesized OZD. This degree of activity was then compared with that of other faults within the southern California region that have a similar style of faulting. The geologic considerations included tectonic setting, style of faulting and deformation, and long-term geologic slip rates for each fault zone. The seismologic data included both historical and instrumentally recorded earthquake data.

To estimate the degree of activity of various southern California faults, it was necessary to assess the geologic slip rates for the NIZD and other strike-slip faults in southern California. A literature search was conducted and available data on fault displacements and slip-rate estimates were compiled (Table G-1, Appendix G). However, because the literature on the NIZD provided a wide range of estimates and little documentation or consistency of results, it was necessary to evaluate long-term geologic slip rates by interpreting subsurface geologic data. Hill (1954, 1971) applied a technique utilizing oil well electric logs, which record the lithologic facies relationships of the layered geologic units, to estimate the total fault displacement that has occurred since these units were deposited (Appendix B). This process was applied in three areas along the NIZD to estimate the geologic slip rates from displacements recorded in upper Miocene and Pliocene rocks. By comparing these data and slip-rate data for other strike-slip faults in the region to the

maximum historical earthquake magnitudes associated with these faults, a slip-rate versus maximum-magnitude relationship was developed. This relationship was then used to estimate the maximum magnitude earthquake along the NIZD.

2.3 Development of Maximum Instrumental Ground-Motion Parameters

The method used to develop maximum earthquake-induced ground motion parameters at the site considered an attenuation relationship of maximum ground motion parameters developed from empirical data. These data consisted of selected earthquake recordings that most closely match the source, travel path and local conditions prevailing at the San Onofre site. Specifically, to accommodate source factors and travel path, recordings were restricted to California earthquakes of a magnitude near that of the estimated maximum magnitude of the NIZD; to accommodate local conditions, only those recording stations situated where soil conditions are similar to those at the San Onofre site were considered. Using the resulting attenuation relationship at the appropriate distance of the site to the hypothesized OZD, instrumental response spectra were calculated for the site. These spectra were then compared to the design basis spectra.

3.0 TECTONIC SETTING

3.1 Regional Setting

The regional tectonics of southern California are dominated by the San Andreas fault system, which is the boundary between the Pacific and North American plates. This system, consisting of the large northwest-trending, right-lateral San Andreas and San Jacinto fault zones, is paralleled to the west by other smaller right-slip fault zones such as the Whittier-Elsinore fault zone, the hypothesized OZD and the San Clemente fault (Figure 2).

Although all these fault zones show evidence of predominant right slip, the faults west of the San Andreas fault zone show an apparent progressively westward decrease in (1) amount of total displacement, (2) continuity of surface trace, and (3) amount of seismic activity.

A detailed discussion of this fault system is presented in Appendix A and concludes that by far the greatest amount of post middle Miocene regional displacement has occured along the San Andreas fault zone; the faults to the west are characterized by smaller total displacements and lower geologic slip rates. Geologic evidence supporting this change in displacement and slip rate is presented in Appendices B and G. The historical earthquake activity also indicates a reduced level of seismic activity westward from the San Andreas fault. Figure 3 is a plot of the seismic activity of magnitude 3.0 and greater in the region from 1947 through 1976 (Hileman and others, 1973) (discussed in Appendix F). The level of activity decreases westward from the San Jacinto zone to the hypothesized OZD.

Focal mechanisms for earthquakes occurring along or adjacent to the hypothesized OZD were studied to evaluate the regional tectonic stresses currently affecting this area. Although there are relatively few earthquakes for which constraints could be adequately established, the horizontal stress axes in the

vicinity of the SCOZD and to the north suggest a general north-south maximum compressive-stress axis, consistent with the regional stresses associated with the regional tectonics of southern California. This is discussed in detail in Appendix F. Local variations in fault-plane orientation were observed, similar to variations observed in other local seismicity studies in the southern California region (Teng and Manov, 1976; Pechmann, 1979; Lee and others, 1979). This pattern of focal mechanisms suggests an assocation with locally varying fault orientations.

3.2 Hypothesized Offshore Zone of Deformation (OZD)

Several geologic features are common to each of the segments of the hypothesized OZD. These are northwest-trending en echelon fault segments, northwest- to west-trending fold axes, and numerous smaller second-order faults intersecting the primary faults, all suggestive of predominant wrench faulting (Harding, 1973). However, there appears to be a progressive change in the amount and style of faulting between the segments. Starting at the north, the NIZD is characterized by discontinuous faults and folds that have evidence of right-lateral displacement of post-middle Miocene basin sediments. The SCOZD to the south has evidence of similar tectonism; however, the SCOZD appears to have more down-to-the-west normal faulting and lacks direct evidence on the amount of lateral displacement present. The RCFZ, at the south end of the hypothesized OZD, has evidence for both strike-slip and normal faulting. Prior investigators of the RCFZ suggest highly differing interpretations, ranging from mostly strike-slip faulting to mostly dip-slip faulting. Locally, folding in the western block of the RCFZ has produced apparent reverse faulting, such as at Mt. Soledad where the western block has been raised.

This apparent change from north to south suggests that areas farther away from the "Big Bend" segment of the San Andreas fault

in the Transverse Ranges experience a progressively lesser influence from the San Andreas wrench faulting. This trend is also consistent with the consideration that the northern portion of the hypothesized OZD abuts the Transverse Range and its associated east-west trending reverse faults. The tectonics of the Transverse Range are believed to be controlled by the same north-south compressional forces responsible for the right-lateral displacement on the San Andreas and related fault systems. The area of interaction of these two tectonic styles appears to be an area of high historic seismicity and stress.

3.2.1 Newport-Inglewood Zone of Deformation (NIZD)

Of the three areas, the NIZD is best documented and has the most complete geologic data base because it has been explored and studied by oil companies, as discussed in Appendix A. The NIZD consists of: a series of short, discontinuous, northwest-trending en echelon, right-lateral faults; a northwest- to west-trending series of relatively shallow drag fold anticlines; and numerous short subsidiary normal and reverse faults. This tectonic style is suggestive of right-lateral, wrench faulting (Harding, 1973).

There are approximately 24 separate faults of significant displacement associated with the NIZD; some of these reach the surface, where they form topographic escarpments in Pleistocene alluvial materials (Barrows, 1974). Displacement on these faults is dominantly right-lateral; however, where faults are associated with major folds, some exhibit normal, reverse, or left-lateral displacement. Drag folding, possibly associated with deep-seated wrench faulting, has apparently formed the numerous anticlinal folds in the basin sediments along the trend of the zone. These anticlines and associated faults form structural traps for the major oil fields along the NIZD.

Historical earthquake activity on the hypothesized OZD is dominated by the occurrence of the magnitude 6.3 (M_s) Long Beach earthquake of 11 March 1933. This earthquake is associated with the NIZD and thus its source parameters are the best representation of large earthquakes on this zone. The style of faulting of the 1933 earthquake was evaluated by waveform analysis of teleseismic bodywave records of the earthquake, as desribed in Appendix E. The best-fit focal mechanism is right-slip on a N40°W-trending fault. This matches the geologic observations of orientation of the NIZD (Appendix A) and also agrees with the aftershock pattern (Appendix E) (Hileman and others, 1973). The waveform study indicates that the focal depth is 10 kilometers and the seismic moment is 4.2 - 6.2 x 10^{25} dyne-cm. The calculated average displacement is 31 to 46 centimeters, and a low stress drop of approximately 10 bars is indicated.

To the north, the NIZD merges with and/or is overridden by the Santa Monica Mountains along the Santa Monica fault; to the south, it branches into several splay faults that appear to die out against the San Joaquin Hills structral high and its offshore extension. The majority of geologic data regarding this trend of folds and faults is restricted to the post-middle Miocene sediments of the Los Angeles sedimentary basin. Scant data are available on the nature of the discontinuity in the basement rocks.

Two distinctly different basement rock types have been recognized on either side of the NIZD: a so-called continental facies on the east, and an oceanic facies on the west (Woodford and others, 1954; Hill, 1971). This basement discontinuity has been attributed to either large-scale strike-slip faulting and/or overthrusting (Woodford and others, 1954) or to subduction of the oceanic rocks by the overriding continental rocks during Mesozoic time (Hill, 1971). Only limited data are available on post-

Mesozoic deformation of these basement rocks. A maximum apparent vertical separation of 4000 feet in the basement rocks was found in the Long Beach area, but generally it averages less than 1000 feet along the length of the zone (Yerkes and others, 1965). There are no basement rock data available to evaluate the amount of possible lateral displacement that might have occurred since the Mesozoic. The basement discontinuity roughly corresponds to a Bouguer anomaly along the NIZD (Harrison and others, 1966); however, the Bouguer anomaly terminates near the San Joaquin structural high. Other similar anomalies have been noted to the south, however, they are farther offshore than are the SCOZD or the RCFZ.

The most recent period of deformation along the NIZD appears to have begun contemporaneously with the deposition of upper Miocene marine sediments and has continued more or less intermittently through at least Pleistocene time. Inception of wrench faulting is suggested by many north-trending normal faults observed in the subsurface along the NIZD that are restricted to the Miocene and lowest Pliocene units and do not displace the overlying younger units. Several geologic observations support continued deformation since Miocene: (1) the Miocene units are displaced laterally a greater distance than are the overlying younger units, as discussed in Appendix B; (2) these Miocene units also show more structural relief on the major anticlinal structures than do the younger units, which shows evidence of structure growth during deposition; and (3) the time-displacement plots discussed in Section 4 of this report and presented in Appendix B suggest that intermittent horizontal displacement has produced a relatively consistent average slip rate since late Miocene.

3.2.2 South Coast Offshore Zone of Deformation (SCOZD)

The tectonic structure of the South Coast Offshore zone of deformation (SCOZD) was evaluated through interpretation of offshore geophysical reflection profiles (Western Geophysical,

1972). This interpretation indicates the apparent tectonic deformation of two deeply buried reflecting horizons, and shows the SCOZD to consist of a zone of branching and discontinuous faults trending south to southeast about 8 kilometers (5 miles) seaward of the SONGS site. Local northwest- to west-trending folds in the shallower horizons are also associated with this zone and, together with the faults, appear to reflect a tectonic style similar to that of the NIZD. These interpretations of the geophysical data show the individual faults to be most continuous on the acoustic basement (Horizon C) and less continuous in the younger rocks, such as those represented by Horizon B. This apparent decrease in fault length and continuity in the younger units is also similar to the NIZD. One of the major differences between the two zones is that normal faulting may be more prominent on the SCOZD than on the NIZD. Deep reflection seismic profiling across the SCOZD indicates that the acoustic basement could be displaced vertically, down to the west, from 1000 to 3000 feet. Gravity data in the Los Angeles basin exhibits a Bouguer anomaly coincident with the NIZD basement discontinuity. This Bouguer anomaly does not continue south to coincide with the SCOZD; however, a similar Bouguer anomaly exists 16 kilometers (10 miles) to the west of the SCOZD. Other differences are the more gentle nature of the folds, the lack of any prominent fault scarps on the sea floor along the SCOZD, and the lack of physical evidence for estimating the amount of lateral displacement on the various fault segments of the SCOZD. A more detailed discussion of this zone is presented in Appendices A and D.

3.2.3 Rose Canyon Fault Zone (RCFZ)

The Rose Canyon fault zone (RCFZ) consists of several northwest-striking faults, both offshore north of La Jolla and onshore in the San Diego area. The full extent of the RCFZ is not well known, but it is believed to die out toward the north in the vicinity of Oceanside and toward the south in the vicinity of San Diego Bay. However, both a northward extension to the SCOZD and

a southward extension to faults in Mexico have been suggested in the literature.

In the offshore segment north of La Jolla, the zone is dominated by northwest-trending, en echelon faults and folds. The onshore segment adjacent to La Jolla has been interpreted as having evidence of right-lateral displacement (Kennedy, 1975; Moore and Kennedy, 1975). Folding is evident along the western block, which has produced both normal and reverse fault relationships across the RCFZ (Appendices A and C). A strike-slip style of deformation within the RCFZ has been suggested on the basis of the postulated displaced stratigraphic units and features such as slickensides that have been observed on individual faults within the zone. Measurements of displacements are difficult to corroborate and those reported in the literature are not well documented or confirmed by supportive evidence. Although evidence for vertical displacement has been found at some locations, the sense of displacement is inconsistent throughout the zone. Kennedy (1975) reported that the rocks on the west side of faults in the zone have moved relatively up in some areas and down in other areas. In the San Diego area, a Bouguer anomaly is about 19 kilometers (12 miles) west of the RCFZ; however, none coincides the the RCFZ. Kennedy (1975) indicates that continental type igneous and metamorphic rocks form the basement on both sides of the RCFZ.

3.3 Tectonic Model for the Hypothesized OZD

Because of the similarities in structural style among the three segments of the hypothesized OZD, and because of the extensive and high-quality data regarding the style and amount of deformation along the NIZD, the NIZD has been selected as a model for the purpose of characterizing the hypothesized OZD. The available surface and subsurface geologic data allows a higher degree of accuracy in assessing the amount and frequency of faulting and folding for the purpose of estimating the maximum

earthquake to be assigned to the hypothesized OZD. Of the three segments of the hypothesized OZD, the NIZD has by far the highest levels of both historical and recorded seismic activity. It has produced two damaging earthquakes, one in Inglewood in 1920, having an estimated magnitude of 4.9, and the other in Long Beach in 1933, having a recorded magnitude of 6.3. The NIZD is considered to be a conservative model for other segments because (1) it has a higher level of historical seismicity; (2) it has the most prominent surficial anticlines and short but prominent fault scarps; (3) it is coincident with a Mesozoic basement rock discontinuity not known beneath the SCOZD or the RCFZ; and (4) it is closer to the influence of the interaction between the San Andreas fault system and the Transverse Range than are the other segments of the hypothesized OZD.

4.0 MAXIMUM EARTHQUAKE

4.1 Slip-Rate Data Base

In reviewing the geologic and seismic conditions along the hypothesized OZD, many different kinds of data were gathered and reviewed. This section briefly discusses the sources of data most valuable to the assessment of the maximum earthquake that may be associated with the hypothesized OZD. The data base includes geologic, seismologic, geophysical, and slip-rate data. Details of this data base and its utilization are given in Appendices B, C and D.

On a regional basis, there is abundant geologic information on both the structure and stratigraphy of southern California; but on a local basis, especially when attempting to define the size and frequency of displacements associated with even major fault zones, the data are limited. An extensive literature search was conducted for each of the major strike-slip fault zones in southern California to compile the data and interpretations regarding displacement of geologic units in order to estimate the slip rate (during Miocene to Holocene time) for each fault.

A summary of the published geologic data and estimated slip rates for the NIZD are presented in Table B-1 of Appendix B. Wide variations and inconsistencies exist among the published values for horizontal and vertical displacements across the NIZD. To evaluate the published data and arrive at consistent displacement values, Hill's (1954) technique of correlating offset geologic facies across a fault was used to estimate the displacements of identifiable and correlatable intervals on logs. This is a subsurface technique utilizing both structural data and electric log data from oil wells (Appendix B). These displacement estimates and existing data on the ages of the stratigraphic units (Nardin and Henyey, 1978; Knapp and others, 1962) were used to calculate geologic slip rates. The results provided consistent slip rates that correspond to the higher values of

most published data. The displacement on the NIZD is confirmed to be dominantly right-slip and is calculated to have a long-term slip rate of 0.5 mm/yr since late Micocene. The vertical to horizontal ratio of faulting is estimated to range from 1:10 to 1:20 (Appendix B). The consistency of the horizontal slip rate data is demonstrated by comparing the results of three slip rate estimates (described in Appendix B): for the Long Beach, Seal Beach and Huntington Beach oil fields, as presented in Figures 4 and 5.

Data on the SCOZD was provided primarily by marine geophysical surveys. A review of these data, discussed in Appendix D, indicates that a combination of minimal available stratigraphic control, variable record quality, wide spacing of survey lines, and variations in seismic signature allow significant variations in interpretation. These data characterize the structural style of deformation, but provide no data for estimating geologic slip rate.

Published and unpublished geologic data regarding the RCFZ suggest highly variable amounts of displacement and lack the evidence necessary to estimate consistent slip rates along the fault zone (Appendix C).

Data were gathered on fault displacement, geologic slip rates, and magnitudes of historical earthquakes for major strike-slip faults in southern California. These data were augmented by the inclusion of other strike-slip faults in California, Alaska, and other areas of the world, as discussed in Appendix G. A summary of geologic slip rates and magnitudes for the major historical earthquakes along these faults is presented in Table 2.

4.2 Analysis of Data

A review of the slip-rate data developed for the various strike-slip faults in the southern California region (Table 2) indicates

that both geologic slip rate and the magnitude of the largest historical earthquakes decrease to the west, beginning with the largest value on the San Andreas fault zone and decreasing with each successive major strike slip fault toward the west. Recent investigations and analyses of the relationships between geologic and seismologic characteristics of faults and earthquakes suggest that there is a substantial basis for establishing a relationship between geologic slip rates on a fault and the size of the largest earthquake on that fault.

Empirically (Slemmons, 1977) and theoretically (Kanamori and Anderson, 1975) it has been found that earthquake magnitude (M_S) is proportional to the logarithm of the associated displacement of the fault on which the earthquake occurred (Appendix H). The slope of the proportionality for strike-slip faults having earthquakes of magnitude approximately 6.5 and larger is somewhat larger than unity. It is also noted that the slip rate on a particular fault can be measured by the sum of the fault displacements associated with all the earthquake activity on the fault as a function of time (Brune, 1968; Molnar, 1979). In general, the total amount of displacement on a fault is dominated by the individual displacements associated with the single or several largest earthquakes to occur during the selected time period: for example, Brune (1968) found that one-third of the total slip on the Imperial fault for the period 1934-1963 was produced by the single largest earthquake. Thus, as is discussed in greater detail in Appendix H, these theoretical and empirical relationships and observations suggest that the logarithmic value of the slip rate scales linearly with the size of the largest earthquakes associated with the sliping fault.

Considering these observations, Figure 6 was constructed by plotting the geologic slip-rate data from Tables 2 and 3 and the magnitudes of the larger events on these faults in a semi-log format of slip rate versus magnitude. The pattern of historic

earthquake data presented on Figure 6 indicates a trend of increasing maximum earthquakes with increasing geologic slip rate. This observation together with an evaluation of the slip rate and magnitude parameters suggests that an upper-bound limit may exist to the right of the data points. Section 4.3 below studies the relationship between the upper limit of the historical data and the estimated maximum magnitude on several of the most extensively studied strike slip faults in California.

4.3 Magnitude of Maximum Earthquake

It is possible to calculate a return period for any magnitude earthquake on a fault with a given geologic slip rate; however, such calculations do not limit the maximum magnitude. Accepted limiting magnitudes have been established by several lines of argument for well studied faults such as those discussed below for California. To examine the relationship between the upper limit of the historical data in Figure 6 and the magnitudes of the maximum earthquakes for these faults, authoritative estimates of the magnitudes of the maximum design* earthquakes for four of the most extensively studied of the faults (San Andreas, San Jacinto, Calaveras and Hayward) were taken from the literature. These estimates, which are based on the empirical relationships between fault length and earthquake magnitude as summarized by Slemmons (1977), indicate maximum design earthquake magnitudes for the four faults as follows:** San Andreas, M 8-1/2; San Jacinto, M 7-1/2; Calaveras, M 7; and Hayward, M 6-3/4 (Figure 7). The use of independently selected maximum design earthquakes derived from interpretation of the geologic record provides a logical means to extend the short historical seismicity record to represent the substantially longer time base

* The maximum earthquake considered likely to be generated by future displacement on a particular fault.

** In order not to leave the impression of high accuracy, these estimates have been rounded to the nearest one-quarter fraction.

required for conservative seismic design purposes. An evelope of those four points defines a line that is parallel to and slightly right of the maximum historic magnitudes on Figure 6: the parallelism supports the expectation of an approximately log-linear relationship between maximum magnitude and geologic slip rate for strike-slip faults in the magnitude range 6-1/2 to 8. The maximum-earthquake line slightly to the right of the empirical data suggests a degree of conservatism that is appropriate to estimating the magnitudes of the maximum design earthquakes that may be associated with the faults represented on Figure 7.

This outer bounding line or limit was then used to estimate the maximum earthquake magnitude for the NIZD. The slip rate of 0.5 mm/yr, previously calculated for the NIZD, when entered into the graph, Figure 7, results in a maximum earthquake magnitude of about M 6-1/2. The NIZD is considered to conservatively represent the earthquake potential of the hypothesized OZD, as discussed in Section 3.3. Therefore, the maximum earthquake magnitude that may be conservatively associated with the hypothesized OZD is M 6-1/2.

5.0 MAXIMUM SITE GROUND-MOTION PARAMETERS

5.1 Attenuation of Ground Motion

The ground motion that occurs at a site during an earthquake results from a complex interaction of source factors, travel path effects and local site conditions. For the San Onofre site, these conditions were considered in the evaluation of the direct application of published attenuation relationships to develop site ground motion parameters.

Major plant structures at the San Onofre site are underlain by San Mateo formation sand that extends to a depth of about 275 meters. This material is a very dense formation sand exhibiting some apparent cohesion due to the dense, efficient packing of individual sand grains. Based on the extensive static and dynamic testing of this material and numerous response analyses performed on a soil profile characterizing the site (documented in the FSAR), the site has been classified as a deep, very stiff soil site. This classification was used in the screening of ground-motion recordings considered in the development of ground-motion parameters.

A large number of recently published attenuation relationships have been critically reviewed; and it has been found that none of the relationships is directly applicable to the San Onofre site because the site conditions used in these relationships were not applicable to the San Onofre site. Other limitations of some of the published relationships include: no documentation of distance extrapolation, magnitude not adequately considered, definition of source distance not consistent or inaccurate, types of magnitudes considered for various data points not consistent or unknown, and the poor fit of relationships to data at magnitude 6-1/2. For these reasons, a site-specific attenuation relationship has been developed for the SONGS site.

5.2 Development of Site-Specific Attenuation Relationships

The development of a site-specific attenuation relationship applicable to the San Onofre site included two basic steps: (1) the selection of earthquake recordings by screening them according to source factors, travel path and local site conditions appropriate to the San Onofre site; and (2) the regression analysis of peak acceleration and response spectral values for the selected accelerograms. The screening of available accelerograms was accomplished considering the following criteria:

Source Factors:

- Earthquakes of approximate magnitude 6-1/2 (M_L) were considered.
- Earthquakes having focal depths less than 20 km were considered.

Travel Path Effects:

- Accelerograms recorded in the Western United States were considered (i.e., same geographic locale).
- Accelerograms recorded at source distances of less than 130 km were used.

Local Site Conditions:

- Accelerograms recorded at recording stations on deep, very stiff soils were used.

The results of the above screening process led to the selection of 56 accelerograms obtained during seven earthquakes in the magnitude (M_L) range 6.3 to 6.5 as summarized on Table J-1. Further details of the selection of accelerograms are presented in Appendix J. Attenuation relationships for peak acceleration and response spectral velocities (damping = 0.02) in the period range 0.04 to 2 seconds were derived through regression analyses of peak acceleration and response spectral values for the

selected accelerograms. A regression equation of the following form was formulated:

$$\begin{Bmatrix} a \\ S_v \end{Bmatrix} = \alpha' \, (R+C)^{\beta} \, \varepsilon'$$

where a = peak acceleration in g's

S_v = spectral velocity in cm/sec (damping = 0.02) at period T

R = source-to-site distance in km

α' and β = regression coefficients

C = magnitude-dependent constant

ε' = random error term

The parameter C is essentially a normalizing parameter for distance; it has the effect of constraining values of peak acceleration or spectral velocity to physically reasonable values at very close distances (within a few kilometers) from the earthquake source. Its use in attenuation relationships was initially proposed by Esteva (1970). The studies presented in Appendix I indicated that for magnitude $M_L \simeq 6\text{-}1/2$, a value of C equal to 20 is appropriate. This value of C was used in the site-specific regression analysis. The details of the analysis are presented in Appendix J.

Examination of the selected data set indicated that the number of data points from the 1971 San Fernando earthquake is extremely large compared to the number of data points from other earthquakes. In this case, the regression equations derived from using the total data set may be biased by the characteristics of the 1971 San Fernando earthquake. To reduce such bias, but still utilizing the San Fernando data, the attenuation relationships for peak acceleration and response spectra were developed by a weighted analysis in which a weight is assigned to each data point such that in given distance intervals the influence of each earthquake is represented equally in the analysis. The general

procedure is as follows: (1) the distance to the zone of energy release is divided into discrete intervals; (2) for a given distance interval, the number of data points from each earthquake is determined; (3) since it is desired that each earthquake should have the same influence on the regression equation, a weight of $1/n_i$), where n_i is the number of data points for the i^{th} earthquake in the given distance interval, is assigned to each data point for the i^{th} earthquake; (4) weighted regression analysis is then carried out to obtain estimates of the regression coefficients and stardard error. The effect of the weights on the regression analysis is that the square of the deviation of the observed data value from the predicted value is multiplied by the weight of the data point to obtain the contribution of that point to the total sum of square of deviations. It is this total sum which is minimized to obtain the regression equation. Further details of the weighting scheme described above are provided in Appendix J.

The results of the analyses in terms of the site-specific attenuation relationships are summarized in Figure 8, which shows the data points and the mean and 84th-percentile attenuation curves. Similar relationships were developed for the attenuation of pseudo relative velocity for 25 individual periods in the period range of 0.04 to 2 seconds. As an example, the attenuation curves and associated data points for a period of 0.1 seconds are presented on Figure 9.

5.3 Calculated Peak Instrumental Accelerations

From the attenuation relationships developed from the weighted regression analyses (see Appendices I and J) the mean and 84th-percentile peak accelerations can be obtained for a desired source distance. For a source distance of 10 kilometers, the resulting values are summarized below. The 10-kilometer distance corresponds to the equivalent closest distance of 8 kilometers from the San Onofre site to the hypothesized OZD and an estimated

depth of 6 kilometers to the center of energy release and is consistent with the treatment of data in the regression analysis.

Data Base	Peak Acceleration at R = 10 km (g's) Mean	84th Percentile
Soil and Rock* Site Data Set (222 points)	0.37	0.54
Soil Site* Data Set (196 points)	0.32	0.45
Site-Specific** Data Set (56 points)	0.42	0.57

* Described in Appendix I.
** Described in Appendix J.

From the results summarized above, it can be seen that in this case, use of the site-specific data set results in higher accelerations than those obtained using a data set which is less site-specific (all soil sites) or non site-specific (all soil and rock sites).

5.4 Calculated Instrumental Response Spectra

Relationships were developed for mean and 84th-percentile pseudo-relative velocity response spectra (damping = 0.02) for the period range 0.04 to 2 seconds. The relationship for period T = 0.1 seconds are presented in Appendix J (Equations J-7a and b). The mean and 84th-percentile values obtained from these equations for a distance of 10 kilometers are 11.2 cm/sec and 15.1 cm/sec. Using relationships applicable to other periods, mean and 84th-percentile pseudo-velocity response spectra for the maximum earthquake on the hypothesized OZD were computed for the period range 0.04 to 2 seconds. These spectra are presented in Figure 10. The computed mean and 84th-percentile values of peak

instrumental acceleration for the site-specific data set (0.42g and 0.57g, respectively) are also shown in Figure 10.

5.5 Comparison of Instrumental Spectra and Design Basis Spectra

Figure 11 presents a comparison of the 84th-percentile spectrum derived using recorded data (that is, the "instrumental" spectrum) with the design basis (DBE) spectrum for SONGS. It is noted that the DBE spectrum exceeds the instrumental spectrum at all periods.

6.0 CONCLUSIONS

Analysis of the seismicity along the hypothesized OZD shows that the NIZD is by far the most active segment, although small earthquakes occur throughout the area. Based on this observation and geologic factors, the NIZD has been used as a conservative model for the hypothesized OZD. From the analyses of slip rates and earthquake magnitudes for strike-slip faults in southern California and elsewhere, the maximum magnitude for the hypothesized OZD is M 6-1/2.

The instrumental spectrum corresponding to the maximum earthquake on the hypothesized OZD (magnitude 6-1/2 occurring at a closest distance of 8 kilometers from the San Onofre site) falls below the design basis spectrum throughout the frequency range of interest. The instrumental spectrum is a quantification of the response spectral content based on 84th percentile values of the motions that may be recorded at SONGS during the postulated maximum earthquake on the hypothesized OZD. This instrumental spectrum is inappropriate for design but it does provide a basis for selecting a design spectrum after it is appropriately modified in various period ranges. General guides as to possible range of modification factors are provided by Newmark (1975, 1977), Newmark and Hall (1978), and Blume (1977a, 1978). According to these general guides, the ground-motion values selected for design may be considerably lower than the expected isolated peak instrumental readings.

Thus, the DBE spectrum for SONGS is considerably greater than that which may be derived as a design spectrum based on the instrumental spectrum shown in Figure 11. Accordingly, the DBE spectrum is a very conservative representation of the design spectrum corresponding to the maximum earthquake on the hypothesized OZD.

Table 1: Flow Diagram of Methodology for Developing Maximum Instrumental Ground Motion Parameters for the Songs Site

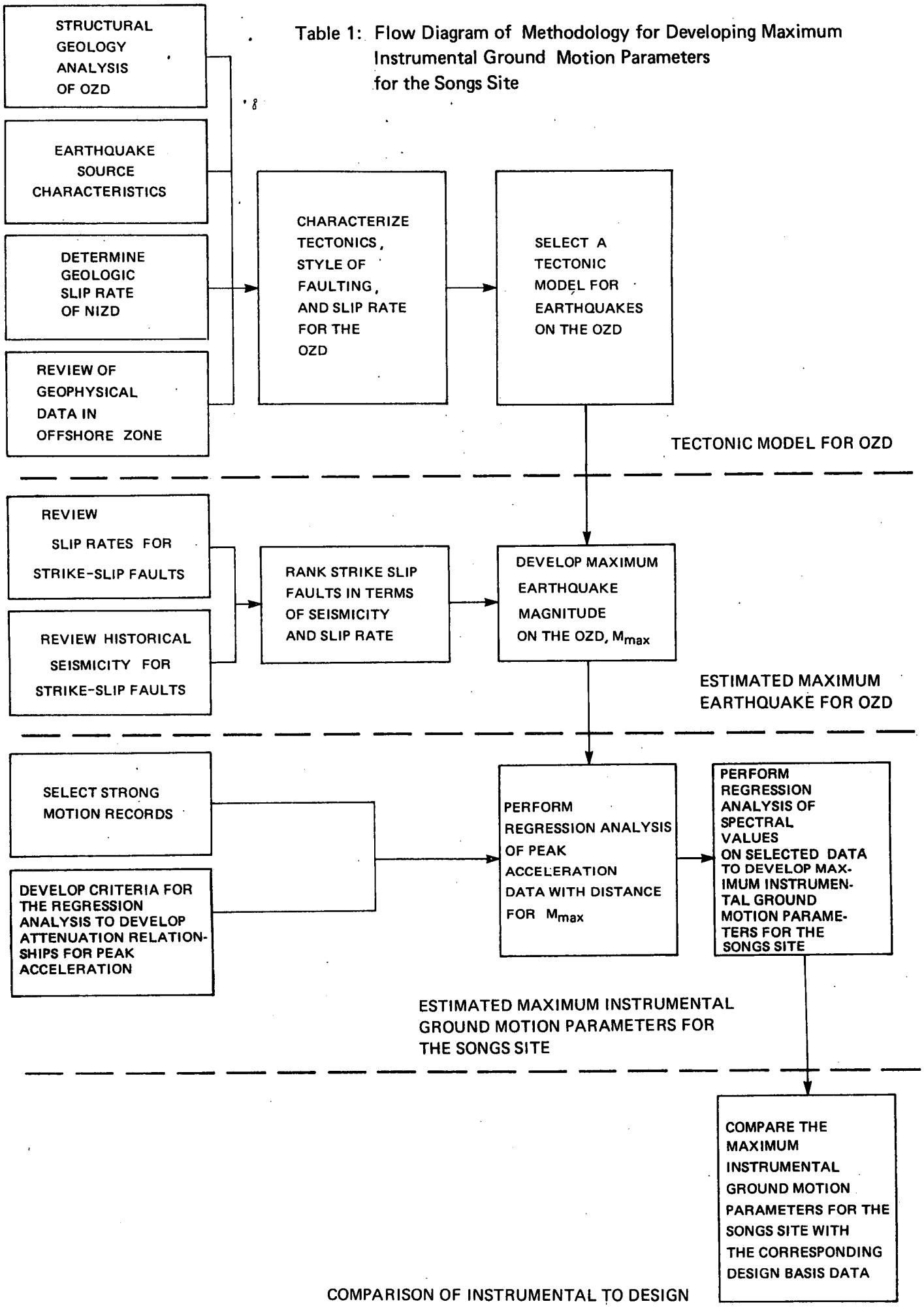

TABLE 2

SUMMARY OF SLIP RATES AND
MAXIMUM HISTORIC EARTHQUAKE MAGNITUDES

Fault	Slip Rate (mm/yr)	Age of Offset Geologic Features	Maximum Earthquake Magnitude (M_s)
Sumatra	66	Pleistocene	7.6
Fairweather	58	Holocene	7.9
San Andreas	37	Holocene	8.3
N. Anatolian	20	Miocene	7.9
San Gregorio	16	Pleistocene	6.1
Motagua	8	Holocene	7.5
Jordan-Dead Sea	7.5	Pleistocene	7.2
San Jacinto	7.1	Pliocene-Holocene	7.1
Hayward	5	Miocene	6.7
Tanna	3.2	Pleistocene	7.1
Calaveras	1.6	Miocene & Pleistocene	6.6
Whittier-Elsinore	1.2	Miocene-Holocene	6.5
Newport-Inglewood	0.5	Miocene-Pliocene	6.3
Antioch	0.03	Eocene & Miocene	4.9

NOTE: For details of slip rate and earthquake data sources, see Table G-1.

TABLE 3

ESTIMATED SLIP RATES FOR STRIKE-SLIP FAULTS
WHICH HAVE NOT EXPERIENCED LARGE HISTORIC EARTHQUAKES

Name	Geologic Slip Rate (mm/yr)	Reference
Denali (Alaska)	35	Richter and Matson, 1971
Totschunda (Alaska)	33	Richter and Matson, 1971
Lembang (W. Java)	30	Tjia, 1968
Alpine (New Zealand)	25	Wellman and Wilson, 1964
Darvaz (Asia)	13	Trifonov, 1978
Bocono (Venezuela)	9	Rod, 1956
Garlock (California)	5.4	Burke and others, 1979
Atera (Japan)	5.3	Sugimura and Matsuda, 1965
Telemazar (Asia)	2.5	Wellman, 1965
Walker Lane (Nevada)	2.1	Slemmons, personal communication, 1979
Big Pine (California)	2.0	Lamar and others, 1973

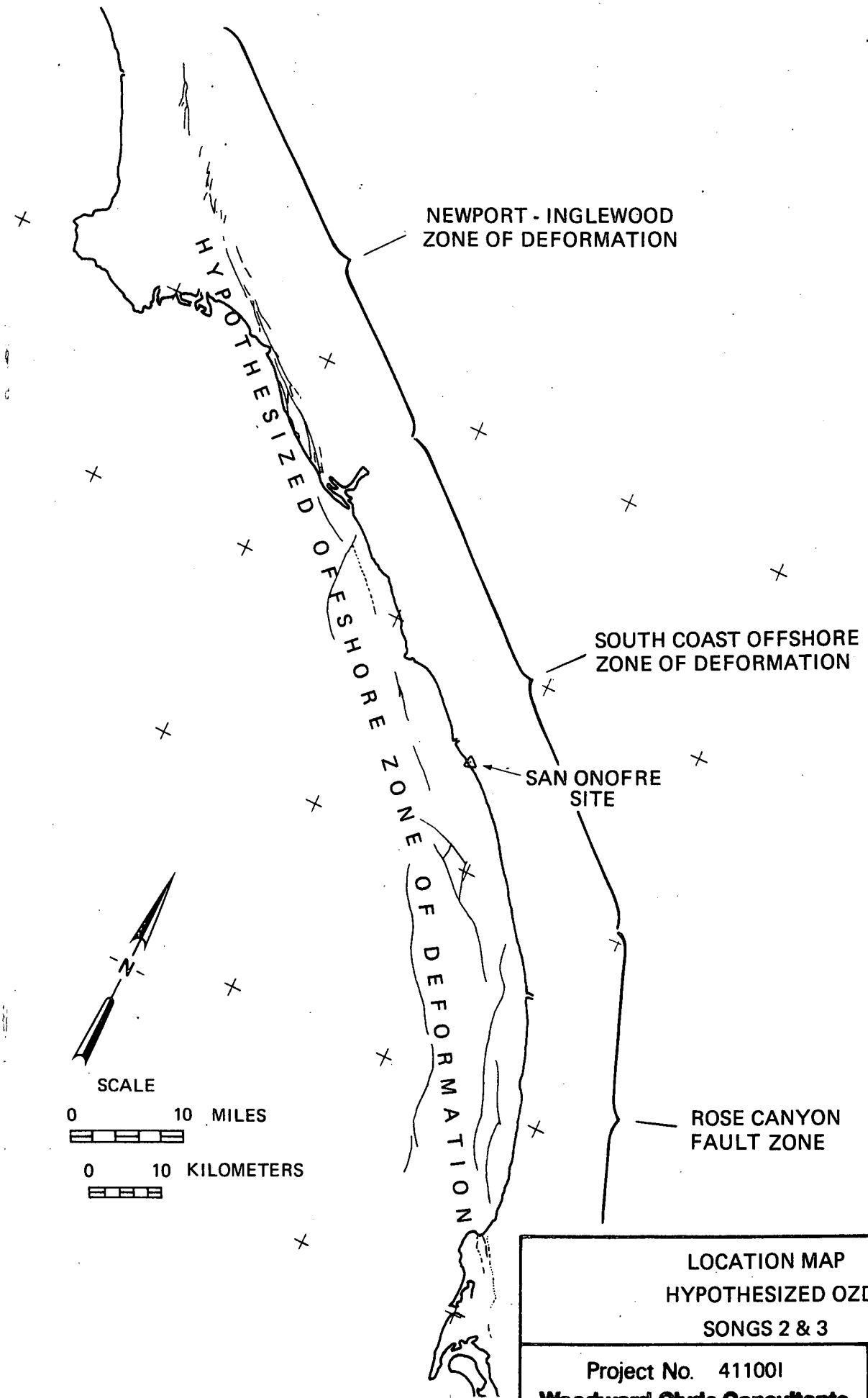

LOCATION MAP
HYPOTHESIZED OZD
SONGS 2 & 3

Project No. 411001
Woodward-Clyde Consultants

Figure 1

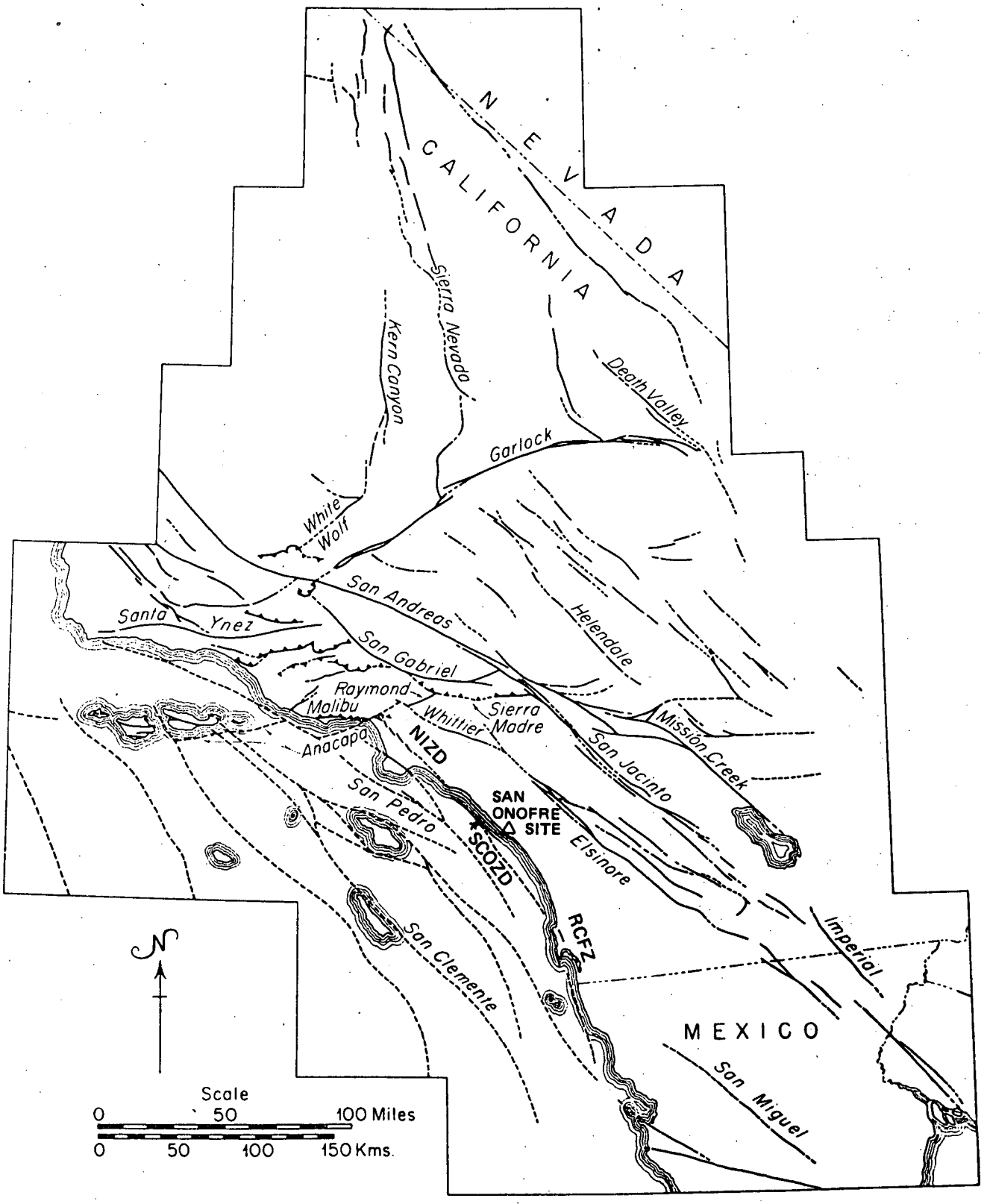

(Modified from Allen et al, 1965; California Department of Water Resources, 1964a; Emery, 1960; Hill, 1916).

MAP OF MAJOR FAULTS IN SOUTHERN CALIFORNIA SONGS 2 & 3	
Project No. 411001 **Woodward-Clyde Consultants**	Figure 2

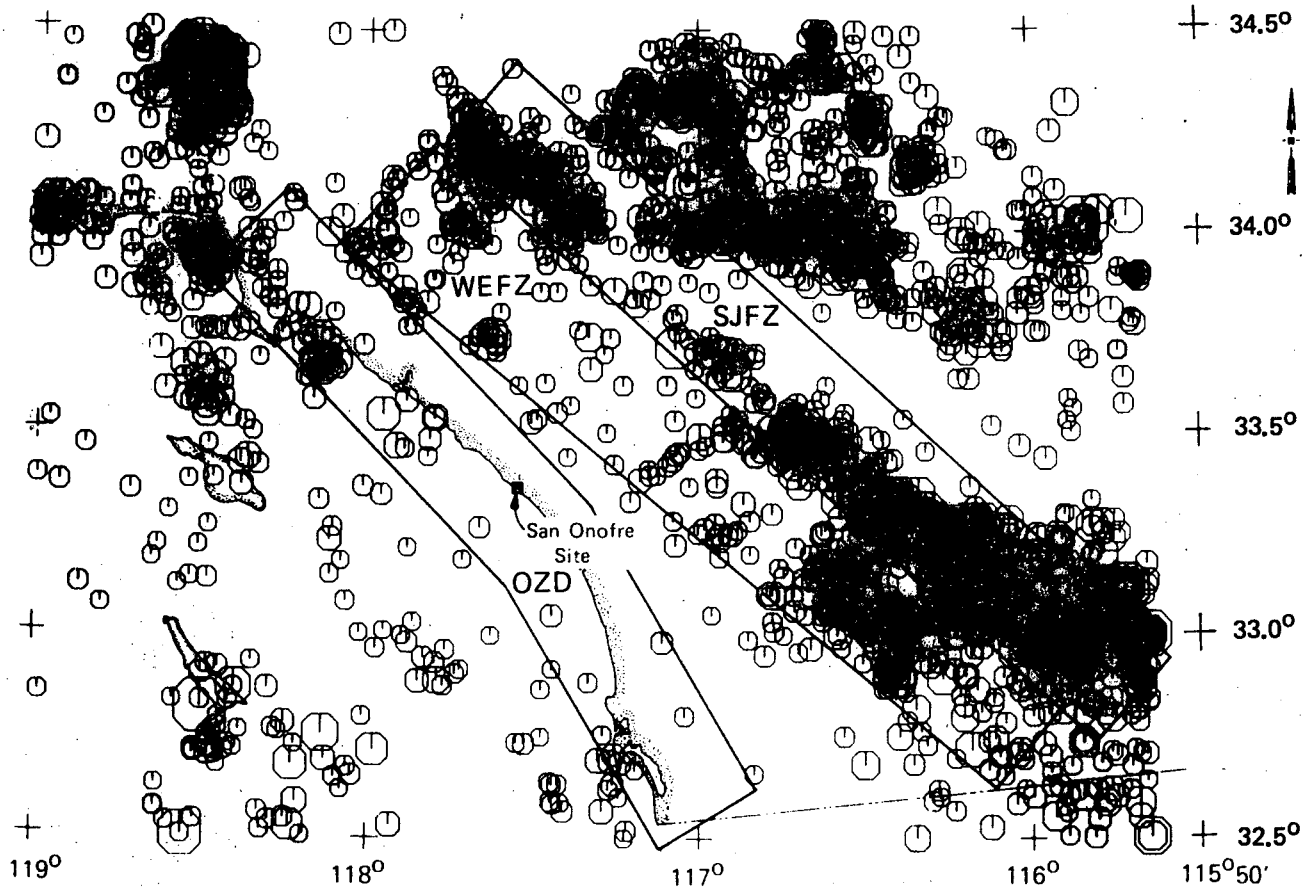

EXPLANATION

Reported Magnitude

7.0

6.0

5.0

4.0

3.0

0 50 100 miles

0 50 100 km

Data Source: Hileman and others, 1973, and California Institute of Technology

OZD – Offshore Zone of Deformation

WEFZ – Whittier – Elsinore fault zone

SJFZ – San Jacinto fault zone

SEISMICITY – 1947 to 1976
MAGNITUDE ≥3
SONGS 2 & 3

Project No. 41100I
Woodward-Clyde Consultants

Figure 3

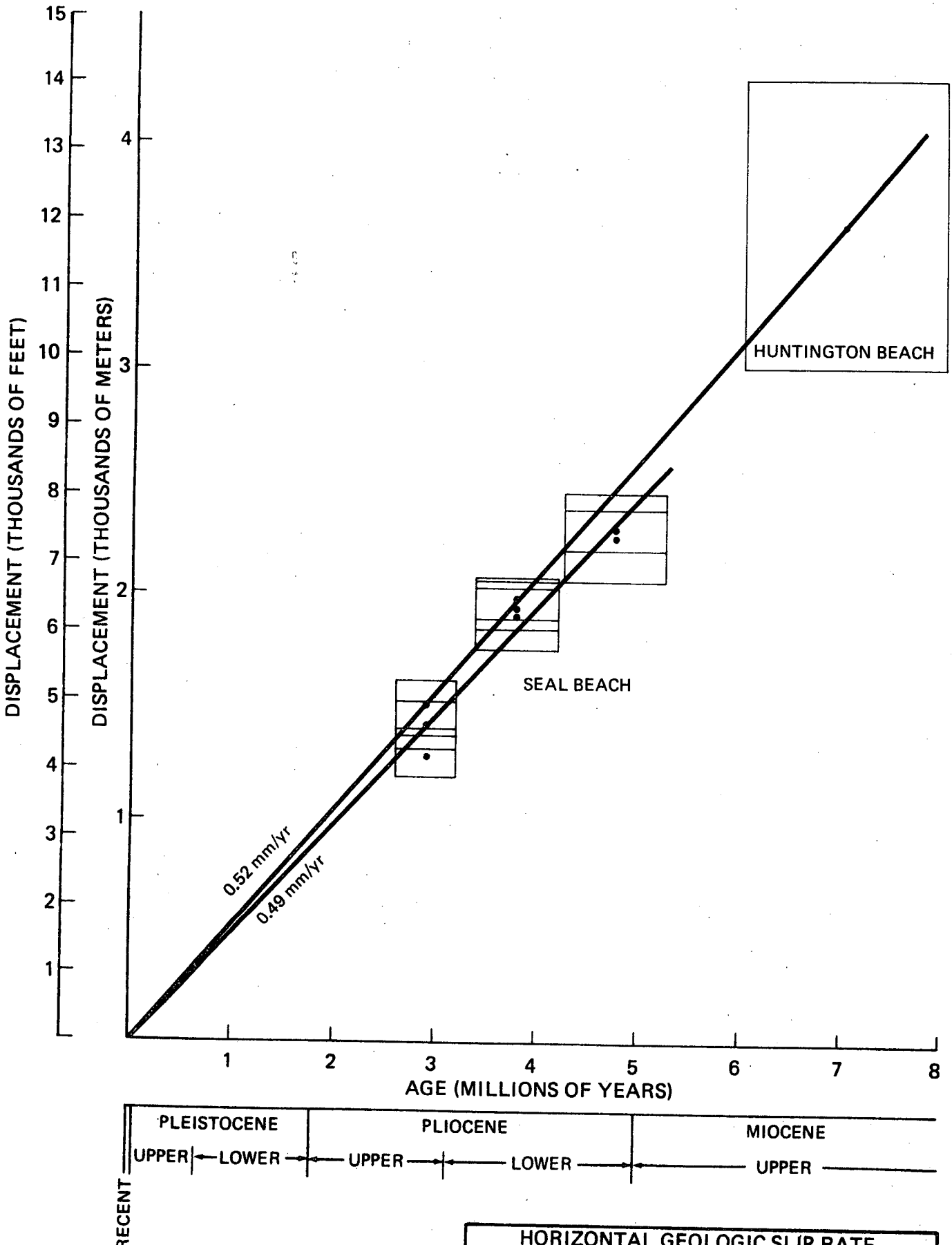

EXPLANATION

Box represents limits of accuracy

HORIZONTAL GEOLOGIC SLIP RATE,
SEAL BEACH AND HUNTINGTON BEACH,
NEWPORT INGLEWOOD ZONE
OF DEFORMATION
SONGS 2 & 3

Project No. 411001
Woodward-Clyde Consultants

Figure 4

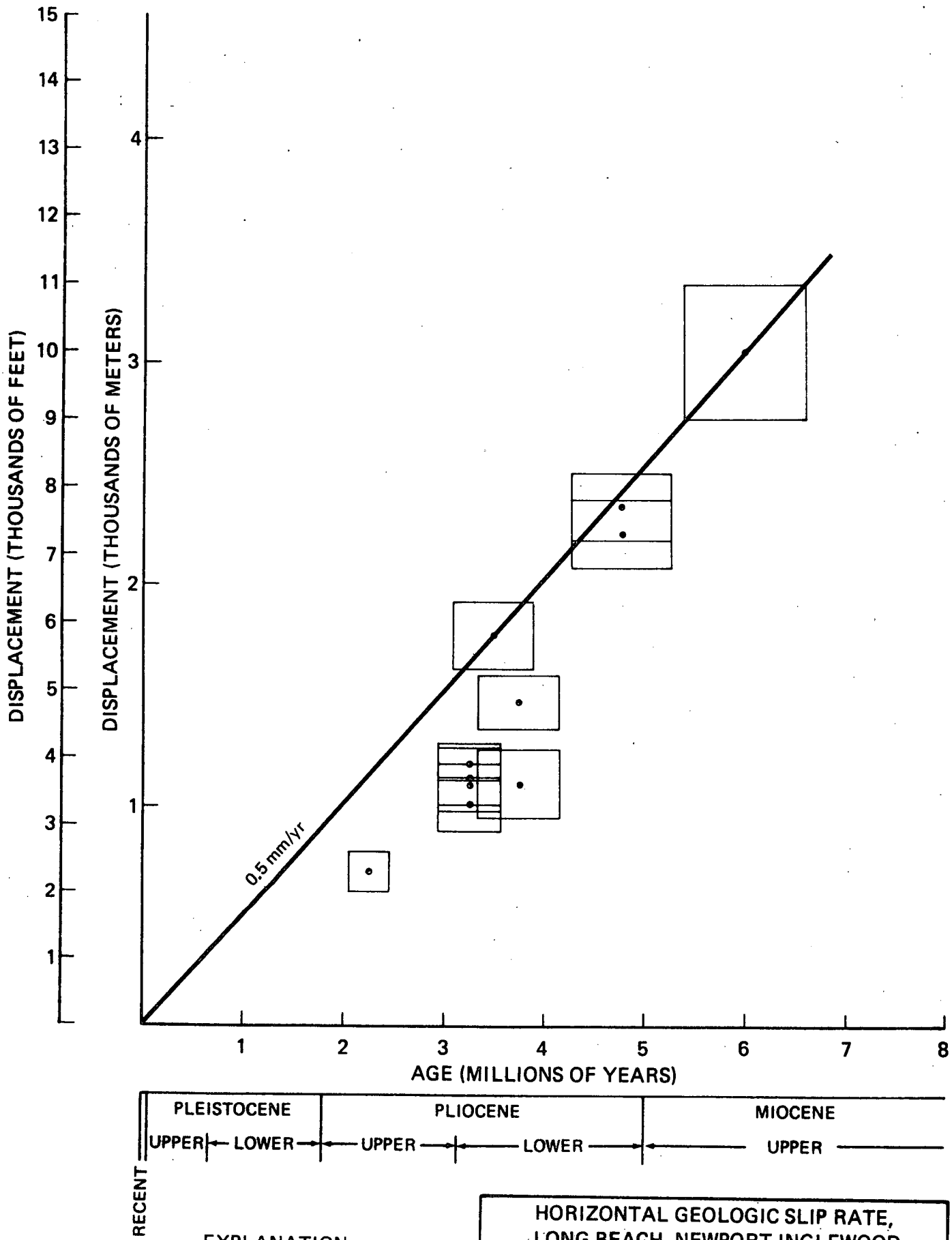

HORIZONTAL GEOLOGIC SLIP RATE,
LONG BEACH, NEWPORT INGLEWOOD
ZONE OF DEFORMATION
SONGS 2 & 3

Project No. 411001

Woodward-Clyde Consultants

Figure 5

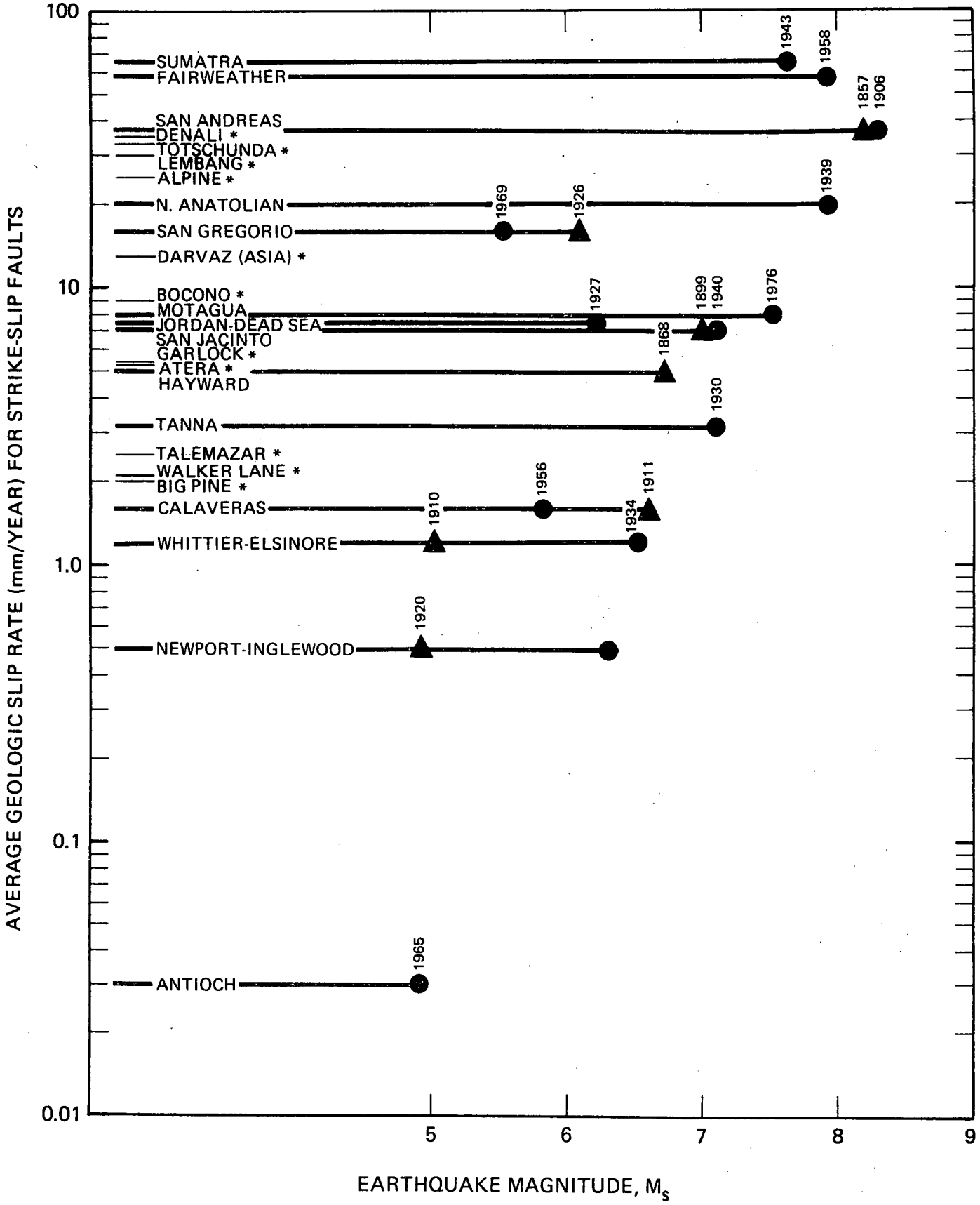

EXPLANATION

- ● Maximum instrumental recordings
- ▲ Maximum pre-instrumental estimates
- — Range over which smaller earthquakes occur
- * No associated large earthquake

GEOLOGIC SLIP RATE vs HISTORIC MAGNITUDE FOR STRIKE-SLIP FAULTS
SONGS 2 & 3

Project No. 411001
Woodward-Clyde Consultants

Figure 6

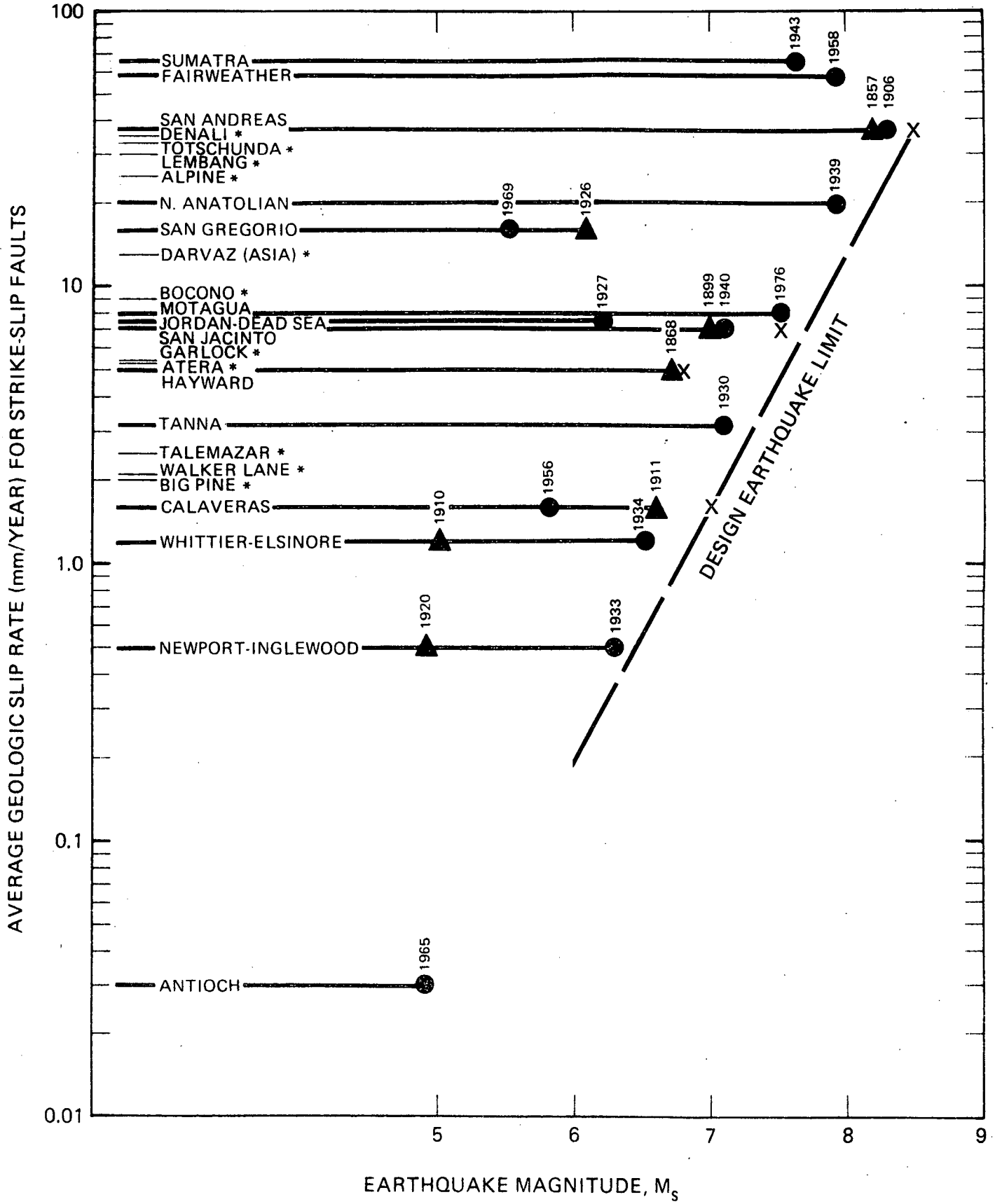

EXPLANATION

- Maximum instrumental recordings
- Maximum pre-instrumental estimates
- Range over which smaller earthquakes occur
- * No associated large earthquake
- X Maximum design earthquake

GEOLOGIC SLIP RATE vs MAGNITUDE
SHOWING DESIGN EARTHQUAKE LIMIT
FOR STRIKE-SLIP FAULTS
SONGS 2 & 3

Project No. 411001
Woodward-Clyde Consultants

Figure 7

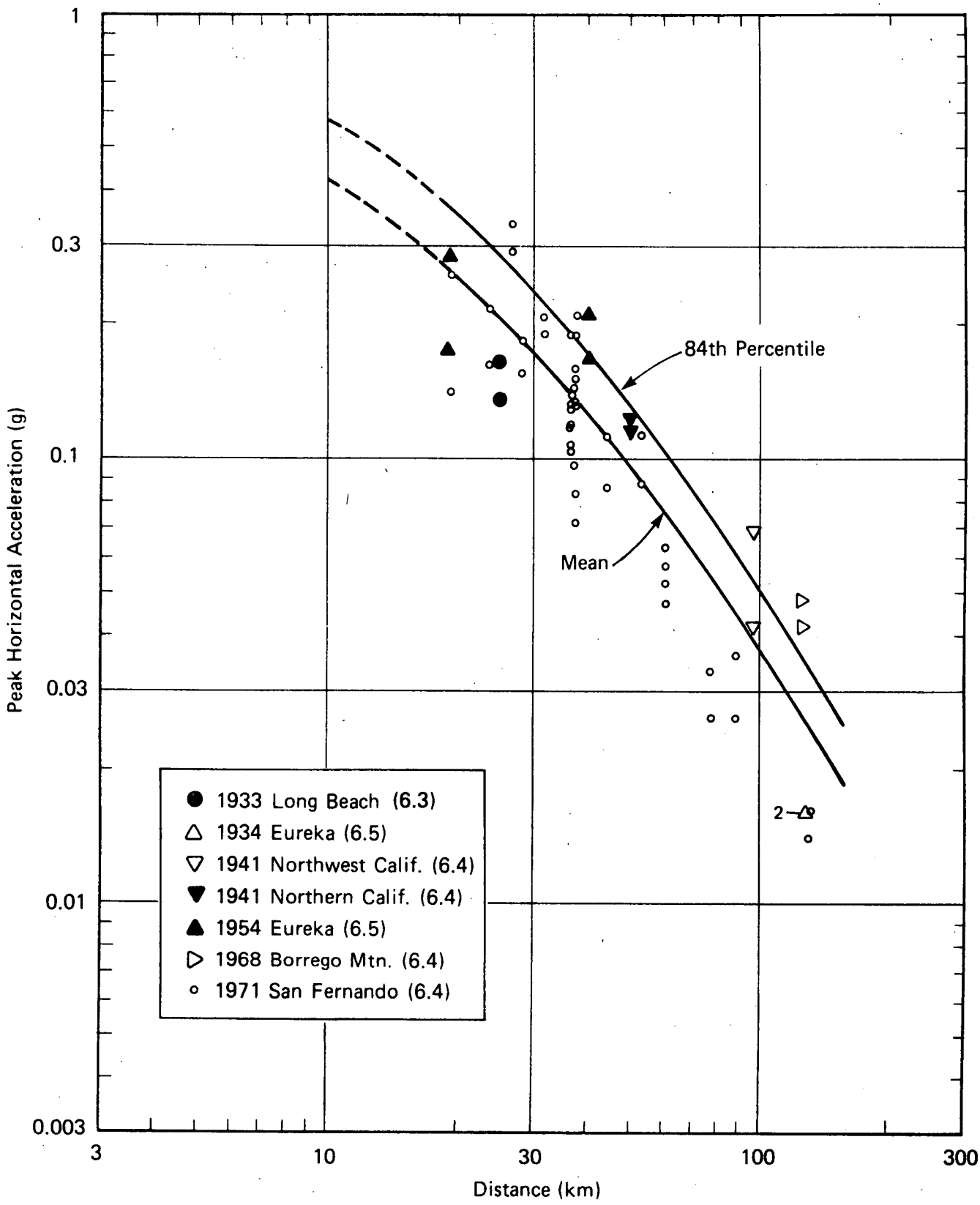

RESULTS OF SITE-SPECIFIC REGRESSION ANALYSIS FOR PEAK ACCELERATION – MAGNITUDE ≈ 6.5
SONGS 2 & 3

Project No. 411001
Woodward-Clyde Consultants

Figure 8

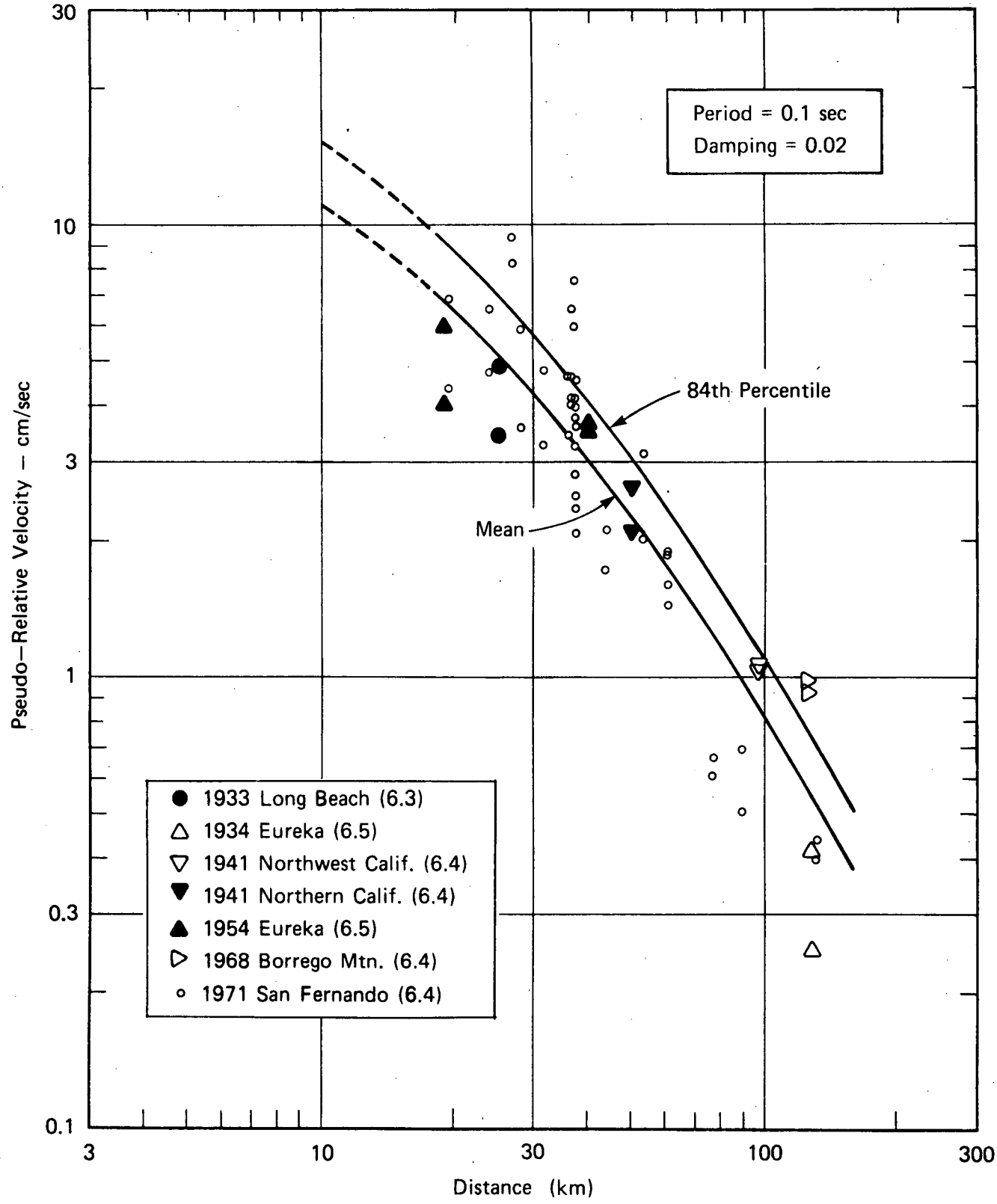

RESULTS OF SITE-SPECIFIC REGRESSION ANALYSIS FOR SPECTRAL VELOCITY (T = 0.1 sec) – MAGNITUDE ≈ 6.5 SONGS 2 & 3

Project No. 411001
Woodward-Clyde Consultants

Figure 9

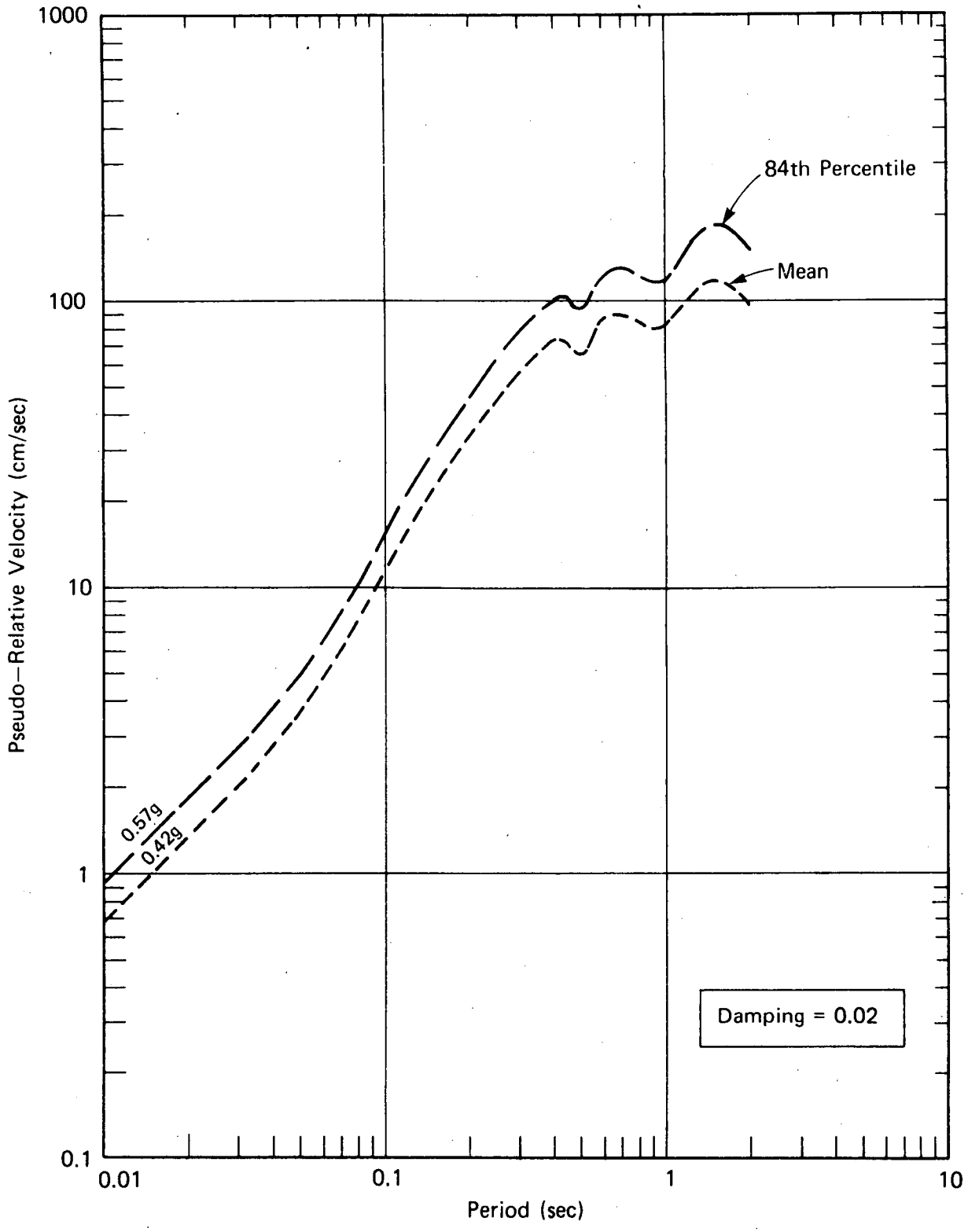

EMPIRICALLY DERIVED MEAN AND 84th PERCENTILE SPECTRA — MAGNITUDE ≈ 6.5, DISTANCE = 10 km SONGS 2 & 3

Project No. 411001
Woodward-Clyde Consultants

Figure 10

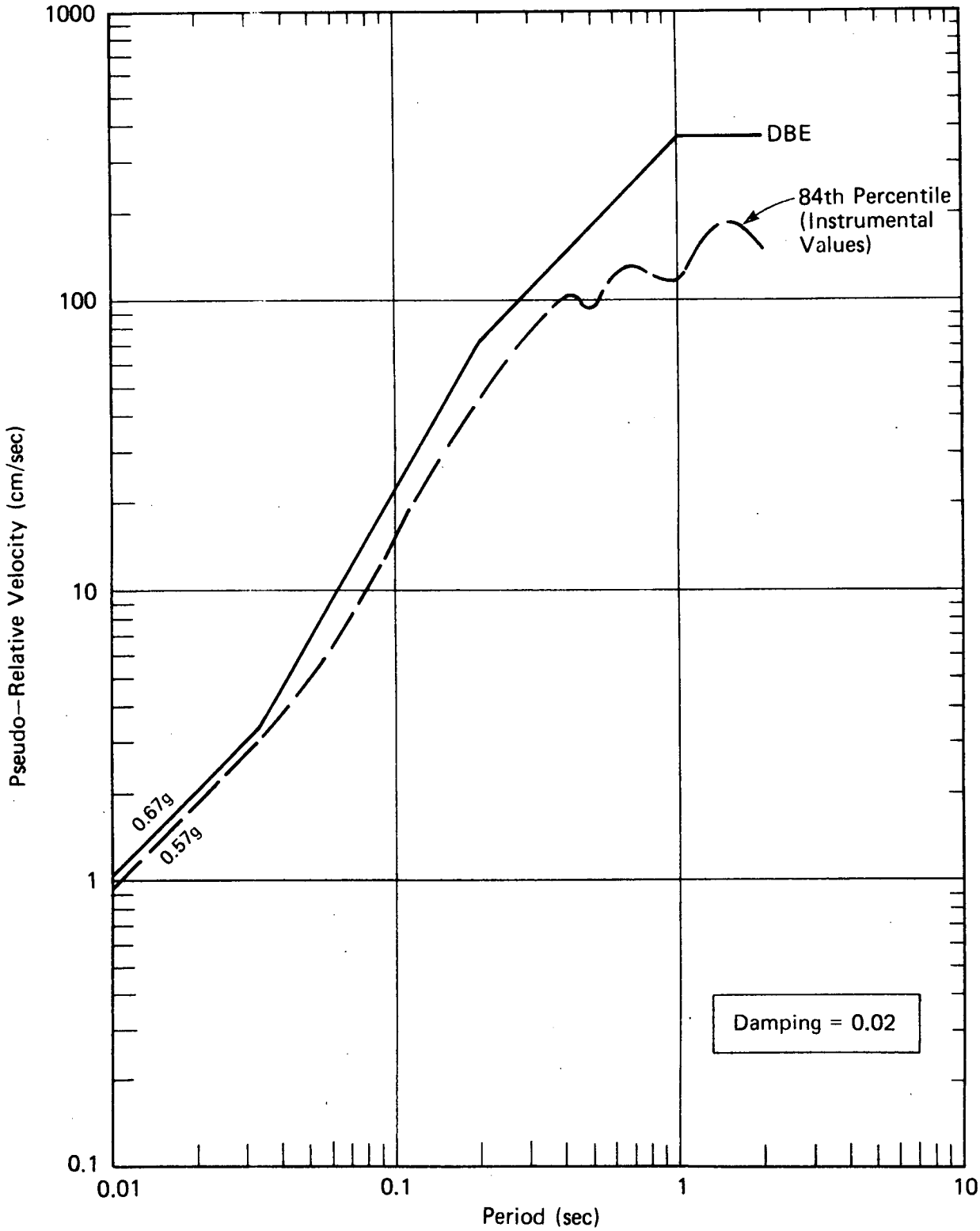

COMPARISON OF 84th PERCENTILE INSTRUMENTAL SPECTRUM WITH SONGS DBE SPECTRUM
SONGS 2 & 3

Project No. 41100I
Woodward-Clyde Consultants

Figure 11

APPENDIX A
TECTONIC SETTING OF THE OFFSHORE ZONE OF DEFORMATION

A-1 INTRODUCTION

For purposes of this appendix, the hypothesized offshore zone of deformation (OZD) will be discussed by the three segments along its trend. From northwest to southeast, these segments are:

1. The Newport-Inglewood zone of deformation (NIZD)
2. The South Coast Offshore zone of deformation (SCOZD)
3. The Rose Canyon fault zone (RCFZ)

This appendix has been prepared to document the style of faulting along the hypothesized OZD, and to develop the thesis that the northerly NIZD can be used as a conservative representation of the central SCOZD opposite the site. The appendix is composed of the six subsections that follow. Section A-2 describes the regional tectonic setting and is followed by Section A-3, which describes the structural setting of the hypothesized OZD. Sections A-4, A-5 and A-6 describe the NIZD, SCOZD and RCFZ, respectively. A summary of the relevant characteristics of the hypothesized OZD is presented in Section A-7.

A-2 REGIONAL TECTONIC SETTING

The regional tectonics of southern California are dominated by the San Andreas fault system, which is believed to represent the boundary between the Pacific and North American Plates. This system consists of the large northwest-trending San Andreas and San Jacinto fault zones and is paralleled to the west by other smaller fault zones such as the Whittier-Elsinore fault zone and the hypothesized OZD that are, like the San Andreas system, right-lateral strike-slip features. The apparent uniformity in deformational style among the zones suggests the presence of a

dominanting regional-scale strain regime in southern California, especially south of the Transverse Ranges. This regional strain may extend farther offshore than the hypothesized OZD to include faults such as the San Clemente fault (Junger, 1976; Howell, 1976).

While all these fault zones show evidence of predominant right-lateral offset, the faults to the west of the San Andreas zone show an apparent progressive westward decrease in total displacement, continuity of surface trace, and amount of seismic activity.

Representative strike-slip displacements measured on these faults are:

Feature	Total Displacement (km)	Age of Displaced Units	Source
San Andreas	480 to 700	Cretaceous to Miocene	Hill-Hobson, 1968; Ehlig et al, 1975
San Jacinto	5.2 to 24	Post Cretaceous Middle Pleistocene	Sharp, 1967; Sharp, 1978
Whittier-Elsinore	8 to 13	Tertiary	Weber, 1977
OZD (NIZD)	3 $\pm$	Upper Miocene	Hill, 1971

These values indicate two conclusions: (1) by far the greatest amount of regional displacement is taken up on the San Andreas fault zone; and (2) the decrease in total displacements indicates relative slower geologic slip rates and lower degrees of activity of faults west from the San Andreas fault zone.

Geomorphic evidence also supports these conclusions. The trace of the San Andreas is readily visible as a continuous scar in Pleistocene and Holocene sediments throughout its entire length

(Crowell, 1975). Proceeding westerly, the geomorphic expression of the en echelon segments of the San Jacinto (Claremont, Casa Loma, Coyote Creek, Superstition Hills, Superstition Mountain and Imperial faults) are quite prominent, while some traces of the Whittier-Elsinore are often difficult to locate at the surface and have the geomorphic appearance of being inactive (Weber, 1977b). Finally, there are few surface traces of the hypothesized OZD, and the majority of the data on that zone have been accumulated through subsurface exploration by petroleum companies (NIZD), marine geophysics (SCOZD, RCFZ), and by surface geology (RCFZ). The geophysical studies of the SCOZD in the general locale of the SONGS site suggest that the segments of the zone may increase in length and continuity with depth, however, they exhibit a discrete and discontinuous character in the shallower units at depths of 5,000 to 10,000 feet below the present sea floor (Appendix D).

The regional east-to-west decreases in geologic displacement and historic seismicity from the San Andreas to the OZD suggest that there has been an east-to-west gradient in strain from the inception of the present strain regime in the Miocene until the present day. Such a strain gradient would result in decrease in displacement and event frequency and magnitude toward the west. Evidence supporting this trend is presented in Appendices B and G.

A-3 HYPOTHESIZED OZD STRUCTURAL SETTING AND DATA BASE

The three elements of the hypothesized OZD (NIZD, SCOZD, RCFZ) have been studied by various methods and to different degrees.

The NIZD has been studied in great detail by the petroleum companies, and a great deal of high-quality subsurface data are available (California Division of Oil and Gas, Long Beach). The NIZD historically is the most active of the three elements of the hypothesized OZD, being responsible for the 1920 M 4.9 and the

1933 M 6.3 events and, therefore, provides the best source of data for seismologic studies along the hypothesized OZD.

The SCOZD lies offshore between Laguna Beach and Oceanside where no confirmed evidence of Holocene displacement exists along its trace. All studies have been done using marine geophysical methods (Western Geophysical, 1972; Appendix D). Those studies have shown: (1) the zone is made up of discrete, discontinuous features (Appendix D; Junger, 1976; Ziony and others, 1974); and (2) these features decrease in length and continuity upward into the younger units (Appendix D). Seismicity is very low and no major historic earthquakes are known to have occurred along the zone.

The RCFZ lies both onshore and offshore, and has produced no historic large earthquakes in the past 200 years. Although frequently studied, little hard data exists about the RCFZ onshore because it is largely covered by young alluvial and lagoonal sediments, and because much evidence may have been destroyed in the urbanization of the area. The offshore segment has been studied primarily through offshore geophysical methods (Kennedy and others, 1978).

Because there is abundant data on the NIZD, there is a strong motivation to use the NIZD as the tectonic model for the SCOZD opposite the site. The tectonic setting of the NIZD and the SCOZD appear to be adequately similar so that it seems reasonable to use NIZD data to estimate a maximum earthquake anywhere on the hypothesized OZD, and then to transfer that maximum earthquake to the SCOZD opposite the site. To assist in evaluating the NIZD as a model, the three elements of the hypothesized OZD have been evaluated separately and a discussion of each is presented in the following sections.

A-4 NEWPORT-INGLEWOOD ZONE OF DEFORMATION

The NIZD is a northwest-trending zone considered to be the source of the Long Beach earthquake of 1933 (M 6.3), the Inglewood earthquake of 1920 (M 4.9) and many smaller earthquakes. The zone is traceable for approximately 70 kilometers (44 miles) as a complex zone of discontinuous faults and folds that exhibit strong evidence for dominant right-lateral slip. At its northwestern terminous near Beverly Hills, it curves to the west, right-laterally offsets and merges with the Santa Monica fault zone west of the intersection (Lang and Dreessen, 1975). Its southeasternmost expression on land is at the Santa Ana River flood plain and Newport Mesa where it splays into two main branches and a series of smaller, right-lateral faults (Ingram, 1968). This zone of deformation is the expression of cumulative right-lateral wrench faulting in the basement rock (Harding, 1973).

There are 24 separate faults of significant displacement found in the subsurface along the NIZD (Barrows, 1974). Some of these reach the surface where they form topographic escarpments in Pleistocene alluvial materials, however, no Holocene displacements have been found. Apparent stratigraphic separation on these faults is dominantly right-lateral; but where they are associated with major folds, second and third order normal, reverse and left-lateral faults are also found. Minor faults are abundant, with parallel and divergent trends to the major faults.

Deep-seated wrench faulting has presumably formed numerous anticlinal folds along the NIZD (Harding, 1973). These anticlines and associated faults form structural traps for the major oil fields distributed along the length of the fault zone. The folds show a maximum of up to 3000 feet of structural relief in the Miocene sedimentary formations on several of the larger structures (Yerkes and others, 1965).

A-4.1 Basement Rocks

The basement surface beneath the NIZD, based on limited data, is generally several hundred to one thousand feet higher on the southwest than the northeast side of the fault. This apparent displacement, however, is also in the same sense and is coincident with the dip of the western flank of the Los Angeles basin and thus may not be due entirely to faulting. Local faulting in the Long Beach oil field has produced a maximum of up to 4000 feet of apparent vertical displacement. While the faulting in the overlying Miocene and Pliocene sedimentary rocks can be shown to be discontinuous, the faulting pattern in the crystalline basement rocks is poorly defined, and no data are available on the amount of lateral displacement that might have taken place.

The basement rocks on either side of the fault zone have been divided into western and eastern basement complexes (Woodford and others, 1954; Yerkes and others, 1965). The western basement consists of low- to medium-grade metamorphic rocks found in numerous wells southwest of the fault, in outcrops at the Palos Verdes Hills, and at Catalina Island. The eastern basement consists of granitic intrusive rocks and Jurassic metasedimentary and metavolcanic rocks found in a well near Beverly Hills at the northwest limit of the Newport-Inglewood zone and in the Santa Ana Mountains. Hill (1971) has suggested that this zone separating these two basement complexes may represent a Mesozoic subduction zone with the rocks to the west representing oceanic crust and the rocks to the east continental crust. This hypothesized subduction zone may continue to the south in the offshore, however, it does not follow the hypothesized OZD into the San Diego area because the eastern complex lies on both sides of the RCFZ. Bouguer gravity data, presented in the PSAR Appendix A-1 suggest that this basement contact lies from 16 to 19 kilometers offshore from the site and is not coincident with the SCOZD.

A-4.2 Character of Sedimentary Rocks

The Newport-Inglewood zone of deformation parallels the southwestern flank of a doubly plunging major syncline that is well expressed at the basement surface and is referred to as the Los Angeles sedimentary basin (Yerkes and other, 1965). The syncline reaches depths of up to 35,000 feet at the basement surface beneath the city of Downey, based on projection of subsurface geology and on gravity surveys.

Overlying the basement surface is a thick sequence of marine sedimentary rocks of Miocene through late Pleistocene age with minor local volcanic rocks. In the vicinity of the NIZD these units are 10,000 to 14,000 feet thick. The middle Miocene rocks are a varied succession of marine clastic sediments, volcanic rocks, and schist breccia. The upper Miocene rocks are clastic marine sediments. The Pliocene rocks are a repetitiously interbedded sequence of fine to coarse, clastic, marine sediments. The lower Pleistocene deposits are a succession of marine silt, sand and gravel. Upper Pleistocene deposits are both shallow water, marine and nonmarine deposits.

A-4.3 Timing and Rate of Deformation

The latest period of deformation along the NIZD appears to have begun soon after formation of the Los Angeles sedimentary basin and deposition of the middle Miocene marine sediments and to have continued on through Pleistocene time. The observations leading to this conclusion are: (1) the Miocene units are displaced laterally a greater distance than are the overlying units, showing that displacement was occurring contemporaneously with deposition of the younger units (refer to Appendix B); (2) the Miocene units also show the greatest structural relief on the major anticlinal structures, indicating that they were growing structures through the Plio-Pleistocene; and (3) many of the north-south oriented normal faults observed in the subsurface along the fault zone are restricted to the Miocene and lowest

Pliocene units, also indicating a lesser degree of faulting and deformation in the younger units. Observations of progressively lesser amounts of lateral displacements in the Pliocene and Pleistocene sediments confirm the continuing nature of the faulting. The time versus displacement plots (Figures B-7 and B-8) suggest that a relatively constant long term rate of deformation has persisted from as early as the deposition of late Miocene sediments up to the present time. Examination of these figures suggests that this rate has averaged approximately 0.5 mm/yr, offsetting the upper Miocene units up to 3.5 kilometers and the upper Pliocene approximately 1 kilometer.

A-4.4 Sense of Major Deformation

The initiation of late Miocene deformation along the NIZD is believed to coincide with the time when San Andreas wrench faulting started dominating southern California tectonics. During late Miocene time, the regional stresses in the NIZD were manifested as relatively short normal faults with northwest to northerly trends. Based on surface geologic mapping, oil field data and offshore geophysical data, these short faults can be shown to displace the Miocene strata along the entire zone. Some of these faults also displace deeply buried lower Pliocene formations in several of the oil fields along the NIZD, however, they generally do not extend into the overlying upper Pliocene or Pleistocene formations. This northwest to northerly oriented normal faulting suggests east-west extension during late Miocene to early Pliocene time, and could represent the inception of regional right-lateral shear along the NIZD (Harding, 1973; Yeats, 1973).

As sedimentation continued in the Los Angeles basin, and right-lateral shearing continued throughout the Pliocene, the existing structural pattern of the NIZD developed, i.e., a series of discontinuous northwest trending en echelon faults and drag folds (Harding, 1973). Most of the observed deformation is consistent

with the fault model of Moody and Hill (1956) wherein second- and third-order faults may form adjacent to the main lateral fault.

The NIZD displays several types of evidence, both structural and sedimentary, that support its identification as a wrench fault system: (1) laterally offset fold axes and fold flanks; (2) horizontal slickensides in deep well cores; (3) offset similar stratigraphic facies relationships and juxtaposed dissimilar facies; (4) highly variable nature of the zone of deformation; (5) en echelon fold and fault patterns; (6) indicated strike-slip genesis of secondary associated structures; (7) parallelism of zone with other documented wrench faults; and (8) clay model studies (Harding, 1973). In summary the geologic evidence indicates dominant right-lateral displacement beginning in the late Miocene, initially causing northwest to northerly oriented normal faulting, and then progressing to the formation of right-stepping en echelon folds and discontinuous left-stepping en echelon right-lateral faults. This deformation pattern appears to have continued through the Pleistocene and is believed to be still active today (however, there is no documented evidence of Holocene surface displacement along the zone).

A-5 SOUTH COAST OFFSHORE ZONE OF DEFORMATION

The SCOZD and related offshore faults form a zone of faulting and folding that trends northwesterly and passes about 8 kilometers (5 miles) offshore from the SONGS site. Existing interpretations of geophysical data from the area (Appendix D) suggest that the SCOZD and related features exhibit structural characteristics consistent with regional north-south compression and resultant right-lateral shear strain, similar to many features along the NIZD. High-resolution profiles near San Onofre and Camp Pendleton (Fugro, 1978; Woodward-Clyde Consultants, 1978) indicate that the SCOZD locally intersects the sea floor. However, the SCOZD is not extensively overlain by Pleistocene or Holocene sediments, and it is not known whether or not these

younger units are displaced.

The SCOZD has been mapped on the acoustic basement (Horizon C, Western Geophysical, 1972) that is found at depths of about 10,000 feet below mudline. The younger rocks such as those represented by Horizon B are less continuous and more difficult to define. Numerous related parallel and subparallel branching lateral faults and normal faults that trend at 45 to 60 degrees to the SCOZD are recognized on Horizon C, but are not continuous across Horizon B (e.g., Figures D-1 and D-2).

The general structural setting of faults and folds identified from offshore geophysical data are indicative of the development of right-lateral shear as suggested by Harding (1973) for the NIZD. Small north-trending normal faults suggest incipient right-lateral shear while the main northwest-trending fault segments represent continued deformation along the shear zone.

A-6 ROSE CANYON FAULT ZONE

The Rose Canyon fault zone (RCFZ) consists of several northwest-striking faults in the San Diego area of southern California. The zone has been classified as a Quaternary fault zone by the California Division of Mines and Geology over the region from offshore of La Jolla to the Mexican border (Jennings, 1975). The full extent of the Rose Canyon zone is not well known but is believed to die out toward the north in the vicinity of Oceanside and toward the south in the vicinity of San Diego Bay. However, both a northward extension to the SCOZD and a southward extension to faults in Mexico have been suggested (Corey, 1954; Emery, 1960; King, 1969; Wiegand, 1970; Moore and Kennedy, 1975; Moore, 1972).

Kennedy (1975) has mapped and studied the area through which the Rose Canyon fault zone trends and has presented a review of the general geology and stratigraphy of the region. The late

Cretaceous, Eocene, Pliocene, Pleistocene and Holocene marine and nonmarine sedimentary rocks of the area are underlain by an igneous and metamorphic basement complex of Mesozoic age on ether side of the fault zone. The most common rocks in the area are a series of marine, lagoonal, and nonmarine, gently folded and faulted sedimentary rocks of Eocene age that were deposited during a period of regional downwarping.

A strike-slip style of faulting within the RCFZ has been suggested on the basis of postulated offset stratigraphic units and evidence such as slickensides that have been observed on individual faults within the zone. Actual measurements of laterally offset features are neither well documented nor confirmed by supportive evidence and, therefore, no quantitative analysis has been made here. Estimates of the amount of displacement along the faults in the RCFZ are highly variable; these are presented in Appendix C of this report. Although evidence for vertical displacement has been found at a number of locations, the sense of displacement is not consistent along the zone. Kennedy (1975) reported that the rocks on the west side of faults had moved relatively up in some areas and down in other areas.

Two periods of tectonic deformation have been recognized for the area in and around the Rose Canyon fault zone. Kennedy (1975) reported that the rocks in the area were chaotically deformed during a pre-mid-Cretaceous period. The Upper Cretaceous and younger units have been gently to moderately folded and faulted during a late Tertiary and Quaternary period. Although there is abundant evidence for active faulting in the zone during the Pleistocene (Kern, 1971), suggestions of Holocene activity have been based solely on indirect evidence such as historic seismicity and evidence for faulting of undated but presumed Holocene sediments offshore (Moore, 1972).

A-7 HYPOTHESIZED OZD SUMMARY

Three segments of the hypothesized OZD have been evaluated by various techniques including conventional field mapping (RCFZ and NIZD), offshore geophysics (SCOZD and RCFZ), and subsurface exploration by the oil industry (NIZD). Features common to each area are typically northwest-trending fault segments, northwest to west oriented fold axes, and numerous smaller second order faults intersecting the primary faults; however, there appears to be a progressive change in the amount and style of faulting between the segments. Starting at the north, the NIZD is characterized by discontinuous faults and folds and exhibits evidence of right-lateral displacement of post mid-Miocene basin sediments suggestive of predominant wrench faulting. The SCOZD offshore to the south exhibits evidence of similar tectonism but with evidently more down-to-the-west normal fault displacement and less direct evidence of lateral displacement. The RCFZ at the south end of the hypothesized OZD exhibits evidence for both strike-slip and normal faulting, but interpretations by prior investigators yield highly differing opinions of the dominant style of faulting. Locally, folding in the western block of the RCFZ has even produced possible reverse faulting at Mt. Soledad where the western block has been raised.

This apparent change from north to south suggests that areas farther away from the "Big Bend" segment of the San Andreas fault in the Transverse Range experience a progressively lesser influence from the San Andreas wrench faulting. This trend is also consistent with the consideration that the northern portion of the hypothesized OZD abuts the Transverse Range and its associated east-west trending reverse faults. The tectonics of the Transverse Range are believed to be controlled by the same north-south compressional forces responsible for the right-lateral displacement on the San Andreas and related fault systems. The area of interaction of these two tectonic styles appears to be an area of high historic seismicity and stress.

The structural similarities of the three segments along the hypothesized OZD support an overall dominant right-lateral tectonic strain along the zone since Miocene time. The differences between the segments point to the conservative nature of using the NIZD as a model to represent the rest of the hypothesized OZD. These significant differences include: greater Quaternary deformation, higher historic seismic activity and higher stress regime at the north end of the hypothesized OZD. The specific characteristics of the hypothesized OZD that have led to using the NIZD as a valid and conservative representation of the SCOZD are listed below.

Structural Similarities Along the Hypothesized OZD

1. The three elements of the OZD all trend northwesterly and form an en echelon zone.

2. Discontinuous en echelon right-lateral faults characterize each segment of the zone.

3. The existence, location and orientations of many anticlinal folds along the hypothesized OZD suggest drag along deep-seated right-lateral shears.

4. Local dip-slip is present along each element of the OZD, but is not consistent throughout the zone and is not dominant.

5. Orientations of many of the small, north-trending, normal faults in Miocene units suggest the inception of right-lateral shear in the late Miocene along the zone.

Differences that Lead to Conservatism of Model

1. Quaternary deformation is most prominent along the NIZD.

2. Historic seismicity indicates the highest degree of activity is on the NIZD.

3. The NIZD is coincident with a major bedrock discontinuity which appears to be responding to the higher stress regime of the Transverse Range and "Big Bend" of the San Andreas fault zone. Such a bedrock discontinuity is not coincident with the southern portions of the hypothesized OZD.

APPENDIX B
ESTIMATES OF DISPLACEMENT ALONG THE NEWPORT-INGLEWOOD ZONE OF DEFORMATION BASED ON E-LOG CORRELATIONS

B-1 INTRODUCTION

In order to obtain more definitive data on geologic slip rates, a separate investigation along the Newport-Inglewood zone of deformation (NIZD) was conducted as a part of this study. Hill (1954 and 1971) has discussed the methodology of determining lateral displacements across faults by matching sedimentary rock facies and stratigraphic thicknesses, and stated that electric log (E-log) correlations of these facies changes along the NIZD demonstrated approximately 3 kilometers of right-lateral slip. Due to the large number of oil fields associated with the NIZD (Figure B-1), and thus abundant structural and stratigraphic control, plus the availability of well data and E-logs, it was decided to use Hill's technique for determining fault displacements of facies changes and then, by relating these displacements to the age of the units displayed, estimate the geologic slip rate along the NIZD.

Hill's technique is based on the fact that E-logs record the interbedded sandstone and siltstone facies that are encountered in a well. By comparing E-logs from two adjacent wells, one can determine what facies changes have occurred between the wells for any specified horizon. Thus a series or line of wells with E-logs can show graphically what facies changes are occurring adjacent to the NIZD. It is possible to match these facies changes within each horizon across a lateral fault by comparing an E-log or series of E-logs from one side of the fault with those from the other side.

These correlations can produce unique matches with a high degree of certainty; however, the accuracy of determining exact displacements is limited by several factors: (1) spacing between control or correlation wells; (2) distance from wells to the fault; and (3) the possibility that the facies changes can be occurring at an oblique angle to the fault. However, when considering displacements ranging from 1 to 3 kilometers, these error limits, which can generally be held down to 200 to 300 meters, represent less than 20% and generally no more than 10% of the calculated displacement at any one place of measurement. Combining numerous measurements at several locations along the zone can further reduce these error limits.

B-2 METHODOLOGY

The present study was divided into two phases. The first phase of the study consisted of a review of the available published literature pertaining to the NIZD in general, and the structure and stratigraphy of oil fields in particular. The second phase evaluated specific displacements at selected sites using oil well data.

The objective of the first phase was to evaluate the relative displacements, both horizontal and vertical, along the fault zone. In addition, locations that would provide the best opportunities to examine the displacements along the fault in more detail using E-log correlations were identified. Criteria used in the selection process included: (1) the fault zone in the study area should be narrow and well defined, with a high degree of assurance that all or most of the zone of faulting was being spanned by the data set; (2) subsurface structure and stratigraphy should be relatively simple and well understood; and (3) there should be a sufficient number of oil wells from which data would be available.

The data regarding horizontal and vertical displacement obtained from the literature review are presented in Table B-1. On the basis of those data, displacement along the NIZD is predominantly right-lateral strike-slip in character. The data also suggested that the Long Beach, Seal Beach and Huntington Beach oil fields were the most promising localities for further analysis.

The second phase of the study involved the evaluation of horizontal and vertical displacements in the three oil fields selected for detailed analysis. Data used to evaluate displacements along the fault in the three oil fields included interpreted cross sections, stratigraphic information, and E-logs available from the California Division of Oil and Gas. Copies of each of the logs and cross sections used are on file at Southern California Edison and Woodward-Clyde Consultants.

B-2.1 Horizontal Displacements

Within each of the fields studied, selected stratigraphic horizons represented on E-logs from correlation wells on one side of the fault were compared to the same horizons in reference wells across the fault. The best correlation of E-log signatures, representing facies relationships, was selected between the correlation and reference wells. Reconstruction of Miocene and Pliocene facies locations were further confirmed by comparing facies changes along the fault zone through correlation of several additional wells on opposite sides of the fault.

The E-log for the correlation well seldom provided an exact match with a log from one of the reference wells, such that the former position of the facies reported in a correlation well was usually judged to have been at some point intermediate between two of the reference wells. The horizontal displacement was estimated by the distance between the present location of the correlation well and its correlation position evaluated with respect to the reference wells. The horizontal displacements have been assigned

plus and minus values that represent the distance between the nearest reference well location and the selected correlation position. Examples of correlations of E-log data are presented in Figures B-2 and B-3.

In the Seal Beach example (Figure B-2), the location of Well 49 (correlation well, Figure B-4) was established as lying between Wells 52 and A-62 (reference wells) based on the overall E-log signature correlation of similar sandstone-siltstone facies within the correlation interval (Lower Pliocene zone B2-C). Further examination of the reference well logs showed distinctive thickening of sandy units near the top and bottom of the correlation interval toward the southeast and a thickening of two middle sandy units toward the northwest. Based on the above example, the correlation of Well 49 was judged to be closer to Well 52 than to Well A-62. This correlation procedure was also applied to Well LW2 to establish its most probable correlation relative to the reference wells. This procedure confirmed the first correlation and the offsets of facies changes along the fault traces.

The Long Beach example (Figure B-3) indicates the correlation of Well Dodge 3 (correlation well, Figure B-5) between Wells B-18 and B-38. Examination of the characteristics of the reference well logs showed a distinctive change from a sandy facies to a more silty facies toward the southeast. The log from Well Dodge-3 was judged to be most similar to that for Well B-18 based on the charactersitics of the E-logs. Most notable on the log from Well Dodge-3 are the blocky shape of the record of the uppermost sandy unit, and the presence of the three lower sandy units that were recorded as a serrated funnel-shaped signature, making this log most similar to that for Well B-18, but distinctly different from the log for Well B-38.

Data available from the files of the California Division of Oil and Gas and from the American Association of Petroleum Geologists (Knapp and others, 1962) made it possible to relate the correlation intervals on the E-logs to various stratigraphic units. The ages of the stratigraphic units were based on the Upper Cenozoic Stratigraphic Column of the Western Los Angeles Basin (Nardin and Henyey, 1978). The range of possible geologic age for each E-log correlation interval was estimated on the basis of the relative position of the interval within a known stratigraphic unit.

The locations of the wells from which data were used are shown in Figures B-4 through B-6. The estimates of horizontal displacements, on a well-by-well basis, for the three oil fields studied are detailed in Tables B-2 through B-4. Horizontal displacements with respect to time are presented graphically in Figures B-7 and B-8; the boxes surrounding each data point reflect the possible range of uncertainty associated with each time and displacement estimate.

B-2.2 Vertical Displacements

The study of vertical displacement along the onshore portion of the NIZD consisted of a review of the structural data available from the published literature and from the E-log correlation of selected wells in the Long Beach and Seal Beach oil fields. The data available from the literature are presented in Table B-1.

Examination of the vertical displacement and separation data for the Long Beach and Seal Beach fields indicates that the measureable separation is, in large part, a function of the effects of folding and the location being studied. A review of the structural contour map of the top of the Brown Zone (Lower Pliocene) at the Long Beach field (Figure B-9) shows that vertical displacement across the NIZD decreases from the crest of the fold to each nose of the doubly plunging structure. At the

crest of the anticline, the vertical separation for the top of the Brown Zone is about 800 feet. The amount of displacement decreases to the northwest and southeast along the fault trend to the extremities where the fold is least developed. In these areas, the vertical displacement across the fault is approximately 100 and 200 feet at the northwest and southeast extremities of the field, respectively. This simple relationship of decreasing vertical displacement away from the crest demonstrates that a sizeable part of the vertical separation across the fault in the Long Beach field results from local folding. The vertical separation influenced least by folding occurs along the fault at the outer limits of the field and is from 100 to 200 feet within the Brown Zone (Early Pliocene). This is considered the best estimate for the maximum vertical separation within the lower Pliocene attributable to tectonic displacement of faults at depth at the Long Beach field. It is on the same order of magnitude as the vertical separation observed in the Seal Beach oil field where folding is much more gentle.

B-3 SUMMARY AND CONCLUSIONS

Because of the wide variations in and inconsistencies among published values for horizontal and vertical displacements across the NIZD, E-log data from oil fields along the fault zone were used to determine the displacements of identifiable and correlative lithologic facies. The displacement estimates, coupled with existing stratigraphic-time information, were used to calculate slip rates. The displacement on the NIZD is dominantly right-lateral strike-slip in character with a long-term slip rate of approximately 0.5 mm/yr. The vertical to horizontal ratio of tectonic displacement is estimated to vary between 1:10 and 1:20.

TABLE B-1

Published Displacement Data
Newport-Inglewood Zone of Deformation

Fault Name	Location	Reference	Fault Orientation	Displacement	Comments
Inglewood	Inglewood oil field	Driver, 1943	Strike: N22°W Dip: 60° to 80°W Normal and right lateral	Horizontal: "As much as 1500 ft" (top of Gyroidina zone - Pliocene age)	p. 307
				Vertical: 275 ft based on surface escarpment, down on the west	p. 307- based on Moody's unpublished report
		Castle and Yerks, 1976	---	Horizontal: 3000-4000 ft, top of Gyroidina zone. Displacement since middle or late Pliocene	p. 5
				Horizontal: 1500-2000 ft, apparent topographic offset of the hills along the Inglewood fault, since Quaternary time; 100-150, apparent offset of a stream channel	p. 5
				Vertical: 200 ft, offset of Pleistocene deposits	p. 5
		Wright and others, 1973	---	Horizontal: 4000 ft, top of Rubel zone based on displaced anticlinal axis	Displacement since late Pliocene
		Yerkes and others, 1965	---	Vertical: 4000 ft of vertical separation on the basement, down on the west	p. A48; plate 4, section E-F
				Vertical: does not exceed 1000 ft for separation of Pliocene age strata	p. A48
				Vertical: 200 ft at base of Pleistocene	
		Poland and others, 1959	Strike: N20°W	Vertical: throw is about 1000 ft from an oil zone at a depth of 2000 ft, down on the west	p. 75
				Horizontal: "May be five times as great as the vertical component"	p. 75
Potrero	Potrero oil field (east area)	Willis and Ballantyne, 1943	Strike: N25°W Dip: 72° SW to vertical Normal and right lateral	Horizontal: 1200 ft apparent displacement of fold axis, "D" contour horizon (upper Repetto)	p. 310-311
				Vertical: "Throw at the crest of the fold is about 270 ft, "D" contour horizon (upper Repetto), down on the west"	Fault zone about 100 to 200 ft wide, p. 310
				Vertical: "Stratigraphic throw of 25-115 ft", based on core and electric logs	p. 310

(TABLE B-1 Cont.)

Fault Name	Location	Reference	Fault Orientation	Displacement	Comments
Potrero (Cont.)	Potrero oil field (east area)	Johnson, 1961	Strike: N23°W Dip: 88° to 82°SW Normal and right lateral	Horizontal: 1600 ft, displacement of fold axis, 52-3 E-log horizon	p. 70
				Vertical: 230 ft, measured between crests of the displaced fold axis, 52-3 E-log horizon, down on the west	P. 70
		Poland and others, 1959	Strike: N25°W Dip: 72° to 88°W Normal and right lateral	Horizontal: 1200 ft	Quotes Willis and Ballantyne, (1943) p. 72
				Vertical: throw about 100 ft, base of water bearing zone, Pleistocene age	
Townsite	Potrero oil field (east area)	Willis and Ballantyne, 1943	Strike: nearly parallel to the Potrero Fault Dip: to the east, reverse and right lateral	Horizontal: 600 ft offset of fold axis	Townsite fault lines up with the main fault through the Inglewood oil field, p.311
				Vertical: stratigraphic throw of 100 ft down on the west	
		Johnson, 1961	High angle reverse	Horizontal: "large component of horizontal displacement"	p. 70
				Vertical: apparent throw of 100 ft	
Inglewood	Rosecrans oil field	Foster, 1954	Strike: N19°W Dip: Vertical Normal	Down on the east	NE trending thrust faults occur west of the fault
	South Rosecrans oil field	Foster, 1954	Strike: N19°W Dip: Vertical	Down on the east (?)	Should be down on the west (Barrows, 1974)
"Regional Shear Zone"	Dominquez oil field	Graves, 1954	Strike: N38°W Dip: 80° to 85°NE Normal and left lateral	---	"Thought to be a member of the Newport-Inglewood shear zone system"; "movement along the regional shear... appears to be left lateral rather than right lateral". Map Sheet 32
"Fault Zone"	---	Grinsfelder, 1943	Strike: N38°W High angle	Vertical: Maximum apparent vertical throw is 200 ft	"Main movement...roughly parallel with the Inglewood Rift", p. 318 "Below 4000 ft the effects of faulting become more evident". p. 318

(TABLE B-1 Cont.)

Fault Name	Location	Reference	Fault Orientation	Displacement	Comments
Cherry Hill	Long Beach oil field	Stolz, 1943	Strike: N47°W Dip: Steeply NE Reverse and right lateral	Vertical: "Maximum throw of 1000 ft"	p. 324
		Dudley, 1954	---	Horizontal: Approximate 3000 ft for the Brown zone, right lateral	Suggested by subsurface contours, Map Sheet 34
				Vertical: Brown zone "raised nearly 700 ft with respect to the position of the zone on the southwest side"	
		Ingram, 1968	---	Vertical: "Northern block upthrown as much as 700 ft, however displacement decreases towards the southeast"	p. 9
				Horizontal: "Considerable strike-slip movement along this fault"	p. 9
		Yerkes and others, 1965	---	Horizontal: 300 - 5000 ft, right lateral slip, "as measured in oil bearing strata", lower Pliocene	Quotes a number of other workers, p. A48
				Vertical: 4000 ft separation of the basement surface	p. A48
				Vertical: "Separation in strata of Pliocene age commonly does not exceed 1000 ft, and at the base of the Pleistocene, 200 ft"	p. A48
		Poland and others, 1956	---	Vertical: 200 to 300 ft, base of San Pedro Formation	p. 98
		Hill, 1954	---	Horizontal: "Electric log correlations demonstrate a few miles of right lateral slip"	p. 10
Northeast Flank	Long Beach oil field	Stolz, 1943	Strike: N44°W Dip: Steeply SW High angle reverse	Vertical: "Maximum throw is 500 ft	p. 324
		Poland and others, 1956	---	Vertical: "Throw is probably 200 ft", base of San Pedro Formation	p. 99
				Vertical: 250 ft at the base of the upper Pilo.	

(TABLE B-1 Cont.)

Fault Name	Location	Reference	Fault Orientation	Displacement	Comments
Seal Beach	Seal Beach oil field	Bowes, 1943	Strike: N50°W Dip: Nearly vertical to northwest, Normal	Vertical: "Downward displacement of 150 to 200 ft, down on the north", top of Selover zone (middle-lower Pico)	"Faulting probably increases with depth", p. 325-326 "Structural and stratigraphic conditions suggest that diastrophic activity began before the deposition of lower Pliocene sediments" p. 327
Faults "A" and "B"	Seal Beach oil field	Calif. Div. Oil and Gas Data Sheet 1974, Seal Beach Oil Field	Strike: N50°W Dip: Northwest	---	Map sheet indicats right lateral movement
Inglewood (High School)	Sunset Beach oil field	Allen and Hazenbush, 1957	Strike: N45°W Dip: Steeply west Normal	---	"With the exception of the Inglewood fault, few faults extend up into the Pliocene beds and those that do are minor in displacement" p. 48
		Barrows, 1974	Strike: N44°W Dip: Steeply west Normal	Vertical: 375 ft at a depth of 5000 ft	Plate V of Allen and Hazenbush (1957)
Newport-Inglewood Zone "Master Longitudinal Fault"	SW of Bolsa Chica mesa	Poland, 1959	Strike: N44°W Dip: Steeply SW Normal and right lateral	Vertical: 100 to 200 ft at the base of the fresh-water zone (base of upper Pico)	p. 102
Newport-Inglewood	Bolsa Chica mesa	DWR, 1968	Strike: N44°W Dip: Vertical to steeply SW Normal and right lateral	Vertical: 35 ft, upper Pleistocene; 50 ft, lower Pleistocene Vertical: 300 ft apparent down drop of the main aquifer	p. 36 P. 36, between two faults forming a graben

(TABLE B-1 Cont.)

Fault Name	Location	Reference	Fault Orientation	Displacement	Comments
Newport-Inglewood (North Branch)	Santa Ana gap area	DWR, 1966	Strike: N45°W Dip: Vertical to steeply SW Normal and right lateral	Horizontal: "May total 6 miles since middle Miocene"	Based on studies in the Hungtington Beach oil field conducted by other agencies, p. 20
				Horizontal: "1/2 mile or more horizontal separation in the San Pedro Formation	Estimated from differences of stratigraphy and microfossil content that cannot be explained by simple vertical separation of beds. p. 21
				Vertical: Apparent displacement as much as 2000 ft within upper Miocene strata	p. 20
				Vertical: As great as 300 ft, lower Pleistocene strata (San Pedro beds) "However, lateral displacement of San Pedro beds is of much greater magnitude"	p. 21
Inglewood-Newport	Huntington Beach oil field	Hazenbush and Allen, 1958	Strike: N45°W Dip: Vertical to steeply SW Right lateral and normal	Horizontal: "May total 6 miles since middle Miocene time"	p. 17
				Vertical: "Displacement across the Inglewood fault system vary from 1200 ft at the southeast end of the field to none near the center"	"System has the appearance of a hinge fault", p. 17
Ingelwood	West Newport Beach oil field	Corwin, 1946	Strike: N45°W Normal	Vertical: About 300 ft, down on the west	p. 11
Inglewood (two branches: Ingelwood and North Branch)	West Newport Beach oil field	Hunter and Allen, 1956	Stike: N45°W Dip: Steeply SW Normal and right lateral	Vertical: "Displacement across the system are as great as 2000 ft"	p. 16
				Horizontal: "Horizontal movements of large magnitude have also occurred"	p. 16

TABLE B-2 - Horizontal Displacement, E-Log Data - Long Beach Oil Field

Correlation Well		Reference Well		Correlation E-Log Horizon			Distance Between Wells (ft)	Estimated Horizontal Displacement (ft)	Comments (Basis for Correlation)
Name	Depth Interval (Thickness,ft)	Name	Depth Interval (Thickness,ft)	Horizon (Zone)	Stratigraphic Unit	Age (Million of Years)			
Sudduth 7	3910-4100 (190)	Amebco 2	4325-4525 (200)	J-M (lower Alamitos)	Repetto	Lower Plio. (3.75±.4)	3600	3600±500	Correlates between Amebco 1 and Encinas 1. Closest with Amebco 2 based on similar sandy horizons and thickness.
Recknagel Carlin 1	3250-3910 (660)	Encinas 1	3850-4590 (710)	TW-J (lower Wilbur)	Repetto	Lower Plio. (3.25±.3)	3900	3600±300	Closest with Encinas 1 based on similar individual sandy horizons and thinning facies to the east.
Olsen-Oliver Wallace 1	2040-2490 (450)	Amebco 1	2350-2880 (530)	Above the C horizon	Pico	Upper Plio. (2.25±.2)	2000	2300±300	Correlates well with Amebco 1 based on facies change. May be to the west based on thickness of individual horizons.
Morton-Dolly Dodge 3	3680-3890 (210)	Texaco B-18	2720-2930 (210)	Lower Wilbur Sand	Repetto	Lower Plio. (3.25±.3)	3700	3900±250	Correlates between Texaco B-18 and Texaco B-38. Closest with B-18 based on sandy horizons at the top of interval with serrated funnel shaped sands below.
Acme Dr. Co. Farrell 2-1	4010-4380 (370)	Cresson Comm. 16	2550-2790 (240)	Lower Wilbur Sand	Repetto	Lower Plio. (3.25±.3)	3500	3700±500	Farrell 2-1 correlates near Cresson 8 and 16 and Texaco C-8. Closest to and may be further than Cresson 16. Based on four sandy horizons near the top of the Wilbur.
Morton-Dolly Dodge 3	5770-6230 (460)	Dormax 1	3860-4220 (360)	W-Z Lower Brown	Repetto	Lower Plio. (4.75±.5)	7300	7500±500	Correlates closest to Dormax 1 than Pala 3, based on silty and sandy horizons.
Acme Dr. Co. Farrell 2-1	5890-6270 (380)	West of Pala 3	4400-4800 (400)	W-Z	Repetto	Lower Plio. (4.75±.5)	7500	7300±500	Correlates between Dormax 1 and Pala 3. Closest to Pala 3 based on E-log characteristics of the interval.
Alamitos 48A	5490-5840 (350)	Field 28	6440-6860 (420)	AH-AL	Puente	U. Miocene (6.0±.6)	11000	10000±100	Alamitos 48A correlates between Field B-28 and Malcom Davis 8, which penetrate through the fault zone. Closest to Field 28 based on thickening sandy horizon.
Acme Dr. Co. Farrell 2-1	4790-5230 (440)	F.F. Richards Dormax 1	2890-3280 (360)	J to Top of Brown	Lower Alamitos	Lower Plio. (3.75±.4)	4900	4800±400	Correlates between Dormax 1 and Cresson 8. Closest with Dormax 1 based on blocky sands.
Axis Pet. Co. Allied 34	3300-3550 (250)	Shell Oil Pala 3	2500-2730 (230)	Lower Wilbur Sand	Lower Wilbur	Lower Plio (3.25±.3)	3300	3300±400	Correlates between Pala 3 and Denni 9. Closest with Pala 3 based on sandy horizons and facies changes.
Axis Pet. Co. Allied 34	3550-3900 (350)	ARCO Fry 5	3210-3550 (340)	Top of Alamitos to J	Alamitos	Lower Plio. (3.5±.4)	6100	5800±500	Correlates between TC 1 and Fry 5. Closest to Fry 5 based on sandy-silt sequence at the top and bottom of the interval.

TABLE B-3 - Horizontal Displacement, E-Log Data - Seal Beach Oil Field

Correlation Well		Reference Well		Correlation E-Log Horizon			Distance Between Wells (ft)	Estimated Horizontal Displacement (ft)	Comments (Basis for Correlation)
Name	Depth Interval (Thickness,ft)	Name	Depth Interval (Thickness,ft)	Horizon (Zone)	Stratigraphic Unit	Age (Million of Years)			
Hellman 49	2610-3075 (465)	Bixby A64	2620-3050 (430)	A4-A5	Pico	Upper Plio. (2.9±.3)	4300	4650±350	Correlates betwen Bixby A62 and Bixby A64. Closest with A64 based on the upper blocky sand development and lateral facies changes.
Helman 49	3990-4440 (450)	San Gabriel 52	3860-4350 (510)	B2-C	Repetto	Lower Plio. (3.75±.4)	6800	6500±300	Correlates between Bixby A62 and San Gabriel 52. Closest to San Gabriel 52 based on similar sandy horizons and location with respect to facies changes.
Helman 49	4855-5160 (305)	San Gabriel 51	4745-5065 (320)	E-G (Selover)	Repetto	Lower Plio. (4.75±.5)	8000	7400±650	Correlates between San Gabriel 51 and San Gabriel 52. Closest with 51 based on individual sandy horizons and facies changes.
Bryant LW-2	2590-3070 (480)	San Gabriel 52	2670-3100 (430)	A4-A5	Pico	Upper Plio. (2.9±.3)	4500	4200±300	Correlates between San Gabriel 52 and Bixby A62. Closest to San Gabriel 52. Based on similar E-log characteristics and relative thickness of sandy facies.
Bryant LW-2	4020-4505 (485)	San Gabriel 51	3840-4320 (480)	B2-B4	Repetto	Lower Plio. (3.75±.4)	5800	6250±500	Correlates closest with San Gabriel 51, but is probably NW of 51 based on E-log characteristics and thinning facies changes and thickness.
Hellman 45	2710-3255 (545)	Bixby A64	2620-3050 (430)	A4-A5	Pico	Upper Plio. (2.9±.3)	4600	4950±350	Correlates between Bixby A62 and Bixby A64. Closest with A64 based on similar development of the upper sandy horizons and facies changes.
Hellman 45	4235-4735 (500)	Bixby A62	3890-4315 (435)	B2-C	Repetto	Lower Plio. (3.75±.4)	6000	6350±300	Correlates between Bixby A62 and San Gabriel 52. Closest with A62 based on development of sandy horizons near the top and overall facies changes.
Hellman 45	5180-5540 (360)	San Gabriel 52	4710-5000 (290)	E-G (Selover)	Repetto	Lower Plio. (4.75±.5)	7200	7500±300	Correlates between San Gabriel 52 and San Gabriel 51. Closest to 52 based on overall E-log characteristics and facies changes near the bottom of the interval.

TABLE B-4 - Horizontal Displacement, E-Log Data - Huntington Beach Oil Field

Correlation Well		Reference Well		Correlation E-Log Horizon			Distance Between Wells (ft)	Estimated Horizontal Displacement (ft)	Comments (Basis for Correlation)
Name	Depth Interval (Thickness,ft)	Name	Depth Interval (Thickness,ft)	Horizon (Zone)	Stratigraphic Unit	Age (Million of Years)			
Signal Oil and Gas S-41	2540-3100 (560)	Rothschild Oil Diehl 1	3625-4130 (405)	Div. "A"	Puente	Upper Mio. (6-8)	12000	12000±2100	Correlates closest with Diehl 1 based on reasonable similarity in thickness and E-log characteristics.

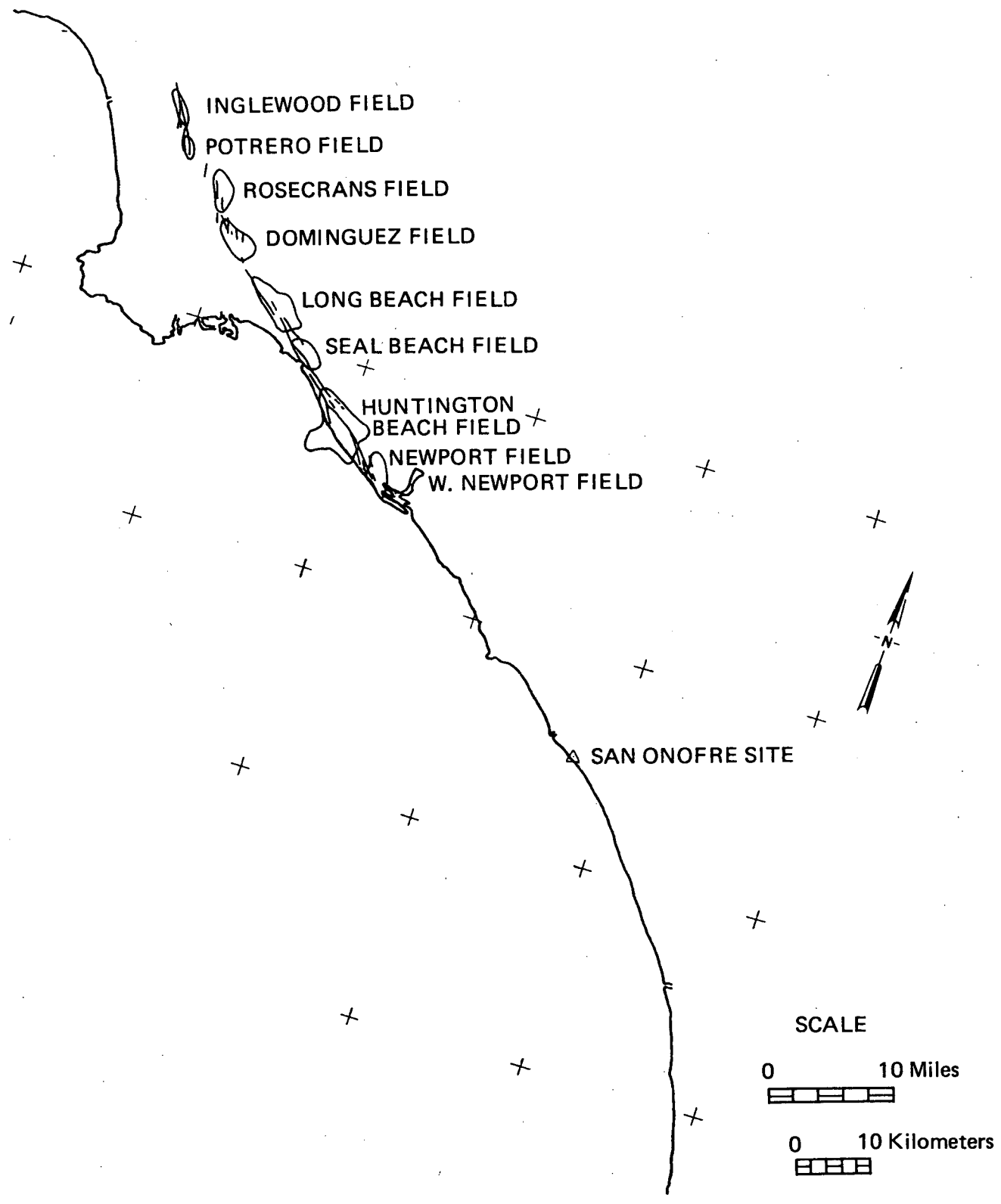

APPROXIMATE LOCATION OF MAJOR OIL FIELDS ALONG THE NEWPORT-INGLEWOOD ZONE OF DEFORMATION

SONGS 2 & 3

Project No. 411001

Woodward-Clyde Consultants

Figure B-1

REFERENCE WELLS
Southside of Seal Beach Fault
B3 to B4 Horizon
(Lower Repetto Fm.)

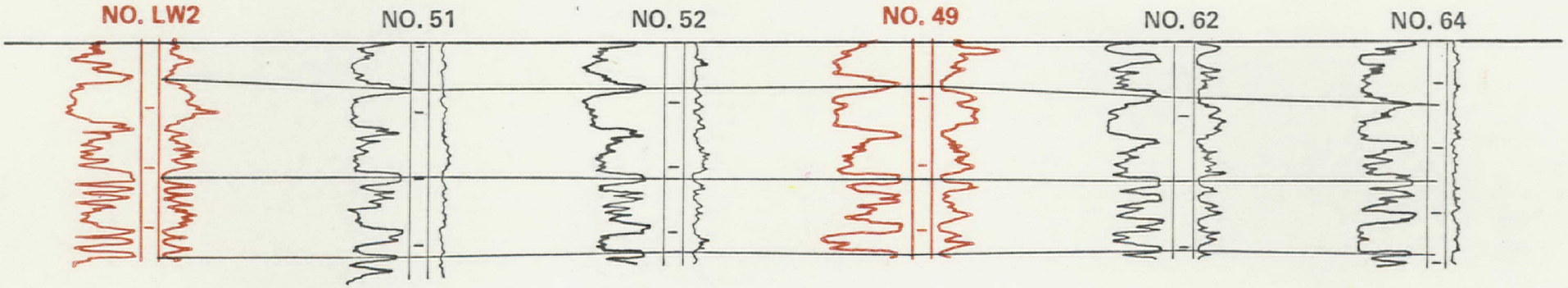

CORRELATION WELLS
Northside of Seal Beach Fault

B3 to B4 Horizon
(Lower Repetto Fm.)

EXPLANATION
E-LOG
Spontaneous-Potential
Resistivity

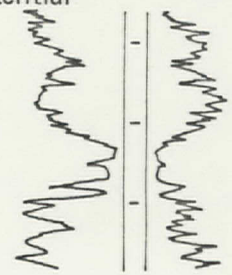

SEAL BEACH OIL FIELD EXAMPLE E-LOGS SONGS 2 & 3	
Project No. 411001 **Woodward-Clyde Consultants**	Figure B-2

REFERENCE WELLS
Northside of Cherry Hill Fault
Lower Wilbur Zone
(Upper Repetto Fm.)

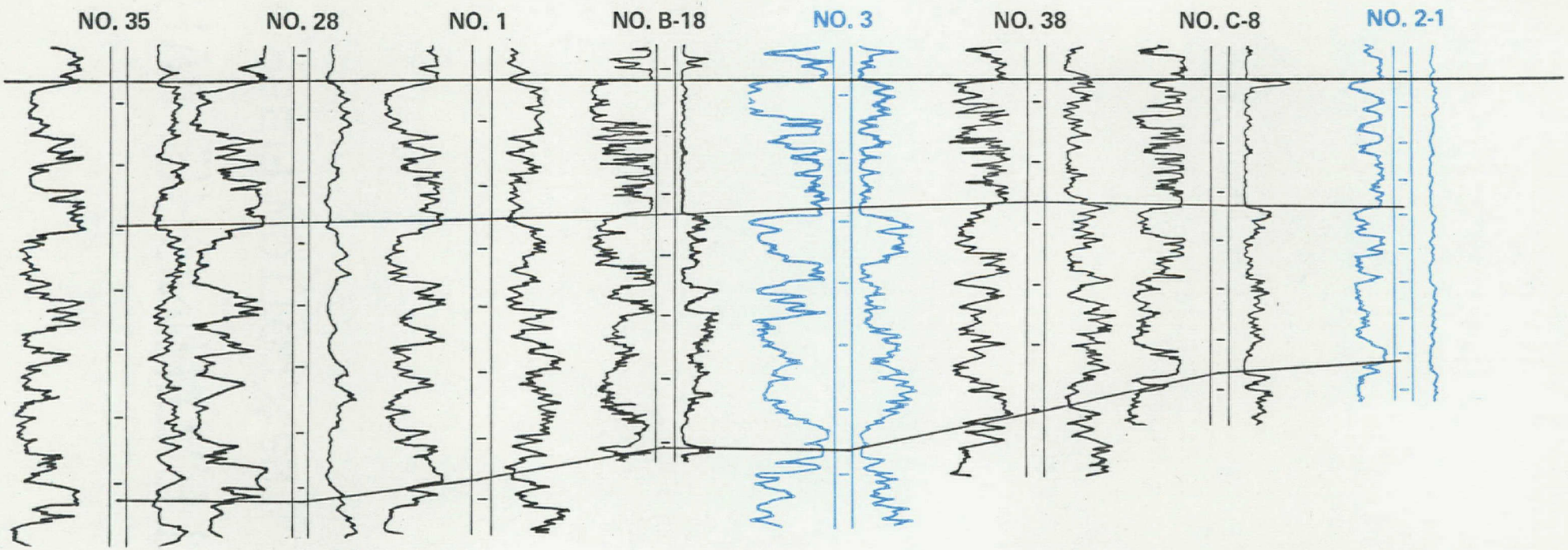

CORRELATION WELLS
Southside of Cherry Hill Fault

Lower Wilbur Zone
(Upper Repetto Fm.)

EXPLANATION

E-LOG

Spontaneous-Potential Resistivity

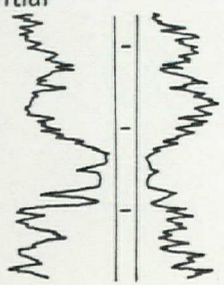

LONG BEACH OIL FIELD EXAMPLE E-LOGS SONGS 2 & 3	
Project No. 411001 **Woodward-Clyde Consultants**	Figure B-3

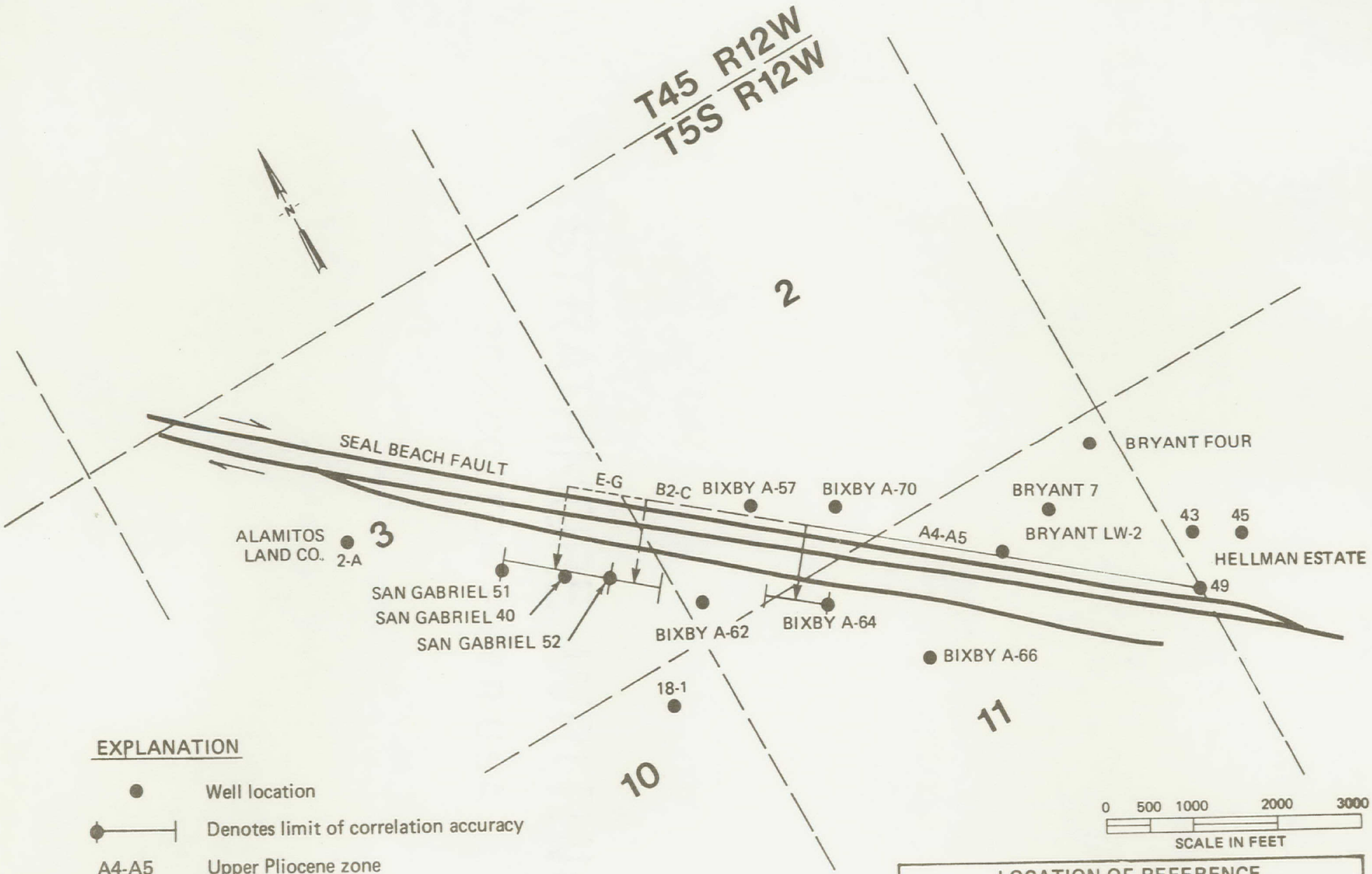

EXPLANATION

- Well location
- Denotes limit of correlation accuracy
- A4-A5 Upper Pliocene zone
- B2-C Lower Pliocene zone
- E-G Lower Pliocene zone
- Denotes total displacement measured from Hillman Estate No. 49

(FAULT TRACE DRAWN ON THE "U" MARKER HORIZON, CDOG, 1974)

0 500 1000 2000 3000
SCALE IN FEET

LOCATION OF REFERENCE AND CORRELATION WELLS – SEAL BEACH OIL FIELD SONGS 2 & 3

Project No. 411001
Woodward-Clyde Consultants

Figure B-4

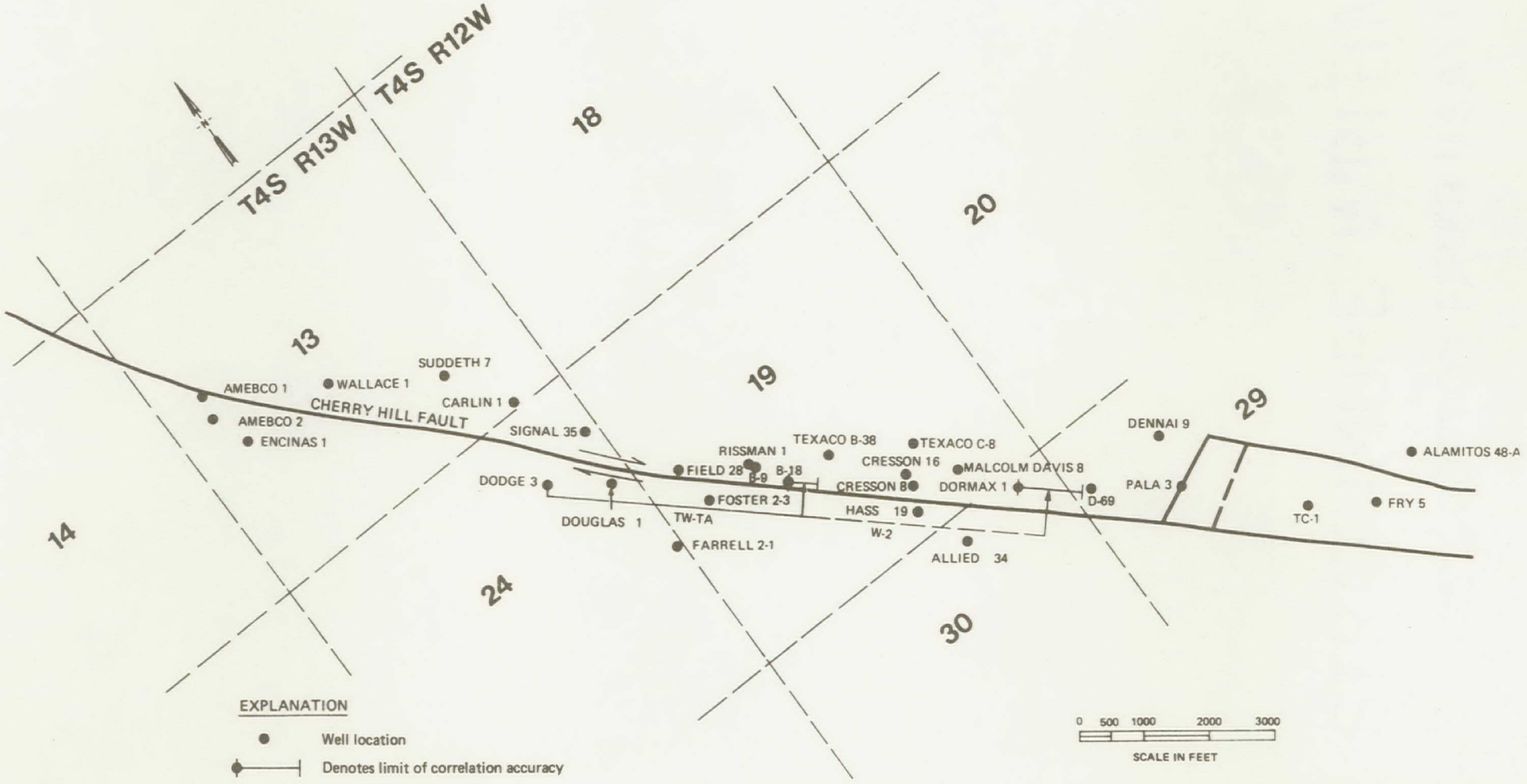

(FAULT TRACE DRAWN ON TOP OF BROWN ZONE, INGRAM, 1968)

LOCATION OF REFERENCE AND CORRELATION WELLS–
LONG BEACH OIL FIELD
SONGS 2&3

Project No. 411001
Woodward-Clyde Consultants

Figure B-5

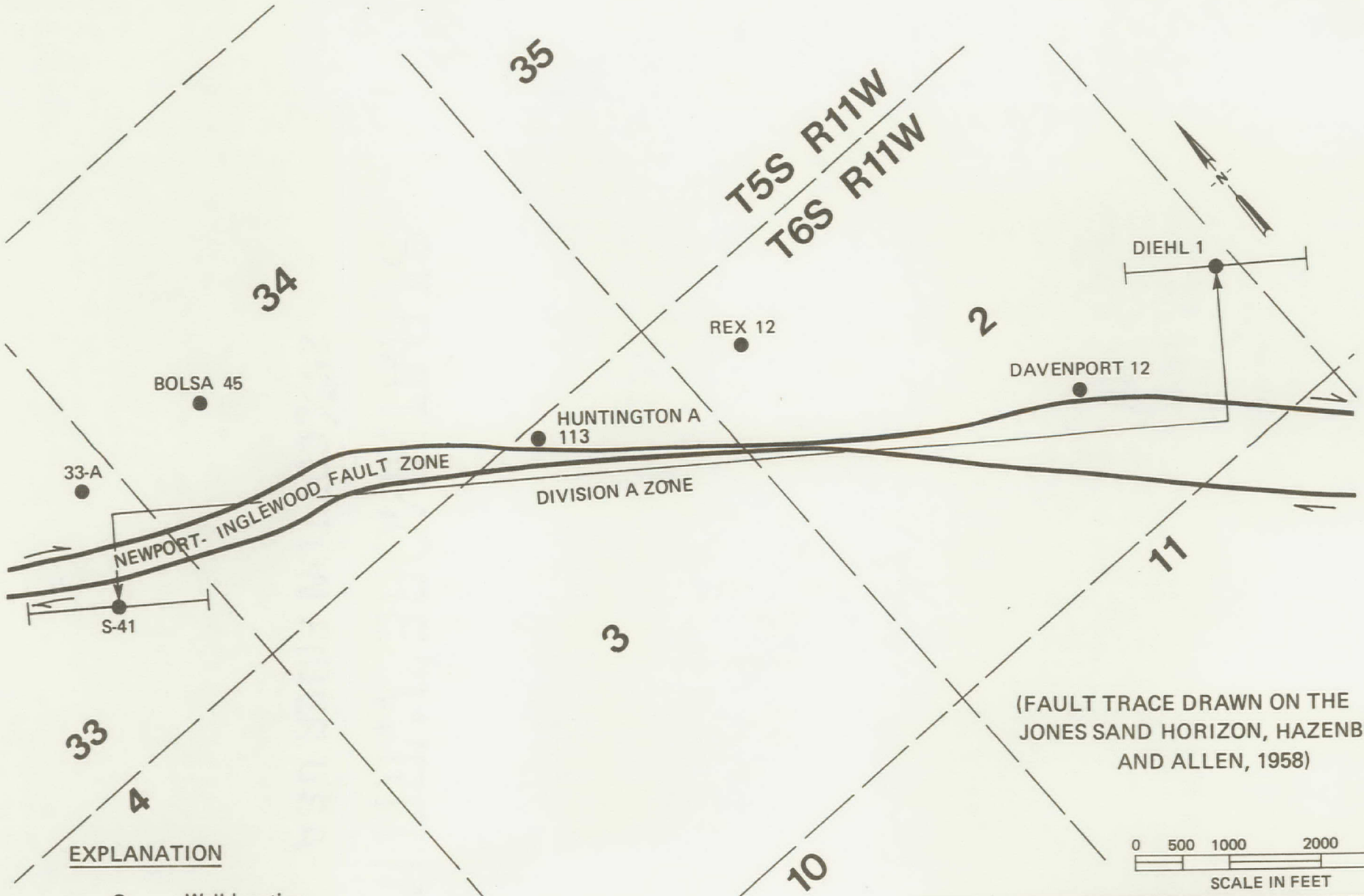

(FAULT TRACE DRAWN ON THE JONES SAND HORIZON, HAZENBUSH AND ALLEN, 1958)

EXPLANATION

- Well location
- Denotes limit of correlation accuracy
- Division A — Upper Miocene
- Denotes total displacement measured from Signal S-41 to Rothschild Diehl-1

0 500 1000 2000 3000

SCALE IN FEET

LOCATION OF REFERENCE AND CORRELATION WELLS – HUNTINGTON BEACH OIL FIELD
SONGS 2 & 3

Project No. 41100I
Woodward-Clyde Consultants

Figure B-6

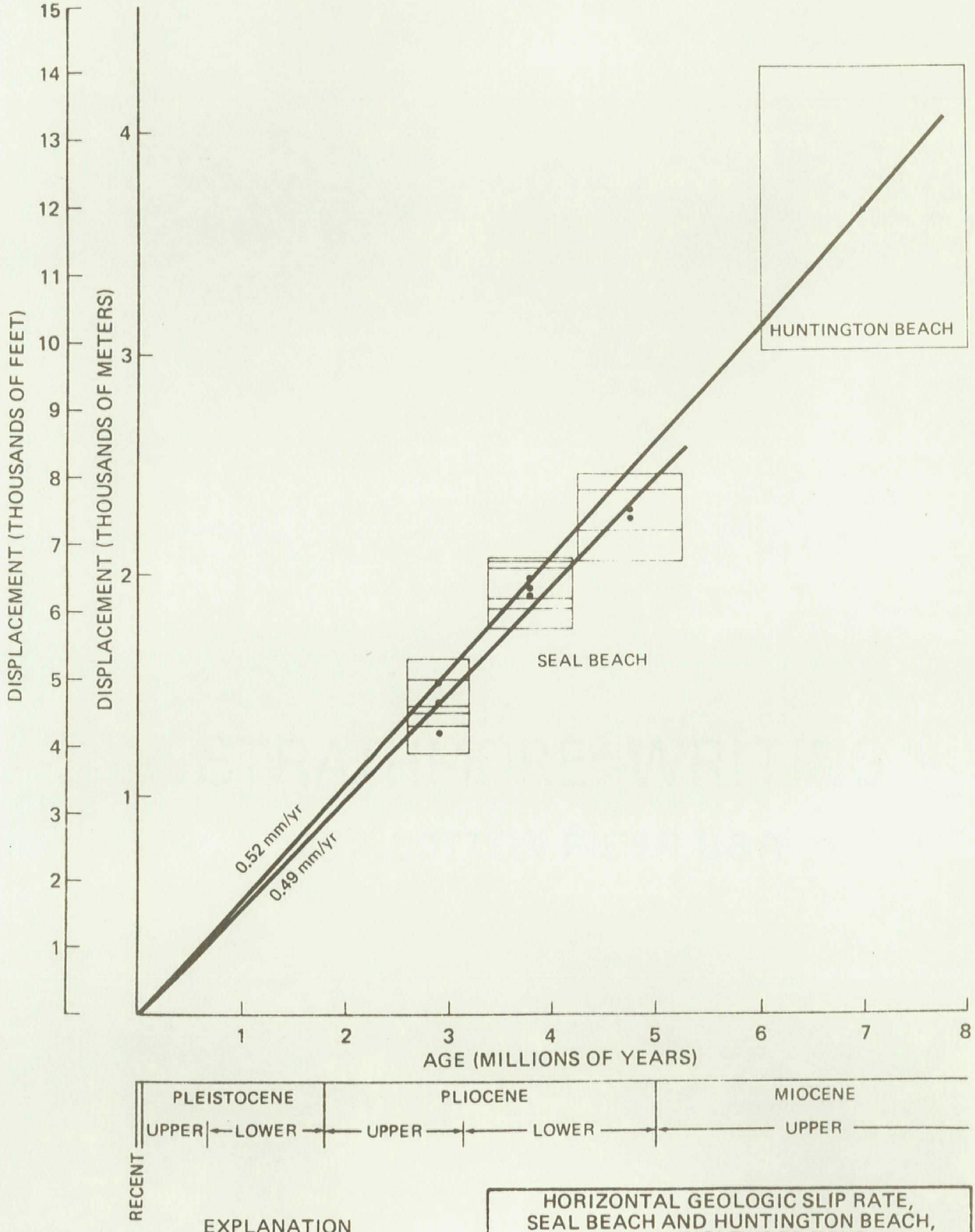

HORIZONTAL GEOLOGIC SLIP RATE,
SEAL BEACH AND HUNTINGTON BEACH,
NEWPORT INGLEWOOD ZONE
OF DEFORMATION
SONGS 2 & 3

Project No. 411001
Woodward-Clyde Consultants

Figure B-7

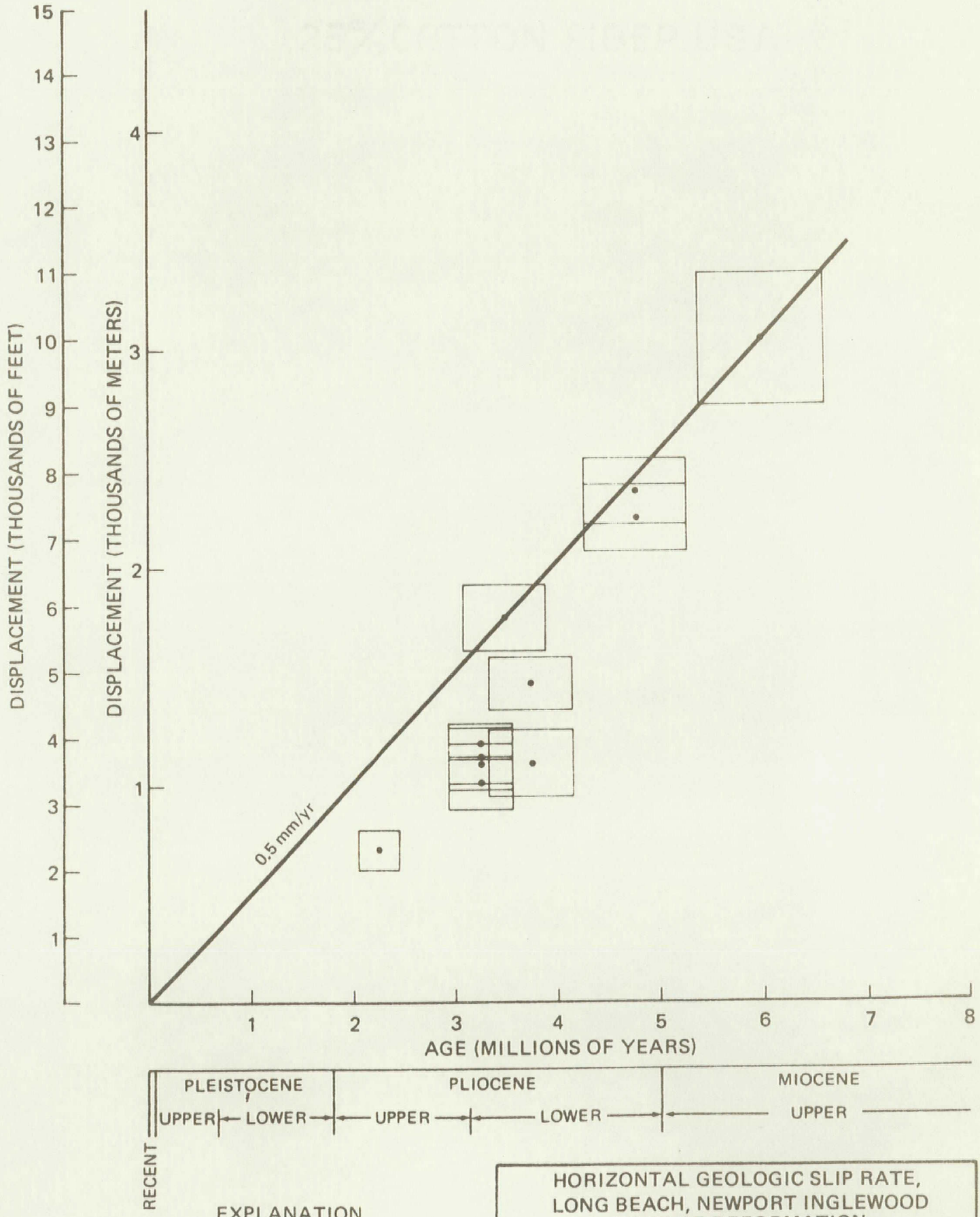

HORIZONTAL GEOLOGIC SLIP RATE,
LONG BEACH, NEWPORT INGLEWOOD
ZONE OF DEFORMATION
SONGS 2 & 3

Project No. 411001
Woodward-Clyde Consultants

Figure B-8

LONG BEACH OIL FIELD, PLATES II & III
VOL. 54, NO. 1

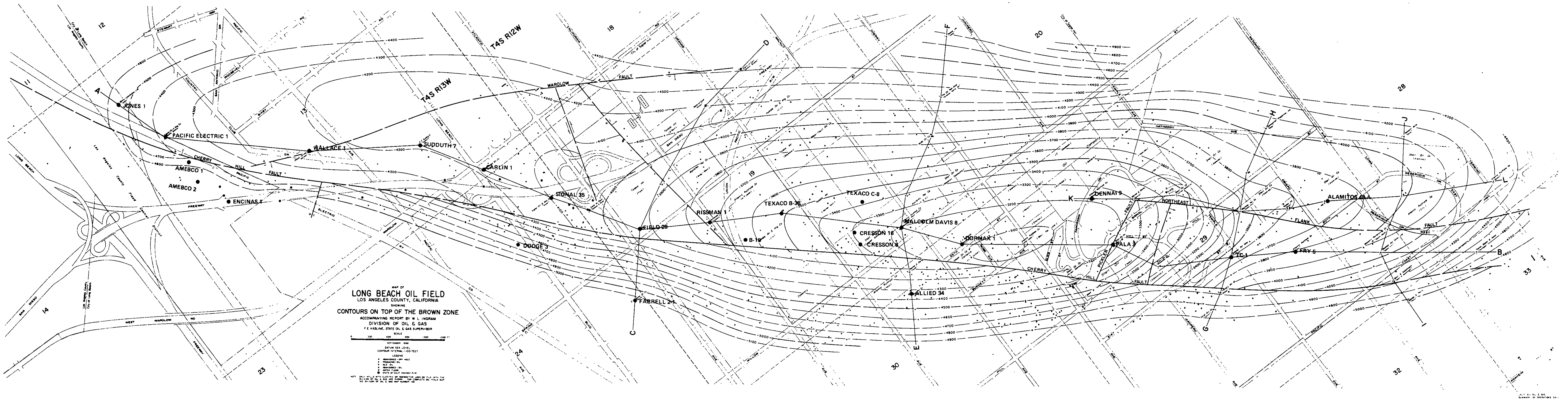

STRUCTURAL CONTOUR MAP,
TOP OF BROWN ZONE
LONG BEACH OIL FIELD
SONGS 2&3

Project No. 411001 **Woodward-Clyde Consultants**	Figure B - 9

APPENDIX C
SLIP-RATE ESTIMATES FOR THE ROSE CANYON FAULT ZONE

Data available in the published literature concerning faulting within the City of San Diego and, in particular, the Rose Canyon fault zone (RCFZ) have been reviewed and are summarized in Table C-1. The main north-northwest trending Quaternary faults in the San Diego area are the RCFZ and the La Nacion fault. Horizontal offsets have been inferred although none have been conclusively demonstrated. Vertical offsets are better known and are accompanied by various absolute age determinations for offset geologic features. The La Nacion fault, six miles east of the RCFZ, is predominately dip-slip with a rate of about 0.13 mm/yr (130 meters of vertical separation on Linda Vista formation estimated to be one million years old). Although the vertical slip rates estimated for the RCFZ are the same order of magnitude as the La Nacion, the RCFZ may be predominately a horizontal-slip fault according to Moore and Kennedy (1975). Table C-1 shows that a wide range of horizontal displacement estimates exist for the RCFZ, and that many of these are often only inferred.

The wide range of displacement data and estimated slip rates in the literature stems from two primary problems: (1) the lack of well defined and well constrained offsets of geologic features; and (2) the lack of accurate age determinations for the stratigraphic units and geomorphic features thought to be offset. For example, the maximum horizontal rate estimate cited is based on the displacement of the San Diego formation, which has not been dated by absolute dating techniques. The age of the San Diego formation is currently given as 2 to 5 million years on the basis of its microfossil content (Moore and Kennedy, 1975). Furthermore, these estimates are based on the premise of an east-

west pinchout line along the northern limits. This analysis, however, is complicated by several factors: (1) the "east-west pinchout line" appears to strike in a more northwesterly direction immediately east of the fault, suggesting that the apparent offset across the fault may be greater than the actual offset; (2) the "pinchout line" may represent a truncated boundary that could have been highly irregular prior to faulting, also amplifying the apparent displacement; and (3) small vertical displacements might lead to large apparent lateral displacements.

A review of the data presented in Table C-1 shows that estimates of apparent horizontal slip rates for the RCFZ range from 0.5 to 3.0 mm/yr. However, as discussed above, due to the questionable nature of the correlations leading to the higher horizontal displacement and slip-rate estimates, and due to lack of geomorphic evidence of lateral faulting, it is most likely that the actual horizontal slip rate is at or below the lower bound of the range given. This lower rate would be similar to the 0.5 mm/yr calculated for the NIZD (see Appendix B).

TABLE C-1

Annotated Bibliography: Rose Canyon Fault Zone and Other Faults in the San Diego Area

Reference	Fault	Style of Faulting	DISPLACEMENT			Displaced Formation & Age	Earthquake Magnitude	Slip Rate	Comments
			Vertical	Displacement Horizontal	Vert/Horiz.				
Artim and Pinckney (1973)	La Nacion fault	Normal down to the west	Pliocene = ∿80m Pleistocene = 85-120m Holocene(?) = ∿1m	None discussed	--	Holocene alluvium 10,980 ± 190 yrs. B.P.	--	None given; Calculated as 0.04-0.2 mm/yr. vertical	See comment on offset alluvium under McEuen and Pinckney (1972).
Kennedy and others (1975)	Rose Canyon fault zone	Right lateral strike-slip and dip-slip	Bay Point Fm. = 10m Lindavista Fm. = 150m Eocene = 800m	Lindavista Fm. = 1m San Diego Fm. = 4m	1/20-1/7	Eocene La Jolla group = 50m.y. Pliocene San Diego Fm. = 2m.y. Pleistocene Lindavista = 1m.y. Late Pleistocene Bay Point = 100,000 yrs.	--	0.1 mm/yr. vertical 1-2 mm/yr. horizontal	Given horizontal displacement of 4km. differs from that of Moore and Kennedy (1975), but does not appear reasonable due to questionable stratigraphic relationships; 1km. offset of the Lindavista Fm. is conceptual and has no direct supportive evidence.
	Point Loma fault zone	Dip-slip	Bay Point Fm. = 5-20m Nestor Terrace = 12m (Kern, 1973) Lindavista Fm. = 100m	--	--	Nestor terrace = 120,000 yrs. (Kern, 1973)	--	0.1 mm/yr. vertical	
	La Nacion fault zone	Dip-slip	Pleistocene = 10-100m San Diego Fm. = 75-125m	--	--	No ages discussed	--	None given. Calculated as 0.01-0.1 mm/yr. vertical	
Kennedy and others (1977)	Spanish Bight, Coronado, and Silver Strand faults	Possible strike-slip and dip-slip	None given	None given	--	Holocene(?) Pleistocene Lindavista Fm. - no absolute age given	--	--	Data based on acoustical profiles.
Kern (1973)	In vicinity of Point Loma fault	Dip-slip	Nestor terrace = 12m	--	--	Nestor terrace = 120,000 yrs.	--	Calculated from data 0.1 mm/yr. vertical	

TABLE C-1 (Continued)

Reference	Fault	Style of Faulting	DISPLACEMENT			Displaced Formation & Age	Earthquake Magnitude	Slip Rate	Comments
			Vertical	Horizontal	Vert/Horiz.				
Kern (1977)	Rose Canyon fault	Right lateral strike-slip and dip-slip	Bird Rock terrace = 19-24m	150m on Nestor terrace	1/3-1/5	Nestor terrace = 120,000 yrs. Birdrock terrace = 80,000 yrs.	--	0.2-0.4 mm/yr. vertical 1.2 mm/yr. horizontal	Identification of offset of terraces is tentative.
Ku and Kern (1974)	In vicinity of Point Loma fault	Dip-slip	Nestor terrace = 13-17m	--	--	Nestor terrace = 120,000 yrs.	--	0.1 mm/yr. vertical	
Liem (1977)	Transverse fault in the Rose Canyon fault zone	Thrust	2.7m	None documented	--	C^{14} dated alluvium = 28,700 yr. $\pm$ 1,500 yrs. B.P.	--	0.09 mm/yr. vertical	Fault identified in 1 trench only. Alternate hypothesis of landsliding cannot be discounted.
McEuen and Pinckney (1972)	Rose Canyon fault zone and associated faults, and La Nacion fault	Right lateral and dip-slip on Rose Canyon. Primarily dip-slip on La Nacion	La Nacion - Pliocene = 70m, Pleistocene = 61m Holocene = 1m+	None given	--	Holocene = less than 11,000 yrs. Late Pleistocene = less than 400,000 yrs.	--	--	Offset Holocene alluvium has been questionably interpreted by several investigators. No documentation for displacements or age for calculation of slip rate.
Moore (1972)	Rose Canyon fault, northwest extension	Assumed strike-slip due to parallel association with Elsinore and San Andreas fault zones	Lindavista Fm. = 130m (no reference) Bay Point Fm. onshore at La Jolla = 30m (Peterson, 1970)	None measured	--	Holocene(?) on sea floor. Pleistocene Lindavista Fm. onshore = 0.5-2.0 m.y. from range suggested by various authors. Late Pleistocene Bay Point Fm. = about 100,000 yrs.	--	0.07-0.3 mm/yr. horizontal	

TABLE C-1

Reference	Fault	Style of Faulting	DISPLACEMENT			Displaced Formation & Age	Earthquake Magnitude	Slip Rate	Comments
			Vertical	Displacement Horizontal	Vert/Horiz.				
Moore and Kennedy (1975)	Southern offshore extension of Rose Canyon fault zone. See Kennedy (1977) reference for update of offshore faulting	Apparent vertical offset down-to-the-east. Also apparent strike-slip right lateral displacement	Holocene(?) = 1-2m Lindavista Fm.(?) = 10m Referenced to other work: Bay Pt. Fm. = 12-30m (Kern, 1973; Peterson, 1970). Lindavista Fm. = 30-130m (Moore, G.W., 1972).	Lindavista Fm. = 1 km San Diego Fm. = 6 km	1/7	Holocene(?) platform on bay floor, = 10,000 yrs. Late Pleistocene Bay Pt. Fm. = 100,000 yrs. Pleistocene Lindavista Fm. = approx. 1 m.y. Pliocene San Diego Fm. 2-5 m.y. (Age of San Diego Fm. is from various sources, summarized in Mandel, 1973).	--	(estimated by author 1 mm/yr. horizontal calculated from data) 0.03-0.3 mm/yr vertical. 0.5-3 mm/yr. horizontal	The 6km horizontal for the San Diego Fm. based on questionable stratigraphic relationships. The 1km post-Quaternary offset at the coastline may be erosional rather than strike separation. No direct evidence is given for offset of the Lindavista Fm.
Simons (1977)	Rose Canyon and La Nacion fault zones	--	--	--	--	--	37 recorded events between M2.3 to M3.7, 1934-1974	--	

APPENDIX D
SOUTH COAST OFFSHORE ZONE OF DEFORMATION
GEOPHYSICAL DATA

Existing interpretations of geophysical data for the area immediately offshore of southern California, south of the Palos Verdes Peninsula, have been reviewed and evaluated. In addition, portions of the raw data on which those interpretations were based were reviewed in an attempt to develop an understanding of the structural style of deformation on the South Coast Offshore zone of deformation (SCOZD). Although the existing interpretations are judged to be generally reasonable, it should be noted that the combination of minimal available stratigraphic control, record quality, wide survey line spacing, and variations in seismic signature allow for significant interpretive latitude and that these interpretations are not definitive for developing horizontal geologic slip rates. The principal results of this data review are summarized below.

The acoustic basement (Horizon C, Western Geophysical, 1972) is believed to be located on the lower to middle Miocene San Onofre Breccia through much of the region, but locally is on crystalline basement (Western Geophysical 1972; Vedder and others, 1974). The earliest displacement of this horizon is considered to be post-middle Miocene. Apparent vertical displacements of 1000 to 3000 feet are indicated on the faults that cut Horizon C (Figure D-1) across the Rose Canyon fault zone (RCFZ), the SCOZD, and a major southwesterly trending branch of the SCOZD. Vertical displacements on most of the other faults are less than 500 feet.

In the SCOZD, Horizon-C faults are reflected as discontinuous breaks and folds at the higher acoustic Horizon B (Figure D-2). An interpretation of post-Miocene structures along the SCOZD

(Vedder and others, 1974) shows a broad, northwest-trending zone of rather uniformly distributed but discontinuous faults, suggestive of the wrench-faulting model of Harding (1973).

Variations among the structural patterns through time suggest that two separate tectonic regimes have produced the recognized features. Structures along the SCOZD on Horizon C appear to be dominated by north- and northwest-oriented normal faulting. This suggests a period of east-west tension across the area and may indicate the onset of regional wrenching (Harding, 1973; Yeats, 1973).

Horizon-B structures are consistent with a north-south compressional environment. The faults in Horizon B, which are younger and shorter faults, indicate continued deformation. Several folds in Horizon B suggest drag folding associated with right-lateral wrench faulting.

High resolution profiles of post-Miocene units near San Onofre (Woodward-Cldye, 1978; Fugro, 1978) indicate a series of faulted folds approximately paralleling the SCOZD. These structures differ from those of the underlying B and C horizon structures in that the faults associated with the folds are not continuous with the faults recognized in Horizons B and C.

Vertical slip rates along the offshore RCFZ and the SCOZD were estimated from the apparent displacement of Western Geophysical's (1972) B and C horizons, with an assumed age for these horizons of 5 and 8 m.y. These vertical displacements and slip rates are considered to be more reliable than possible horizontal displacements that were based on tentative correlations of apparently displaced features across the faults. Calculated vertical slip-rate estimates on the offshore RCFZ range from 0.02 to 0.15 mm/yr over the past 8 m.y., and for the SCOZD, from 0.05 to 0.12 mm/yr over the same period. Horizontal displacement

estimates based on tentative correlations were highly inconsistent and produced a wide scatter of displacements. These horizontal displacements are considered too speculative and too poorly constrained to be used for the calculation of geologic slip rates.

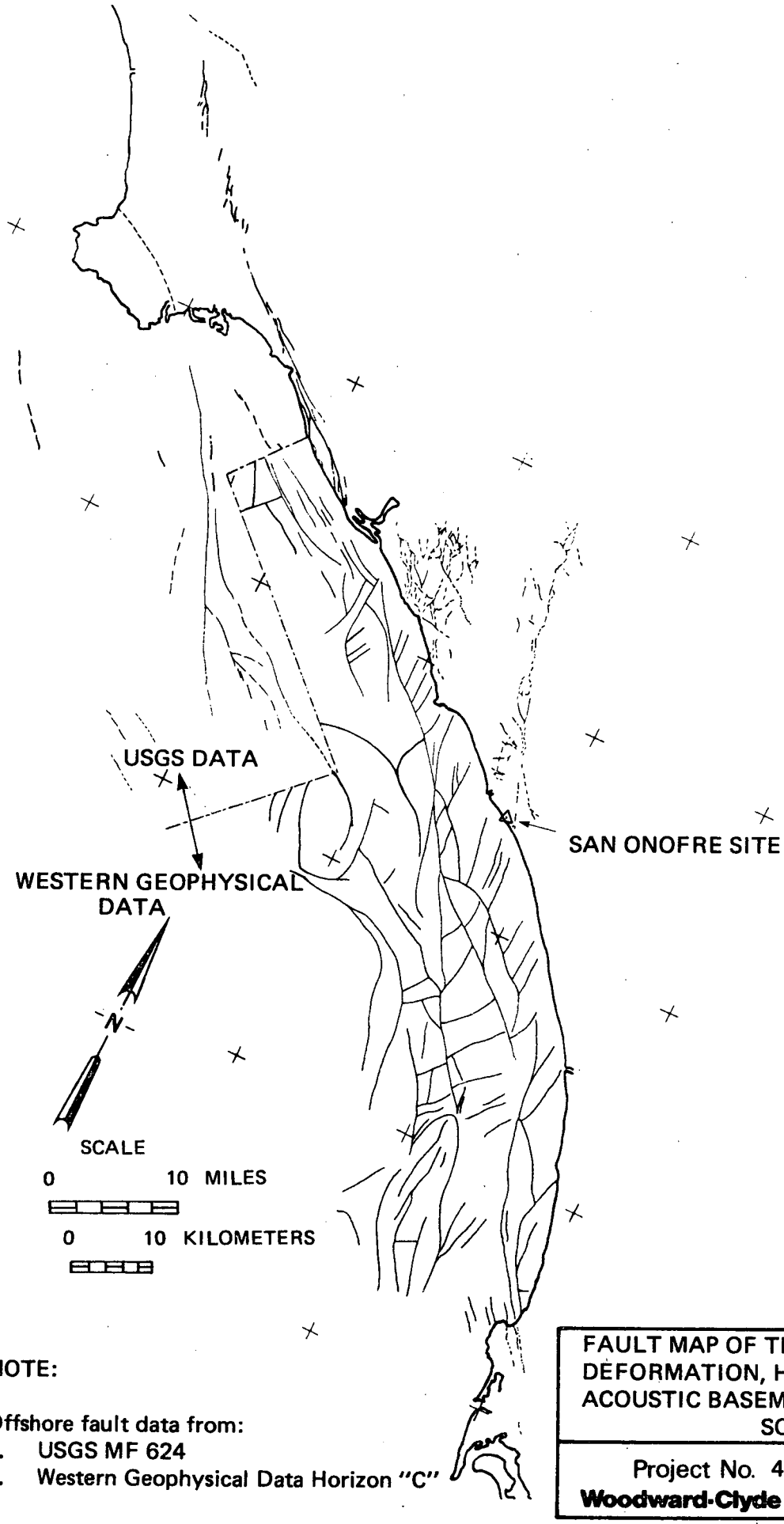

NOTE:

Offshore fault data from:
1. USGS MF 624
2. Western Geophysical Data Horizon "C"

FAULT MAP OF THE OFFSHORE ZONE OF DEFORMATION, HORIZON "C" (EFFECTIVE ACOUSTIC BASEMENT)
SONGS 2 & 3

Project No. 411001
Woodward-Clyde Consultants

Figure D-1

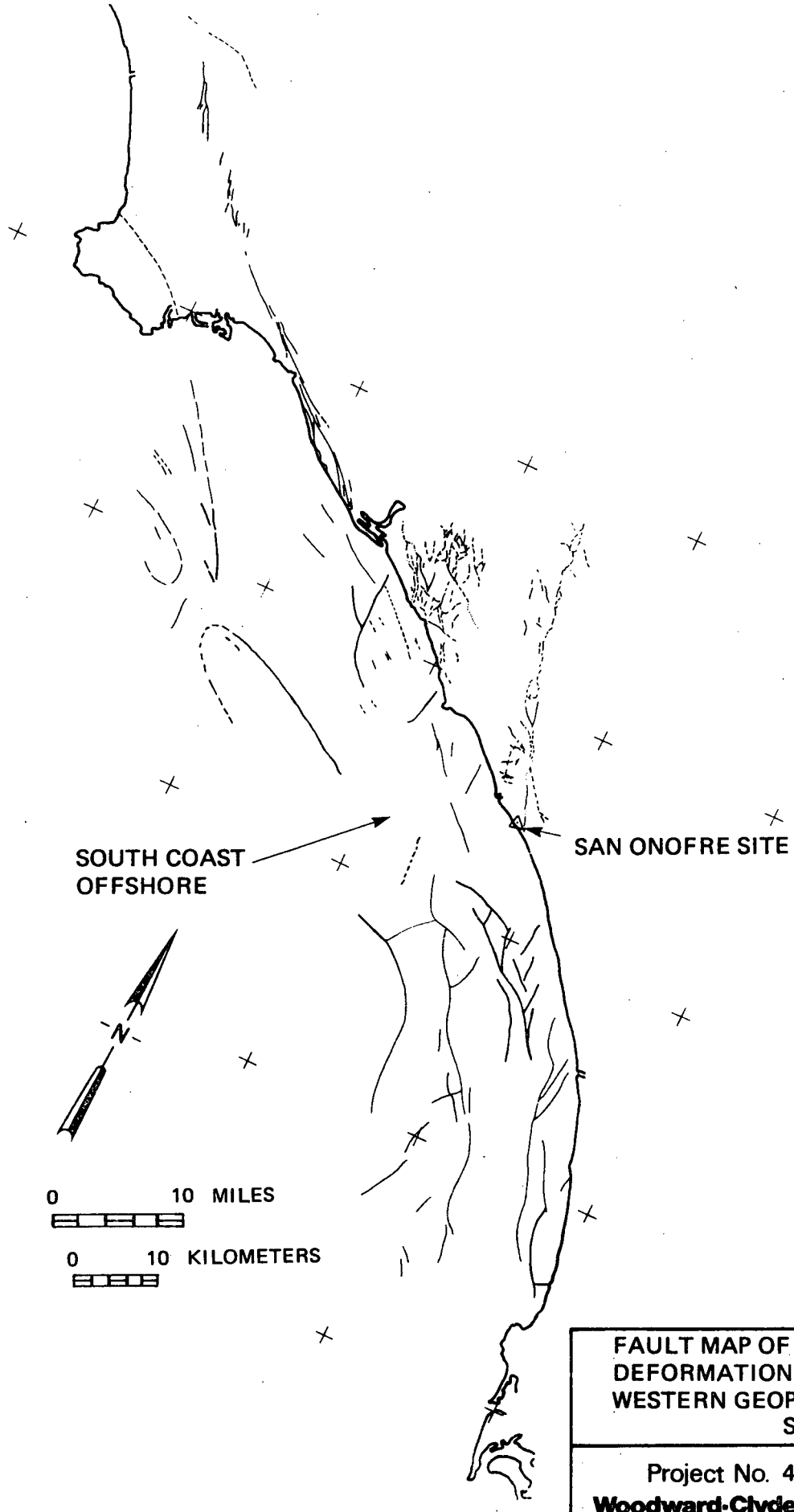

FAULT MAP OF THE OFFSHORE ZONE OF DEFORMATION, HORIZON "B". FROM WESTERN GEOPHYSICAL, 1972.
SONGS 2 & 3

Project No. 411001
Woodward-Clyde Consultants

Figure D-2

APPENDIX E
ANALYSIS OF TELESEISMIC DATA FOR THE 1933 LONG BEACH EARTHQUAKE

E-1 INTRODUCTION

The 1933 Long Beach earthquake is the largest instrumentally recorded earthquake to have occurred on a segment of the hypothesized offshore zone of deformation (OZD). Thus it provides important information about characteristics of possible future earthquakes on the hypothesized OZD. An essential element for understanding the physical relationship between the Long Beach earthquake and its geologic source is the focal mechanism of the earthquake. The P-wave first motions recorded on regional seismograph stations in 1933 are insufficient to fully constrain the mechanism. Consequently, the teleseismic recordings of the 1933 earthquake have also been used to constrain the focal mechanism and other source parameters.

In this study, emphasis is placed on accurately modeling the observed P, pP, and sP phases recorded at teleseismic distances. The modeling procedure is very sensitive to the focal mechanism orientation, and thus the final mechanism is determined by iteratively determining a best fit to both the well-recorded P waveforms and the directions of first motion of a large number of P and S phases.

E-2 DATA COLLECTION

Obtaining seismograms from stations around the world for this relatively old event required substantial investigative work. Many of the records had been archived since 1933; others were lost or sent to researchers in 1933. Within the United States, a few records were obtained from the National Archives; many other records came from individual seismographic stations still in operation. A large percentage of these private stations were and/or are operated by the Jesuits and the quality of the records

is quite good. Several very important close-in data points came from stations operated by Berkeley and Caltech.

Most of the European stations that recorded the event were also contacted. The assistance of Dr. Raikes at Karlsruhe, Germany is gratefully acknowledged in this effort. About 70% of the stations in Europe responded to requests for seismograms. The quality of much of the European data is very good, since many stations used a Galitzin seismograph. This instrument is very similar in characteristics to the current World-Wide Standard Seismograph (WWSS). A very complete list of world-wide seismographic stations, including instrument constants, was published by the National Research Council (McComb and West) in 1931. The effects on the waveforms introduced by the seismograph response were therefore easily included in the modeling procedure.

A complete list of all seismograph stations contacted, the disposition of the records, and the polarities of the P-wave first motions are listed in Table E-1. Distances and azimuths from the stations to the earthquake are also given.

E-3 PRE-PROCESSING OF SEISMOGRAMS

All seismograms that might potentially be modeled in this project were digitized and are shown in Figures E-1 and E-2. Not all of these records were used in the modeling, as indicated in Table E-1. In order to obtain a very accurate representation of the seismogram, the records were photographically enlarged by a factor of 50. The records were then digitized, and the digital seismograms were rotated into a coordinate system more appropriate for the earthquake location. That is, the north-south and the east-west components were vectorially added so that the resultant waveforms corresponded to what would have been recorded if the station had been oriented with one horizontal component pointing towards the earthquake (radial) and the other

perpendicular to it (transverse). The rotated components are plotted in Figure E-2 along with the original components.

The rotation of the S-wave into radial and transverse components naturally decomposes the S-wave into SV (vertically polarized S-wave) and SH (horizontally polarized S-wave). The first motion of the SH wave can be used in focal-mechanism solutions in a manner similar to P-wave first motions. For instance, for a north-striking, right-lateral strike-slip fault, a station due east would record an S-wave with the first motion toward the south. As a vertical component seismograph was not operating at Sitka, the radial component of the P-wave was used in the modeling study. Four of the other five P-waves modeled were recorded by vertical instruments and required only digitizing and plotting at a common time scale (30 mm/min). The remaining P-wave, for station DEB, was not received in time to digitize but was included in the analysis.

E-4 SYNTHETIC SEISMOGRAM THEORY

A complete discussion of the generation of synthetic seismograms is provided in Langston and Helmberger (1975). The following is a brief description of the physics involved in wave propagation and in the method used here for modeling seismic waveforms.

The recorded seismograms represent the end product of a series of operations that modify and distort the seismic energy as it propagates through the earth. First the earthquake itself radiates energy in a non-uniform but well-defined pattern. At any particular azimuth, the energy radiated by the source depends on the orientation of the fault, the time history of the faulting process, and the direction of fault rupture. The earth structure immediately around the source further modifies the seismic energy. Reflections from the surface and discontinuities in the crust appear at teleseismic distances as though they were independent sources with a strength modulated by the strength of

the reflections. As the energy propagates through the earth's mantle, the amplitude decays because of geometrical spreading; and attenuation preferentially reduces the amplitudes of the higher-frequency components of the waveform. The crustal structure at the recording site also modifies the signal. Finally the seismograph itself introduces a significant distortion. In trying to understand what the waves on a seismogram mean, it is extremely important to note that this series of modifications is commutative: no matter in what order the modifications are made, the resulting waveform is the same. All operators, except the source-radiation pattern and the interaction with the crust at the source, can be combined into one effective operator. The time-domain shape of this operator, called SQI, is shown in Figure E-3. Thus SQI contains the effects of source, attenuation, and instrument.

The instrumental constants for the Galitzan Seismographs are described by McComb and West (1931). The attenuation or Q-operator used in this study was developed by Futterman (1962). The parameter that controls the shape of the Q-operator is T* (equals travel time divided by the average Q). For P-waves at teleseismic distances, a T* of 1.0 is a good average value (Langston and Helmberger, 1975). The final operator included in the function SQI is the source dislocation time history. When an extensive data set of both short- and long-period teleseismic recordings are available, this parameter is routinely adjusted as part of the iterative inversion for fitting the wave form. The data set from 1933 is rather limited. The rupture time was adjusted in the early stages of the inversion. The width of the observed pulses require a source duration of about 6.5 $\pm$2 seconds. The rise time for a particle on the fault to reach peak velocity was set at 0.2 seconds. These are reasonable average values, and reasonable variations in their choice will not seriously affect the conclusions of this study.

After the definition and selection of the parameters used in constructing the function SQI, the waveform-fitting process enters into an iterative stage. The parameters defining the orientation of the fault and the depth of the hypocenter are selected. Next, the synthetic seismograms are compared with the data. Perturbations to the fault orientation parameters and source depth are calculated and the next iteration started. This procedure continues until 12 to 15 seconds of the observed P-wave forms are reproduced by the synthetics in a best-fit sense.

The interaction with the source and the crust involves three major phases, as illustrated in Figure E-3. The first P-wave phase (P) leaves the source and enters immediately into the mantle of the earth. The next phase, seen typically on a seismogram for shallow earthquakes, is the P-wave that leaves the source traveling upwards, reflects from the surface of the earth and follows P to the station (pP). Finally an S-wave is converted to a P-wave at the surface (sP) and follows pP to the station. The strengths of these three phases and their time separation depend on: (1) the orientation of the earthquake fault plane; (2) the strength (amplitude) of the reflection or conversion; and (3) the depth of the earthquake. The spike-like Delta-functions on Figures E-3 and E-4 show the relative sizes, polarities, and arrival times for these three phases. The final synthetic seismogram is constructed by adding the waveshape (SQI) together three times, with each waveshape shifted in time corresponding to the arrival time of the phase. The amplitude of SQI is modulated by the three pulse strengths. The synthetic seismograms shown in Figure E-4 agree very well with the observed seismograms presented in Figures E-1 and E-2 and represent the best fit between the observed and synthetic waveforms in terms of both polarity and relative strength of the three phases P, pP, and sP. The synthetic seismograms shown in Figure E-4 are computed with the focal mechanism shown in Figure E-5.

E-5 FOCAL MECHANISM FOR THE 1933 LONG BEACH EARTHQUAKE

It should be noted that the final waveform or synthetic seismogram is a delicate balance between three strongly interfering signals. Small changes in the source orientation can have very dramatic effects on the waveforms. Figure E-6 shows an example of how rapidly the waveforms change for changes in strike and dip of only 10 degrees. Because of these extreme changes to the waveforms with relatively minor changes in fault orientation, the resolution of the strike, dip and rake of the fault plane is quite good. For the focal mechanism discussed below, a change of 10 degrees would strongly violate the waveform data.

All available first-motion data are plotted on a lower hemisphere stereonet in Figure E-5. The first motions of the regional stations as well as the teleseismic synthetics are used. The "+" at station LJA was read as nodal by Dr. Hiroo Kanamori at Caltech (personal communication, 1978). This suggests that the strike of the fault should pass very close to, or through, the station. The best fit to all the data is shown by the indicated fault planes. The fault plane most consistent with the aftershock lineation shown in Figure E-7 and the rupture zone on the NIZD associated with the 1933 Long Beach earthquake shown in Figure E-8 (both striking approximately N45°W) is the plane striking N22°W and dipping 84°SW. However, the number of inconsistent first motions, six, and the lack of complete consistency with the geologic orientation of the earthquake source suggest that additional factors should be evaluated in the focal mechanism determination.

E-6 EFFECT OF DIPPING SEDIMENTARY STRUCTURE ON THE FOCAL MECHANISM AND MOMENT

Two explanations can be considered for the inconsistencies in the focal mechanism shown in Figure E-5:

(1) In some cases, fault zones may be restricted from moving by

a major asperity, so that slip on the fault may occur only after this asperity had been fractured, perhaps along a relatively minor fault that is not perfectly aligned with the N45°W trend of the entire zone. This asperity model is not supported by the present understanding of the geology of the NIZD.

(2) The best-fitting fault plane, Figure E-6, was largely constrained by the upgoing phases pP and sS, so that if a dipping sedimentary wedge were above the earthquake, the take-off azimuths for these phases would be rotated. Figure E-8 shows the depth-to-basement contours for the Los Angeles Basin and supports the suggestion that the dipping structure probably does rotate the azimuths to some extent.

This second possibility of the focal mechanism inconsistencies offers a satisfactory explanation and can be more fully evaluated. Figure E-9 shows both a plan and cross-section view of a ray that leaves the source, interacts with the structure, and continues on to the station BUF. Each time the ray encounters the dipping interface, it is bent towards the direction of maximum dip and causes the change in azimuth. This effect changes the azimuth that the ray must leave the focal sphere in order to travel to the station. For comparison, both the rotated upgoing phase sP and the unaffected downgoing phase P are shown in Figure E-9. The plan view in the lower diagram in Figure E-9 shows that as the S-wave encounters the dipping layer it is bent towards the dip direction. The same phenomena affects the reflected P-wave. Hence, if the ray is to leave the region on an azimuth of N61°E, it must leave the source at N77°E, thus causing a corrective rotation of the takeoff azimuth.

Figure E-10 shows a corrected focal mechanism that assumes a dipping interface with a strike of N15°W and a dip of 5 degrees toward the northeast, a simple model for the Los Angeles basin.

The seismic velocities of 3.0 km/s and 1.7 km/s for the sedimentary wedge were assumed for P and S respectively. This simple dipping interface explains the minor difference between the geology and the seismological interpretation based on a flat-layered earth. The rotated focal mechanism in Figure E-10 has a plane that strikes N40°W, in close agreement with the mapped trend of the NIZD (Figure E-8). The mechanism is pure strike-slip and has no calculable vertical component from the records used.

In order to more fully assess the effect of non-horizontal structure on up-going seismic rays, a more quantitative analysis can be performed to calculate the effect of such structure on the synthetic waveforms. In Figure E-8, along the strike of the NIZD, the basement rocks of the Los Angeles basin dip 5 to 20 degrees to the northeast. However, from a seismological perspective, the immediate overlying sedimentary rocks do not form a significant impedance contrast. Because of the overlying lithostatic load and induration, the seismic velocity of the deepest sediments is quite similar to the basement complex (Kanamori and Hadley, 1975). As the Los Angeles basin has been continuously subsiding during the Miocene (Yerkes and others, 1965) the dip of the basement represents a maximum effective dip. In most sedimentary structures the effect of the lithostatic load or confining pressure on the seismic velocities is as significant as the lithology. This reduces the dip of the acoustic layer from that expected solely from the geology. In consideration of these effects, a low velocity sedimentary unit has been included in the waveform modeling. The dip of the contact has been varied from 0 to 12.5 degrees and the strike has been varied from N60°W to N15°W to encompass various possibilities for the effective Los Angeles basin structure.

The rotation of the azimuth of the up-going phases pP and sP for the stations BUF and SIT was examined for variation of the strike

and dip of the contact over the range of the model described above. For the up-going phases an approximate rule of thumb was found for the source-station geometry of the Long Beach earthquake: the angular distance on the focal sphere that an up-going phase is perturbed by the dipping layer is approximately two to three times the dip angle. Hence for small dip angles (approximately 5 degrees), the migration is not large. With the added constraints of the regional and teleseismic first motion readings (the open and closed symbols on Figure E-6) the extent that the focal-mechanism solution can be modified is rather limited. By varying the dipping layer over the model range, right-lateral strike-slip focal-mechanisms solutions, compatible with the polarity of the up-going phases, range in strike from N22°W to N45°W. Dip angles range from 80°NE to 80°SW.

The addition of a soft, surficial layer substantially complicates the waveform modeling process. In the previous sections, three arrivals were discussed: P, pP and sP. With the addition of the surficial layer, pP and sP are modified by the transmission coefficients that describe what percentage of the incident energy crosses the layer boundaries. In addition, at least two additional rays must be added to the modeling process. These are the equivalent of pP and sP, but they are reflected from the bottom of the layer instead of the surface. If one desires to model the data for an extended record length, additional rays must be computed as well, representing those rays that reflect several times in the layer. These late arrivals have been neglected since primary interest in this study is in the first 12 to 14 seconds of each seismogram.

As with the half-space model, variations of the fault strike, dip and rake of only a few degrees greatly modify the waveform at some or all of the stations. In addition, changes in the dip and strike of the bottom of the low velocity wedge have similarly dramatic effects.

The inversion process of fine-tuning the fault orientation to maximize the correlation between the synthetic seismograms and the data is a fairly lengthy process. Adding a dipping layer and two additional rays easily doubles the complexity of the task. However, for purposes of evaluating the stability of the waveform amplitude estimates when the velocity model is modified to include dipping structure, it is not necessary to completely fine tune the inversion. The resulting moment estimate is discussed in Section E-7.

After mapping out the perturbations to the up-going rays by varying the dipping structure, the velocity model shown in Figure E-9 was used. Although a fault plane solution that gave the correct polarity for all five rays at all six stations could be found manually, matching the amplitude for each ray was a more difficult task. The synthetic seismograms presented in Figure E-11 are a compromise between fitting the correct polarities and the correct amplitudes. The fault orientation used for the calculations is N45°W with a dip of 82°SW and rake -165°. Station STR has been omitted because the azimuth and distance are almost the same as station STU. These synthetics are not optimal and the waveforms only approximately fit the data. Additional fine-tuning of the strike, dip and rake of the fault plane and the strike and dip of the sedimentary section would improve the correlation, but would not significantly alter the associated source parameters.

In conclusion, modeling the effect of shallow dipping sedimentary structures has shown that the up-going rays are systematically rotated by the structure. For the 1933 Long Beach earthquake, located on the edge of the Los Angeles basin, modeling shows that the true fault plane should be rotated counter-clockwise from the best estimate derived from a simple velocity model. For the station geometry for this event, the rotation introduced by the sedimentary wedge primarily affects the strike of the fault

plane. Dip on the strike-slip fault plane is most probably within 10 degrees of vertical.

E-7 ESTIMATION OF ADDITIONAL SOURCE PARAMETERS

The depth of the earthquake can be well constrained by the relative arrival times of the phases P, pP and sP. Clearly, the deeper the earthquake is, the greater the time separation is between the down-going and up-going phases. Similarly, the faster the P- and S-wave velocities are, the shorter the separation is. Relatively good estimates of the crustal velocities are available from several previous studies (Gutenberg, 1955; Shor, 1955; Kanamori and Hadley, 1975). Seismic velocities of 6.3 km/s and 3.5 km/s for P and S were used respectively. The velocity model used was a simple half space. The best-fit depth for the simple half space model is calculated as 11 km. The use of a lower-velocity surficial layer could reduce that calculated value by 1 to 2 km. Thus, a good estimate for the depth of the 1933 Long Beach earthquake is 10 $\pm$1 km.

The numbers shown on Figures E-4 and E-11 adjacent to the synthetic seismograms are the trace amplitudes (in microns) that would be recorded by a Galitzin instrument with unit gain for an earthquake with a moment of 10^{25} dyne-cm. (Moment is the product of the area of the fault, the displacement on the fault and the shear rigidity.) The best estimate of the moment is the average of the ratios of the observed amplitudes and the synthetic amplitudes. The details of this calculation for the six stations initially modeled are listed in Table E-2. The average value estimated for the moment is 6.2×10^{25} dyne-cm.

The moment calculated according to the procedure in Table E-2 but using the amplitudes of the waveforms calculated for the dipping structure (Figure E-11) is somewhat less, with an average value of 4.2×10^{25} dyne-cm. This range of values indicates a measure of the uncertainty in the moment value.

In addition, as the velocity model is quite different than the half-space model used in the previous section and the computer code has been largely altered to handle dipping structures; this second moment estimate provides a nearly independent check on the initial value.

Although the sedimentary wedge rotates the up-going rays, it does not significantly alter the moment calculated from the comparison of synthetic and real seismograms. Since moment and energy release are related, it is physically very reasonable that the geologic structure can alter the radiation pattern but not seriously affect the total energy radiated teleseismically. For a sparsely sampled radiation pattern, the orientation of the fault plane and the calculated moment can be intimately linked. For the Long Beach earthquake, the regional and teleseismic data provide sufficient coverage so that uncertainty introduced by the geologic structure does not degrade the estimated moment.

From the moment of the earthquake it is possible to estimate the average displacement along the fault, provided reliable estimates are available for the fault area. The length of the fault may be estimated from the 1933 earthquake aftershock zone. The total aftershock zone as shown in Figure E-7 is slightly longer than 45 km. However, the aftershocks that occurred during the first day or so following the main shock occurred over a shorter zone, approximately 30 km in length, based on the aftershock locations reported by Hileman and others (1973) and discussed by Wood (1933), Benioff (1938), and Richter (1958). The width of the fault zone is generally considered to be the entire portion of the seismically active crust, a width of about 15 km. A rigidity of 3×10^{11} dyne/cm^2 is in good agreement with average density and S-wave velocities. Combining these parameters with the moment in the equation given in Table E-2 results in an estimated average displacement of 46 cm. Using the estimated moment for the dipping structure gives a displacement of 31 cm.

The relationship between the moment and surface wave magnitude (M_S = 6.3) for this event is compared with a wide range of other earthquakes in Figure E-12 (from Kanamori and Anderson, 1975). This comparison shows that the Long Beach earthquake was a low stress drop event ($\Delta\sigma \simeq 10$ bars). Such events are characterized by relatively small displacements, which is consistent with the calculated 46 cm, given above.

TABLE E-1

SEISMOGRAPHIC STATIONS CONTACTED
STATUS OF RECORDS, POLARITIES AND RECORD QUALITY

Station	Code[1]	Distance (degrees)	Azimuth (degrees E of N)	Status of Records[2]	Polarity[3]	Quality[4]
Pasadena	PAS	0.6	346	1	D	1
Mount Wilson	MWC	0.6	356	1	D	1
Riverside	RVR	0.7	53	1	D	1
La Jolla	LJA	1.0	139	1	N	3
Santa Barbara	SBC	1.7	301	1	C	1
Haiwee	HAI	2.6	0	1	D	1
Tinemaha	TIN	3.5	358	1	D	1
Mt. Hamilton		4.8	323	2		4
Palo Alto	PAL	5.2	320	2	D	2
Berkeley	BKL	5.5	322	2	D	2
San Francisco		5.5	320	2		4
Tucson	TUC	6.2	100	2	D	1
Ukiah		7.0	324	3		
Denver	DEN	12.1	56	2	D	3
Bozeman	BOZ	13.2	22	2	D	1
Spokane		14.0	2	3		
Little Rock	LTR	21.2	80	2	C	1
St. Louis	STL	22.9	69	2	D	3
Madison		24.2	58	3		
Sitka	SIT	26.3	338	2	D	2
Columbia	COL	30.5	78	2		5
Buffalo	BUF	31.8	61	2	N	1
Georgetown		33.1	68	4		
Ottawa		34.2	56	2		4
Seven Falls		*	*	2		5
Halifax		*	*	2		4
Fordham		35.5	65	2		5
Honolulu		37.1	261	2		5
La Paz		72.8	128	2		5

Station	Code [1]	Distance (degrees)	Azimuth (degrees E of N)	Status of Records [2]	Polarity [3]	Quality [4]
Edinburgh		74.8	32	2		4
Kew	KEW	78.9	35	2	D	2
Upsala		79.7	21	3		
De Bilt	DEB	81.0	31	2	D	1
Copenhagen	COP	81.3	26	2		3
Hamburg		82.2	28	3		
Gottingen		83.4	30	3		
Toledo		84.6	45	2		4
Strasbourg	STR	84.7	32	2	D	2
Stuttgart	STU	85.2	32	2	D	2
San Fernando		85.4	49	3		
Zurich		85.9	33	2		4
Granada		86.5	47	3		
Chur		86.7	33	3		
Almeria		87.4	47	3		

Notes:

[1] Station code given for stations used in analysis

* Distance and azimuth not computed

[2] 1 = Polarities Available
2 = Records recovered
3 = Records lost/destroyed
4 = Records ordered but not yet received

[3] D = Dilation
C = Compression
N = Nodal

[4] 1 = Excellent, impulsive
2 = Good
3 = Fair, emergent
4 = Very emergent
5 = not usable

TABLE E-2

MOMENT AND FAULT DISPLACEMENT CALCULATIONS

Station	Phase	Record Amp. (mm)	Gain	Ground Motion (μ)	Synthetic* (μ)	Moment x 10^{25} dyne-cm
STU	P	3.0	930	3.23	.40	8.07
STR	P	2.0	930	2.15	.40	5.37
KEW	P	1.42	930	1.53	.55	2.78
BUF	P	4.86	930	5.23	.97	5.39
SIT	P	4.4	1000	4.4	.55	8.0
DEB	P	2.8	750	3.73	.50	7.46

Average Moment = 6.2×10^{25} dyne-cm

$$\text{Moment} = \mu L w \bar{D}$$

Fault Length, $L = 30$ km

Rigidity, $\mu = 3 \times 10^{11}$ dyne/cm^2

Fault Width, $w = 15$ km

Therefore: Displacement, $\bar{D} = 46$ cm

* Synthetic calculated for moment of 10^{25} dyne-cm.

STU VERT COMP P–WAVE

KEW VERT COMP P–WAVE

BUF VERT COMP P–WAVE

COL E–W
(E UP) S–WAVE (TIME SHIFT)

COL E–W
(E UP) P–WAVE

KEW N–S COMP
(N UP) S–WAVE

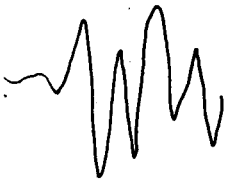

COP E–W
(E UP) S–WAVE

STU E–W COMP
(E–UP) S–WAVE

STR VERT COMP P–WAVE

Note:

Stations are listed in Table E-1.

Events marked "Time Shifted" do not have accurate absolute timing.

Maximum amplitude of records is normalized.

1 minute
SCALE

DIGITIZED ORIGINAL SEISMOGRAMS

SONGS 2 & 3

Project No. 411001
Woodward-Clyde Consultants

Figure E-1

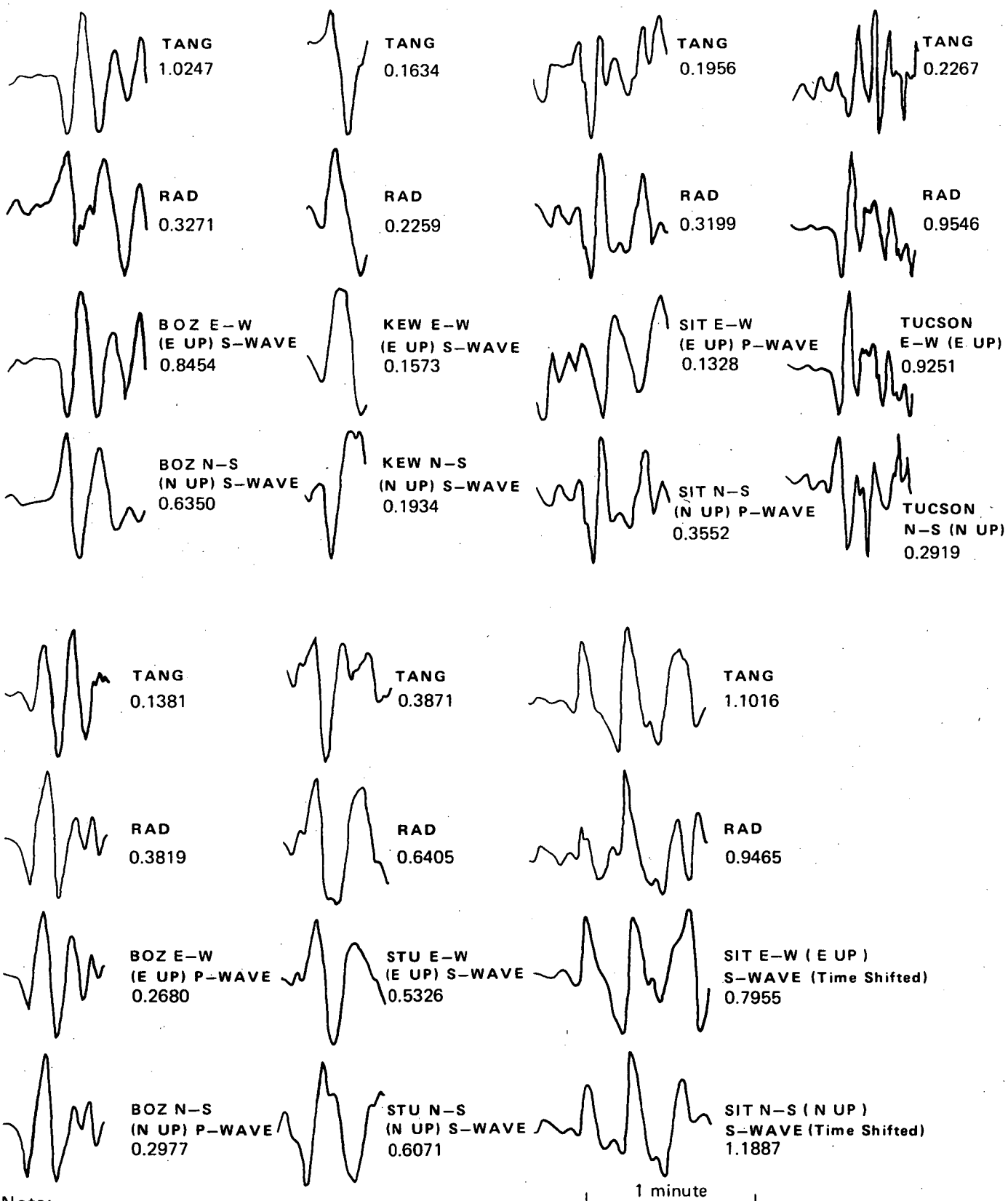

Note:

TANG = Tangential

RAD = Radial

Maximum amplitude of records is normalized; numbers represent relative amplitude Stations listed in Table E-1

DIGITIZED ORIGINAL AND ROTATED (RADIAL AND TRANSVERSE) SEISMOGRAMS SONGS 2 & 3

Project No. 411001

Woodward-Clyde Consultants

Figure E-2

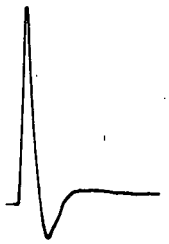

SQI

(Source-Time history, attenuation, and instrument effects operator)

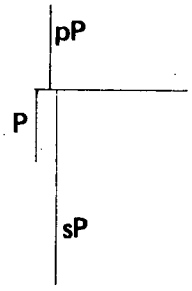

Time sequence and relative amplitude of modeled phases

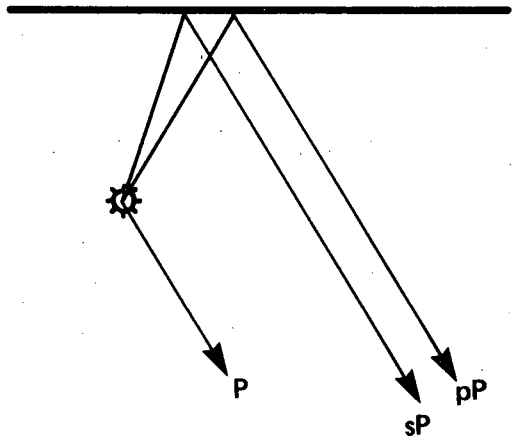

1 minute

SCALE

SYNTHETIC SEISMOGRAM THEORY	
SONGS 2 & 3	
Project No. 411001 **Woodward-Clyde Consultants**	Figure E-3

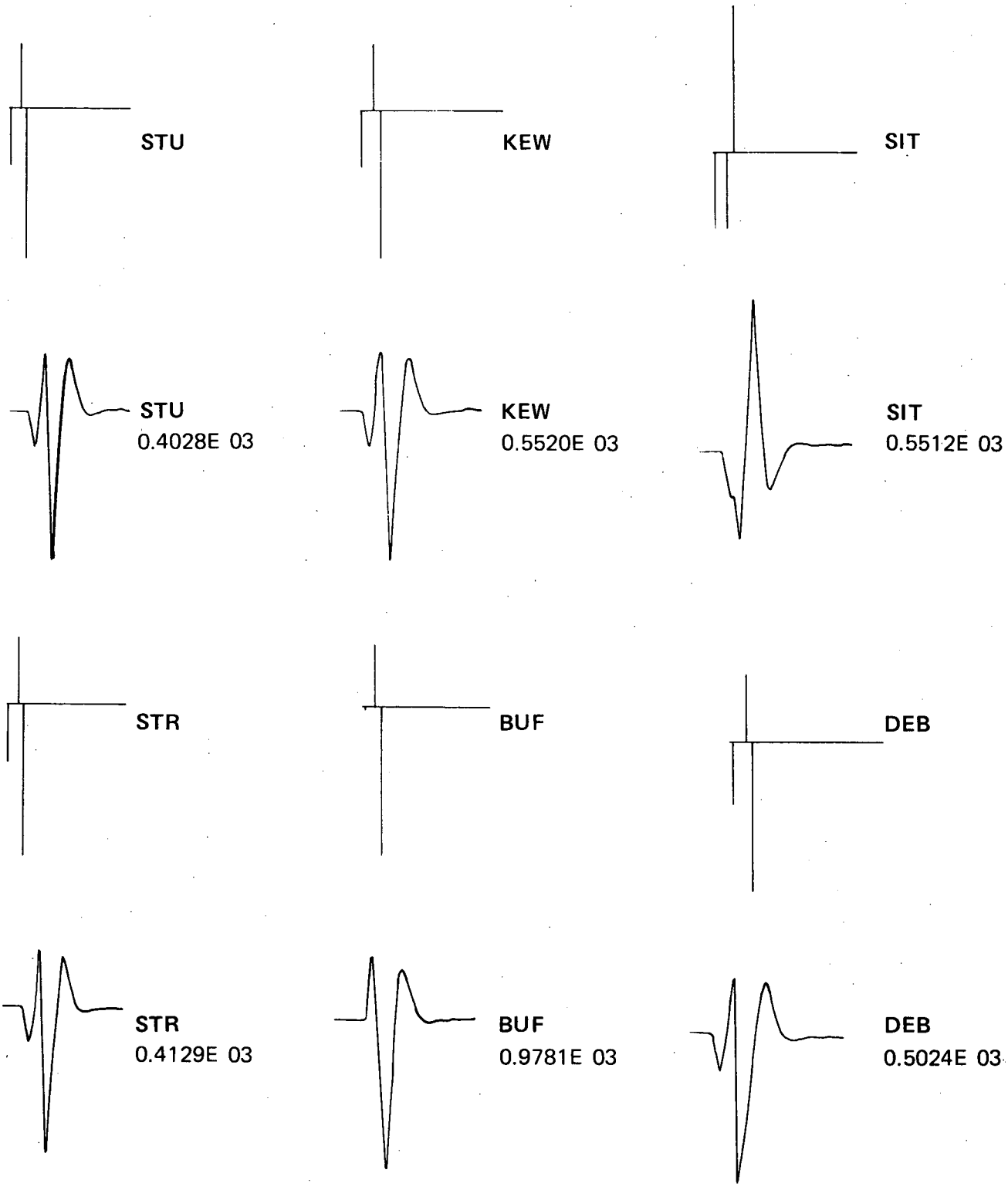

Note:
Numbers represent trace amplitude, see section E-7
Stations listed in table E-1

1 minute
SCALE

P–PHASE TIME FUNCTIONS AND SYNTHETIC SEISMOGRAMS
SONGS 2 & 3

Project No. 411001
Woodward-Clyde Consultants

Figure E-4

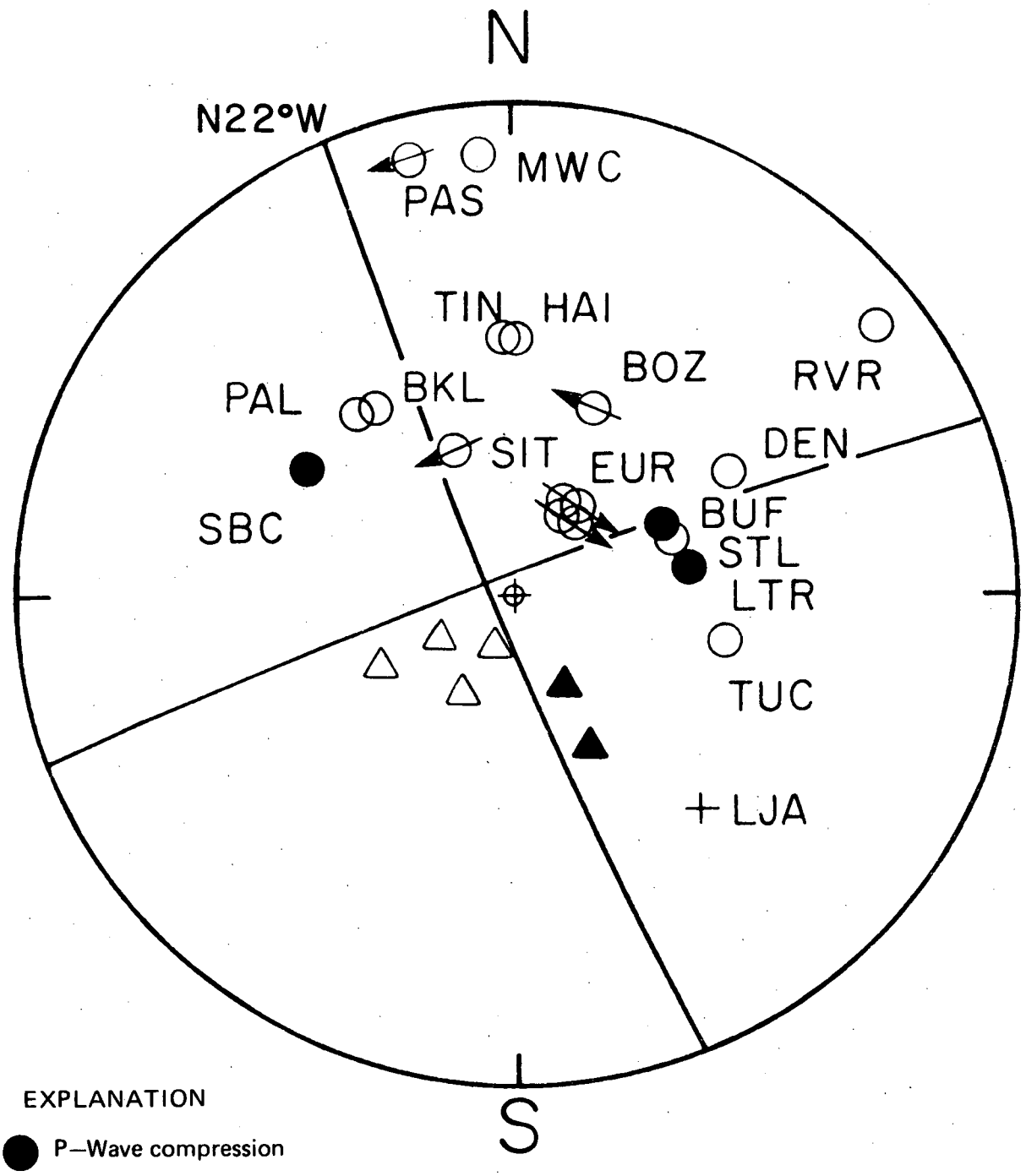

EXPLANATION

- P—Wave compression
- P—Wave dilatation
- pP or sP compression
- pP or sP dilatation
- SH polarization

BEST FIT FOCAL MECHANISM

SONGS 2 & 3

Project No. 411001
Woodward-Clyde Consultants

Figure E-5

STATION: STU

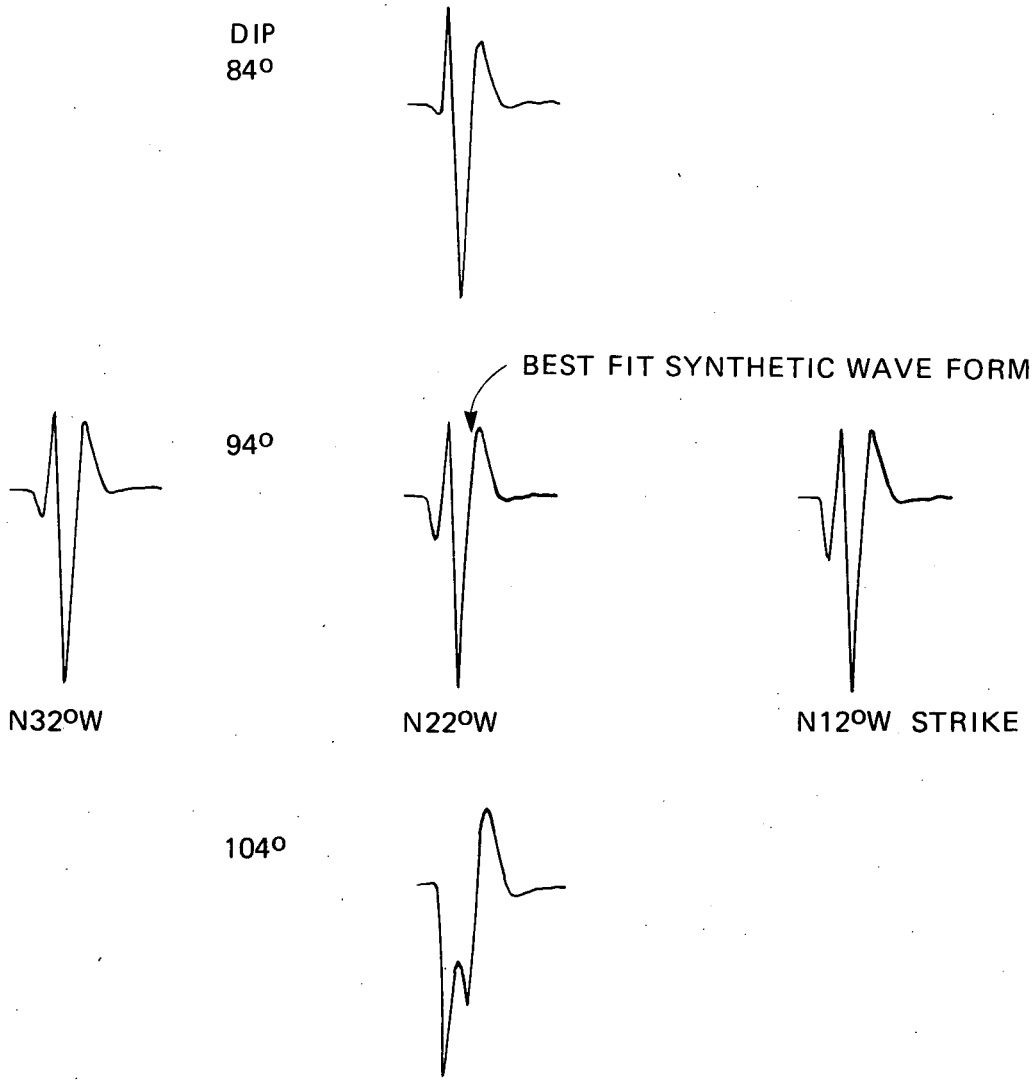

Note: Dip and strike are shifted by 10° from the best fit focal mechanism shown in Figure E-6

1 minute
SCALE

SYNTHETIC WAVEFORM SENSITIVITY SONGS 2 & 3	
Project No. 411001 **Woodward-Clyde Consultants**	Figure E-6

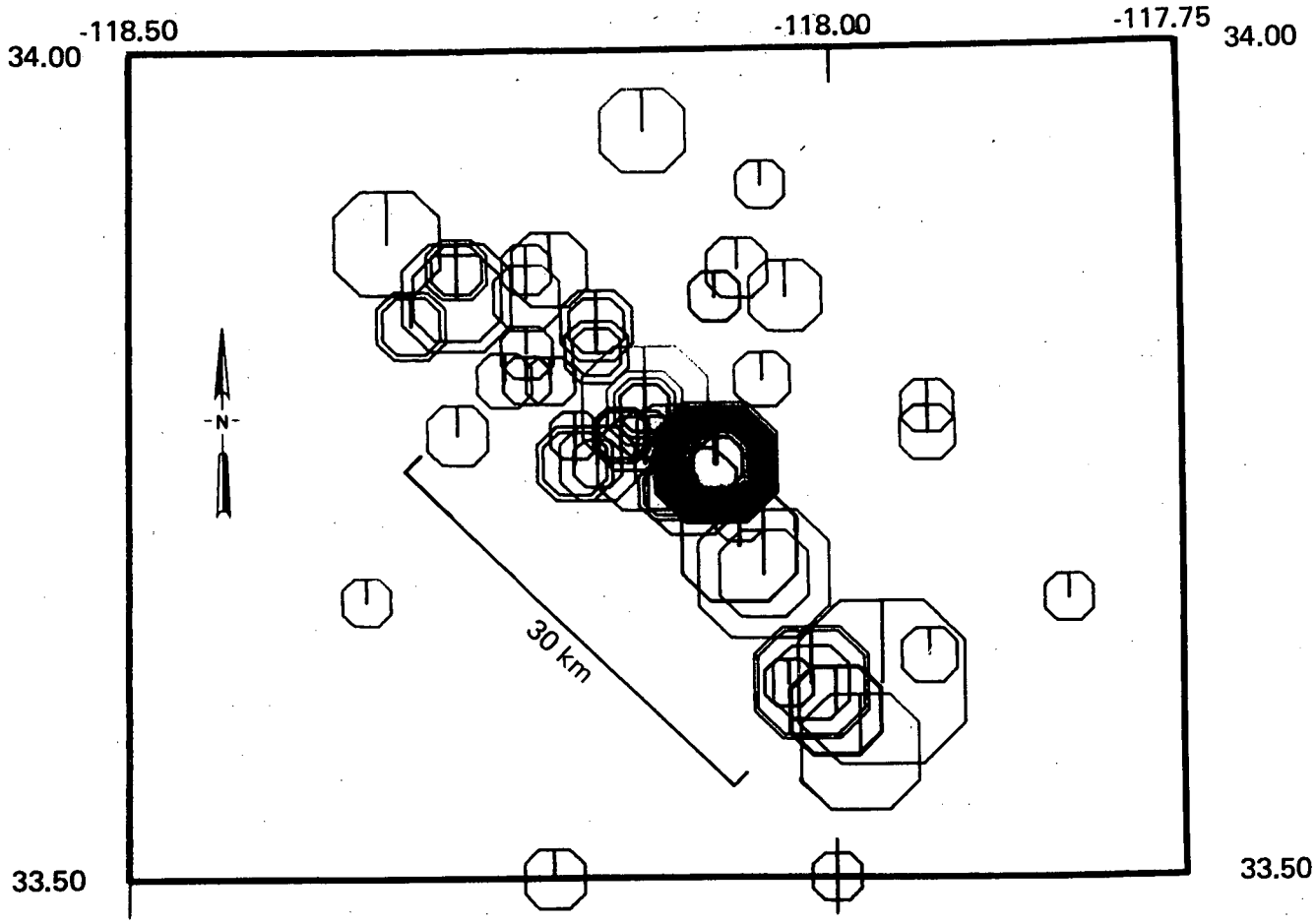

MAGNITUDE

6.0

5.0

4.0

3.0

$M \geq 3.0$

1 January 1933 through 31 December 1933.
Data from Hileman and others, 1973.

SCALE

0 25km

0 25 miles

AFTERSHOCKS OF 1933
LONG BEACH EARTHQUAKE

SONGS 2&3

Project No. 411001
Woodward-Clyde Consultants

Figure E-7

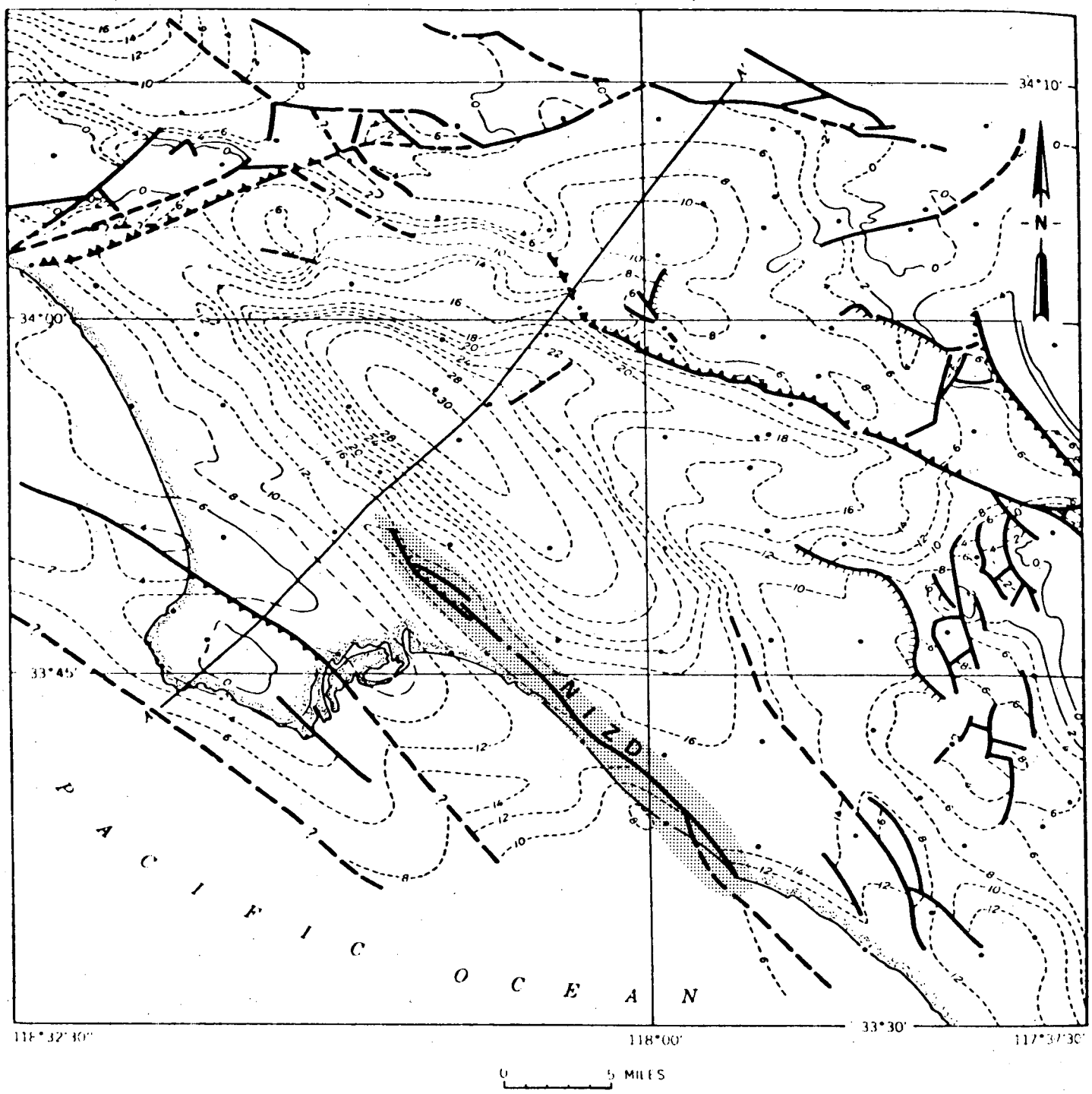

EXPLANATION

Gravity station

Structure contours (thousands of feet)
Drawn on top of basement rocks Long dashes where approximately located, short dashes where questionable. Contour interval 2000 feet, numbers are all zero or minus. Datum is mean sea level.

Approximate extent of 1933 rupture zone.

From: Yerkes and others, 1965

Fault
Queried where doubtful.

Normal fault
Hachures on downthrown side.

Reverse fault, approximately located
Saw-teeth on upthrown side, queried where doubtful.

STRUCTURE CONTOUR MAP ON TOP OF BASEMENT ROCKS IN THE LOS ANGELES BASIN
SONGS 2 & 3

Project No. 411001
Woodward-Clyde Consultants

Figure E-8

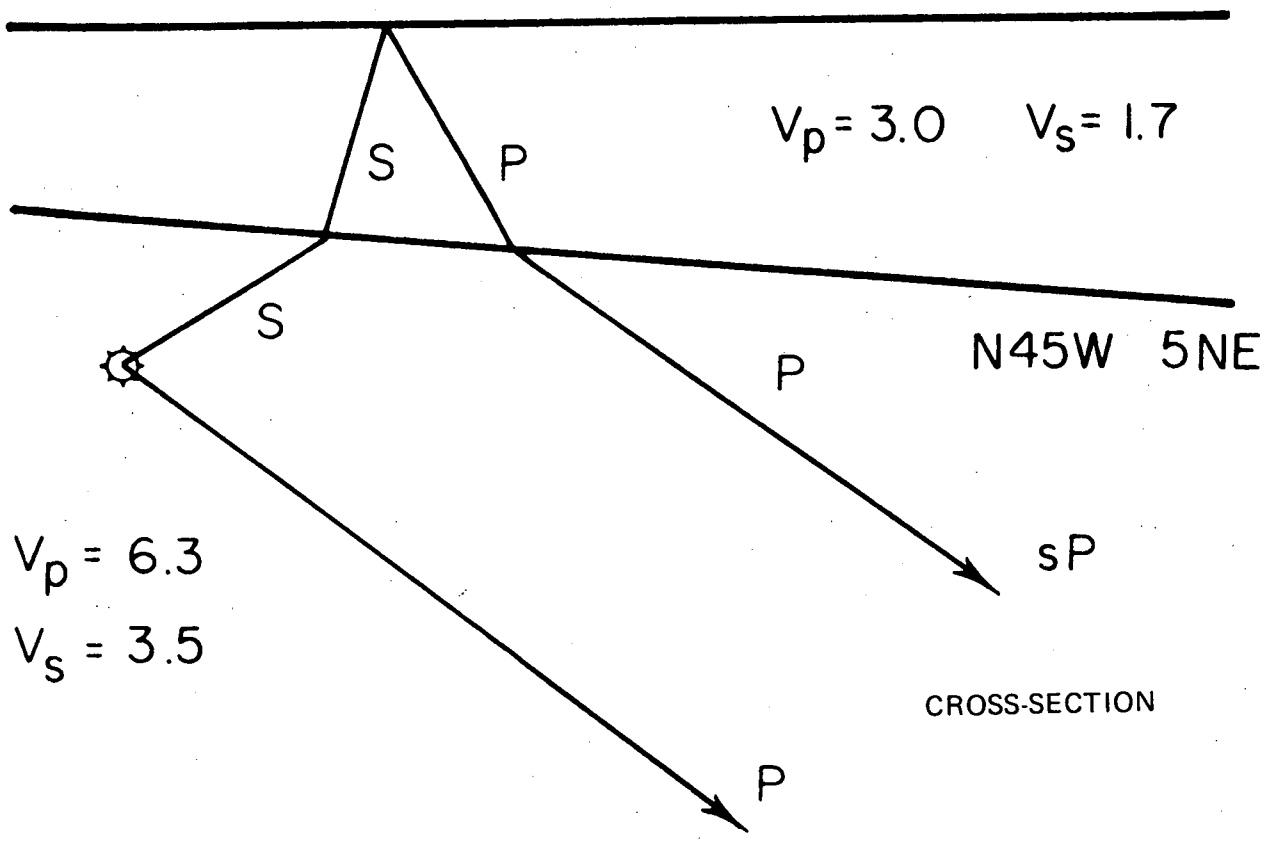

CROSS-SECTION

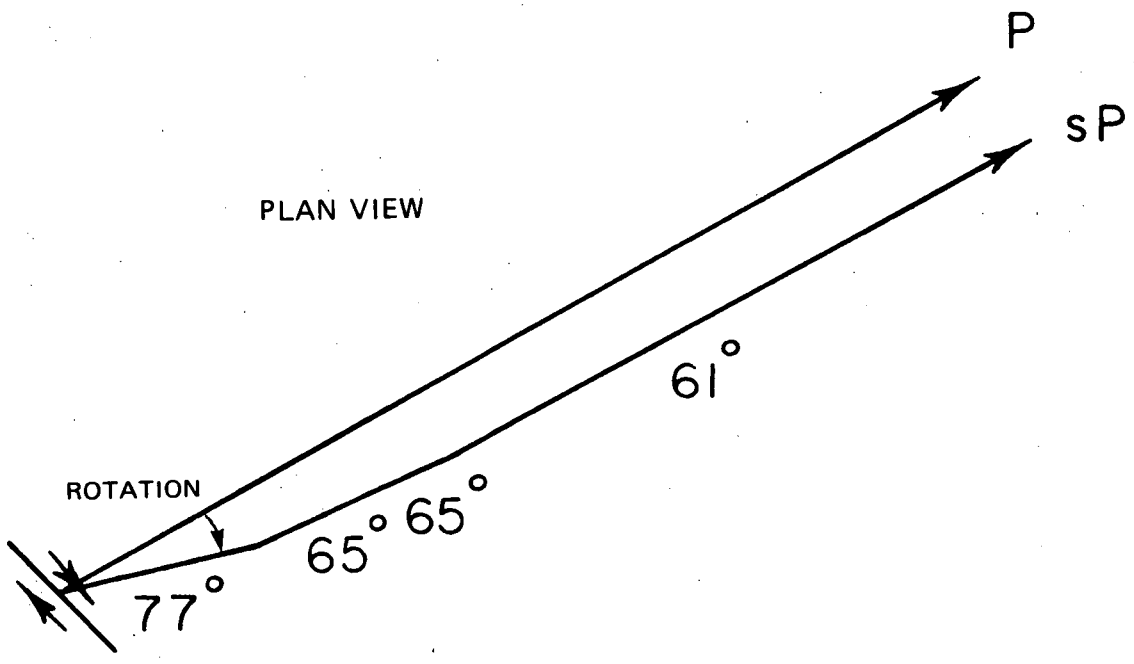

PLAN VIEW

ROTATION OF THE TAKE-OFF AZIMUTH DUE TO BASIN STRUCTURE SONGS 2 & 3	
Project No. 411001 **Woodward-Clyde Consultants**	Figure E-9

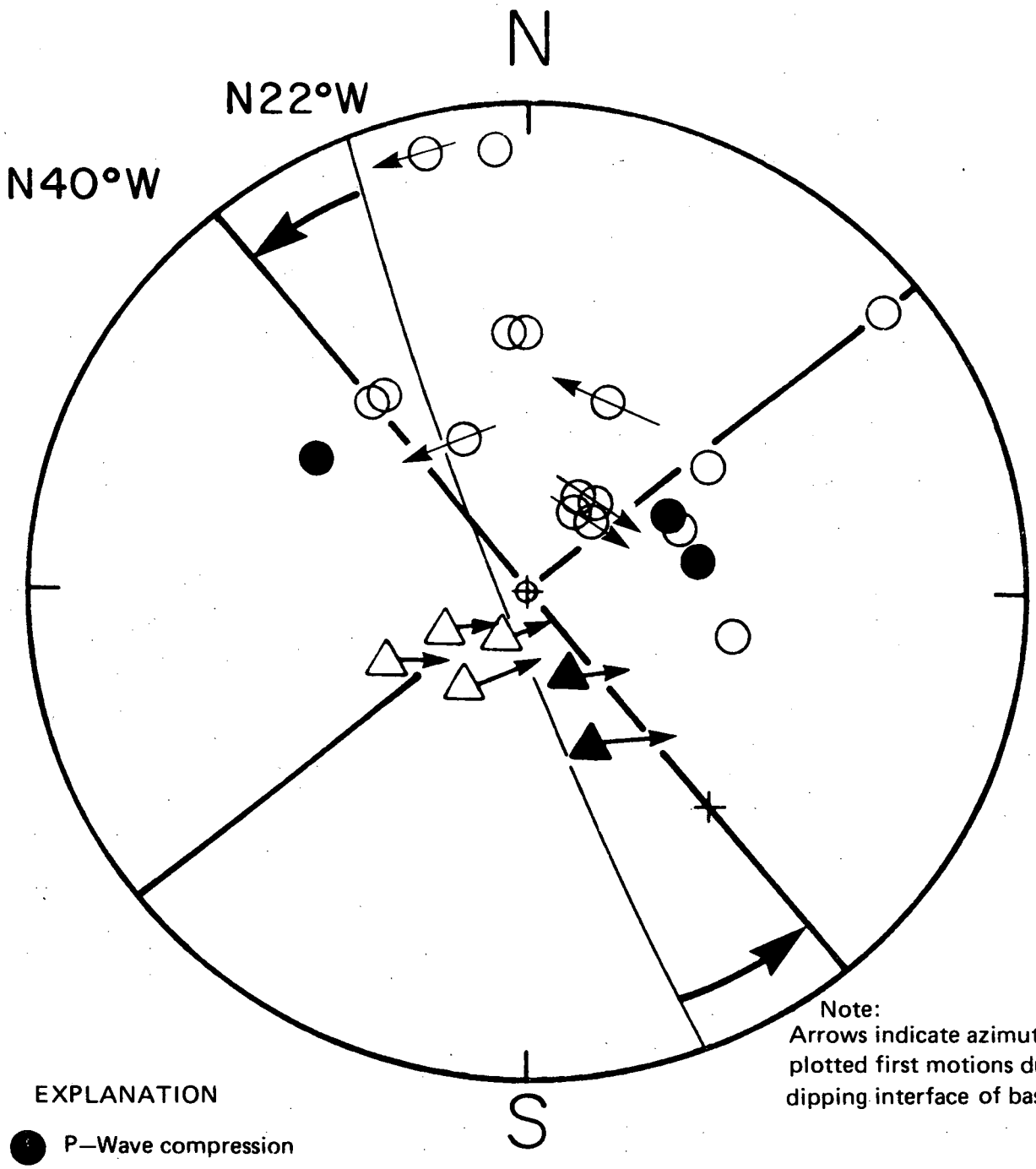

Note:
Arrows indicate azimuthal shifts of plotted first motions due to dipping interface of basin

EXPLANATION

- P—Wave compression
- P—Wave dilatation
- pP or sP compression
- pP or sP dilatation
- SH polarization

ROTATED FAULT PLANE SOLUTION
SONGS 2 & 3

Project No. 411001
Woodward-Clyde Consultants

Figure E-10

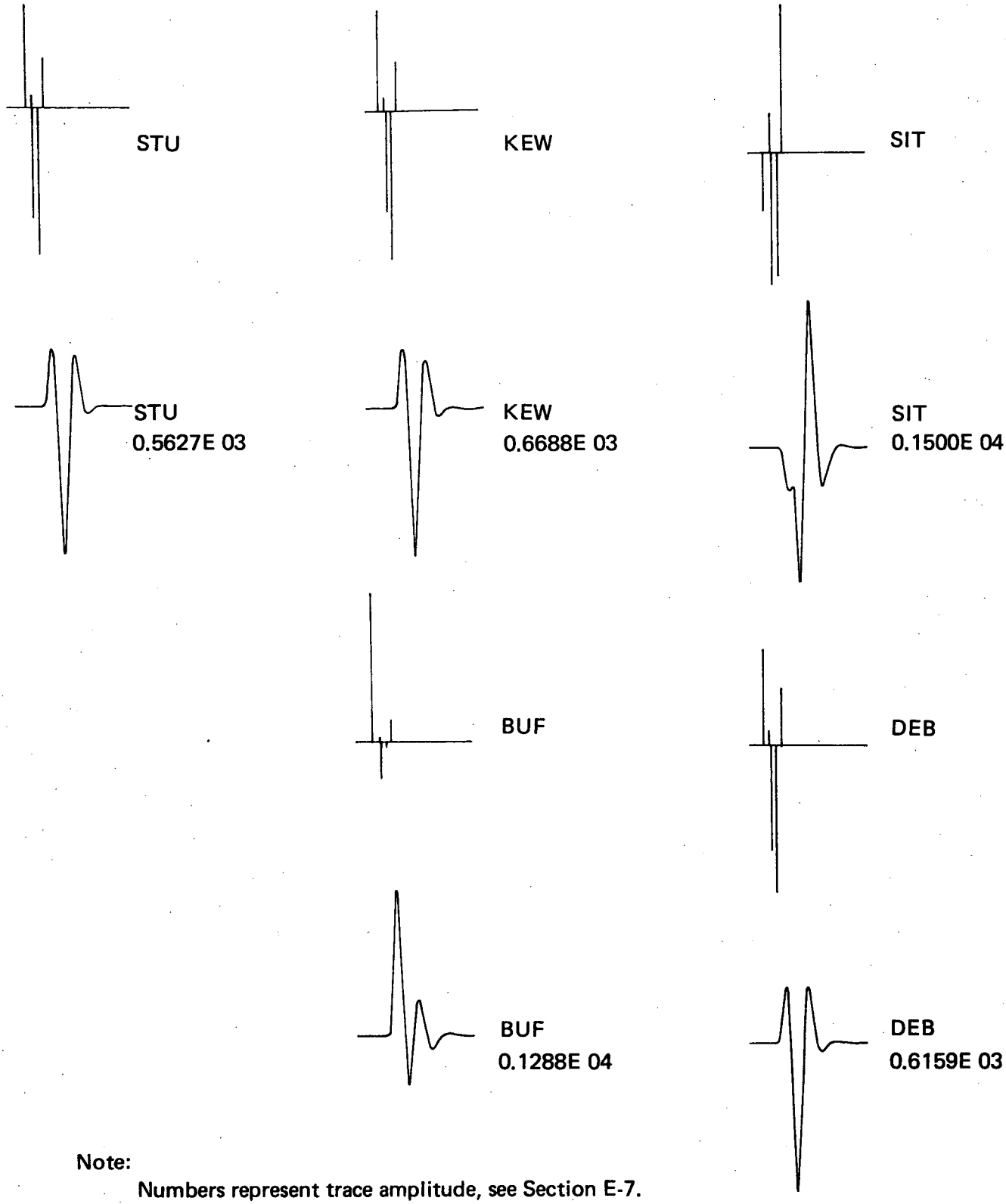

Note:

Numbers represent trace amplitude, see Section E-7.

Stations listed in Table E-1.

1 minute

SCALE

P–PHASE TIME FUNCTIONS AND SYNTHETIC SEISMOGRAMS FOR DIPPING STRUCTURE
SONGS 2 & 3

Project No. 41100I

Woodward-Clyde Consultants

Figure E-11

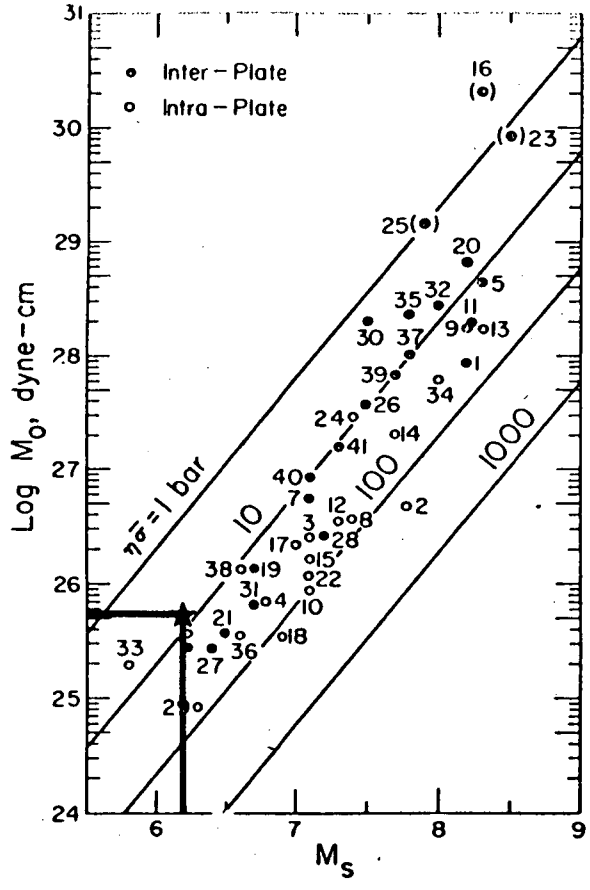

The straight lines are for constant apparent stress.
A rigidity of 3×10^{11} dyne/cm^2 is used.

After Kanamori and Anderson, 1975

RELATION BETWEEN M_s AND M_o	
SONGS 2 & 3	
Project No. 411001 **Woodward-Clyde Consultants**	Figure E-12

APPENDIX F
FOCAL MECHANISMS AND SEISMICITY

In this appendix, two aspects of the seismic environment of the hypothesized offshore zone of deformation (OZD) are discussed: stress axes determined from focal mechanisms (Section F-1), and level of background earthquake activity (Section F-2).

F-1 P-WAVE FAULT MECHANISM STUDIES FOR THE HYPOTHESIZED OFFSHORE ZONE OF DEFORMATION

F-1.1 Introduction

The mechanism of faulting of earthquakes along the Newport-Inglewood zone of deformation (NIZD), South Coast Offshore zone of deformation (SCOZD), and Rose Canyon fault zone (RCFZ) was investigated to evaluate the style of faulting along these fault zones and the consistency of tectonic deformation within different parts of the hypothesized OZD and with the regional stress field in southern California.

In several areas of California, focal mechanisms of small earthquakes bear a variable relationship to the style of faulting on major regional faults. For example, Bolt and others (1971) comprehensively studied focal mechanisms in northern California and identified a prominent pattern of strike-slip along the San Andreas fault. Pechmann (1979) and Lee and others (1979) noted that focal mechanisms in the Transverse Ranges of southern California exhibit a general pattern of north-south compression but contain both thrust and strike-slip mechanisms. The results of the present study are consistent with the pattern of earthquakes in southern California: (1) general north-south maximum compression axis; (2) local variations in fault plane orientation; and (3) pattern of focal mechanisms not necessarily reresentative of nor located on the large or through-going

structural features. The variation in least and intermediate stress axis orientation for the small events studied suggets substantial spatial (and perhaps also temporal) complexity of the fault zones and local variations of the stress fields within the areas studied. The variety of focal mechanisms suggests faults of different orientations. Although this does not rule out the possibility of a major through-going feature, it does not require that interpretation.

F-1.2 Data

The data available for this study were severely limited by the low level of seismic activity and the sparsity of seismographic station coverage, particularly prior to 1976 when the California Institute of Technology (CIT) array was supplemented by CIT and the U.S. Geological Survey (USGS). The hypothesized OZD region indicated in Figure F-1 was searched for candidate earthquakes for first motion studies. Areas lying within about 10 kilometers to the east of this zone were also searched. The selection criteria used to identify candidate events were that:

(1) The events be reasonably associated with or adjacent to the NIZD, SCOZD, or RCFZ.

(2) The size of earthquakes be large enough to have produced usable recordings at an adequate number of stations.

(3) The number and azimuthal distribution of recording stations in area of epicenter be sufficient to provide focal mechanism constraint.

Sixty-four earthquakes during the period 1932 through September 1978 were selected for study from the Caltech data catalog. Additional focal mechanism solutions were obtained based on data from the seismic network operated by USC along the NIZD (Teng and Manov, 1976).

Routinely listed first motion data from the CIT Seismological Laboratory were gathered for all 64 events. Of these, 20 were found to have enough first motion data for further analysis.

All 20 events listed in Table F-1 were analyzed for focal mechanism solutions using "FOCPLOT" (Whitcomb, 1973). The first-motion data and best-fit fault planes are reproduced in Figures F-2a through F-2s. Projections are on the lower hemisphere using the following crustal velocity model developed by Hadley (1978):

Velocity (km/sec)	Thickness (km)
5.5	3.0
5.7	1.0
5.9	1.5
6.25	16.5
6.7	8.0
7.9	--

F-1.3 Summary of Results

Fault plane solutions are shown in Figure F-3 only for the 15 better constrained mechanisms. The direction of maximum compressive stress exhibits a general north-south orientation, consistent with the regional stress field produced by interaction of the North American and Pacific plates. The offshore data are quite limited, however.

The variety of focal mechanisms suggests faults of different orientations. Although this does not rule out the possibility of a major through-going feature, it does not require that interpretation. The mechanism of the 1933 Long Beach earthquake, found to be pure strike-slip in Appendix E, is represented by very few events in the vicinity of the NIZD.

F-2 COMPARATIVE SEISMIC ACTIVITY FOR FAULT AREAS IN SOUTHERN CALIFORNIA

In general, comparisons of the levels of seismic activity between regions, even those lying within the same tectonic environment, must be evaluated with care. Such comparisons are easily distorted by rapid changes in activity associated with aftershock sequences or earthquake swarms. In the qualitative discussion of this appendix the seismic activity of three zones is examined: the hypothesized OZD, the Whittier-Elsinore fault zone (WEFZ), and the San Jacinto fault zone (SJFZ). Earthquake data are presented in Figures F-1, F-4 and F-5 for these zones in order to illustrate similarities and differences in seismicity. The data source used is the record of instrumentally detected and located earthquakes compiled since 1932 by the California Institute of Technology (Hileman and others, 1973, with later data from Caltech files).

Figure F-1 shows the earthquakes of magnitude 4 and greater for the period 1 January 1932 through 30 September 1976. Boundaries are shown for the three zones of interest, and are sufficiently broad to include earthquakes that may be somewhat mislocated with respect to the surface fault traces on the local deformation zones. The zone boundaries were defined with respect to the zones indicated on the map of Jennings (1975) and based on the discussions of Appendix A. The zones shown in Figure F-1 are dominated by the occurrence of two large earthquake sequences: the 1933 Long Beach earthquake and aftershocks in the northern portion of the hypothesized OZD, and the 1968 Borrego earthquake sequence in the southern portion of the SJFZ. The SJFZ is rather well defined by magnitude 4 and greater earthquakes over its entire indicated length. The hypothesized OZD and WEFZ are incompletely defined as linear zones by the earthquakes shown in Figure F-1.

The magnitude levels of both detectability and locatability of the earthquakes during the study period have decreased as a function of the increasing density with time of seismograph station coverage over the area shown in Figure F-1. Based on the station distribution, it appears that earthquakes as small as magnitude near 3.0 have been locatable over the entire study area since 1932 (Hileman and others, 1973). While coverage down to this level probably has not been complete during periods of very high seismic activity, such as during the 1933 earthquake sequence, for the present qualitative purposes this approximation is adequate.

In Figure F-4, epicenters of earthquakes with magnitude between 3 and 4 are added to the data shown in Figure F-1. The inclusion of data on all events of magnitude 3 and larger provides a different perspective on the nature of seismic activity in the three zones. In all cases, regions which appear aseismic in Figure F-1 are seen to have had scattered seismic activity in the magnitude range of 3 to 4. For the SCOZD, the data in Figure F-4 do not reveal a linear pattern of activity that would support the interpretation of a through-going fault zone. The distributed activity that is evidenced there indicates that there are scattered sources of small earthquakes within or adjacent to the SCOZD.

In Figure F-5, the data from Figure F-4 are replotted to include only the time period 1947-1976. This effectively removes the 1933 aftershock activity from the NIZD and reveals the pattern of background seismic activity for the NIZD in comparison with the remainder of the hypothesized OZD. In this later time period, the NIZD continues to exhibit a linear pattern of activity along its trend, while the more southerly portion of the hypothesized OZD does not.

TABLE F-1

EARTHQUAKES WITH FOCAL MECHANISMS PLOTTED IN FIGURE F-1

Event No.*	Date	Quality of Mechanism
1	27 October 1969	poorly constrained
2	28 December 1973	fair
3**	3 January 1975	fair
4	27 January 1975	poorly constrained
5	7 March 1976	poorly constrained
6	11 July 1976	fair
7	16 July 1976	poorly constrained
8	19 July 1976	fair
9	25 March 1977	fair
10	7 June 1977	fair
11	29 June 1977	poorly constrained
12	16 October 1977	poorly constrained
13	8 February 1978	fair
14	25 October 1978	poorly constrained
15	29 October 1978	fair

EARTHQUAKES NOT PLOTTED

	14 December 1974	not constrained
	7 May 1976	not constrained
	1 February 1977	not constrained
	31 March 1977	not constrained
	20 January 1978	not constrained

* Focal mechanisms and first motions are presented in Figures F-2a through F-2s

** From Southern California Edison, Geotechnical Studies, Southern Orange County, California, February 1976.

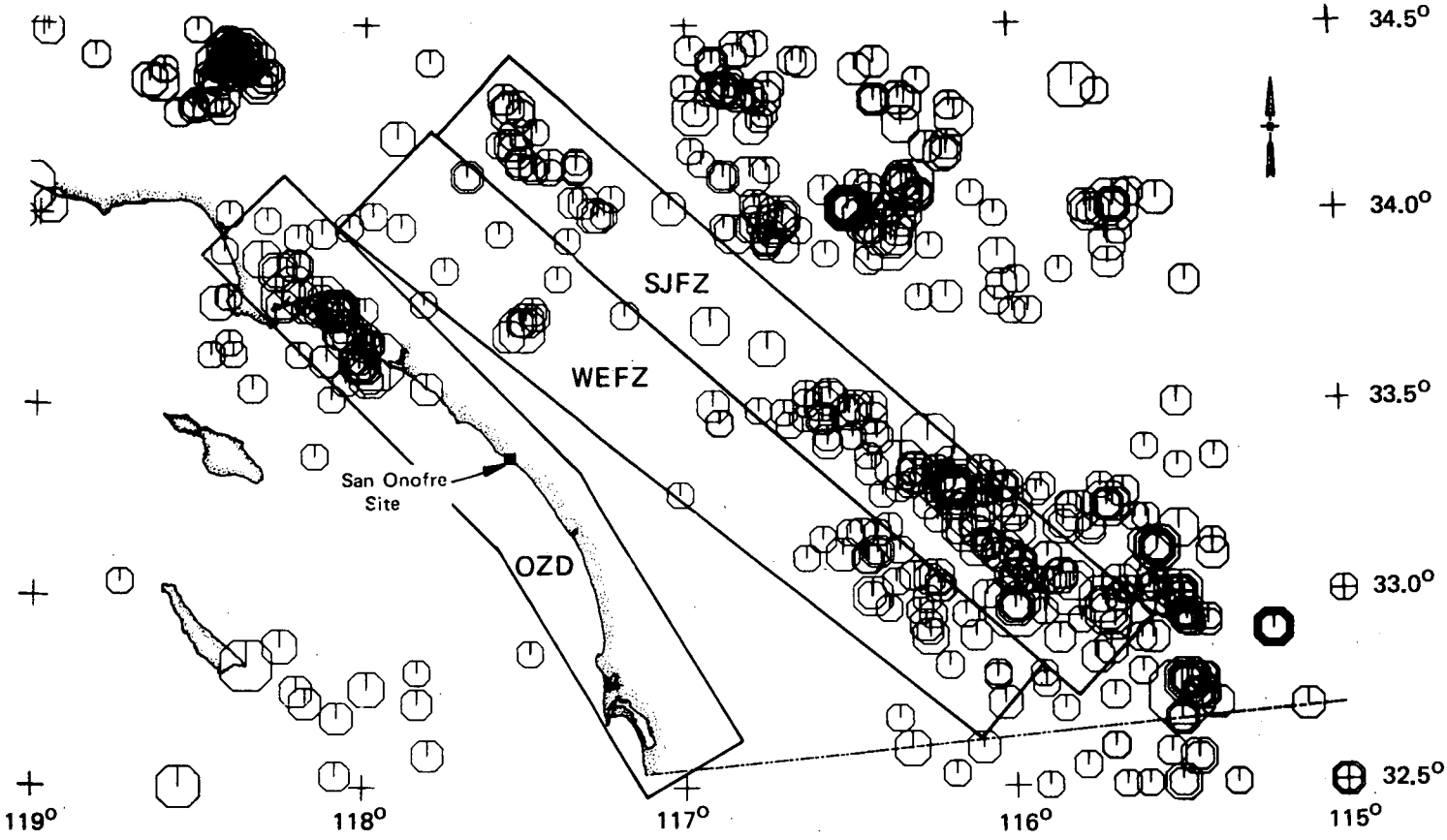

EXPLANATION

Reported Magnitude

7.0

6.0

5.0

4.0

3.0

0 50 100 miles

0 50 100 km

Data Source: Hileman and others, 1973, and California Institute of Technology

OZD – Offshore Zone of Deformation

WEFZ – Whittier – Elsinore fault zone

SJFZ – San Jacinto fault zone

SEISMICITY – 1932 TO 1976
MAGNITUDE ≥4
SONGS 2 & 3

Project No. 41100I
Woodward-Clyde Consultants

Figure F-1

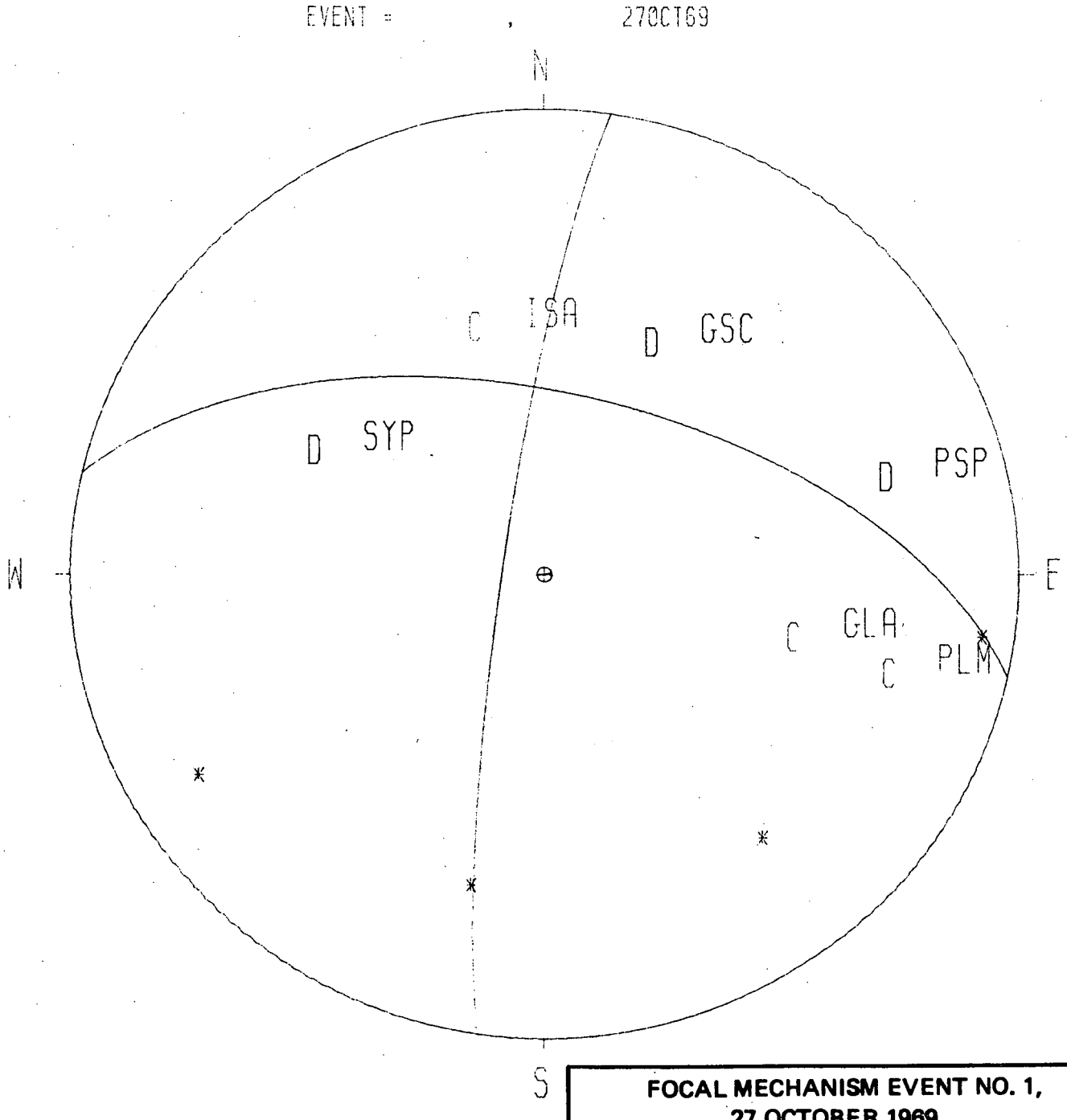

FOCAL MECHANISM EVENT NO. 1,
27 OCTOBER 1969

SONGS 2 & 3

Project No. 411001
Woodward-Clyde Consultants

Figure F-2a

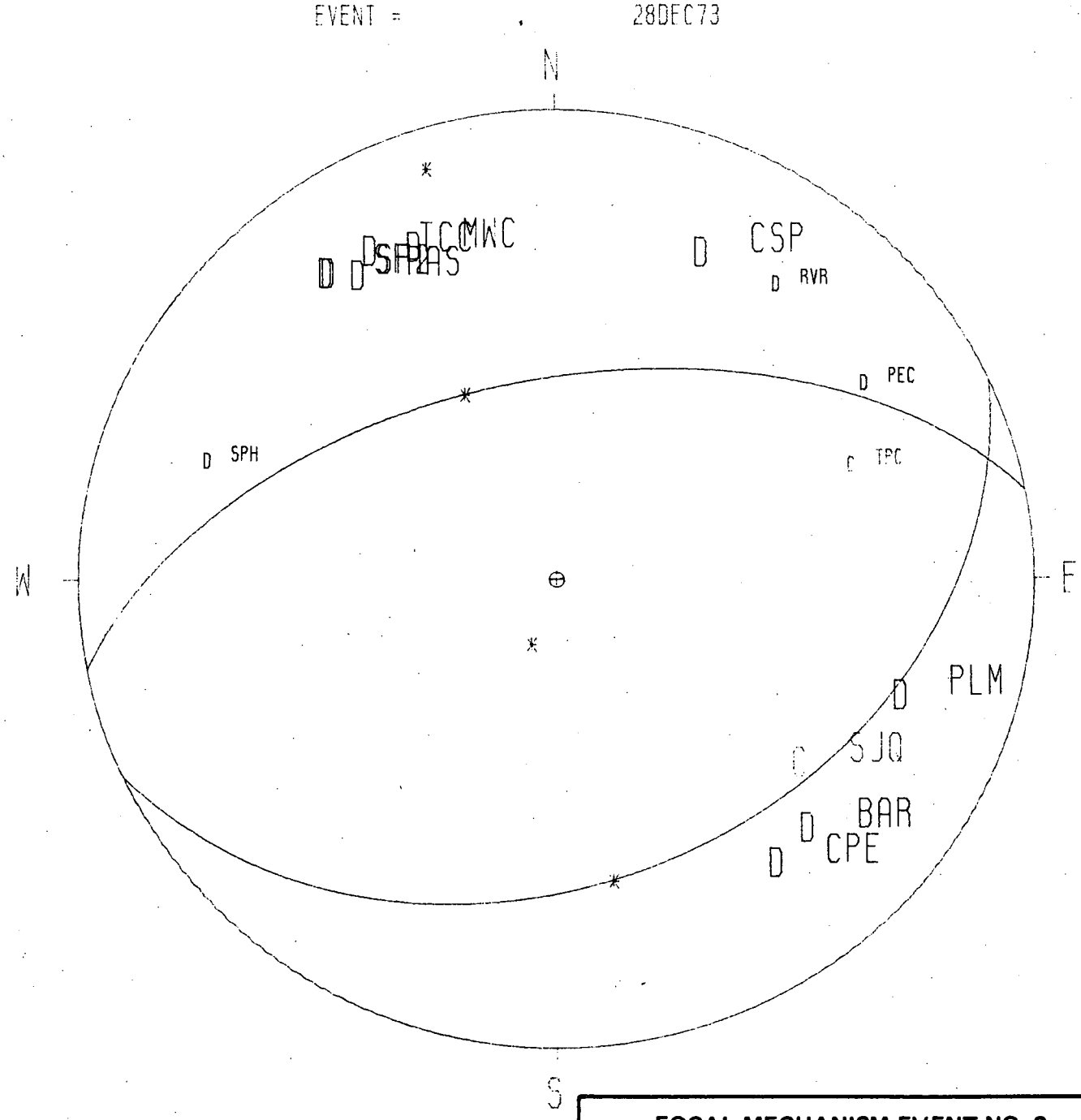

FOCAL MECHANISM EVENT NO. 2,
28 DECEMBER 1973
SONGS 2 & 3

Project No. 411001
Woodward-Clyde Consultants

Figure F-2b

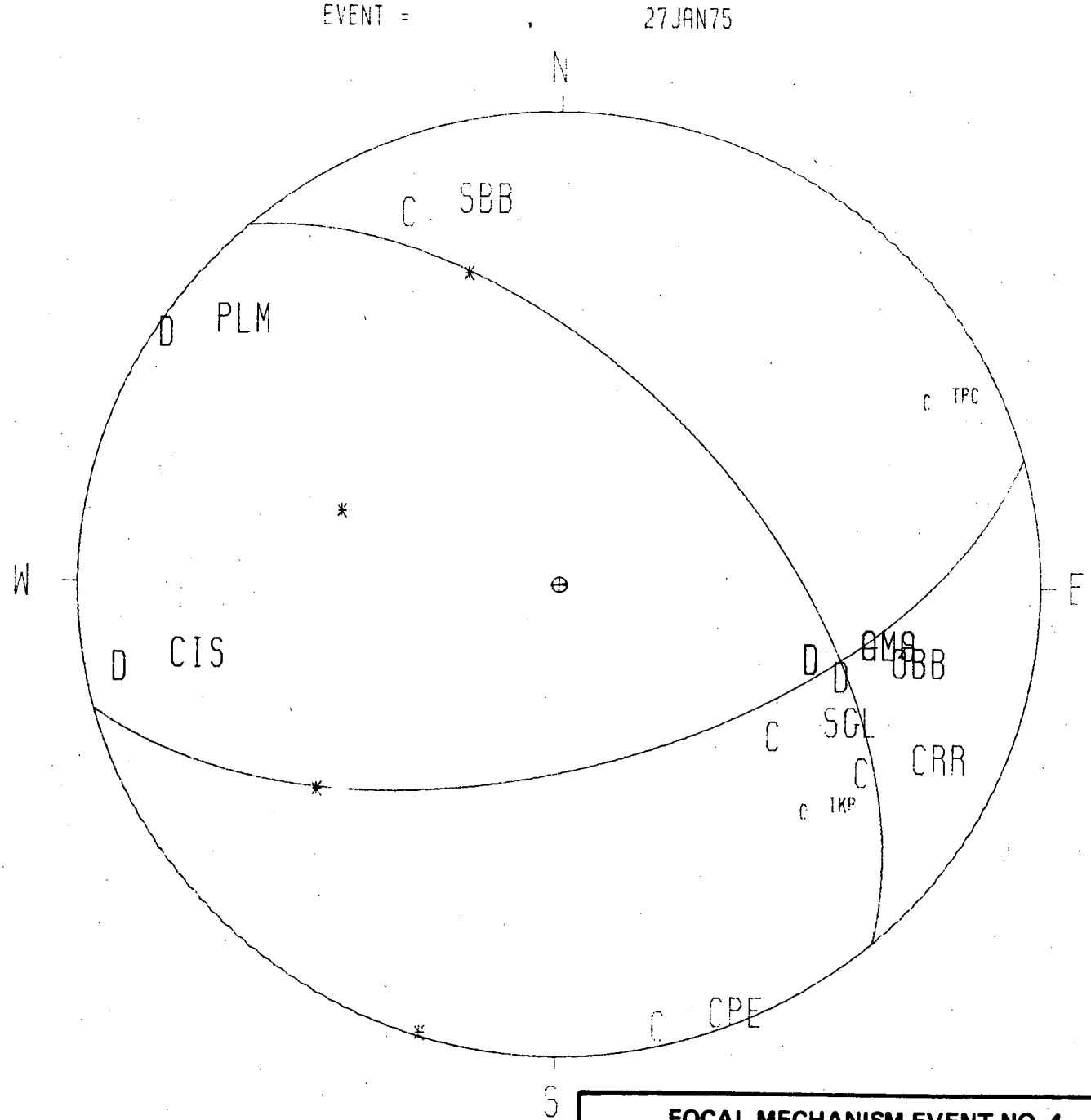

FOCAL MECHANISM EVENT NO. 4,
27 JANUARY 1975
SONGS 2 & 3

Project No. 411001 **Woodward-Clyde Consultants**	Figure F-2c

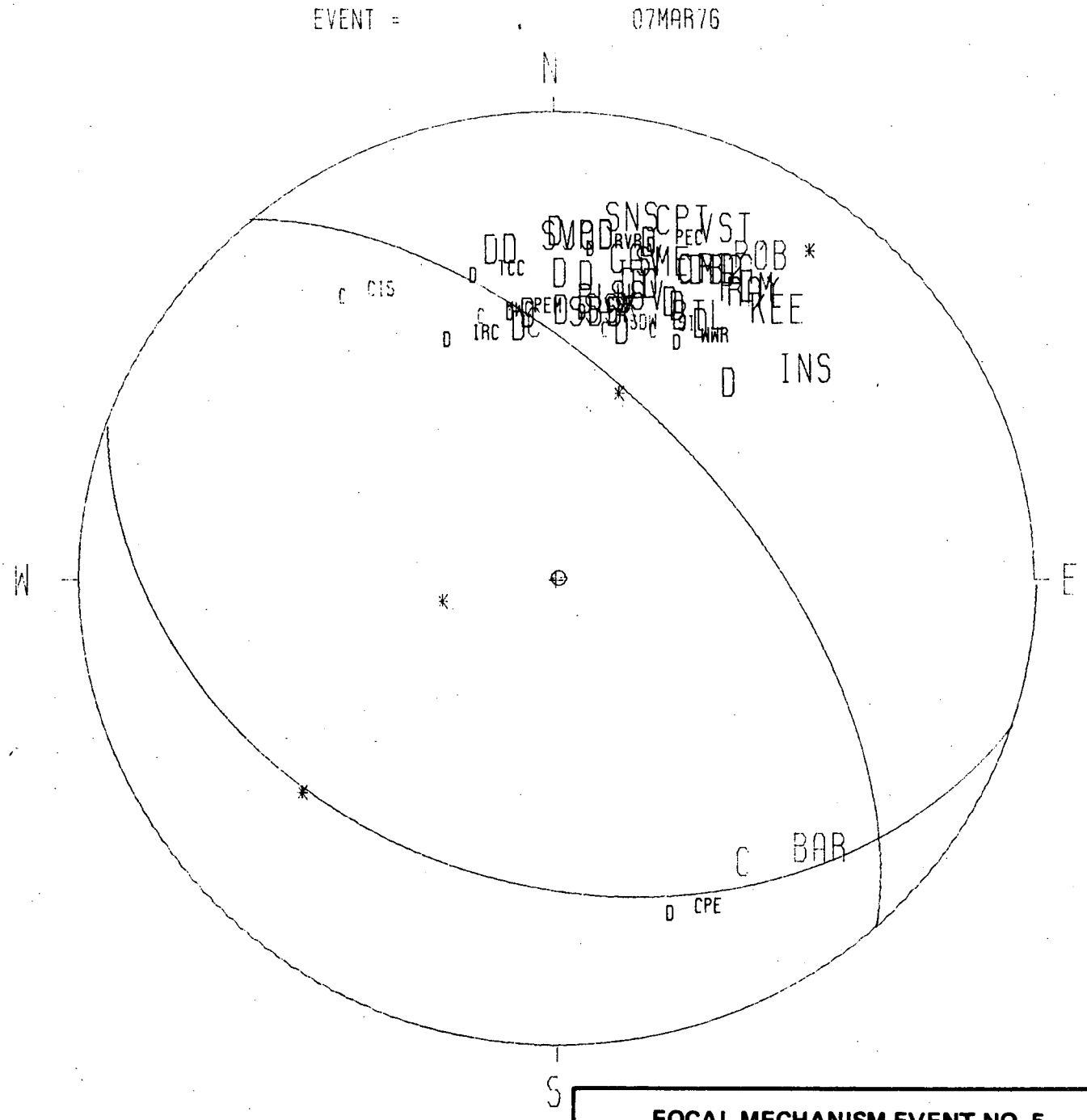

FOCAL MECHANISM EVENT NO. 5,
7 MARCH 1976
SONGS 2 & 3

Project No. 411001
Woodward-Clyde Consultants

Figure F-2d

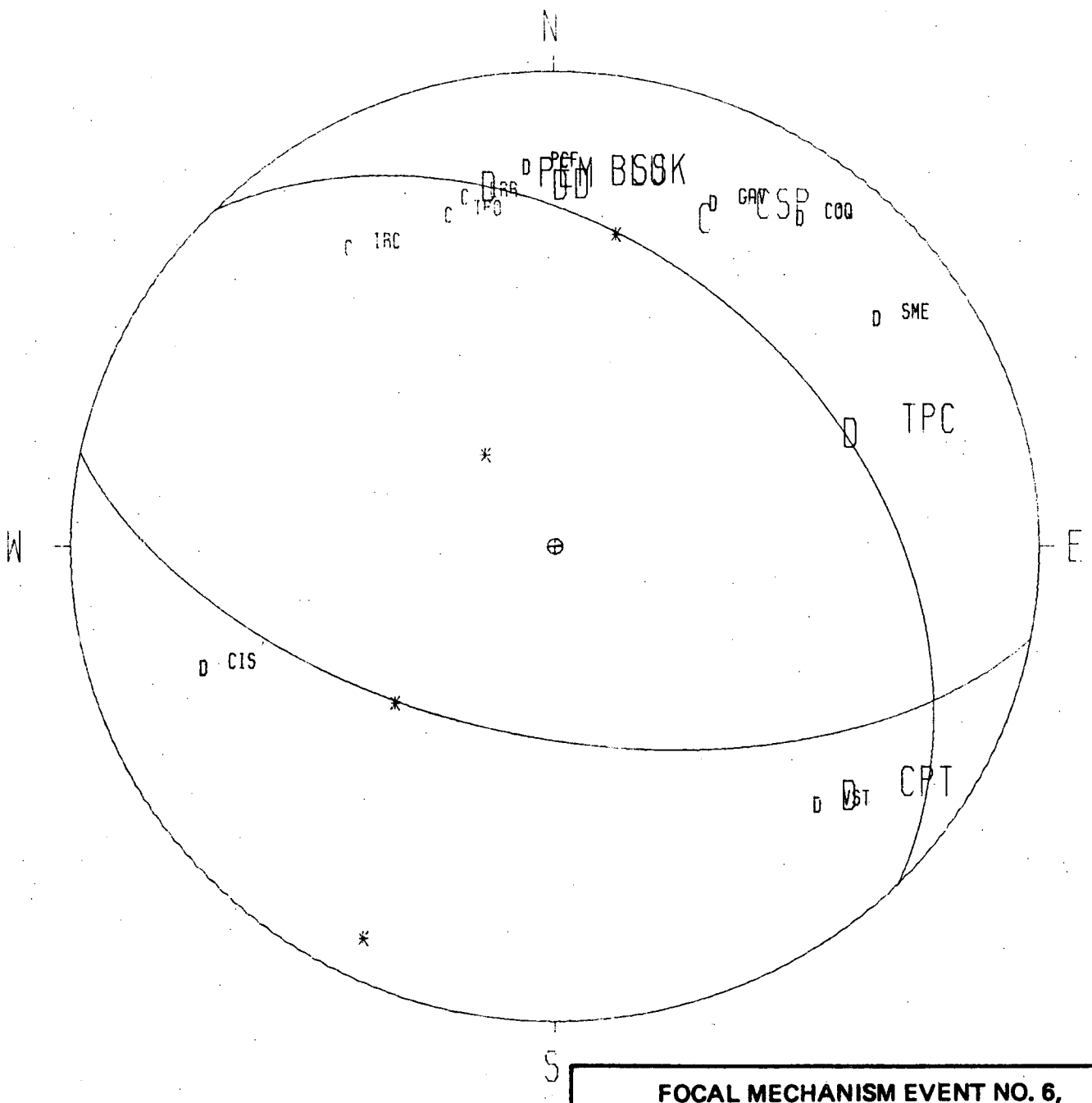

FOCAL MECHANISM EVENT NO. 6,
11 JULY 1976
SONGS 2 & 3

Project No. 411001
Woodward-Clyde Consultants

Figure F-2e

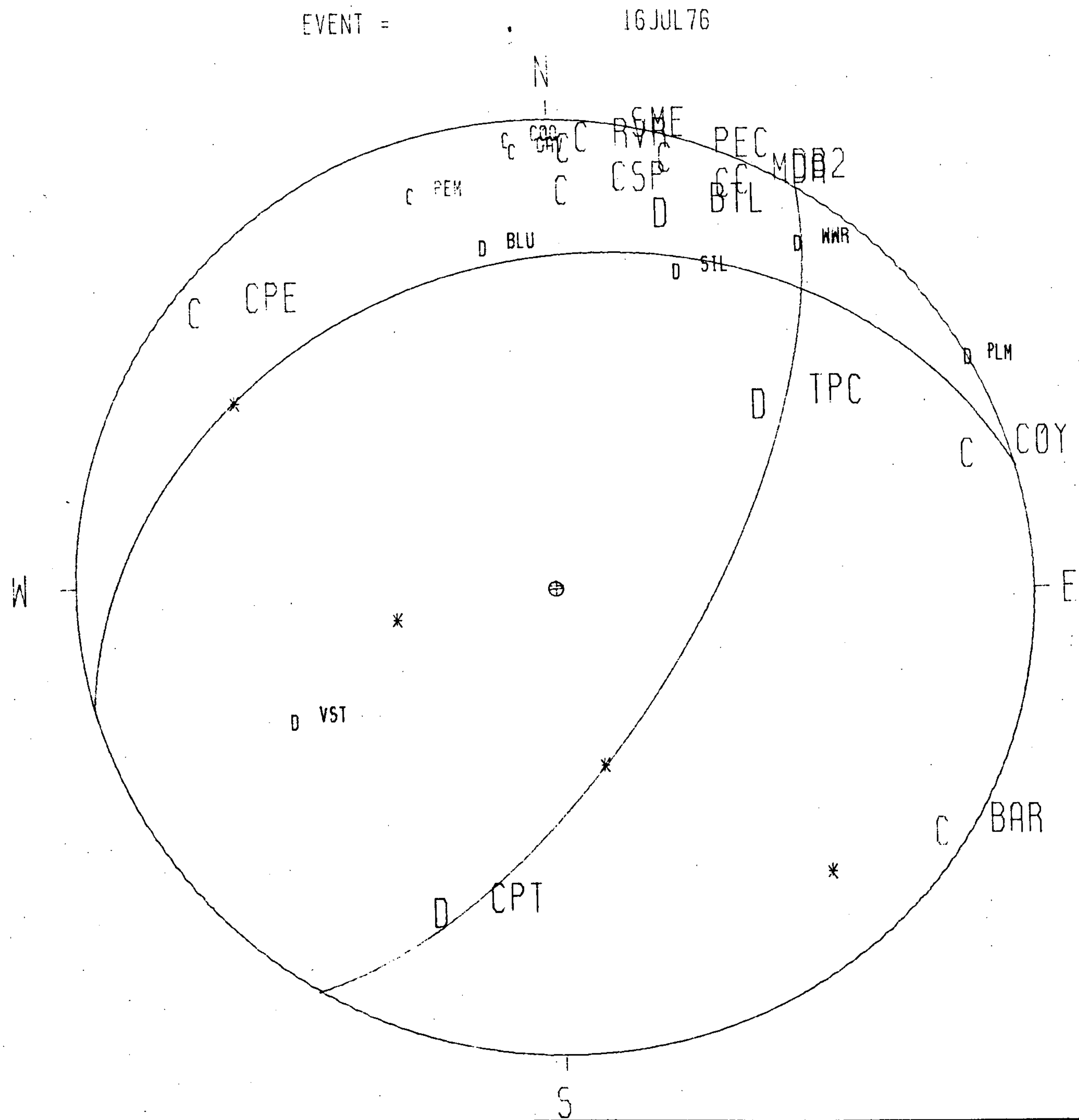

FOCAL MECHANISM EVENT NO. 7,
16 JULY 1976

SONGS 2 & 3

Project No. 41100I **Woodward-Clyde Consultants**	**Figure F-2f**

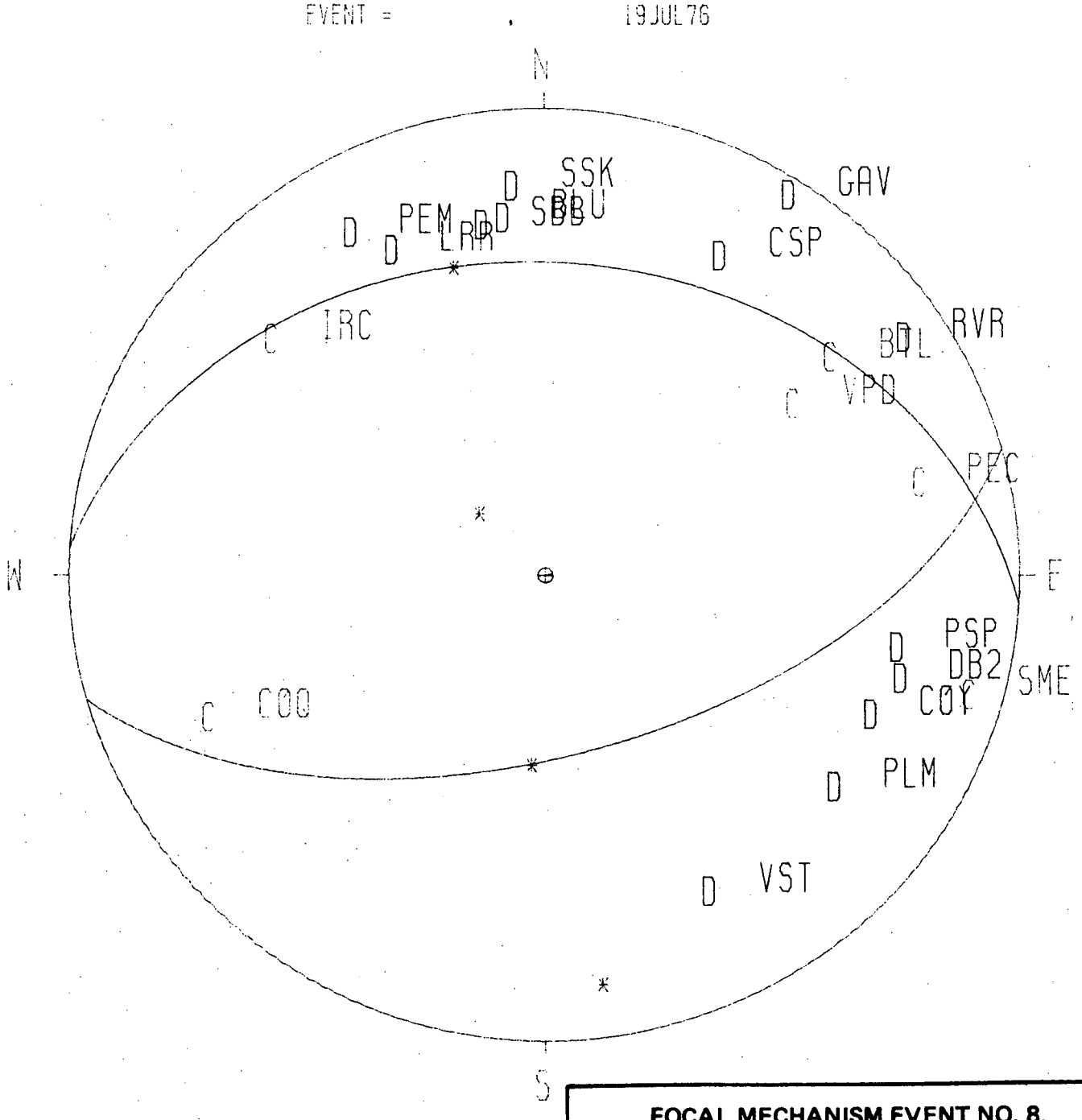

FOCAL MECHANISM EVENT NO. 8,
19 JULY 1976
SONGS 2 & 3

Project No. 411001
Woodward-Clyde Consultants

Figure F-2g

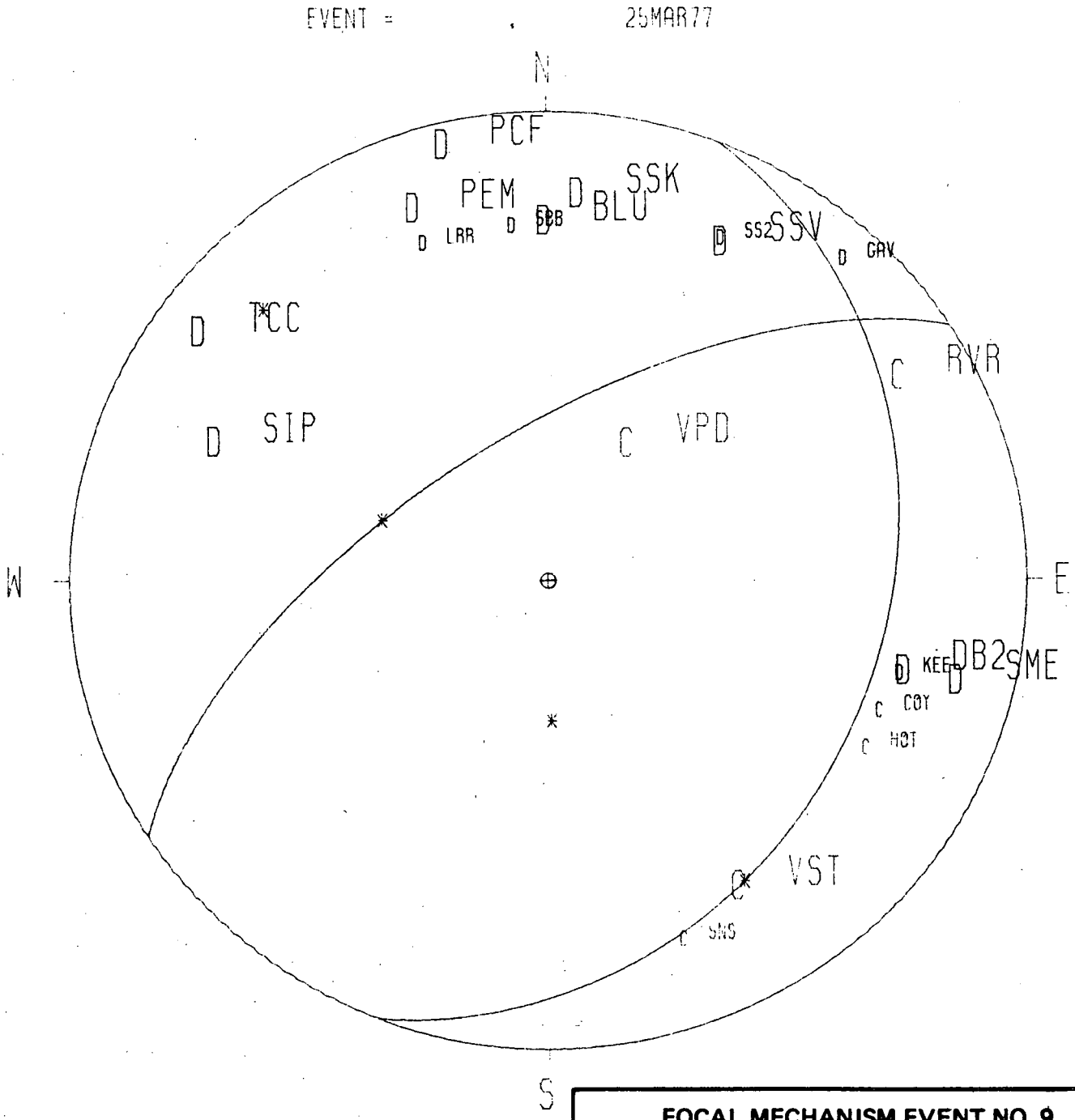

FOCAL MECHANISM EVENT NO. 9,
25 MARCH 1977
SONGS 2 & 3

Project No. 411001 **Woodward-Clyde Consultants**	Figure F-2h

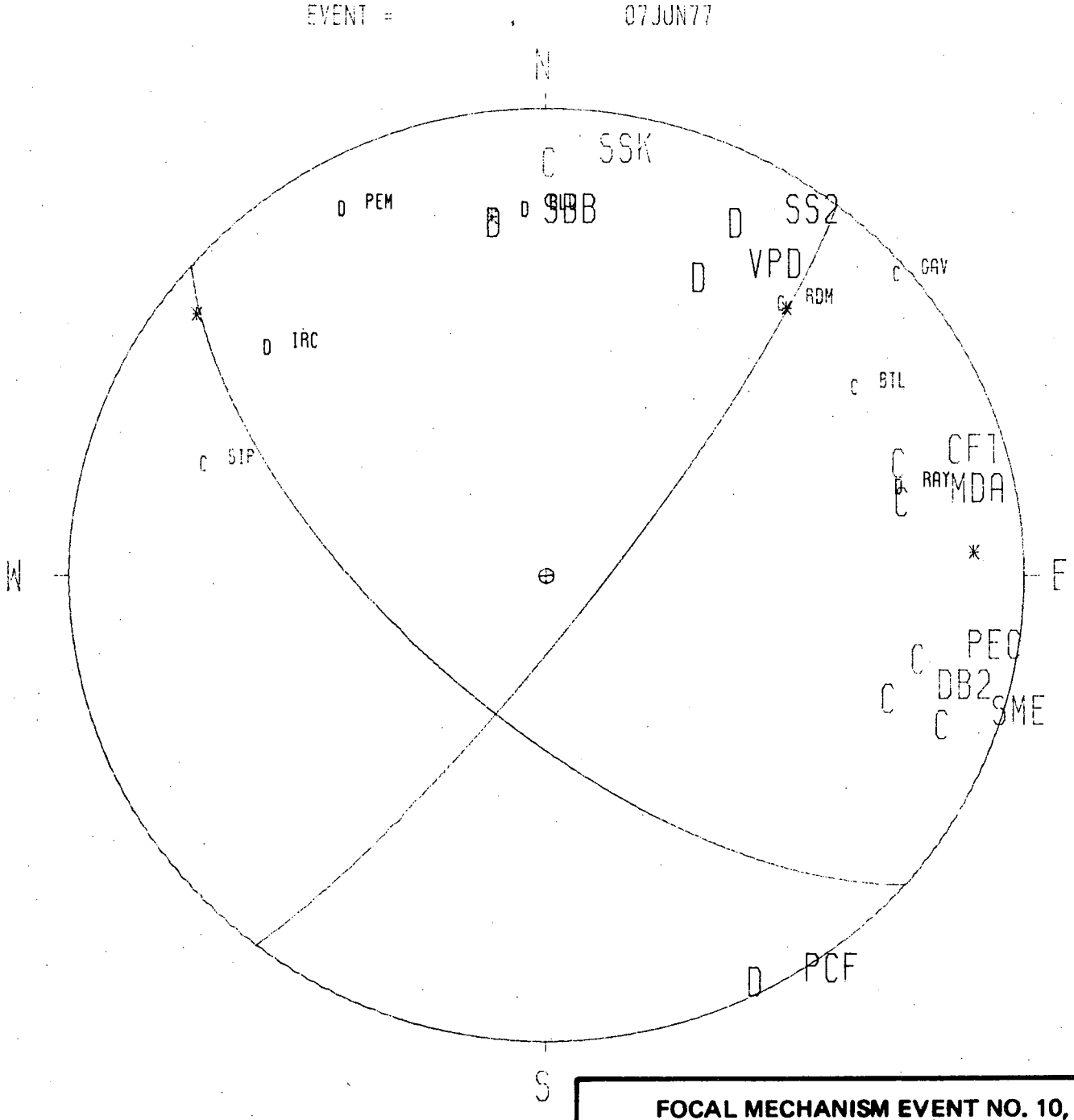

FOCAL MECHANISM EVENT NO. 10,
7 JUNE 1977
SONGS 2 & 3

Project No. 411001 **Woodward-Clyde Consultants**	Figure F-21

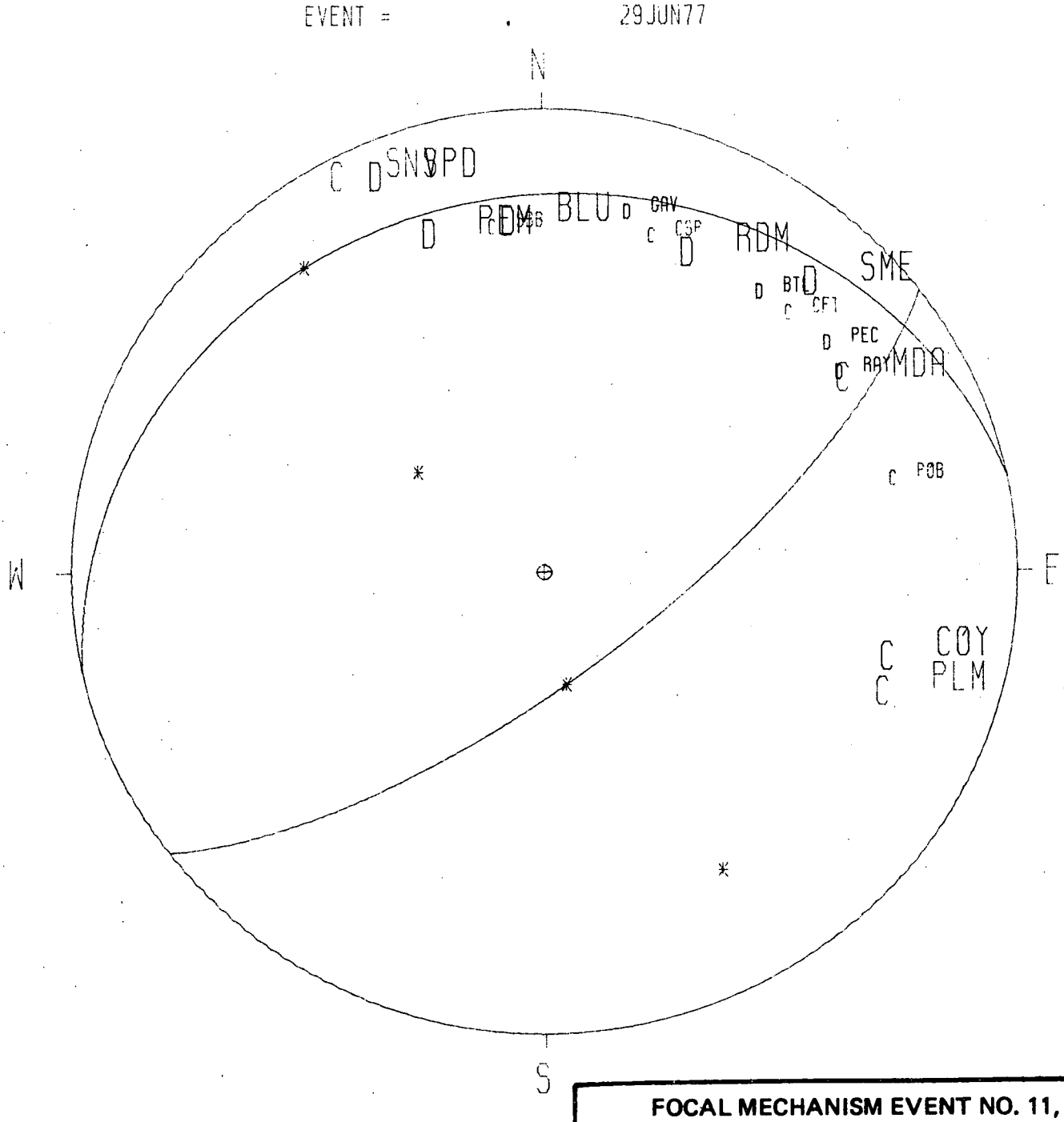

FOCAL MECHANISM EVENT NO. 11,
29 JUNE 1977
SONGS 2 & 3

Project No. 411001
Woodward-Clyde Consultants

Figure F-2j

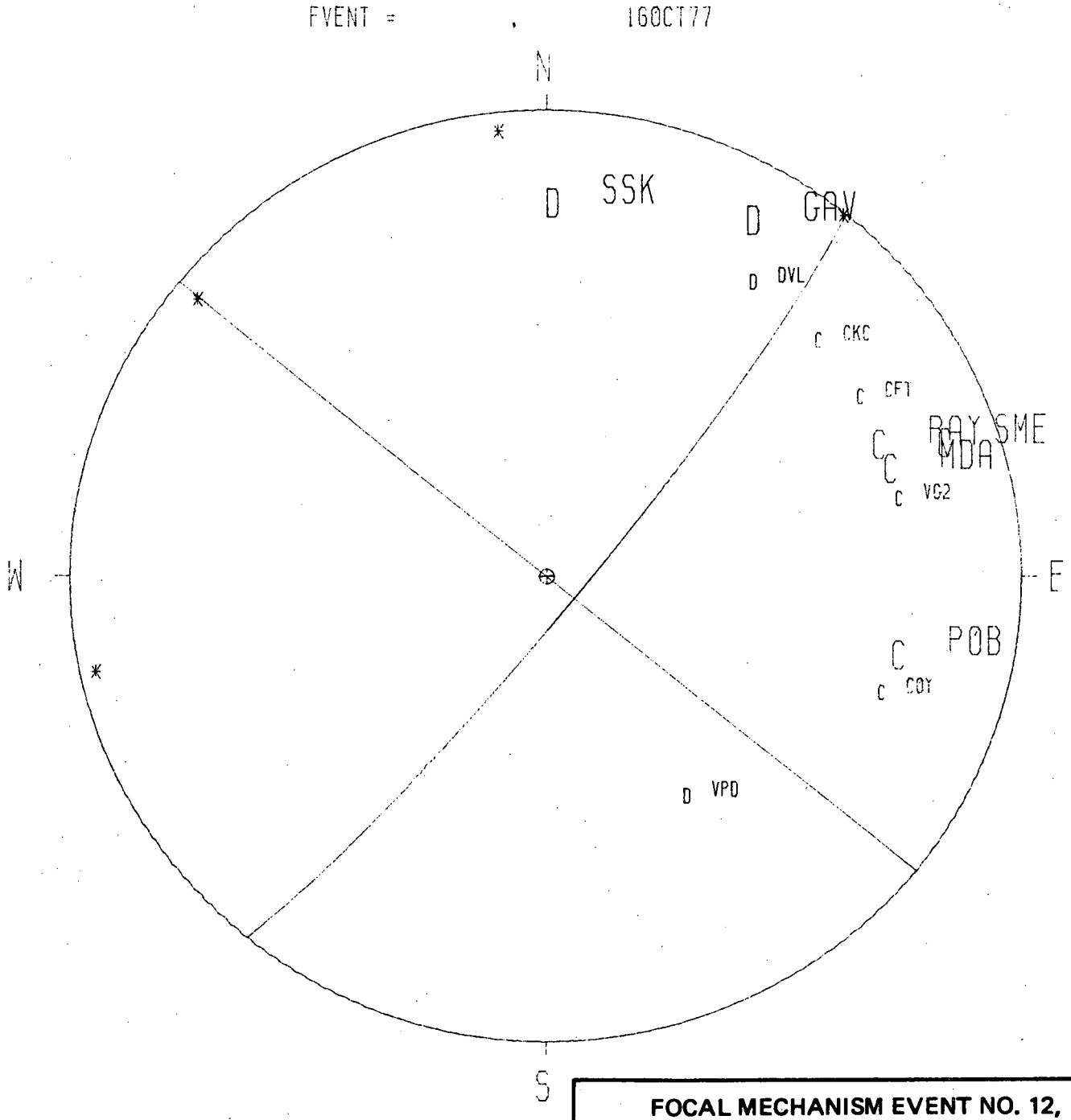

FOCAL MECHANISM EVENT NO. 12,
16 OCTOBER 1977
SONGS 2 & 3

Project No. 411001
Woodward-Clyde Consultants

Figure F-2k

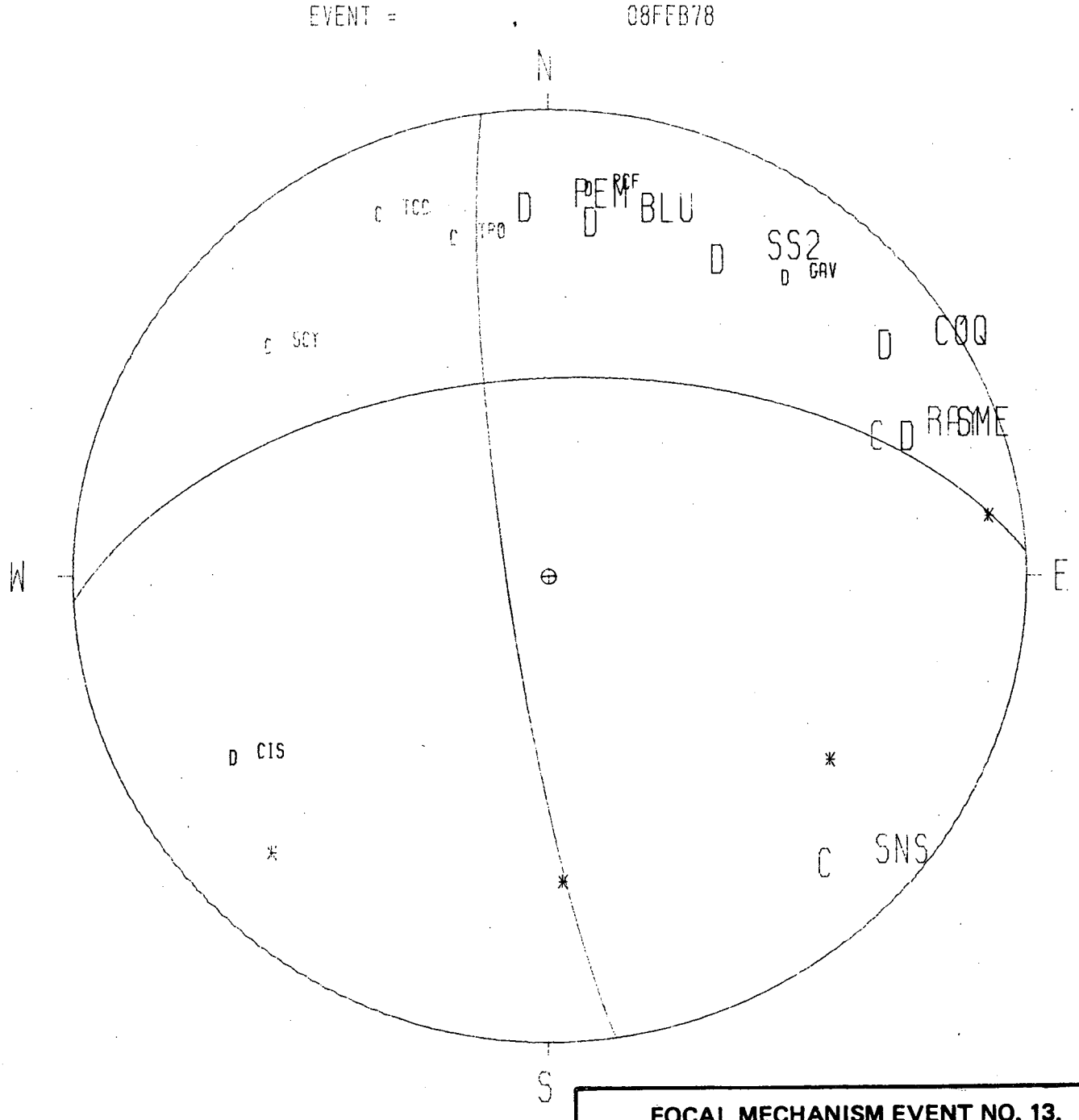

FOCAL MECHANISM EVENT NO. 13,
8 FEBRUARY 1978
SONGS 2 & 3

Project No. 411001
Woodward-Clyde Consultants

Figure F-21

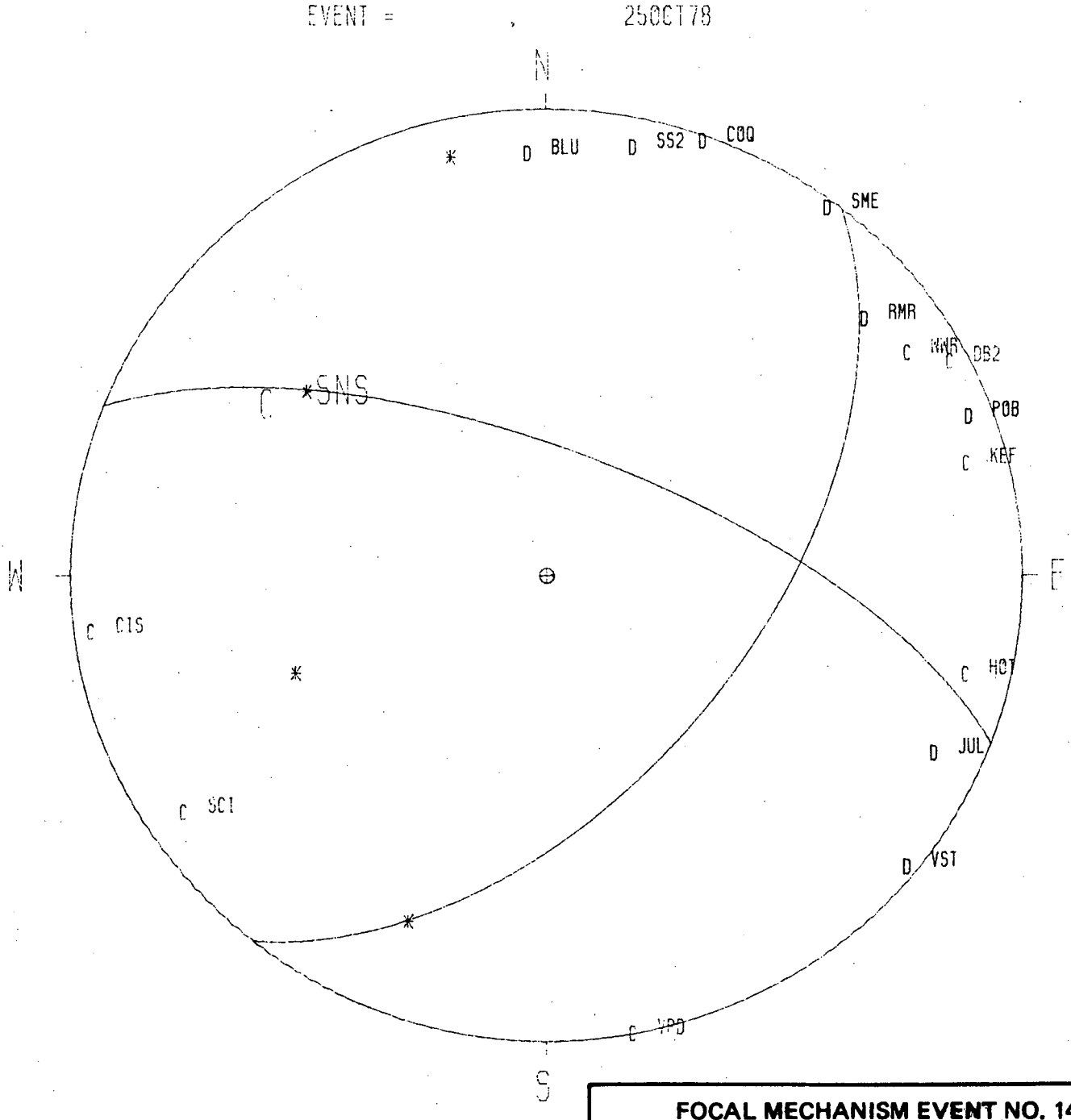

FOCAL MECHANISM EVENT NO. 14,
25 OCTOBER 1978
SONGS 2 & 3

Project No. 411001
Woodward-Clyde Consultants

Figure F-2m

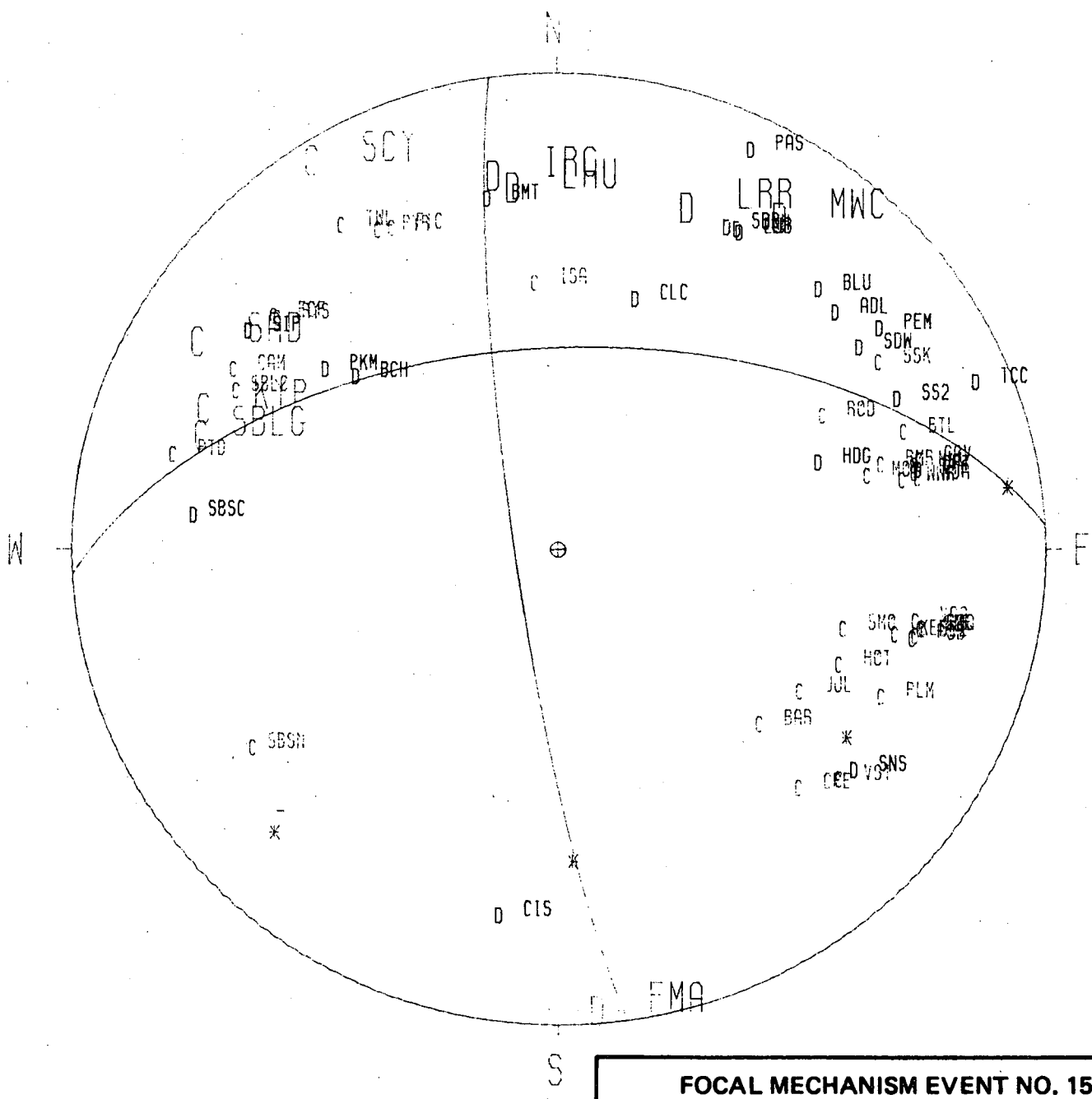

FOCAL MECHANISM EVENT NO. 15,
29 OCTOBER 1978
SONGS 2 & 3

Project No. 411001
Woodward-Clyde Consultants

Figure F-2n

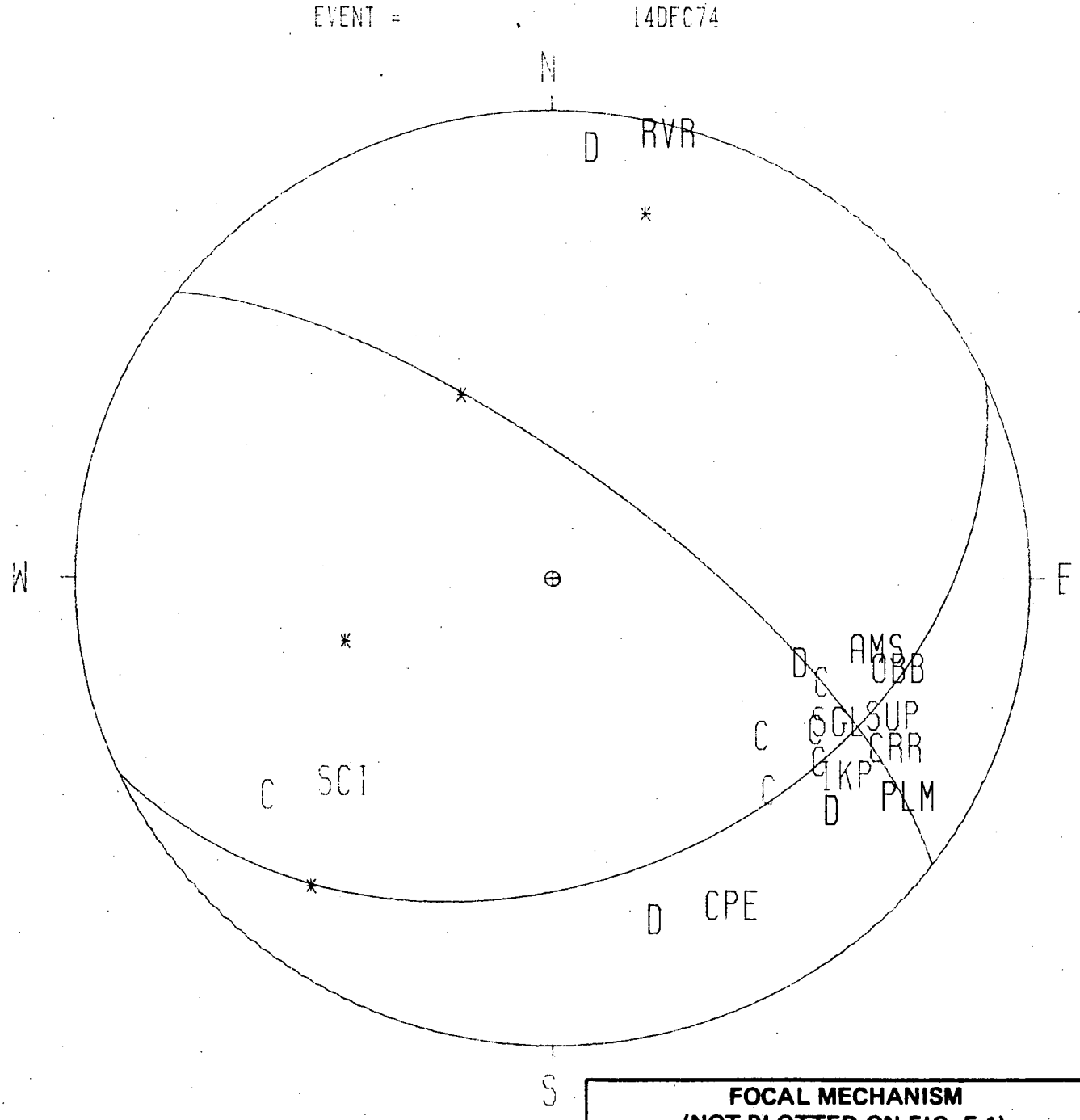

FOCAL MECHANISM
(NOT PLOTTED ON FIG. F-1),
14 DECEMBER 1974
SONGS 2 & 3

Project No. 411001
Woodward-Clyde Consultants

Figure F-2o

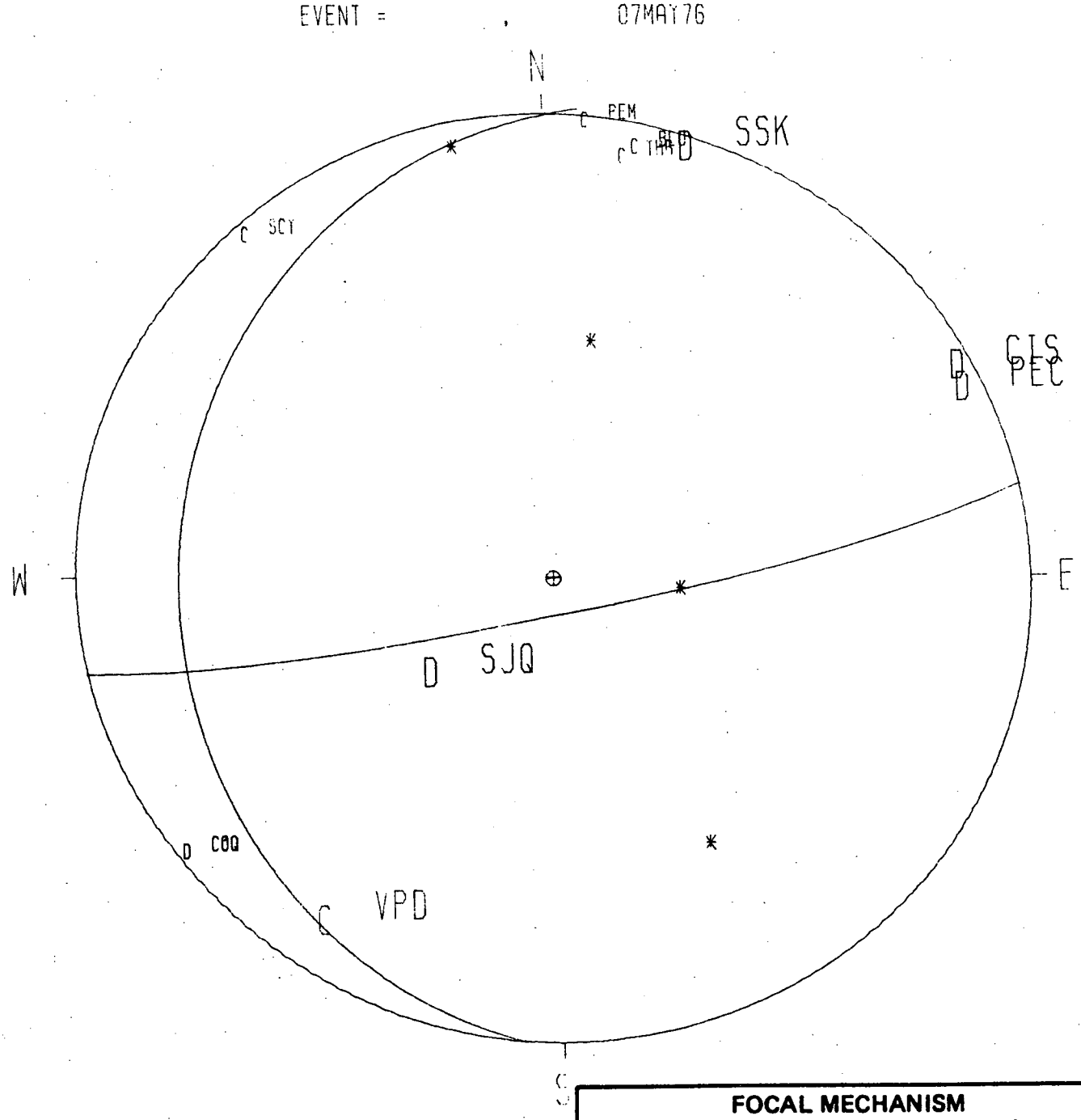

FOCAL MECHANISM
(NOT PLOTTED ON FIG. F-1),
7 MAY 1976
SONGS 2 & 3

Project No. 411001
Woodward-Clyde Consultants

Figure F-2p

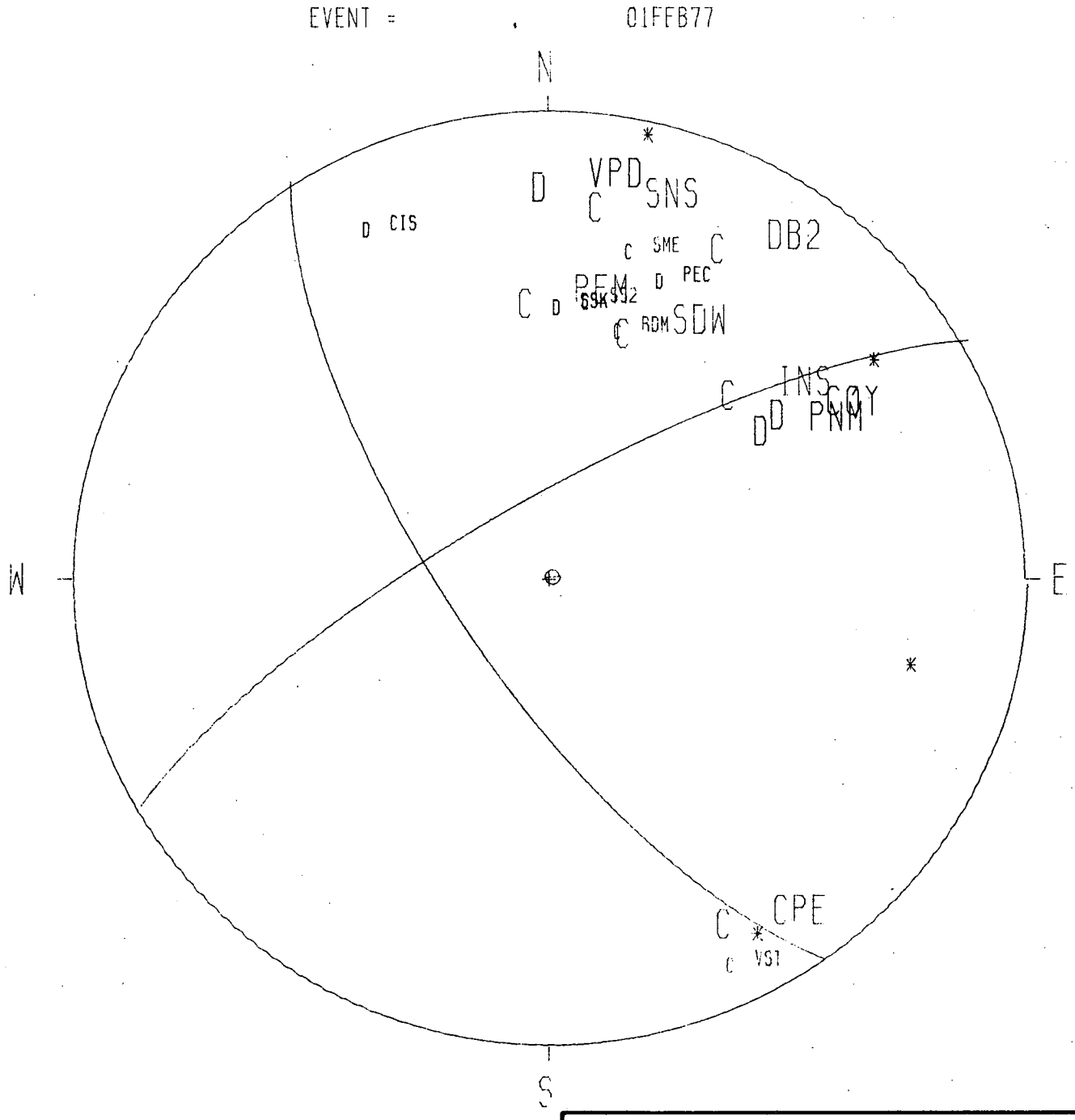

FOCAL MECHANISM
(NOT PLOTTED ON FIG. F-1),
1 FEBRUARY 1977
SONGS 2 & 3

Project No. 41100I
Woodward-Clyde Consultants

Figure F-2q

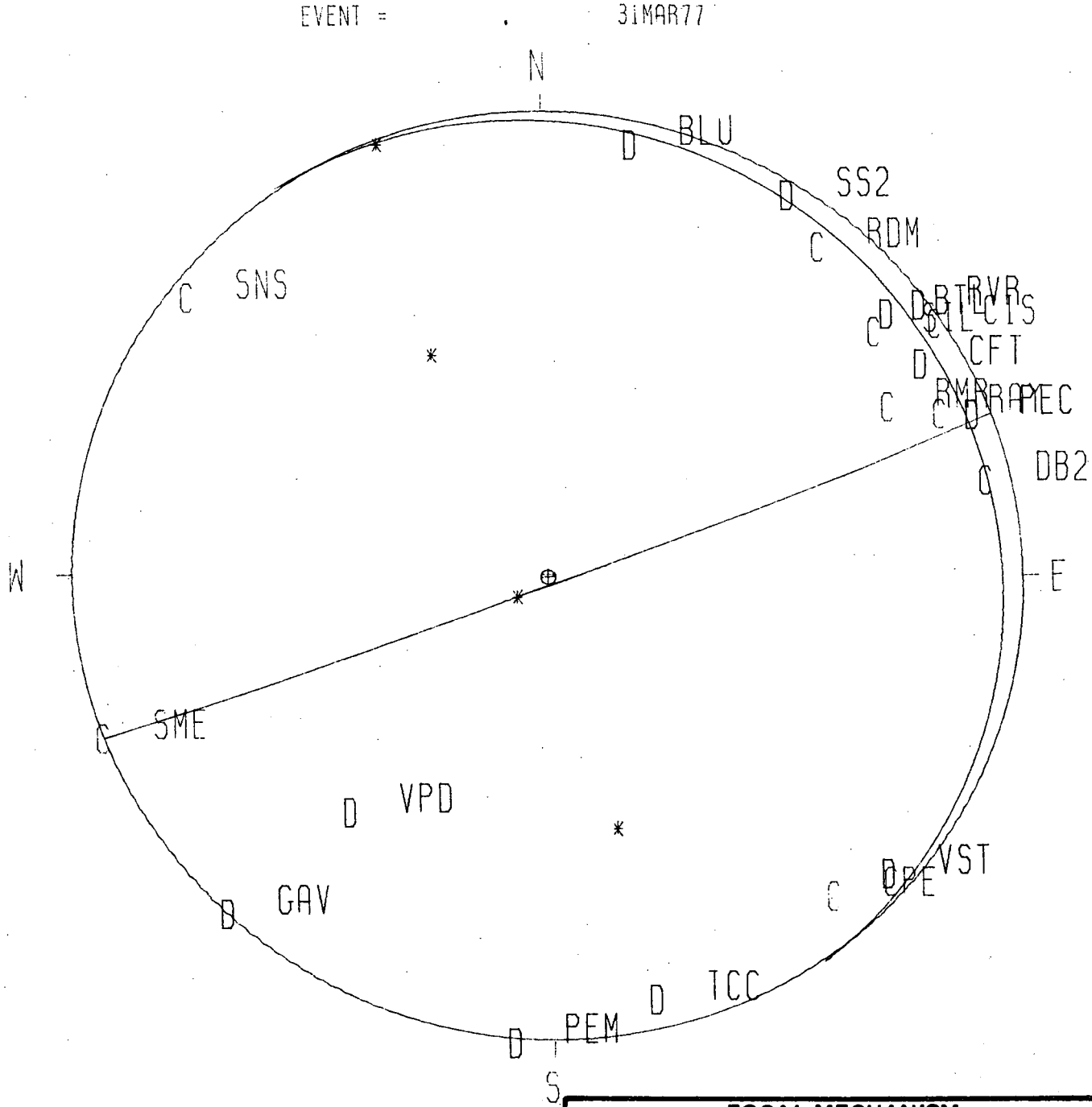

FOCAL MECHANISM
(NOT PLOTTED ON FIG. F-1),
31 MARCH 1977
SONGS 2 & 3

Project No. 411001
Woodward-Clyde Consultants

Figure F-2r

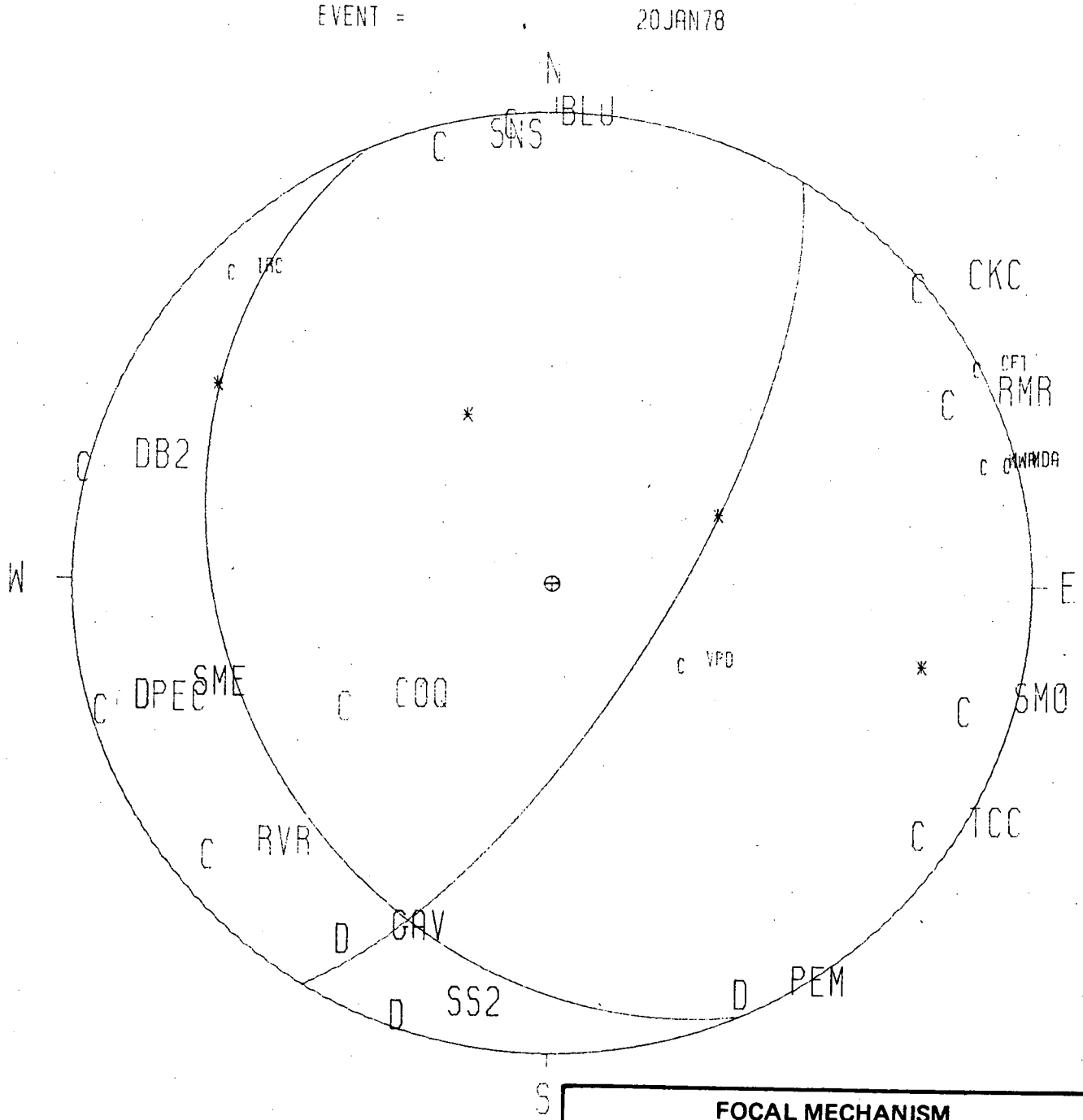

FOCAL MECHANISM
(NOT PLOTTED ON FIG. F-1),
20 JANUARY 1978
SONGS 2 & 3

Project No. 411001 **Woodward-Clyde Consultants**	Figure F-2s

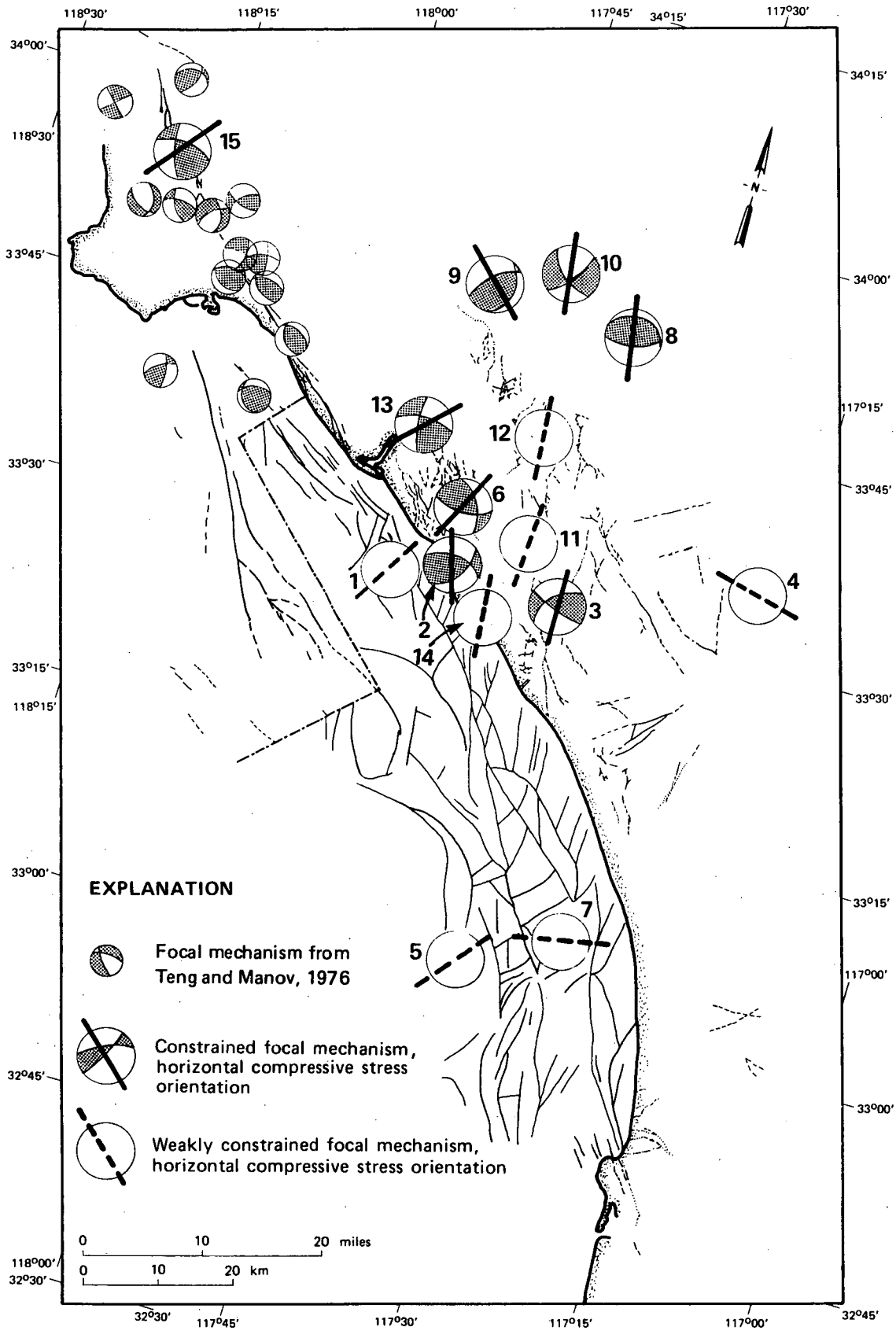

Note: Numbers refer to Table F-1

FOCAL MECHANISMS AND HORIZONTAL COMPRESSIVE STRESS ORIENTATIONS
SONGS 2 & 3

Project No. 411001
Woodward-Clyde Consultants

Figure F-3

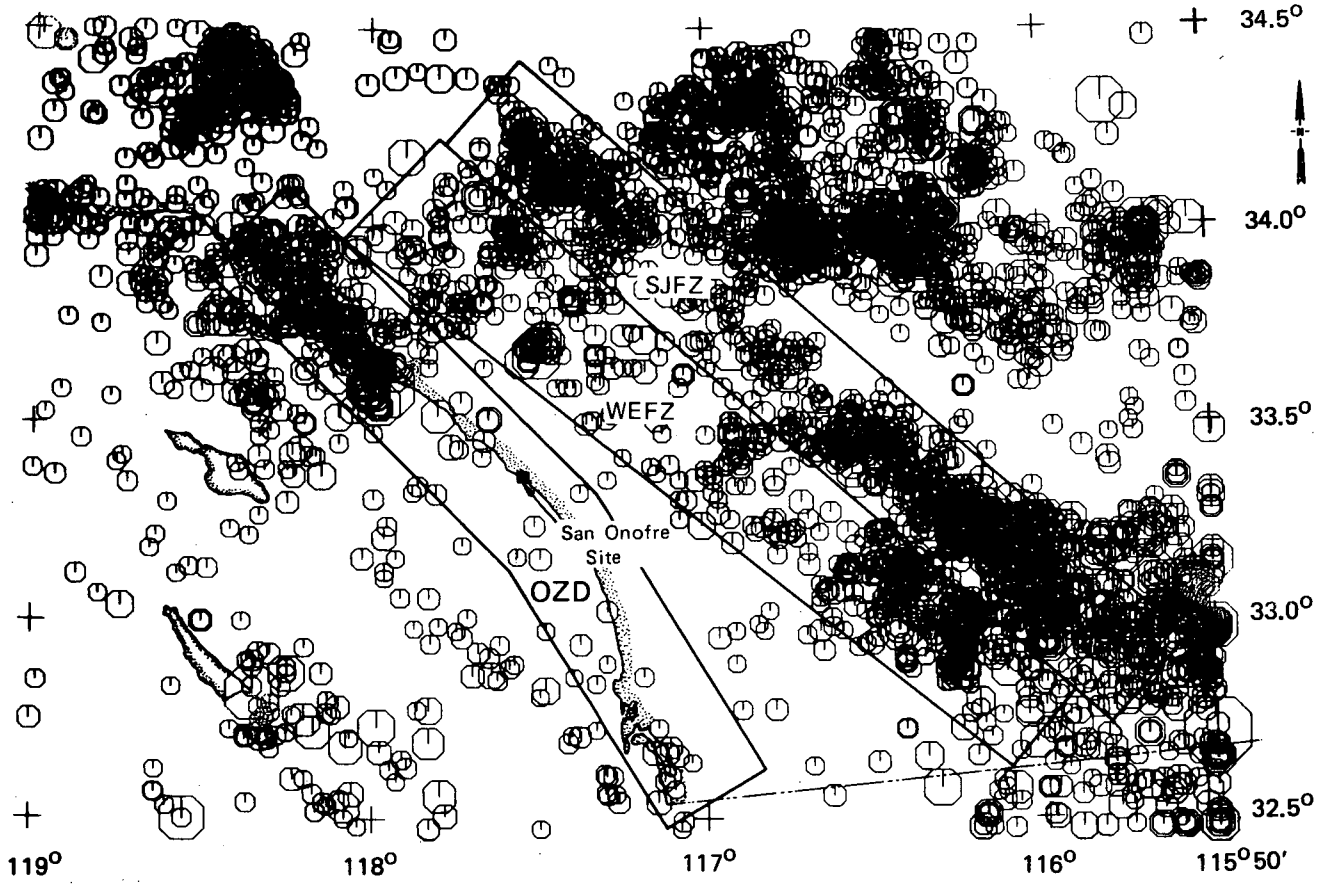

EXPLANATION

Reported Magnitude

7.0

6.0

5.0

4.0

3.0

OZD – Offshore Zone of Deformation

WEFZ – Whittier – Elsinore fault zone

SJFZ – San Jacinto fault zone

0 50 100 miles

0 50 100 km

Data Source: Hileman and others, 1973, and California Institute of Technology

SEISMICITY – 1932 TO 1976
MAGNITUDE ≥3
SONGS 2 & 3

Project No. 41100I
Woodward-Clyde Consultants

Figure F-4

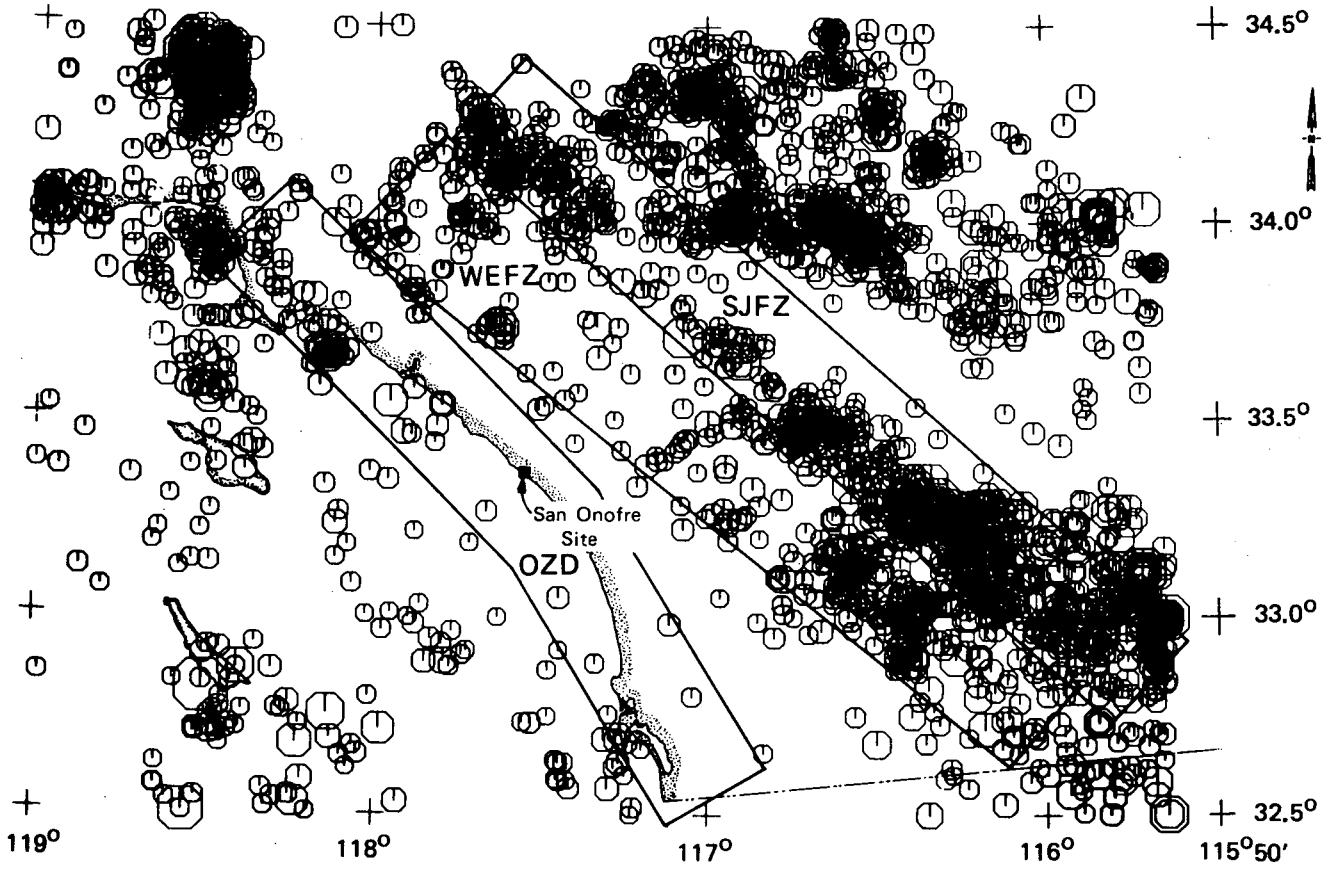

EXPLANATION

Reported Magnitude

7.0

6.0

5.0

4.0

3.0

0 50 100 miles

0 50 100 km

Data Source: Hileman and others, 1973, and California Institute of Technology

OZD – Offshore Zone of Deformation

WEFZ – Whittier – Elsinore fault zone

SJFZ – San Jacinto fault zone

SEISMICITY – 1947 TO 1976
MAGNITUDE ≥3
SONGS 2 & 3

Project No. 41100I
Woodward-Clyde Consultants

Figure F-5

APPENDIX G
GEOLOGIC DISPLACEMENT AND SLIP RATE DATA FOR STRIKE-SLIP FAULTS

The data available for analysis in the evaluation of geologic slip rates on strike-slip faults from a variety of locations are summarized and documented in this appendix. Geologic slip rates for faults are based on the cumulative offset of geologic features related to the ages of those features. The slip rates reflect the cumulative effects of discrete displacements during seismic events and during aseismic slip. Thus, geologic slip rates are long term (longer than historic records) average rates of slip for faults and they portray, in a geologic sense, the degree of activity of faults. If the net displacements of geologic and geomorphic features can be determined, and if the ages of the features determined, an average geologic slip rate for that fault can be calculated. Further, if slip-rate data are available for several faults, the relative degree of activity and thus the hazard-producing potential of those faults can be compared (Cluff, 1978).

The data in Tables G-1 and G-2 were obtained from the published literature and through personal communications from workers who have studied one or more of the listed faults. Those data presented in Table G-1 include all recognized values for slip rate on each fault and the largest magnitude earthquake known to be associated with each listed fault. All of the faults listed in Table G-1 were selected to meet four criteria:

(1) Each is thought to be dominantly strike-slip in character. This is important because the hypothesized OZD and most of the other principal faults in California south of the Transverse Ranges are interpreted as dominantly strike-slip.

(2) Both displacement data and temporal data (Quaternary preferred) are available, allowing geologic slip rates to be calculated. Sometimes the ages of displaced features are only approximately known, and qualifying information is presented in the "comments" column of Table G-1 when appropriate.

(3) The geologic displacement data are the result of field observations or mapping studies, and therefore reflect the offset of mappable units. Data based on geophysical interpretation of offshore tectonic relationships which can not be verified as unique geologic solutions, and geodetic slip-rate data, which represent only short periods of time, have not been used for this study of geologic slip rates.

(4) Each of the listed faults has produced a large earthquake and it seems reasonable to assume that some of these probably approach the maximum for the fault. For consistency, most magnitude data are in terms of surface wave magnitude (M_S), except as noted.

Table G-1 presents earthquake magnitude, geologic displacement, age of displaced units and geologic slip rate data available in the published literature. The maximum reported earthquakes that are presented often have several magnitude interpretations. When a value for slip rate was not specially presented in a publication but displacement and temporal data were listed, that information was used to calculate the slip rates presented in Table G-1. Unless otherwise indicated under "comments", the slip rate values have been calculated as a part of the present investigation. Assumptions necessary to calculate those values are also listed.

Table G-2 presents slip rate data on additional strike slip faults for which no confirmed major historic earthquake magnitudes could be obtained. Selection of the faults were based on the same criteria as those presented in Table G-1 with the exception of item (4) above concerning historic large earthquakes.

TABLE G-1
Strike-Slip Faults
Earthquake, Displacement and Geologic Slip Rate Data

Fault Name	Maximum Reported Earthquake	Fault Type	Displacement or Slip Rate Reference	Displacement Data: Geologic Unit	Displacement Data: Geologic Age	Displacement Data: Amt. Displ.	Geologic Slip Rate: Vert. (mm/yr.)	Geologic Slip Rate: Horiz. (mm/yr.)	Geologic Slip Rate: Vert./Horiz.	Comments
San Andreas (north of Cholame)	8.3 (1906) (Richter, 1958)	Right lateral	Clark & Nielsen, 1973	Point of Rocks, Sandstone, Kreyenhagen Shale, Butano Sandstone & Twobar Shale	Eocene	305 to 330km		14-28		Displacement derived by stratigraphic, sedimentation and paleogeographic studies. Inception of faulting taken to be 12m.y. to 22.5m.y. (Crowell, 1975; Dibblee, 1975; Ehlig, Ehlert & Crowe, 1975).
			Huffman, 1972	Clastic sediments	late Miocene (5m.y.)	234±8km		47		Studies of source areas of late Miocene clastic deposits; at least one change of slip rate in the last 22m.y.
			Addicott, 1968	"Lincoln Stage"	Oligocene (22.5m.y.)	322km		14		Zoogeographic study of middle Tertiary marine basins in central California used to determine amounts of displacement.
				"Vaqueros Stage"	early Miocene (~15m.y.)	274km		18		
				"Temblor Stage"	mid. Miocene (~12m.y.)	209km		17		
				"Margartian Stage"	late Miocene (5m.y.)	129km		26		
			Cummings, 1968	Corte Madera facies	early Pleistocene (1 to 3 m.y.)	28km		10-30		Offset of Corte Madera facies of Santa Clara Formation; age estimated to be between 1 and 3 m.y.
			Wentworth, 1968	strata of Anchor Bay	Lt. Campanion or early Maestrichtian (Cretaceous)	270 to 350km		12-29		Upper limit of 350km displacement is uncertain and could be more. Inception of faulting taken to be between 12m.y. and 22.5m.y. (Crowell, 1975; Dibblee, 1975; Ehlig, Ehlert, & Crowe, 1975).
			Jahns, 1969	---	post-Oligocene (22.5m.y.)	---		13		Inferred slip rate compiled from published results of independent field work by ten investigators.
			Dickert, 1968	Monterey Formation & Claremont shale	mid. Miocene (~12m.y.)	32km		3		Constraints for determining offsets are poor. Correlated peak concentrations of phosphatic facies of Tertiary marine sediment.
				Phosphatic	mid. Miocene	104km		9		

(TABLE G-1 Continued)

Fault Name	Maximum Reported Earthquake	Fault Type	Displacement or Slip Rate Reference	Displacement Data: Geologic Unit	Displacement Data: Geologic Age	Displacement Data: Amt. Displ.	Geologic Slip Rate: Vert. (mm/yr.)	Geologic Slip Rate: Horiz. (mm/yr.)	Geologic Slip Rate: Vert./ Horiz.	Comments
San Andreas (cont. north of Cholame)			Dickert, 1968 (cont.)	Lambert & Santos phosphatic shales	early Miocene (15m.y.)	290m		19		
				Butano Sandstone & San Lorenzo Formations	late Eocene	386km		17-26		Inception of faulting taken to be between no older than 22.5m.y. (Crowell, 1975; Dibblee, 1975; Ehlig, Ehlert, & Crowe, 1975).
San Andreas (Cholame to Cajon Pass	8.2 (1857) (Slemmons, 1977)	Right lateral	Clifton, 1968	salmon-colored sandstone	late Miocene (5m.y.)	16 to 24km		3-7		Considered minimum displacement because source for sandstone could be from more distant area.
			Crowell, 1973	---	late Miocene (5m.y.)	260km		52		Displacement for south of "big bend". Questionable data.
			Crowell, 1962	Sierra Pelona shist, Paleocene to Miocene rocks	early Miocene (~15m.y.)	209km		14		
			Huffman, Turner	Pinnacles volcanic rocks,	22m.y.	295km		13		K-Ar age dating, continuity of Miocene shoreline and geochemistry used in correlating Miocene volcanic rocks.
				Neenach Volcanic Formation, volcanic rocks of San Juan Bautista & Blue Ridge-Brush Mtn.	23.5m.y.	311km		13		
			Barrows and others, 1976	Harold Formation	older Quaternary (~.8m.y.)	8km		10		Pelona Schist-bearing Harold Formation offset minimum of 4.9 to 5 miles. Said to be late Quaternary thus .8m.y. assumed to be young age for which slip rate was approxinated.
			Howell, 1975	Maniobra Formation, Eocene Shoreline, Eocene sediments	Eocene	260km		12-22		Comparison of lithology, fauna and paleogeography of Eocene clastic sediments. Inception of faulting taken to be 12m.y. to 22.5m.y. (Crowell, 1975; Dibblee, 1975; Ehlig, Ehlert & Crowe, 1975).
			Ehlig, Ehlert, and Crowe, 1975	Mint Canyon Formation & Caliente Formation	Miocene (12m.y.)	297 to 307km		25		Relates clasts of Mint Canyon Formation to volcanic complex source in Chocolate Mtns. Pre-Cenozoic basement offset same amount and 12m.y. said to be the youngest parts of offset formation.

(TABLE G-1 Continued)

Fault Name	Maximum Reported Earthquake	Fault Type	Displacement or Slip Rate Reference	Displacement Data: Geologic Unit	Displacement Data: Geologic Age	Displacement Data: Amt. Displ.	Geologic Slip Rate: Vert. (mm/yr.)	Geologic Slip Rate: Horiz. (mm/yr.)	Geologic Slip Rate: Vert./ Horiz.	Comments
San Andreas (cont. Cholame to Cajon Pass)		Right lateral	Dibblee, 1975	Vaqueros & Punchbowl Formations	early Miocene (~15m.y.)	150km		10		Questionable whether formations are equivalent in age.
			Ehlig, 1975	alluvium	early Pleistocene (1.8m.y.)	16km	minor	9		Offset of alluvium from drainages of San Gabriel Mtns. Uplift of San Gabriel Mtns. implied by tilting of 30° of Pleistocene alluvium. Age of displacement assumed to be 1.8m.y. and could be less.
			Vedder, 1975	Tertiary marine basin	middle Miocene (~12m.y.)	300km		25		Correlates Tertiary marine sediments of Temblor and Caliente Ranges with those east of Salton Sea.
					early Pliocene (3.5m.y.)	80km		23		
			Wallace, 1975	---	---	---		14-21	1/10 to 1/20	Slip rate and ratio based on scarp morphology in Carrizo Plain.
			Sieh, 1978 (in press)	Wallace Creek	Holocene (3420±160 yrs.)	118 to 138m	minor	34-41		Radiocarbon age date. Slip rate from text; average is 37mm/yr.
			Sieh, 1978	marsh deposits	Recent (1800 to 500 AD)	---		30		Based on average recurrence interval of 160 years per event, number of events and displacement of 1857 earthquake; slip rate by personal communication.
San Andreas (south of) Cajon Pass)	6.5 (1948) (Real and others, 1978)	Right lateral	Crowell, 1962	Precambrian terraces	---	300km		13-25		Inception of faulting taken to be between 12m.y. and 22.5m.y. (Crowell, 1975; Dibblee, 1975; Ehlig, Ehlert & Crowe, 1975).
			Haxel & Dillon, 1973	granitic rocks	Tertiary	50km		2-4		K-Ar age of 62m.y. ties granitic rocks between Cargo Muchaco & Picacho areas. Inception of faulting taken to be between 12m.y. and 22.5m.y. (Crowell, 1975; Dibblee, 1975; Ehlig, Ehlert & Crowe, 1975).

(TABLE G-1 Continued)

Fault Name	Maximum Reported Earthquake	Fault Type	Displacement or Slip Rate Reference	Displacement Data			Geologic Slip Rate			Comments
				Geologic Unit	Geologic Age	Amt. Displ.	Vert. (mm/yr.)	Horiz. (mm/yr.)	Vert./ Horiz.	
San Andreas (Cont. south of Cajon Pass)			Peterson, 1975	Coachella Fanglomerate	Miocene (10m.y.)	215km		21.5		Fanglomerate deposit derived from source area near Cargo Muchacho Mtns. 10.0±1m.y. is age of dike 25m from base of 1500m. thick fanglomerate. Slip rate taken from text valid for north branch only.
			Babcock, 1974	Salt Creek, Borrego and Shavers Well Formations	Pleistocene (30,000 yrs.)	850m		28		Time constraint for offset is poor; assumed to be greater than 30,000 yrs.
			Proctor, 1968	conglomerate	late Pleistocene or early Holocene (~10,000 yrs.)	245m		25		Poor constraint on age of conglomerate. Assumed to be approximately 10,000 years.

(TABLE G-1 Continued)

Fault Name	Maximum Reported Earthquake	Fault Type	Displacement or Slip Rate Reference	Displacement Data: Geologic Unit	Displacement Data: Geologic Age	Displacement Data: Amt. Displ.	Geologic Slip Rate: Vert. (mm/yr.)	Geologic Slip Rate: Horiz. (mm/yr.)	Geologic Slip Rate: Vert./ Horiz.	Comments
San Jacinto	7 (1890, 1899) (Thatcher and others, 1975)	Right-lateral	Sharp, 1967	lower Bautista beds	early Irvingtonian (0.8-1.45m.y.)	5.2km 0.3km vert.	0.21-0.38	3.6-6.5		Early Irvingtonian age assigned by Lamar and others (1973). Horizontal displacement is maximum, vertical is inferred.
				upper Bautista beds	Irvingtonian (0.5-1.2m.y)	2.6km		2.2-5.2		Middle Irvingtonian age; age limits are inferred.
				basement units	mid. to late Cretaceous	24km 1.6-3.25 km vert.	0.23-0.65	3.4-4.8		Slip is post-late Cretaceous, possibly all post-mid Miocene. Age 5 to 7 m.y. used as start of displacement
				sedimentary units	Pliocene (3-5m.y.)	18-19.5km		3.6-6.5		Claremont segment of the fault. Faulting occurred post-early Pliocene.
				bedrock in San Gabriel Mts.	---	11km		1.8-3.6		Bedrock of unknown age displaced on two segments of fault in Lytle Creek area. Post-late Miocene age used as start of displacement.
			Clark and others, 1972	Lake Cahuilla sediments	Holocene (3080+600, C^{14} age)	1.7m vertical	0.55-2	3.0-3.8	1/2.7	Trenching across the Coyote Creek fault. Sharp (1967) implies an equal amount of slip for Clark fault (Clark and others, 1972) in this vicinity, so total slip rate for the fault zone may be 6mm/yr.
			Sieh, personal communication, 1978	sediments and peat	Holocene (approx. 2000 yrs.)	---		3		Results are preliminary with horizontal displacement inferred from most recent displacement.
Whittier-Elsinore	6.5 (1934, Mexico) (Lamar and others, 1973) 6.0 (1910) (Real and others, 1978)	Right-lateral	Heath, 1954	Puente Fm. (Whittier)	Pliocene	3.7km 3.1km vert.	0.52-1.0	0.62-1.2		Whittier fault; vertical displacement varies. Both values are maximum.
				stream channels (Whittier)	Pleistocene?	2.5km		1.3(?)		Stream channel displaced as much as 2.5km; age unknown. Low quality.
			Weber, 1977a	fault in Silverado Fm.	Paleocene	9.5km		0.79-1.2		Inception of faulting assumed to be Miocene.

Fault Name	Maximum Reported Earthquake	Fault Type	Displacement or Slip Rate Reference	Displacement Data: Geologic Unit	Displacement Data: Geologic Age	Displacement Data: Amt. Displ.	Geologic Slip Rate: Vert. (mm/yr.)	Geologic Slip Rate: Horiz. (mm/yr.)	Geologic Slip Rate: Vert./Horiz.	Comments
Whittier-Elsinore (cont.)			Weber, 1977b	Bedford Canyon Fm, pegmatite dikes, contact of Bedford Canyon Fm. & Santiago Peak Volcanics	late Cretaceous	9-11km		0.9-1.6 (0.36-0.55)		Faulting began no earlier than post-Paleocene, more likely post-mid. Miocene, also calculated for post-Eocene (post-Sespe).
				Sespe-Vaqueros contact	late Eocene	10-13km		1.0-1.8 (0.4-0.65)		Very poorly defined contact, and poorly constrained maximum displacement. Age of faulting assumed post-mid. Miocene, also calculated for post-Eocene.
				Perris surface	9m.y.	180-400m vertical	0.02-0.04	---		Moderately well-controlled correlation of upland erosional surfaces.
				Basement	late Cretaceous	1220m vertical	0.12-0.17 (0.05-0.06)	---		Faulting assumed to start in mid. Miocene across Eagle fault segment. Also calculated for post-Eocene. Net displacement probably lower.
			Kennedy, 1977	Santa Rosa Basalt	8.3±0.5 m.y.	300m dip-slip	0.036	---		Radiometric date on basalt.
				unconsolidated sediments	Pleistocene (0.7-2m.y.)	5km		2.5-7.0		Evidence for displacement poorly shown on map. Age of unit poorly constrained.
			Sage, 1973	sediments	Paleocene	40km		2.7-5.0		Sage suggests post-Miocene displacement; amount of displacement poorly-constrained, based on reconstruction of paleogeography.
			Lamar and others, 1973	sediments	pre-Pliocene	32km		2.6-4.0		Lamar and others' estimate based on Lamar's thesis using paleogeographic reconstruction. Both Lamar and Sage (1973) assume pre-Pliocene displacement. Amount and age poorly constrained.
				Puente Fm.	lower Pliocene	4.7-4.8km		0.9-1.6		Based in part on displacement of cross-faults; Whittier fault.
				stream channels	Pleistocene	2.4km		1.2(?)		Whittier fault; age unknown.

Fault Name	Maximum Reported Earthquake	Fault Type	Displacement or Slip Rate Reference	Displacement Data: Geologic Unit	Displacement Data: Geologic Age	Displacement Data: Amt. Displ.	Geologic Slip Rate: Vert. (mm/yr.)	Geologic Slip Rate: Horiz. (mm/yr.)	Geologic Slip Rate: Vert./ Horiz.	Comments
Whittier-Elsinore (cont.)			Yerkes, 1972	offset faults	upper Mohnian	4 6km		0.38-0.58		This value assumes all displacement along fault is strike slip.
			Durham and Yerkes, 1964 Yerkes and others, 1965	sediments	upper Mohnian	1.2-4.6km 0.6-4.3 km vert.	.05-0.54	0.10-0.58		These values are calculated from distribution of vertical slip on Whittier fault as reported by Yerkes.
			Hannon, personal communication, 1978	sediments	Holocene (4000-5000 yrs.)	30-46 cm vert.	0.06-0.11			Preliminary data on Whittier fault; data unpublished.
San Gregorio	6.1 (1926 (Greene and others, 1973)	Right lateral	Weber and Lajoie, 1977	marine terraces	Pleistocene (120,000 to 200,000 yrs.)	---		6.3-16		Rates given for entire fault zone; individual traces are less. Zone consists of 3 traces where studied. 16 mm/yr. is preferred (Weber, personal communication, 1977).
Calaveras	6.6 (1911) (Toppozada and others, 1978)	Right lateral	Saul, 1967	stream channel	Pleistocene	0.8km		0.4-1.6		Northern end of Calaveras; lesser development of Quaternary fault traces than in south.
				Tertiary sediments	Eocene	19km		1.6-2.4		Assumed start of faulting at end of mid-Miocene.
			Crittenden, 1951	faults in Miocene units	post-Miocene	5km		0.8-1.2		Assumed start in early Pliocene.
			Herd, 1978	---	---	---		1.2-1.5		Does not give basis of rate.
Hayward	6.7 (1868) (Slemmons, 1977)	Right lateral	Prowell, 1974	Volcanic	Pliocene-Miocene	---		5		Slip rate based on set of data points by Prowell (1974).
Antioch	4.9 (1965) (McEvilly and Casaday, 1967)	Right lateral	Knuepfer, 1977	Tuff unit	mid-Miocene	0.18-0.66km		0.01-0.07		Poorly constrained displacement.
			Burke and Helley, 1973	Norton-ville Shale	late Eocene	1.2km		0.02-0.03		Apparent mapped displacement; poorly constrained.

(TABLE G-1 Continued)

Fault Name	Maximum Reported Earthquake	Fault Type	Displacement or Slip Rate Reference	Displacement Data: Geologic Unit	Displacement Data: Geologic Age	Displacement Data: Amt. Displ.	Geologic Slip Rate: Vert. (mm/yr.)	Geologic Slip Rate: Horiz. (mm/yr.)	Geologic Slip Rate: Vert./ Horiz.	Comments
Fairweather (Alaska)	Ms 7.9 (1958) (Plafker and others, 1978)	Right lateral	Plafker and others, 1978	glacial deposits	Holocene (940± 200 yrs.)	55m		58		Plafker prefers 58mm/yr. rate as more accurate and consistent for past 100,000 yrs.
				glacial deposits	Holocene (1300±200 yrs)	50m		38		
N. Anatolian (Turkey)	7.9 (1939) (Richter, 1958; Ambrasseys, 1970)	Right lateral	Wellman, 1969	---	Miocene (17.5m.y.)	350?km		20		Displacement data taken from Pavoni (1961).
	Ms 7.8 (same earthquake) (Geller and Kanamori, 1977)		Ambrasseys, 1970	---	Historic (30 yrs.)	90cm		30		Average displacement represented by 1939-1967 earthquakes.
				---	Historic (12 yrs.)	24cm		20		Local rate of creep.
Khangay (Bolnai) (Mongolia)	Ms 8.2 (1905) (Geller & Kanamori, 1977)	Left lateral	Wellman, 1969	---	---	---		20		Rate of slip estimated by Wellman from geomorphic appearance of fault trace. No geologic data basis.
	8.7 (same earthquake) (Richter, 1958)			---	---	---		---		
Bogdu (Lake Valley) (Mongolia	Ms 8.0 (1957) (Abe & Kanamori, in press, 1979)	Left lateral	Wellman, 1969	---	---	---		30	1/3.5	Rate of slip estimated by Wellman from geomorphic appearance of fault trace. No geologic data basis.
	8.3 (same earthquake) (Slemmons, 1977)			---	---	---		---		
Dasht-E Bayas	7.2 (1968) (Tchalenko and Berberian, 1975)	Left lateral, reverse	Tchalenko and Berberian, 1975	limestone	Cretaceous (65m.y.)	4km		0.06		65m.y. assumed as minimum age.
				sediments	Eocene (37m.y.)	400m		0.01		37m.y. assumed as minimum age.
					Holocene (10,000 yrs.)	8-24m		0.8-2.4		10,000 years assumed as maximum; geologic slip rate may be higher.
				sediments	Cretaceous (65m.y.)	1km (vert.)	0.015	---	1/4	

(TABLE G-1 Continued)

Fault Name	Maximum Reported Earthquake	Fault Type	Displacement or Slip Rate Reference	Displacement Data			Geologic Slip Rate			Comments
				Geologic Unit	Geologic Age	Amt. Displ.	Vert. (mm/yr.)	Horiz. (mm/yr.)	Vert./ Horiz.	
Shahrud (Iran)	7.25 (1962) (Slemmons, 1977)	Left lateral, reverse	Wellman, 1965 Wellman, 1969	streams	Holocene (10,000 yrs.)	100m		10		8 streams offset 100 meters, age assumed to be 10,000 years by Wellman, 1969.
										Richter (1958) indicates that no fault trace due to the earthquake was found.
Kopet-Dagh (Iran)	7.3 (1948) (Gutenberg and Richter, 1954) 7.6 (Same earthquake) (Richter, 1958)	Right lateral	Trifonov, 1978	wall of Chugundor Fortress	Middle ages (475 to 1475 yrs.)	2.5m		1.7-5.3	1/3 to 1/7	Vert./horiz. ratios by Trifonov.
										Middle Ages ranged from 500-1500 AD.
				irrigation systems	5th C., B.C. (2,500 yrs.)	9m		3.6		Younger irrigation systems offset progressively less.
				geomorphic	Holocene-Pleistocene (10,000 yrs.)	55-60m		6.0		10,000 years assumed as age. Trifonov suggests that slip rate is 1.5 to 2.0 mm/yr.
			Trifonov, 1971	irrigation systems	1,000-2,000 yrs.	8m		4-8		The main trace in Parou area.
Tanna (Japan)	7.1 (1930) (Slemmons 1977)	Left lateral	Matsuda, 1976	Taga volcanics	Pleistocene	1km		3.2		Slip rate from graph, Matsuda (1976)
Motagua (Guatamala)	7.5 (1976) (Plafker, 1976)	Left lateral	Plafker, 1976	---	---	---		20		Correlates slip rate of 20mm/yr between Caribbean and N. American plates with Motagua fault.
			Schwartz, Cluff and Donnelly, 1979 (in press)	alluvial terrace	Quaternary (~10,000 yrs.)	60m		6-10		Age of offset was estimated by authors to be 10,000 years old. Slip rate from text.
El Pilar (Venezuela)	6.7 (1957) (Sykes and Ewing, 1965)	Right lateral	Metz, 1968	---	---	5-15km		1-3		Age of 5m.y. for the inception of present strike-slip tectonic framework (Dewey, 1972) assumed for calculating slip rate for this report.
			Wellman, 1969	---	Cretaceous	475km		5		Long term slip rate from text based on data from Rod (1956). Age of fault's inception could be much younger.

(TABLE G-1 Continued)

Fault Name	Maximum Reported Earthquake	Fault Type	Displacement or Slip Rate Reference	Displacement Data: Geologic Unit	Displacement Data: Geologic Age	Displacement Data: Amt. Displ.	Geologic Slip Rate: Vert. (mm/yr.)	Geologic Slip Rate: Horiz. (mm/yr.)	Geologic Slip Rate: Vert./ Horiz.	Comments
Bocono (Venezuela)	8+1/4 (1812) (Woodward-Clyde Consultants, 1969)	Right lateral	Schubert and Sifontes, 1970	Victoria & Zerpa lateral moraines	Pleistocene (10,000 yrs.)	66m		7		Style of faulting is in debate; earthquake magnitude and location estimate from historical records.
			Dewey, 1972	---	5m.y.	50km		10		Based on other sources. Some normal thrust component implied by Dewey (1972) and Maresch (1974).
			Rod, 1956	glacial moraines	Pleistocene (10,000 yrs.)	80-100m		8-10		Based on field evidence. Style of faulting in debate.
Magellanes (Chile)	7 3/4 (1949-1950) (Winslow, 1978)	Left lateral	Winslow, 1976 and 1978	---	Miocene	100km		4-20		Minor compressional or normal components of slip. Insufficient data for age of offset said to be as young as Miocene (5m.y. to 22.5m.y).
Alpine (New Zealand)	none since 1830 (Scholz, 1973)	Right lateral, reverse	Wellman, 1969	---	base of Cretaceous	480km		30		Does not discuss basis for slip rate. Long term slip rate of 5mm/yr. also given.
			Scholz and others, 1973	---	post-Jurassic	450km		38		Data from Wellman (1955). Inception of fault said to be upper Miocene (12m.y.) by Christoffel (1971).
				lamprophyre dikes	mid. Cretaceous	120-150km		10-13		Data from Grindley (1963) and Wellman and Cooper (1971). Inception of fault said to be upper Miocene (12m.y.) by Christoffel (1971).
				glacial & post-glacial features	---	---	10			Derived from Wellman (1955) and Suggate, (1963, 1968)
								<10	1/1	Derived from Clark and Wellman (1959) and Wellman and Cooper (1971).
			Wellman, 1964					25		Southern end of Alpine fault In central part of fault Wellman, (1964) suggests that displacement of terraces indicate equal horizontal and vertical movement. Suggate and Lensen (1973) inferred little or no horizontal movement in Quaternary.

Fault Name	Maximum Reported Earthquake	Fault Type	Displacement or Slip Rate Reference	Displacement Data: Geologic Unit	Displacement Data: Geologic Age	Displacement Data: Amt. Displ.	Geologic Slip Rate: Vert. (mm/yr.)	Geologic Slip Rate: Horiz. (mm/yr.)	Geologic Slip Rate: Vert./ Horiz.	Comments
Hope (New Zealand	6.7 (1888) (Slemmons, 1977)	Right lateral, reverse(?)	Scholz and others 1973	---	post-Miocene (5m.y.)	20km		4		Displacement and age from Freund (1971) and Clayton (1966).
			Lensen, 1975	---	post-glacial (~18,000yrs.)	60-70m		3-4	1/3	60-70m. right-lateral offsets in Marlborough area assumed to be associated with Wairau, Awatere, Clarence, and Hope faults. Lateral slip rate across the shear zone (Marlborough fault system) is assessed to be 14-18mm/yr. and vertical slip rate +5 and -5 mm/yr.
Wairarapa (New Zealand	8 (1855) (Slemmons, 1977	Right lateral, reverse	Lensen and Vella, 1971	Waiohine terrace	20,000 to 22,000 yrs	120m		5-6		Tectonic environment indicates thrusting of Pacific plate under Australian plate.
			Wellman, 1972	---	---	---		24		Data from south part of North Island.
Sumatra	7.6 (1943 (Gutenberg and Richter, 1954)	Right lateral	Tjia, 1973	Toba ignimbrite	less than 300,000	20km		66		Radiometric age of ignimbrite given by Tjia (1973).
			Katili and Hehuwat, 1967	---	---	---		5-7		Tjia (1973) quotes Katili and Hehuwat (1967) for slip rate.
Jordan-Dead Sea	6.2 (1927) (Ben-Menahem and others, 1976)	Left lateral	Zak and Freund, 1966	Marl	20,000	150m		7.5		Offset data taken in association with multiple offsets.
			Quennell, 1958	sediments	Pliocene (5m.y.)	45km		9		Second phase of faulting that began after great sedimentation cycle at beginning of Pliocene. Age is estimated.
			Ben-Menahem and others, 1976	---	Pliocene (3-4m.y.)	---		6.5-10		Data taken from Freund and others (1970) and from Girdler (1958).

TABLE G-2

ESTIMATED SLIP RATES FOR STRIKE-SLIP FAULTS
WHICH HAVE NOT EXPERIENCED LARGE HISTORIC EARTHQUAKES

Name	Geologic Slip Rate (mm/yr)	Reference
Denali (Alaska)	35	Richter and Matson, 1971
Totschunda (Alaska)	33	Richter and Matson, 1971
Lembang (W. Java)	30	Tjia, 1968
Darvaz (Asia)	13	Trifonov, 1978
Garlock (California)	5.4	Burke and others, 1979
Atera (Japan)	5.3	Sugimura and Matsuda, 1965
Telemazar (Asia)	2.5	Wellman, 1965
Walker Lane (Nevada)	2.1	Slemmons, personal communication, 1979
Big Pine (California)	2.0	Lamar and others, 1973

APPENDIX H
RELATIONSHIP BETWEEN SLIP RATE AND MAGNITUDE

H-1 INTRODUCTION

In this appendix, observational data and theoretical considerations relating geologic and seismologic earthquake parameters are discussed. The central result of this work is the development of a relationship between observed geologic slip rates on individual strike-slip faults and maximum earthquakes associated with those faults.

This approach represents development of a procedure for determining maximum earthquakes that does not depend solely on the conventional fault-length versus magnitude method. Recently, several workers have noted explicit difficulties and inaccuracies in using such a method (see for example, Bolt, 1978; Chinnery, 1979; and Wyss, 1979). The approach presented here avoids the central problem of directly estimating the length of fault rupture during a future earthquake based on some subjective estimate of some fraction of the fault breaking during the event. It should be noted that this approach represents a different look at some of the same data used in the conventional design earthquake approach and takes into consideration available geologic data and current knowledge of the theory of earthquake sources.

Sections H-2, H-3 and H-4 respectively describe background information, theoretical considerations and the use of empirical data to develop the relationship between slip rate and magnitude.

H-2 BACKGROUND

In a simple physical model of an earthquake, tectonic stress is rapidly released in a stress drop of $\Delta\sigma$ averaged over a fault with a length of L and width w. An average displacement $\bar{D}$ is produced across the fault. Along with these physical parameters for a given earthquake, a surface wave magnitude M_S and seismic moment M_O can be determined from instrumental recordings of the seismic waves. Kanamori and Anderson (1975) and Geller (1976) have discussed the interrelationships of these earthquake parameters in detail. The earthquake parameters that can be observed directly in the field are produced by intersection of the earthquake rupture surface with the earth's surface. This has occurred historically in several hundred cases for which surface fault displacements and surface rupture lengths have been measured and recorded (e.g., Slemmons, 1977). These surface effects usually are associated with fault zones on which numerous past episodes of displacement have occurred during the Quaternary. Allen (1975) has noted this association on a worldwide basis and points out that, for the California area, there is virtually a one-to-one correlation between large earthquakes and faults that have been active in the Quaternary.

There are close numerical and physical relationships between the observed geologic features and the measured and calculated seismological parameters. Observations of length of fault rupture and displacement in individual earthquakes have provided an important observational constraint on the mathematical characterization of these parameters in seismological models and their derived parameters. These relationships are reviewed by Kanamori and Anderson (1975), Geller (1976) and Slemmons (1977). In Section H-3 that follows, these relationships are used to characterize and support a relationship between the geologic observation of long-term (geologic) slip rate on a fault and the maximum surface-wave magnitude that can be associated with the fault.

H-3 THEORETICAL CONSIDERATIONS

H-3.1 Magnitude Versus Displacement

In discussing theoretical and empirical constraints on earthquake parameters, Kanamori and Anderson (1975) show that surface-wave magnitude (M_S) is related to the dimension of earthquake sources. Using assumptions appropriate for strike-slip faulting, Geller (1976) similarly notes that M_S is proportional to n log L, where L is fault-rupture length and n is a function of magnitude and varies from 0 to 3. Using the assumption of constant stress drop leads to the similarity condition of constant $\bar{D}/L$ (Kanamori and Anderson, 1975). The data considered by Kanamori and Anderson (1975) for stress drop of California strike-slip faults range from about 15 to 30 bars, and for world-wide data, from about 5 to 100 bars. The tectonic consistency in California suggests that constant stress drop is an appropriate assumption for this discussion. From the above, the following relationships hold for the indicated magnitude ranges (Geller, 1976):

$$M_S \simeq 3 \log \bar{D} \text{ for } M_S < 6.67 \qquad \text{(H-1)}$$
$$M_S \simeq 2 \log \bar{D} \text{ for } 6.67 < M_S < 8.1$$
$$M_S \simeq \log \bar{D} \text{ for } 8.1 < M_S < 8.2$$
$$M_S \simeq \text{constant for further increase in fault dimensions}$$

These relationships illustrate the saturation of the M_S magnitude scale for very large earthquakes with M_S limited to 8.2 or so. They also point out that the predicted shape of a model-based magnitude-displacement relationship is dependent upon the simplified model assumptions used to predict the spectral shape of larger earthquakes. As Geller (1976) notes, the scaling relationships fit the oberved data fairly well but are "averages" and should not be used to predict parameters of a particular earthquake. This model summary indicates that there is a direct relationship between M_S and log $\bar{D}$ with a slope in the range of about 1 to 2 for the magnitude range 6-1/2 and larger.

Equations H-1 have been investigated on a purely empirical basis by Slemmons (1977) using surface fault displacements observed for worldwide strike-slip earthquakes. He finds the best-fit relationship,

$$M_s \propto 1.2 \log \bar{D} \qquad \text{(H-2)}$$

for earthquakes of moderate and large magnitude.

This section has established a relation between M_s and $\bar{D}$ within the limits of the assumptions in the theoretical models and interpretations by Kanamori and Anderson (1975) and Geller (1976). In the next section, the average seismic slip $\bar{D}$ is related to the measured long-term slip on faults based on geologic field measurements.

H-3.2 Average Slip Rate Versus Displacement and Magnitude

The average slip rate on a fault can be related to the summed displacement of earthquakes occurring on the fault. Brune (1968), Smith (1976) and Anderson (1979) show that the rate of slip on an individual fault may be calculated from the total seismic moment as a function of time for the fault. The seismic moment is defined as

$$M_o = \mu L w \bar{D} \qquad \text{(H-3)}$$

where μ is the rigidity modulus. The moments for a suite of earthquakes occurring during a given time period may be added to determine the total displacement for that time period, $\bar{D}_{sum}$, along the total fault length, L_{tot},

$$\bar{D}_{sum} = \frac{1}{\mu L_{tot} w} \sum M_o \qquad \text{(H-4)}$$

where the fault width, w, is considered constant. If it is

assumed that there is no aseismic slip or fault creep, then all the displacement that occurs on a fault must be represented by earthquakes with moments contributing to the total moment in Equation H-3. The quantity $\bar{D}_{sum}$/(time interval) thus represents the average geologic slip rate inferred from geologic field evidence.

It is important to note that most of the slip on a given fault is contributed by the largest earthquakes (Brune, 1968; Molnar, 1979). The number of earthquakes as a function of magnitude is found to be given by the relationship

$$\text{Log } N = a - bM_S \qquad \text{(H-5)}$$

where a and b are constants (Richter, 1958). The value of b in California is about 0.8. Thus for every unit decrease in magnitude there should be about 6.3 (= antilog 0.8) times as many earthquakes on a given fault. Kanamori and Anderson (1975) observe that $M_S \propto 3/2 \log M_O$ for the magnitude range 6 to 8. Thus the moment (and consequently displacement) will accumulate much more rapidly for larger earthquakes. Even if the b-value were 1.0 or greater, the slip at a given point would still be dominated by the displacements of the largest earthquakes because the smaller earthquakes also have smaller rupture lengths and thus add their smaller displacement over a smaller area. Brune (1968) found that about one-third of the total moment for earthquakes occurring in the Imperial Valley in the interval 1934-1963 was produced by the single largest earthquake.

The above observation is important in evaluating the largest earthquakes that can occur on a particular fault based on observations of slip rate, for it means that the slip rate for a given time period is a direct measure of the larger earthquakes that have occurred on the fault during that period. It should be noted that, with respect to Equation H-4, both total displacement

or average slip rate and total fault length bear a simple mathematical relationship to the total seismic moment and thus to the largest earthquake to occur on a fault. In many previous studies total fault length has been used to develop a means of assessing maximum earthquake magnitude. This discussion, representing recent understanding of the mechanics of earthquake occurrence, suggests that slip rate is also related to maximum earthquake magnitudes on active faults.

It should be noted again that the theoretical proportionality of Equations H-1 and its extension to slip rate and maximum magnitude are dependent upon fundamental assumptions about earthquake sources. These theoretical considerations are intended as a guide to interpreting the slip rate and magnitude data discussed in Section H-4 below.

H-4 EMPIRICAL RELATIONSHIPS

Empirical relationships between the recorded size of historic earthquakes and the best estimates for geologic slip rates measured on the causative fault suggest that a relatively simple relationship exists between the geologic slip rate on a fault and the magnitude of the maximum event which may occur on that fault. Observations of the occurrence of surface displacements related to individual earthquakes suggest that observed surface geologic displacements (except aseismic fault creep) result from the larger earthquakes. That is, the total slip during periods of time longer than the recurrence interval of large events is primarily the result of the major events, rather than the summed effect of many smaller events. Observations of California's strike-slip faults also show that the larger faults exhibit higher geologic slip rates and have historically produced the largest magnitude earthquakes. The large geologic slip rates on major faults such as the San Andreas are explained by either more frequent displacement events or larger-displacement events, or a combination of those factors, than are found on faults with lower

geologic slip rates. Faults with relatively low geologic slip rates do not generate such large earthquakes or large displacements, as are observed on faults with relatively high geologic slip rates. Thus relationships between slip rate and displacement per event suggest that a relationship exists between maximum magnitude earthquake and geologic slip rate.

Figure H-1 was constructed from the data base provided in Appendix G and Table H-1 in order to examine the relationship between the magnitudes of the largest historic earthquakes and the geologic slip rates for faults with the characteristics and style of southern California strike-slip faults. The best estimates of geologic slip rates, based on the most reliable data, and maximum earthquake magnitudes were selected from Appendix G. Table H-1 presents all of the maximum historic earthquakes and other significant earthquakes associated with the respective faults with slip-rate data; these data are shown on Figure H-1. Some data summarized in Appendix G were not used because of poor control in the correlation of offset geologic features, poorly defined ages for offset features, or other similar problems that led to low confidence in the data. In a few cases, earthquakes were eliminated from consideration because the largest-magnitude earthquake associated with the fault was based on unreliable early historic records or because the assignment of that earthquake to that fault was doubtful.

The pattern of historic earthquake data presented on Figure H-1 indicates a trend of increasing maximum earthquakes with increasing geologic slip rate. This observation together with an evaluation of the slip rate and magnitude parameters suggests that an upper-bound limit may exist to the right of the data points. Although the recurrence time on faults may be up to several centuries, collection of fault data on a worldwide basis should allow for obtaining a number of earthquake events which would approach this upper limit. It is possible to calculate a

return period for any magnitude earthquake on a fault with a given geologic slip rate; however, such calculations do not limit the maximum magnitude. Accepted limiting magnitudes have been established by several lines of argument for well studied faults such as those discussed below for California.

To examine the relation between the upper limit of the historical data on Figure H-1 and the magnitude of the maximum earthquakes for these faults, authoritative estimates of the magnitudes of the maximum design* earthquakes for four of the most extensively studied of the faults (San Andreas, San Jacinto, Calaveras and Hayward) were taken from the literature. These estimates, which are based on the empirical relationships between fault length and magnitude as summarized by Slemmons (1977), indicate maximum design earthquake magnitudes for the four faults as follows:** San Andreas, M 8-1/2; San Jacinto, M 7-1/2; Calaveras, M 7; and Hayward M-6-3/4. When plotted, as on Figure H-2, an envelope of those four data points defines a line that is parallel to and slightly to the right of the maximum historic magnitudes on Figure H-1. The parallelism shown on Figure H-2 supports the expectation of an approximately log-linear relationship between maximum magnitude and geologic slip-rate for strike-slip faults in the magnitude range of 6-1/2 to 8. The fact that the maximum earthquake line lies slightly to the right of the empirical data suggests the degree of conservatism that is appropriate in estimating the magnitudes of the maximum design earthquakes that should be anticipated on the faults.

A short discussion of each of the faults used for the construction of Figure H-1 is presented in the subsections that

---

* The maximum earthquake considered likely to be generated by future movement on a particular fault.

** In order not to leave the impression of high accuracy, these estimates have been rounded to the nearest one quarter fraction.

follow. The slip-rate data are the best estimates based on current knowledge of the faults. The discussions are based on the results of an evaluation of available published data, and they present the rationale for selection of the particular geologic slip rates used in the graph. Specifically, the subsections presented below and respective faults are as follows:

Subsection	Fault or Fault Segment
H-4.1	San Andreas
H-4.2	San Jacinto
H-4.3	Whittier-Elsinore
H-4.4	Newport-Inglewood
H-4.5	San Gregorio
H-4.6	Calaveras
H-4.7	Hayward
H-4.8	Antioch
H-4.9	Fairweather (Alaska)
H-4.10	North Anatolian (Turkey)
H-4.11	Motagua (Guatamala)
H-4.12	Tanna (Japan)
H-4.13	Jordan-Dead Sea (Middle East)
H-4.14	Sumatra (Indonesia)

H-4.1 San Andreas Fault

The detailed trenching, age-dating and stream-offset studies by Sieh (1977, 1978) are considered to be the most reliable documentation of younger fault displacments along the San Andreas fault. Sieh (1978) recognized as many as nine earthquake events that incrementally offset streams and marsh sediments deposited between 500 and 1800 A.D. Based on studies at Pallett and Wallace Creeks, Sieh (1977) derived a slip rate of 30 to 37 mm/yr. Based on current knowledge, Sieh indicates a preference for the 37 mm/yr rate.

H-4.2 San Jacinto Fault

The San Jacinto fault zone consists of several en echelon fault segments characterized by individual displacement and seismic histories. Table G-1 is a summary of displacements on segments for which available data are sufficient for determining rates of slip. The independent history of individual segments and uncertainty in time constraints are largely responsible for the various slip rates which range between 1.8 and 7.1 mm/yr. Sharp (1978) has most recently revised his earlier estimates of slip rate upward to the 7.1 mm/yr figure based on the correlation of an ash bed underlying offset gravels to the Bishop ash dated at 0.73 million years. The slip rate given is thought to be a minimum but is derived from the best available information.

H-4.3 Whittier Elsinore Fault

Reference sources in which lateral displacement and time constraints were considered acceptable include Weber (1977a, b) and Lamar and others (1973). Based on these data, an average lateral slip rate of 1.2 mm/yr was calculated for use in Figure H-1. The vertical slip rate is at least an order of magnitude lower than the lateral slip rate.

H-4.4 Newport-Inglewood Zone of Deformation

Literature sources of displacement data and ages of displacements were generally found to be of low confidence and quoted values varied considerably. This study took the published data into consideration, performed an evaluation of offset facies based on E-log data from oil wells, and computed a slip rate of approximately 0.5 mm/yr. This rate envelopes the majority of slip rates calculated from the literature. For a more detailed discussion of the NIZD, refer to Appendix D.

H-4.5 San Gregorio Fault

The displacement history of marine terraces was studied by Weber and Lajoie (1977) by which they evaluated the slip rate. Weber

(personal communication, 1977) believes the best estimate of slip rate is 16 mm/yr for the San Gregorio fault.

H-4.6 Calaveras Fault

Total lateral displacement and late Miocene inception of the Calaveras fault was reported by Saul (1967). Post-Miocene displacement was reported by Crittenden (1951). Based on these authors' investigations, the slip rate for the Calaveras fault appears to lie between 0.8 and 2.4 mm/yr. The average slip rate of 1.6 mm/yr was selected for use in this report.

H-4.7 Hayward Fault

Offsets of Pliocene and Miocene volcanic units across the Hayward fault have been correlated on the bais of petrography, mineralogy and stratigraphy. Prowell (1974) discussed the correlations and plotted offset distances versus time to derive a slip rate that varies between 5 and 8 mm/yr for the Hayward fault. Prowell (1974) suggested that the fault is slowing down since Miocene time. The 5 mm/yr rate provided by the youngest (Pliocene) offset was used for this report.

H-4.8 Antioch Fault

Knuepfer (1977) and Burke and Helley (1973) have provided slip-rate estimates that range from 0.01 to 0.07 mm/yr based on offsets of Miocene and Eocene age rocks. Knuepfer (personal communication, 1979) suggests that the best estimate is about 0.03 mm/yr, which is used in this report.

H-4.9 Fairweather Fault (Alaska)

Holocene displacement and slip rate have been determined by Plafker and others (1978). Plafker suggests that the slip rate of 58 mm/yr is most accurate and feels that this rate is probably consistent over the past 100,000 years.

H-4.10 North Anatolian Fault (Turkey)

The slip rate for the North Anatolian fault was calculated by Wellman (1969) to be 20 mm/yr based on the total lateral displacement of Miocene rocks reported by Pavoni (1961). Ambraseys (1970) lends support to the 20 mm/yr slip rate by considering the historic rate of displacement resulting from major earthquakes.

H-4.11 Motagua Fault (Guatamala)

The Motagua fault and its tectonic setting within a major crustal plate boundary have been studied recently because of a major earthquake (M 7.5) on 4 February 1976 (Plafker, 1976). Schwartz and others (1979, in press) have examined the displacement of a Quaternary terrace deposit and have provided a preliminary geologic slip rate between 6 and 10 mm/yr. For the purpose of this report, the rate of 8 mm/yr was deemed appropriate. The rate of 20 mm/yr suggested by Plafker (1976) is most likely distributed among several parallel Guatamalan faults in addition to the Motagua fault.

H-4.12 Tanna Fault (Japan)

Based on work by Kuno (1936), Matsuda (1976) estimates a slip rate of about 3.2 mm/yr for the Tanna fault. Matsuda assigns a Pleistocene age to the 1 km offset of the Taga volcano and then calculates the slip rate.

H-4.13 Jordon-Dead Sea Fault (Middle East)

Several authors (Zak and Freund, 1966; Quennell, 1956; Ben-Menahem and others, 1976) have calculated slip rates that vary between 6.5 to 10 mm/yr. Quennell (1956) and Ben-Menahem and others (1976) base their slip rates on offset Miocene and Pliocene rocks. Zak and Freund (1966) base their slip rate estimate on 150-meter offsets of the Lisan Marl, which is about 20,000 years old in its upper beds. The 7.5 mm/yr slip rate given by Zak and Freund (1966) is selected for this report

because several offsets are used in the calculation and it best represents the degree of activity in the Quaternary time.

H-4.14 Sumatra Fault (Indonesia)

Tjia (1973) has suggested that a slip rate of at least 66 mm/yr should be assigned to the Sumatra fault. The rate is based on a 20 km offset of the Toba ignimbrite, which has been age dated at less than 300,000 years by radiometric techniques.

TABLE H-1

SUMMARY OF SLIP RATES AND
MAXIMUM HISTORIC EARTHQUAKE MAGNITUDES

Fault	Slip Rate (mm/yr)	Age of Offset Geologic Features	Maximum Earthquake Magnitude (M_s)
Sumatra	66	Pleistocene	7.6
Fairweather	58	Holocene	7.9
San Andreas	37	Holocene	8.3
N. Anatolian	20	Miocene	7.9
San Gregorio	16	Pleistocene	6.1
Motagua	8	Holocene	7.5
Jordan-Dead Sea	7.5	Pleistocene	7.2
San Jacinto	7.1	Pliocene-Holocene	7.1
Hayward	5	Miocene	6.7
Tanna	3.2	Pleistocene	7.1
Calaveras	1.6	Miocene & Pleistocene	6.6
Whittier-Elsinore	1.2	Miocene-Holocene	6.5
Newport-Inglewood	0.5	Miocene-Pliocene	6.3
Antioch	0.03	Eocene & Miocene	4.9

NOTE: For details of slip rate and earthquake data sources, see Table G-1.

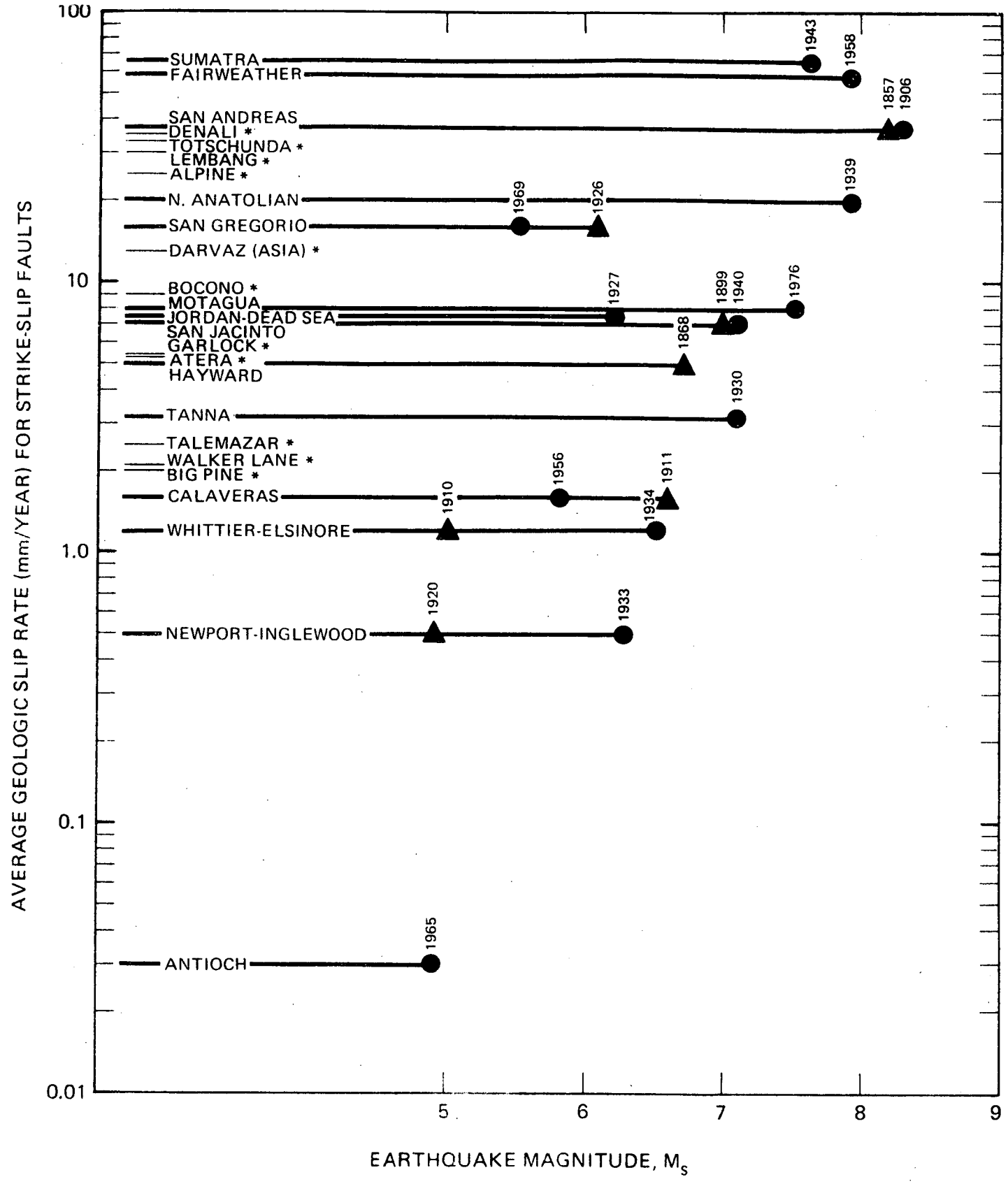

EXPLANATION

- Maximum instrumental recordings
- Maximum pre-instrumental estimates
- Range over which smaller earthquakes occur
- * No associated large earthquake

GEOLOGIC SLIP RATE vs HISTORIC MAGNITUDE FOR STRIKE-SLIP FAULTS
SONGS 2 & 3

Project No. 411001
Woodward-Clyde Consultants

Figure H-1

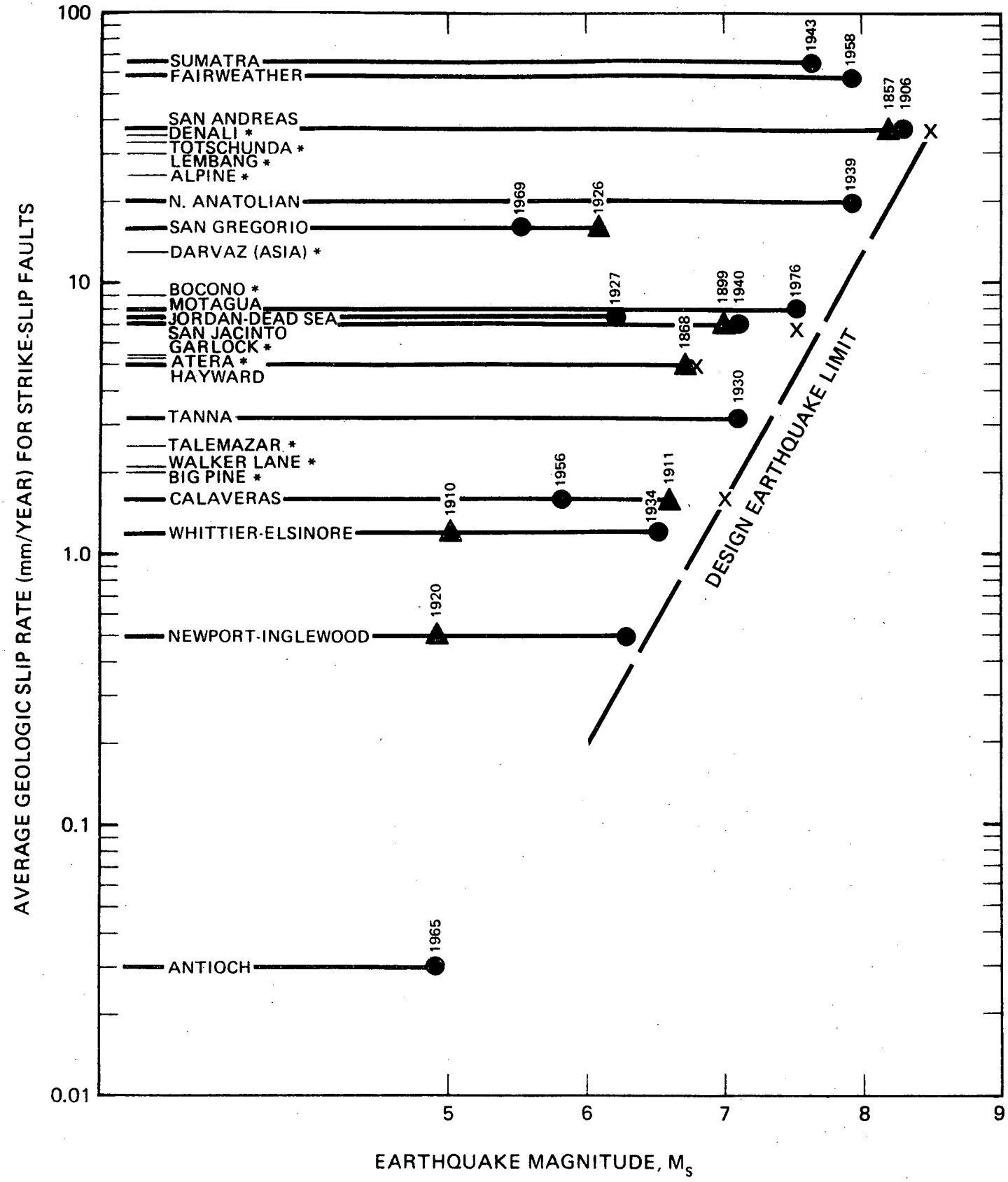

EXPLANATION

- ● Maximum instrumental recordings
- ▲ Maximum pre-instrumental estimates
- — Range over which smaller earthquakes occur
- * No associated large earthquake
- X Maximum design earthquake

GEOLOGIC SLIP RATE vs MAGNITUDE SHOWING DESIGN EARTHQUAKE LIMIT FOR STRIKE-SLIP FAULTS
SONGS 2 & 3

Project No. 411001
Woodward-Clyde Consultants

Figure H-2

APPENDIX I
DEVELOPMENT OF PEAK-ACCELERATION ATTENUATION RELATIONSHIPS FOR SOIL SITE AND COMBINED SOIL AND ROCK SITE DATA SETS

I-1 INTRODUCTION

This appendix contains the results of analyses to develop and examine attenuation relationships for peak horizontal acceleration using as a data base all available high-quality, digitized and uniformly processed recordings obtained from western United States earthquakes with magnitude M_L approximately equal to 6.5. One objective of these analyses was to compare less site-specific (all soil sites) and non site-specific (all soil and rock sites) attenuation relationships with site-specific (deep, very stiff soil sites) relationships developed in Appendix J for SONGS. The analyis procedure was the same as that used in developing site-specific relationships so that the comparisons and conclusions derived therefrom would be meaningful.

Another objective of these analyses was to examine the form of the attenuation relationship used in the site-specific analyses. The relationship used is of the following general form:

$$a = b_1 e^{b_2 M} (R+C)^{b_3} \qquad \text{(I-1)}$$

Parameter C is essentially a normalizing parameter for distance; its use was initially proposed by Esteva (1970). It has the effect of flattening the attenuation relationship at close source-to-site distances, thus constraining the peak acceleration at close distances to physically reasonably values. The form of Equation I-1 has has been used by many investigators; the parameter C has been assigned a constant value (typically 25 kilometers) independently of magnitude.

The major limitation of using a constant C is that the dependence of peak acceleration on magnitude is kept independent of distance, whereas magnitude dependence should decrease at smaller distances as indicated by theoretical considerations and analysis of observational data (for example, Hanks and Johnson, 1976).

Incorporating the magnitude effect in a realistic manner while retaining the commonly used form of the relationship can be accomplished if parameter C is non-zero and magnitude-dependent (the larger the magnitude the higher the C).

The analyses presented herein provide a basis for selecting an appropriate value for C for magnitude 6.5 earthquakes. This was accomplished by using a substantially larger number of recordings (196 accelerograms from 12 earthquakes for the all soil site data set compared with a total of only 56 accelerograms from 7 earthquakes for the site-specific soil data set given in Appendix J) covering the distance range of about 10 to 150 kilometers. The all-soil-site data set, rather than the combined soil- and rock-site data set (222 accelerograms from 12 earthquakes), was used because it is desirable to have a reasonably homogeneous data set in examining attenuation trends. Use of the soil-site data set also reduced somewhat the potential bias due to the San Fernando earthquake since the rock-site recordings are all from this one event.

I-2 RECORDS USED IN ANALYSES

The records used in regression analyses are summarized in Table I-1. All the records in the table (222 acceleration values) were used for the combined soil and rock data set. All records from soil sites identified in Table I-1 (196 acceleration values) constituted the soil site data set.

For the records listed in Table I-1, Table I-2 summarizes the number of accelerograms obtained during each earthquake, and

Table I-3 summarizes the number of accelerograms recorded at each station.

I-3 DATA ANALYSIS PROCEDURE AND ANALYSIS RESULTS

The data analysis procedure is identical to that described in detail in Appendix J for the site-specific data set. Weighted regression analyses were made. The number of data points in discrete distance intervals used in the analyses for the soil site data set is summarized below:

Distance Range	Earthquake (Number of Data Points)
5 - 7.1 km	None
7.1 - 10 km	1933 Long Beach (2)
10 - 14.1 km	1940 Imperial Valley (2)
14.1 - 20 km	1954 Eureka (2); 1971 San Fernando (2)
20 - 28.1 km	1933 Long Beach (2); 1971 San Fernando (18)
28.1 - 40 km	1933 Long Beach (2); 1971 San Fernando (92)
40 - 56.6 km	1941 Northern California (2); 1942 Borrego Valley (2); 1954 Eureka (2); 1968 Borrego Mountain (2); 1971 San Fernando (12)
56.6 - 80 km	1934 Lower California (2); 1971 San Fernando (20)
80 - 113.1 km	1941 Northwest California (2); 1971 San Fernando (10); 1968 Borrego Mountain
113.1 - 160 km	1934 Eureka (2); 1954 Lower California (2); 1966 Gulf of California (2); 1968 Borrego Mountain (4); 1971 San Fernando (8)

Peak accelerations for soil sites are plotted versus distance in Figure I-1. The trend of the data shown therein clearly indicates that the attenuation relationship should flatten at closer source-to-site distances. As discussed in Section I-1, simulation of this trend requires that a non-zero value of C be used in the attenuation equation.

To further examine the trend of the data shown in Figure I-1, regression analyses were conducted using these data and values of C ranging from zero to 40. The standard error of estimate obtained from these analyses decreased with increasing C. Thus the analysis results support the trend shown by visual examination of the data and indicate that a non-zero value of C should be used in the regression equation. The results of regression analysis for C = 20 are superimposed on the data in Figure I-1; the relationships shown appear to fit reasonably well the general trend of the data. Therefore, for final regression analyses, C = 20 was selected.

The mean and 84th percentile attenuation relationships derived for the soil site and combined soil and rock site data sets are the following:

Soil Sites

$$a = 49.0\ (R+20)^{-1.48}\ \text{(Mean)} \qquad \text{(I-2a)}$$

$$a = 69.5\ (R+20)^{-1.48}\ \text{(84th Percentile)} \qquad \text{(I-2b)}$$

Soil and Rock Sites

$$a = 92.4\ (R+20)^{-1.62}\ \text{(Mean)} \qquad \text{(I-3a)}$$

$$a = 133.4\ (R+20)^{-1.62}\ \text{(84th Percentile)} \qquad \text{(I-3b)}$$

TABLE I-1

LIST OF RECORDS USED IN ANALYSIS

Earthquake	Richter Magnitude (M_L)	Recording Station (USGS No)	Site Classif.	Source Distance (km)	C.I.T. No.	Comp.	Peak Acc'n (g)
Long Beach (33-3-11)	6.3	288	Soil	25	B021	N08E S82E	0.135 0.163
Long Beach (33-3-11)	6.3	136	Soil	31.5	V314	N39E N51W	0.064 0.100
Long Beach (33-3-11)	6.3	131	Soil	8.7	V315	SOUTH WEST	0.216 0.183
Eureka (34-7-6)	6.5	1023	Soil	128	U294	N45W S45W	0.016 0.016
Lower Calif. (34-12-30)	6.5	117	Soil	62.7	B024	N00E N90E	0.169 0.184
Imperial Valley (40-5-18)	6.4	117	Soil	10.8	A001	S00E S90W	0.359 0.224
Northwest Calif. (41-2-9)	6.4	1023	Soil	97	B027	S45W N45W	0.068 0.042
Northern Calif. (41-10-3)	6.4	1023	Soil	50	U300	N45W S45W	0.123 0.115
Borrego Valley (42-10-21)	6.5	117	Soil	49	T286	NORTH EAST	0.071 0.050
Lower Calif. (54-11-12)	6.3	117	Soil	151	T289	NORTH EAST	0.025 0.031

TABLE I-1 (continued)

Earthquake	Richter Magnitude (M_L)	Recording Station (USGS No)	Site Classif.	Source Distance (km)	C.I.T. No.	Comp.	Peak Acc'n (g)
Eureka (54-12-21)	6.5	1022	Soil	18.9	A008	N11W	0.175
						N79E	0.283
Eureka (54-12-21)	6.5	1023	Soil	40.2	A009	N44E	0.166
						N46W	0.209
Gulf of Calif. (66-8-7)	6.3	117	Soil	149	T293	NORTH	0.015
						EAST	0.015
Borrego Mtn. (68-4-8)	6.4	117	Soil	46	A019	S00W	0.142
						S90W	0.061
Borrego Mtn. (68-4-8)	6.4	277	Soil	104	A020	S00W	0.032
						N90E	0.032
Borrego Mtn. (68-4-8)	6.4	280	Soil	125	B040	N33E	0.042
						N57W	0.048
Borrego Mtn. (68-4-8)	6.4	113	Soil	137	Y370	SOUTH	0.024
						EAST	0.031
San Fernando (71-2-9)	6.4	279	Rock	9.0	C041	S14W	0.730
						N76W	0.730
San Fernando (71-2-9)	6.4	241	Soil	19.3	C048	N00W	0.258
						S90W	0.140
San Fernando (71-2-9)	6.4	151	Soil	37.8	C051	N36E	0.108
						N54W	0.133
San Fernando (71-2-9)	6.4	157	Soil	37.4	C054	N52W	0.150
						S38W	0.130

TABLE I-1 (continued)

Earthquake	Richter Magnitude (M_L)	Recording Station (USGS No)	Site Classif.	Source Distance (km)	C.I.T. No.	Comp.	Peak Acc'n (g)
San Fernando (71-2-9)	6.4	110	Soil	26.6	D056	N21E N69W	0.335 0.289
San Fernando (71-2-9)	6.4	133	Soil	34.0	D057	S00W N90E	0.115 0.153
San Fernando (71-2-9)	6.4	135	Soil	34.0	D058	S00W N90E	0.187 0.217
San Fernando (71-2-9)	6.4	187	Soil	36.7	D059	N46W S44W	0.152 0.164
San Fernando (71-2-9)	6.4	181	Soil	37.2	D062	N38W S52W	0.139 0.147
San Fernando (71-2-9)	6.4	217	Soil	36.5	D065	S00W S90W	0.154 0.163
San Fernando (71-2-9)	6.4	238	Soil	32.1	D068	N00E N90E	0.087 0.102
San Fernando (71-2-9)	6.4	1102	Soil	84.9	E071	S00W N90E	0.034 0.028
San Fernando (71-2-9)	6.4	223	Soil	36.4	E072	N75W N15E	0.088 0.125
San Fernando (71-2-9)	6.4	208	Soil	36.5	E075	N00E S90W	0.142 0.117
San Fernando (71-2-9)	6.4	137	Soil	36.9	E078	N50W S40W	0.137 0.188

TABLE I-1 (continued)

Earthquake	Richter Magnitude (M_L)	Recording Station (USGS No)	Site Classif.	Source Distance (km)	C.I.T. No.	Comp.	Peak Acc'n (g)
San Fernando (71-2-9)	6.4	199	Soil	36.1	E083	S00W N90E	0.168 0.182
San Fernando (71-2-9)	6.4	288	Soil	44.0	F086	N83W S07W	0.111 0.085
San Fernando (71-2-9)	6.4	281	Soil	80.2	E087	S04E S86W	0.029 0.029
San Fernando (71-2-9)	6.4	122	Soil	27.4	F088	S70E S20W	0.274 0.227
San Fernando (71-2-9)	6.4	175	Soil	39.3	F089	S53E S37W	0.141 0.152
San Fernando (71-2-9)	6.4	190	Soil	37.3	F092	S62E S28E	0.071 0.083
San Fernando (71-2-9)	6.4	143	Soil	34.9	F095	S88E S02W	0.100 0.091
San Fernando (71-2-9)	6.4	166	Soil	38.0	F098	S53E S37W	0.252 0.206
San Fernando (71-2-9)	6.4	113	Soil	96.7	F101	S00W N90E	0.039 0.034
San Fernando (71-2-9)	6.4	1096	Soil	65.5	F102	N00E N90E	0.028 0.023
San Fernando (71-2-9)	6.4	269	Soil	36.7	F103	N00E N90W	0.103 0.148

TABLE I-1 (continued)

Earthquake	Richter Magnitude (M_L)	Recording Station (USGS No)	Site Classif.	Source Distance (km)	C.I.T. No.	Comp.	Peak Acc'n (g)
San Fernando (71-2-9)	6.4	1052	Soil	53.1	F104	N00E	0.087
						N90W	0.112
San Fernando (71-2-9)	6.4	140	Soil	35.8	F105	S00W	0.095
						N90E	0.089
San Fernando (71-2-9)	6.4	266	Rock	29.0	G106	S00W	0.096
						S90W	0.204
San Fernando (71-2-9)	6.4	475	Soil	32.0	G107	N00E	0.103
						N90E	0.114
San Fernando (71-2-9)	6.4	264	Soil	31.8	G108	N00E	0.206
						N90E	0.189
San Fernando (71-2-9)	6.4	267	Soil	23.7	G110	S82E	0.215
						S08W	0.160
San Fernando (71-2-9)	6.4	163	Soil	37.8	G112	N38E	0.106
						N52W	0.088
San Fernando (71-2-9)	6.4	262	Soil	27.6	G114	S60E	0.118
						S30W	0.150
San Fernando (71-2-9)	6.4	466	Soil	26.5	H115	N11E	0.225
						N79W	0.152
San Fernando (71-2-9)	6.4	244	Soil	47.5	H118	S45E	0.035
						S45W	0.034
San Fernando (71-2-9)	6.4	482	Soil	36.1	H121	S90W	0.121
						S00W	0.117

TABLE I-1 (continued)

Earthquake	Richter Magnitude (M_L)	Recording Station (USGS No)	Site Classif.	Source Distance (km)	C.I.T. No.	Comp.	Peak Acc'n (g)
San Fernando (71-2-9)	6.4	476	Soil	67.6	H124	S90W S00W	0.035 0.040
San Fernando (71-2-9)	6.4	452	Soil	34.6	I128	N00E S90W	0.062 0.099
San Fernando (71-2-9)	6.4	455	Soil	35.6	I131	N50E N40W	0.202 0.170
San Fernando (71-2-9)	6.4	425	Soil	36.3	I134	N54E S36E	0.103 0.090
San Fernando (71-2-9)	6.4	461	Soil	26.3	I137	S81E S09W	0.148 0.135
San Fernando (71-2-9)	6.4	125	Soil	33.0	J141	N21E S69E	0.152 0.115
San Fernando (71-2-9)	6.4	126	Rock	30.2	J142	S69E S21W	0.200 0.159
San Fernando (71-2-9)	6.4	127	Rock	27.1	J143	N21E N69W	0.147 0.131
San Fernando (71-2-9)	6.4	128	Rock	23.4	J144	N21E N69W	0.374 0.288
San Fernando (71-2-9)	6.4	458	Soil	21.5	J145	S00W S90W	0.118 0.111
San Fernando (71-2-9)	6.4	431	Soil	36.3	J148	N00E S90W	0.116 0.117

TABLE I-1 (continued)

Earthquake	Richter Magnitude (M_L)	Recording Station (USGS No)	Site Classif.	Source Distance (km)	C.I.T. No.	Comp.	Peak Acc'n (g)
San Fernando (71-2-9)	6.4	1039	Rock	140.0	K162	N14E N76W	0.008 0.010
San Fernando (71-2-9)	6.4	220	Soil	28.1	L166	N00E S90W	0.181 0.154
San Fernando (71-2-9)	6.4	280	Soil	131.2	L171	N33E N57W	0.014 0.016
San Fernando (71-2-9)	6.4	437	Soil	38.3	M176	N37E S53E	0.088 0.123
San Fernando (71-2-9)	6.4	1027	Rock	70.2	M179	S00W N90E	0.026 0.057
San Fernando (71-2-9)	6.4	472	Soil	76.3	M180	S00W S90W	0.026 0.033
San Fernando (71-2-9)	6.4	290	Soil	60.3	M183	N65W N25E	0.047 0.057
San Fernando (71-2-9)	6.4	290	Soil	60.3	M184	S65E S25W	0.052 0.063
San Fernando (71-2-9)	6.4	287	Rock	61.4	N187	N75W N15E	0.058 0.081
San Fernando (71-2-9)	6.4	440	Soil	36.4	N188	N54E N36W	0.117 0.129
San Fernando (71-2-9)	6.4	411	Soil	65.0	N191	N65E S25E	0.025 0.043

TABLE I-1 (continued)

Earthquake	Richter Magnitude (M_L)	Recording Station (USGS No)	Site Classif.	Source Distance (km)	C.I.T. No.	Comp.	Peak Acc'n (g)
San Fernando (71-2-9)	6.4	449	Soil	36.6	N192	N29E N61W	0.104 0.107
San Fernando (71-2-9)	6.4	465	Soil	114.4	N195	N33E N57W	0.044 0.034
San Fernando (71-2-9)	6.4	132	Soil	69.5	N196	N76W S14W	0.036 0.038
San Fernando (71-2-9)	6.4	141	Rock	30.2	0198	S00W S90W	0.188 0.180
San Fernando (71-2-9)	6.4	469	Soil	37.7	0199	N28E N62W	0.144 0.259
San Fernando (71-2-9)	6.4	111	Rock	88.4	0202	S85E S85W	0.021 0.016
San Fernando (71-2-9)	6.4	131	Soil	68.9	0204	N00E N90E	0.028 0.021
San Fernando (71-2-9)	6.4	130	Soil	69.2	0205	N21W S69W	0.029 0.030
San Fernando (71-2-9)	6.4	274	Soil	97.3	0206	N00E N90E	0.039 0.047
San Fernando (71-2-9)	6.4	121	Rock	36.3	0207	N56E N34W	0.068 0.103
San Fernando (71-2-9)	6.4	282	Soil	126.8	0208	N42E S48E	0.017 0.019

TABLE I-1 (continued)

Earthquake	Richter Magnitude (M_L)	Recording Station (USGS No)	Site Classif.	Source Distance (km)	C.I.T. No.	Comp.	Peak Acc'n (g)
San Fernando (71-2-9)	6.4	123	Soil	140.7	0210	S45E	0.044
						S45W	0.040
San Fernando (71-2-9)	6.4	226	Soil	32.3	P214	S89W	0.162
						S01E	0.167
San Fernando (71-2-9)	6.4	196	Soil	36.3	P217	S00W	0.122
						N90E	0.097
San Fernando (71-2-9)	6.4	114	Soil	88.7	P220	S00W	0.026
						N90E	0.036
San Fernando (71-2-9)	6.4	104	Rock	33.6	P221	N03E	0.172
						N87W	0.223
San Fernando (71-2-9)	6.4	272	Soil	73.2	P222	S00W	0.027
						S90W	0.026
San Fernando (71-2-9)	6.4	278	Rock	54.9	P223	N55E	0.078
						N35W	0.059
San Fernando (71-2-9)	6.4	247	Soil	49.0	P231	N00E	0.045
						S90W	0.041
San Fernando (71-2-9)	6.4	253	Soil	26.7	Q233	S12W	0.263
						N78W	0.207
San Fernando (71-2-9)	6.4	446	Soil	31.9	Q236	EAST	0.172
						SOUTH	0.130
San Fernando (71-2-9)	6.4	416	Soil	35.8	Q239	SOUTH	0.126
						EAST	0.171

TABLE I-1 (continued)

Earthquake	Richter Magnitude (M_L)	Recording Station (USGS No)	Site Classif.	Source Distance (km)	C.I.T. No.	Comp.	Peak Acc'n (g)
San Fernando (71-2-9)	6.4	172	Soil	37.1	Q241	N37E	0.096
						N53W	0.143
San Fernando (71-2-9)	6.4	145	Soil	37.1	R244	N53W	0.156
						S37W	0.132
San Fernando (71-2-9)	6.4	235	Soil	32.5	R246	SOUTH	0.119
						EAST	0.110
San Fernando (71-2-9)	6.4	232	Soil	32.5	R248	SOUTH	0.192
						EAST	0.230
San Fernando (71-2-9)	6.4	184	Soil	36.5	R249	N44E	0.084
						S46E	0.093
San Fernando (71-2-9)	6.4	148	Soil	37.2	R251	N37E	0.208
						S53E	0.189
San Fernando (71-2-9)	6.4	160	Soil	37.4	R253	N30W	0.256
						S60W	0.232
San Fernando (71-2-9)	6.4	443	Soil	36.2	S255	N08E	0.129
						N82W	0.131
San Fernando (71-2-9)	6.4	205	Soil	40.7	S258	N29E	0.063
						S61E	0.086
San Fernando (71-2-9)	6.4	413	Soil	37.0	S261	N59E	0.102
						N31W	0.111
San Fernando (71-2-9)	6.4	202	Soil	36.3	S265	SOUTH	0.111
						WEST	0.132

TABLE I-1 (continued)

Earthquake	Richter Magnitude (M_L)	Recording Station (USGS No)	Site Classif.	Source Distance (km)	C.I.T. No.	Comp.	Peak Acc'n (g)
San Fernando (71-2-9)	6.4	211	Soil	36.4	S266	NORTH	0.167
						WEST	0.135
San Fernando (71-2-9)	6.4	229	Soil	49.1	S267	NORTH	0.058
						EAST	0.069

TABLE I-2

SUMMARY OF DATA USED IN ANALYSIS - NUMBER OF ACCELEROGRAMS OBTAINED DURING SELECTED EARTHQUAKES

Earthquake	Date	Magnitude (M_L)	Number of Accelerograms
Long Beach	33-3-11	6.3	6
Eureka	34-7-6	6.5	2
Lower Calif.	34-12-30	6.5	2
Imperial Valley	40-5-18	6.4	2
Northwest Calif.	41-2-9	6.4	2
Northern Calif.	41-10-3	6.4	2
Borrego Valley	42-10-21	6.5	2
Lower Calif.	54-11-12	6.3	2
Eureka	54-12-21	6.5	4
Gulf of Calif.	66-8-7	6.3	2
Borrego Mtn.	68-4-8	6.4	8
San Fernando	71-2-9	6.4	188

TABLE I-3

SUMMARY OF DATA USED IN ANALYSIS - NUMBER OF ACCELEROGRAMS RECORDED AT SELECTED STATIONS

USGS No.	Station Name	Number of Accelerograms
104	SANTA ANITA RESERVOIR ARCADIA	2
110	OLD RIDGE ROUTE CWR SITE CASTAIC, CA	2
111	ALLEN RANCH, CEDER SPRINGS CWR SITE, CA	2
112	PUMPHOUSE CEDER SPRINGS CWR SITE	2
113	SCE SUBSTATION COLTON CA	2
114	666 W 19TH ST COSTA MESA	2
116	DEVILS CANYON CWR SITE FILTER PLANT, CA	2
117	EL CENTRO IMPERIAL VALLEY IRRIGATION DIST, CA	12
121	FAIRMONT RESERVOIR	2
122	633 E BROADWAY GLENDALE	2
123	HEMET FIRE STATION	2
125	LAKE HUGHES ARRAY #1, CA	2
126	LAKE HUGHES ARRAY STATION #4	2
127	LAKE HUGHES ARRAY STATION #9	2
128	LAKE HUGHES ARRAY STATION #12	2
130	SCE, TERMINAL ISLAND LONG BEACH	2
131	PUBLIC UTILITIES BLDG. LONG BEACH, CA	4
132	HUMANITIES BLDG. LONG BEACH STATE COLLEGE	2
133	HOLLYWOOD STORAGE BLDG. L.A., CA	2
135	HOLLYWOOD STORAGE PE LOT L.A., CA	2
136	SUBWAY TERMINAL BLDG. L.A., CA	2

137	WATER & POWER BLDG. L.A., CA	2
140	UCLA REACTOR LAB	2
141	GRIFFITH PARK OBS L.A., CA	2
143	120 N ROBERTSON L.A., CA	2
145	222 FIGUEROA STREET L.A., CA	2
148	234 FIGUEROA STREET L.A., CA	2
151	250 E FIRST STREET L.A., CA	2
157	445 FIGUEROA STREET L.A., CA	2
160	533 S FREMONT AVENUE L.A., CA	2
163	611 W SIXTH STREET L.A., CA	2
166	646 S OLIVE STREET L.A., CA	2
172	800 W FIRST STREET L.A., CA	2
175	808 S OLIVE STREET L.A., CA	2
181	1640 MARENGO L.A., CA	2
184	1900 AVENUE OF THE STARS L.A., CA	2
187	1901 AVENUE OF THE STARS L.A., CA	2
190	2011 ZONAL AVEUNE L.A., CA	2
196	3345 WILSHIRE BOULEVARD L.A., CA	2
199	3407 W. SIXTH STREET L.A., CA	2
202	3411 WILSHIRE BOULEVARD L.A., CA	2
205	3440 UNIVERSITY USC	2
208	3470 WILSHIRE BOULEVARD L.A., CA	2
211	3550 WILSHIRE BOULEVARD L.A., CA	2
217	3710 WILSHIRE BOULEVARD L.A., CA	2
220	3838 LANKERSHIM BOULEVARD L.A., CA	2
223	4680 WILSHIRE BOULEVARD L.A., CA	2

226	4867 SUNSET BOULEVARD L.A., CA	2
229	5250 CENTURY BOULEVARD L.A., CA	2
232	6430 SUNSET BOULEVARD L.A., CA	2
235	6464 SUNSET BOULEVARD L.A., CA	2
238	7080 HOLLYWOOD BOULEVARD L.A., CA	2
241	8244 ORION BOULEVARD L.A., CA	2
244	8639 LINCOLN AVEUNE L.A., CA	2
247	9841 AIRPORT BOULEVARD L.A., CA	2
253	14724 VENTURA BOULEVARD L.A., CA	2
262	PALMDALE FIRE STATION	2
264	MILLIKAN LIBRARY, CIT PASADENA, CA	2
266	OLD SEISM LAB CIT	2
267	JPL CIT PASADENA, CA	2
269	PEARBLOSSOM PUMPING PLANT GROUND STATION	2
272	NAVAL RESRCH & EVAL LAB PORT HUENEME, CA	2
274	HALL OF RECORDS SAN BERNARDINO, CA	2
277	SAN DIEGO LIGHT & POWER BLDG., CA	2
278	PUDDINGSTONE DAM ABUTMENT SAN DIMAS, CA	2
279	PACOIMA DAM ABUTMENT, CA	2
280	SAN ONOFRE SCE NUCLEAR POWER PLANT STATION	4
281	ORANGE CO ENG BLDG. SANTA ANA, CA	2
282	FLUID MECH LAB UC SANTA BARBARA GOLETA	2
287	SAN ANTONIO DAM UPLAND	2
288	CMD BLDG. VERNON, CA	4
290	6074 PARK DRIVE WRIGHTWOOD, CA	4
411	2516 VIA TEJON PALOS VERDES ESTATES	2

413	1177 BEVERLY DRIVE L.A., CA	2
416	9100 WILSHIRE BOULEVARD BEVERLY HILLS	2
425	1800 CENTURY PARK E L.A., CA	2
431	616 S NORMANDIE AVENUE L.A., CA	2
437	1150 S HILL STREET L.A., CA	2
440	1880 CENTURY PARK EAST L.A., CA	2
443	6200 WILSHIRE BOULEVARD L.A., CA	2
446	1760 ORCHID STREET L.A., CA	2
449	2500 WILSHIRE BOULEVARD L.A., CA	2
452	435 N OAKHURST BEVERLY HILLS	2
455	450 ROXBURY BEVERLY HILLS	2
458	15107 VANOWEN STREET L.A., CA	2
461	15910 VENTURA BOULEVARD L.A., CA	2
465	CITY HALL SAN JUAN CAPISTRANO	2
466	15250 VENTURA BOULEVARD L.A., CA	2
469	1625 OLYMPIC BOULEVARD L.A., CA	2
472	1 CITY BOULEVARD ORANGE, CA	2
476	2600 NUTWOOD AVENUE FULLERTON, CA	2
482	900 N FREEMONT AVENUE ALHAMBRA, CA	2
1022	EUREKA FEDERAL BLDG., CA	2
1023	FERNDALE CITY HALL, CA	8
1027	TEHACHAPI PUMPING PLANT GORMON	2
1039	ISABELLA AUX DAM ABUTMENT	2
1052	OSO PUMPING PLANT (GORMAN)	2
1096	FORT TEJON	2
1102	WHEELER RIDGE GROUND STATION	2

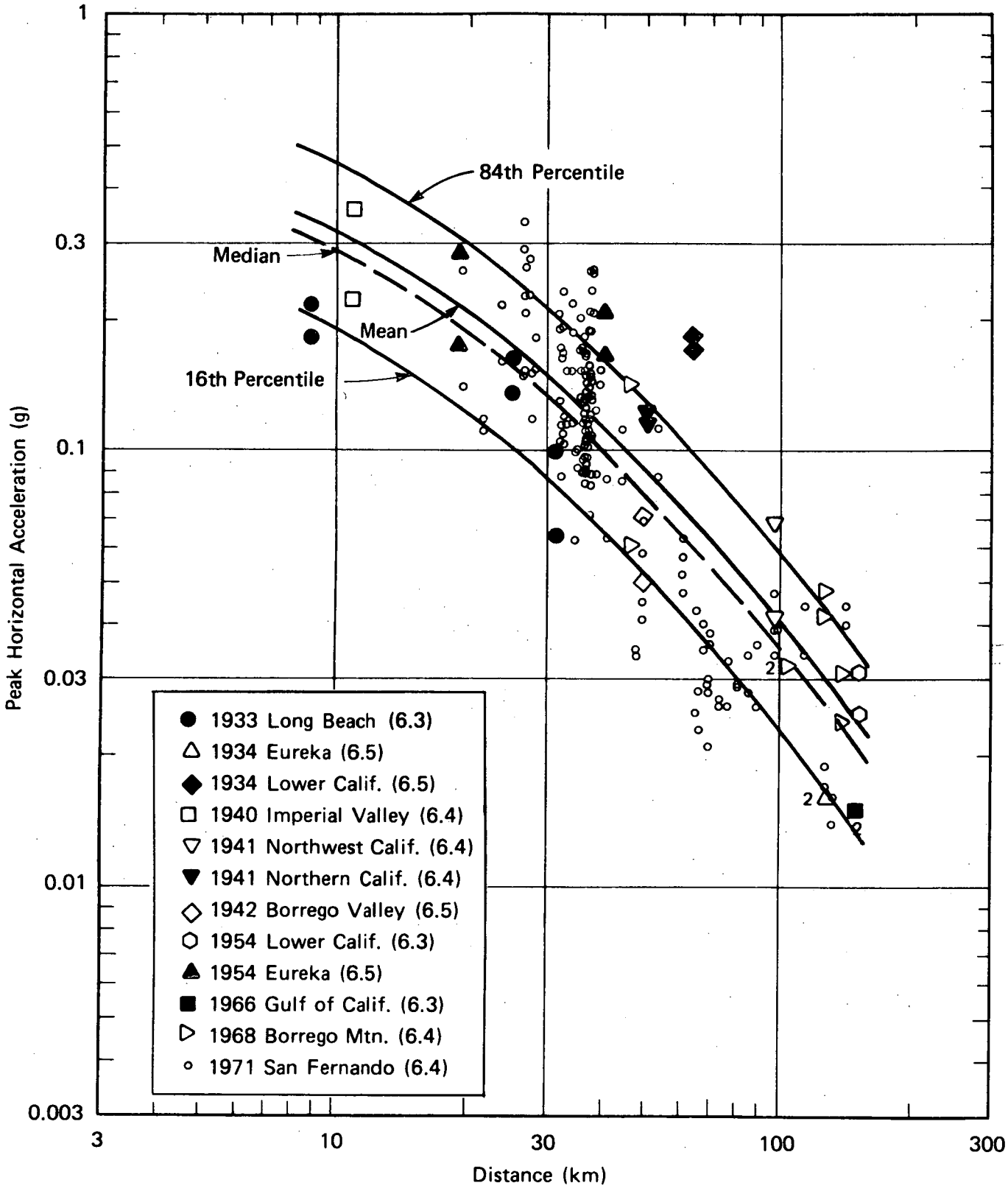

RESULTS OF REGRESSION ANALYSIS
FOR PEAK ACCELERATION –
MAGNITUDE ≈ 6.5, SOIL SITES
SONGS 2 & 3

Project No. 411001
Woodward-Clyde Consultants

Figure I-1

APPENDIX J
DEVELOPMENT OF ATTENUATION RELATIONSHIPS FOR SONGS

J-1 BASIC CONSIDERATIONS IN SELECTING DATA BASE

J-1.1 Factors Affecting Earthquake Ground Motions

The ground motion that occurs at a site during an earthquake is the result of complex interactions among several factors. In the most general way the earthquake ground motions are affected by source factors, travel path, and local conditions. A brief review of each of these factors is given below.

Source factors include stress conditions at the source, type of faulting, rupture dimensions, source depth, rupture propagation, directivity, radiation pattern, etc. At the present time magnitude is the most widely used source parameter in empirically derived expressions for earthquake ground motions. Recent studies (Patwardhan and others, 1978; Idriss, 1978) examining (individually and statistically) recordings from shallow-focus and deep-focus earthquakes have defined a significant effect of source depth on characteristics of ground motions.

Travel path factors include geometric spreading, absorption, inhomogenieties, phase conversion of body waves to surface waves, etc. At the present time, distance is the only parameter used in empirical expressions to describe the effects of travel path on earthquake ground motions.

Factors that can be attributed to local conditions include: subsurface conditions, topographic variations, soil-structure interaction, etc. In currently available empirical expressions only subsurface conditions have been treated in any detail. Recently, a few studies have been made to examine the effects of topography and soil-structure interaction.

J-1.2 Strong Motion Records Selected for Analysis

Recorded data used in developing attenuation relationships for peak acceleration and response spectral velocity were selected using the following criteria:

Consideration of Source Factors:

The accelerograms were recorded during earthquakes of magnitude (M_L) ≃6.5, and the earthquakes were shallow (focal depths less than 20 km for the records used).

Consideration of Travel-Path Factors:

The accelerograms were from strong motion recordings from the Western United States (i.e., the same geographic locale), and the recordings were obtained at distances from the earthquake source not greater than about 130 km.

Consideration of Local Conditions:

The accelerograms were recorded on sites having subsurface conditions generally similar to those at the site of San Onofre Nuclear Generating Station (i.e., deep, very stiff soil sites). Furthermore, the accelerograms were obtained at or near the ground surface in ground floors or basements of buildings or in "free-field" conditions.

Other Considerations:

To the extent possible with available data, a variety of earthquakes and recording stations were represented in the data set. Also to the extent possible, the records were fairly uniformly distributed within the distance range. The accelerograms were uniformly processed using a standard procedure (CIT, 1971-75).

The selected records are summarized in Table J-1. The data set consists of 56 accelerograms obtained during seven earthquakes in

the magnitude (M_L) range 6.3 to 6.5 (see Table J-2) at 22 recording stations (see Table J-3) having site conditions generally similar to the SONGS site.

The definition of distance used in the study is the closest inclined distance from the recording station to a horizontal line on the fault rupture surface that passes through the approximate center of energy release. In general, sufficient information was available on the depth, lateral extent, and geometry of faulting to estimate this distance. However, for records at some stations, particularly the northern California stations at Eureka and Ferndale, this distance is undefined. In these cases, hypocentral distance was used.

J-2 DATA-ANALYSIS PROCEDURE AND ANALYSIS RESULTS

J-2.1 Data-Analysis Procedure

Attenuation relationships for peak acceleration and response spectral velocities (damping = 0.02) in the period range 0.04 to 2 seconds were derived through regression analyses of peak acceleration and response spectral values for the selected accelerograms. A regression equation of the following form was used:

$$\begin{Bmatrix} a \\ S_v \end{Bmatrix} = \alpha' \, (R+C)^{\beta} \, \varepsilon' \qquad \text{(J-1)}$$

where a = peak acceleration in g's

S_v = Spectral velocity in cm/sec (damping = 0.02) at period T

R = Source-to-site distance in km

α' and β = Regression coefficents

C = Magnitude-dependent constant

ε' = Random error term

The parameter C is essentially a normalizing parameter for distance; it has the effect of constraining values of peak

acceleration or spectral velocity to physically reasonable values at very close distances (within a few kilometers) from the earthquake source. Its use in attenuation relationships was initially proposed by Esteva (1970). As discussed in Appendix I, for magnitude M_L 6.5, a value of C equal to 20 is appropriate. This value of C was used in the present analyses.

Taking natural logarithms of both sides in Equation J-1

$$\ln \left\{ \begin{matrix} a \\ S_v \end{matrix} \right\} = \alpha + \beta \ln (R+C) + \varepsilon \qquad \text{(J-2)}$$

where $\alpha = \ln \alpha'$

$\varepsilon = \ln \varepsilon'$

Of the 56 accelerograms (Table J-2) selected to most nearly match the OZD situation, 42 were obtained during the 1971 San Fernando earthquake. Consequently, regression coefficients derived from using the total data set would be biased by that earthquake. For this reason, the attenuation relationships for peak acceleration and response spectra were developed by a weighted regression analysis in which a weight is assigned to each data point such that in given distance intervals the influence of each earthquake is represented equally in the analysis. The general procedure is as follows: (1) the distance to the zone of energy release is divided into discrete intervals; (2) for a given distance interval, the number of data points from each earthquake is determined; (3) since it is desired that each earthquake should have the same influence on the regression equation, a weight of $(1/n_i)$, where n_i is the number of data points for the i^{th} earthquake in the given distance interval, is assigned to each data point for the i^{th} earthquake; and (4) weighted regression analysis is then carried out to obtain estimates of the regression coefficients and standard error. The effect of the weights on the regression analysis is that the square of the deviation of the observed data value from the predicted value is

multiplied by the weight of the data point to obtain the contribution of the point to the total sum of squares of deviations. It is this total sum which is minimized to obtain the regression equation.

The discrete distance intervals were selected to be equally spaced on a logarithmic scale. The selected distance intervals as well as the number of data points in each interval from various earthquakes (listed in Table J-1) are as follows:

Distance Range	Earthquake (Number of Data Points)
10 - 14.1 km	None
14.1 - 20 km	1954 Eureka (2); 1971 San Fernando (2)
20 - 28.1 km	1933 Long Beach (2); 1971 San Fernando (6)
28.1 - 40 km	1971 San Fernando (20)
40 - 56.6 km	1941 Northern California (2); 1954 Eureka (2); 1971 San Fernando (4)
56.6 - 80 km	1971 San Fernando (6)
80 - 113.1 km	1941 Northwest California (2); 1971 San Fernando (2)
113.1 - 160 km	1934 Eureka (2); 1968 Borrego Mountain (2); 1971 San Fernando (2)

As an example, following the general guidelines for the weighted regression anlyses described previously, in the distance interval range of 28.1 to 40 km, a weight of (1/20) was applied to each of the 20 data points from the 1971 San Fernando earthquake; whereas, in the distance range of 40 to 56.6 km, weights of (1/2), (1/2) and (1/4) were applied to data from the 1941 Northern California earthquake, the 1954 Eureka earthquake, and the 1971 San Fernando earthquake, respectively.

J-2.2 Results of Regression Analysis for Peak Acceleration

The regression analyses provided estimates of the regression coefficients α' and β, as well as estimates (s^2) of the variance (σ^2) about the regressions (where s is the estimate of the standard error of prediction in ln a). The attenuation relationship is of the form:

$$\hat{a} = \alpha' (R+20)^{\beta} \text{ (Median)} \qquad \text{(J-3)}$$

from which the mean and 84th percentile relationships are obtained as:

$$\bar{a} = \hat{a}\, e^{s^2/2} \text{ (Mean)} \qquad \text{(J-4)}$$

$$a = \hat{a}\, e^{s} \text{ (84th Percentile)} \qquad \text{(J-5)}$$

The relationships for mean and 84th percentile values for peak acceleration are as follows:

$$a = 161\ (R+20)^{-1.75} \text{ (Mean)} \qquad \text{(J-6a)}$$

$$a = 220\ (R+20)^{-1.75} \text{ (84th Percentile)} \qquad \text{(J-6b)}$$

The attenuation relationships for peak acceleration are presented in Figure J-1 together with the data used in deriving these relationships (from the records in Table J-1).

J-2.3 Results of Regression Analyses for Spectral Velocities

Regression analyses were conducted using the pseudo-relative velocity data corresponding to the records summarized in Table J-1. Attenuation relationships were derived for a total of 25 individual periods in the period range 0.04 to 2 seconds. Relationships for mean and 84th percentile values were obtained using relationships similar to Equations J-4 and J-5.

For a selected period (T = 0.1 sec) the relationships for mean and 84th percentile are given below.

$$S_v\ (\beta=0.02,\ T=0.1\ \text{sec}) = 6900\ (R+20)^{-1.89} \quad \text{(Mean)} \qquad \text{(J-7a)}$$

$$S_v\ (\beta=0.02,\ T=0.1\ \text{sec}) = 9310\ (R+20)^{-1.89} \quad \text{(84th Percentile)} \qquad \text{(J-7b)}$$

Plots of these relationships together with the data used in deriving these relationships are presented in Figure J-2. The complete spectra, for all periods considered, are given in Figure 10 of the main text of this report.

TABLE J-1

LIST OF RECORDS USED IN ANALYSIS

Earthquake (Date)	Richter Magnitude (M_L)	Recording Station (USGS No)	Source Distance (km)	C.I.T. No	Comp.	Peak Acc'n (g)
Long Beach (33-3-11)	6.3	288	25	B021	S08W	0.135
					N82W	0.163
Eureka (34-7-6)	6.5	1023	128	U294	N45W	0.016
					S45W	0.016
Northwest Ca. (41-2-9)	6.4	1023	97	B027	N45E	0.068
					S45E	0.042
Northern Ca. (41-10-3)	6.4	1023	50	U300	N45W	0.123
					S45W	0.115
Eureka (54-12-21)	6.5	1022	18.9	A008	N11W	0.175
					N79E	0.283
Eureka (54-12-21)	6.5	1023	40.2	A009	N44E	0.166
					N46W	0.209
Borrego Mt. (68-4-8)	6.4	280	125	B040	N33E	0.042
					N57W	0.048
San Fernando (71-2-9)	6.4	241	19.3	C048	N00W	0.258
					S90W	0.140
San Fernando (71-2-9)	6.4	157	37.4	C054	N52W	0.150
					S38W	0.130
San Fernando (71-2-9)	6.4	110	26.6	D056	N21E	0.335
					N69W	0.289

TABLE J-1 (continued)

Earthquake (Date)	Richter Magnitude (M_L)	Recording Station (USGS No)	Source Distance (km)	C.I.T. No.	Comp.	Peak Acc'n (g)
San Fernando (71-2-9)	6.4	137	37.4	E078	N50W S40W	0.137 0.188
San Fernando (71-2-9)	6.4	288	44.0	F086	N83W S07W	0.111 0.085
San Fernando (71-2-9)	6.4	190	37.3	F092	S62E S28W	0.071 0.083
San Fernando (71-2-9)	6.4	1052	53.1	F104	N00E N90W	0.087 0.112
San Fernando (71-2-9)	6.4	264	31.8	G108	N00E N90E	0.206 0.189
San Fernando (71-2-9)	6.4	267	23.7	G110	S82E S08W	0.215 0.160
San Fernando (71-2-9)	6.4	431	36.3	J148	N00E S90W	0.116 0.117
San Fernando (71-2-9)	6.4	220	28.1	L166	N00E S90W	0.181 0.154
San Fernando (71-2-9)	6.4	280	131.2	L171	N33E S57W	0.014 0.016
San Fernando (71-2-9)	6.4	472	76.3	M180	S00W S90W	0.026 0.033
San Fernando (71-2-9)	6.4	290	60.3	M183	N65W N25E	0.047 0.057

TABLE J-1 (continued)

Earthquake (Date)	Richter Magnitude (M_L)	Recording Station (USGS No)	Source Distance (km)	C.I.T. No.	Comp.	Peak Acc'n (g)
San Fernando (71-2-9)	6.4	290	60.3	M184	S65E S25W	0.052 0.063
San Fernando (71-2-9)	6.4	449	36.6	N192	N29E N61W	0.104 0.107
San Fernando (71-2-9)	6.4	114	88.7	P220	S00W N90E	0.026 0.036
San Fernando (71-2-9)	6.4	172	37.1	Q241	N37E N53W	0.096 0.143
San Fernando (71-2-9)	6.4	145	37.1	R244	N53W S37W	0.156 0.132
San Fernando (71-2-9)	6.4	148	37.2	R251	N37E S53E	0.208 0.189
San Fernando (71-2-9)	6.4	443	36.2	S255	N08E N82W	0.129 0.131

TABLE J-2

SUMMARY OF DATA USED IN ANALYSIS - NUMBER OF ACCELEROGRAMS OBTAINED DURING SELECTED EARTHQUAKES

Earthquake	M_L	M_s	Number of Accelerograms
Long Beach (33-3-11)	6.3	6.3	2
Eureka (34-7-6)	6.5	-	2
Northwest Calif. (41-2-9)	6.4	-	2
Northern Calif. (41-10-3)	6.4	-	2
Eureka (54-12-21)	6.5	6.6	4
Borrego Mountain (68-4-8)	6.4	6.7	2
San Fernando (71-2-9)	6.4	6.6	42

TABLE J-3

SUMMARY OF DATA USED IN ANALYSIS - NUMBER OF ACCELEROGRAMS RECORDED AT SELECTED STATIONS

USGS No.	Station Name	Number of Accelerograms
110	Castaic, Old Ridge Route	2
114	Costa Mesa, 666 W 19th	2
137	Los Angeles, Water & Power Building	2
145	Los Angeles, 222 Figueroa	2
148	Los Angeles, 234 Figueroa	2
157	Los Angeles, 445 Figueroa	2
172	Los Angeles, 800 W. First Street	2
190	Los Angeles, 2011 Zonal	2
220	Los Angeles, 3838 Lankershim	2
241	Los Angeles, 8244 Orion Boulevard	2
264	Pasadena, Millikan Lib., CIT	2
267	Pasadena, 4800 Oak Grove (JPL)	2
280	San Onofre Nuclear Power Plant	4
288	Vernon, CMD Terminal Building	4

TABLE J-3 (continued)

USGS No.	Station Name	Number of Accelerograms
290	Wrightwood, 6074 Park Drive	4
431	Los Angeles, 616 S. Normandie	2
443	Los Angeles, 6200 Wilshire	2
449	Los Angeles, 2500 Wilshire	2
472	Orange, 1 City Boulevard	2
1022	Eureka Federal Building	2
1023	Ferndale, Old City Hall	8
1052	Oso Pumping Plant (Gorman)	2

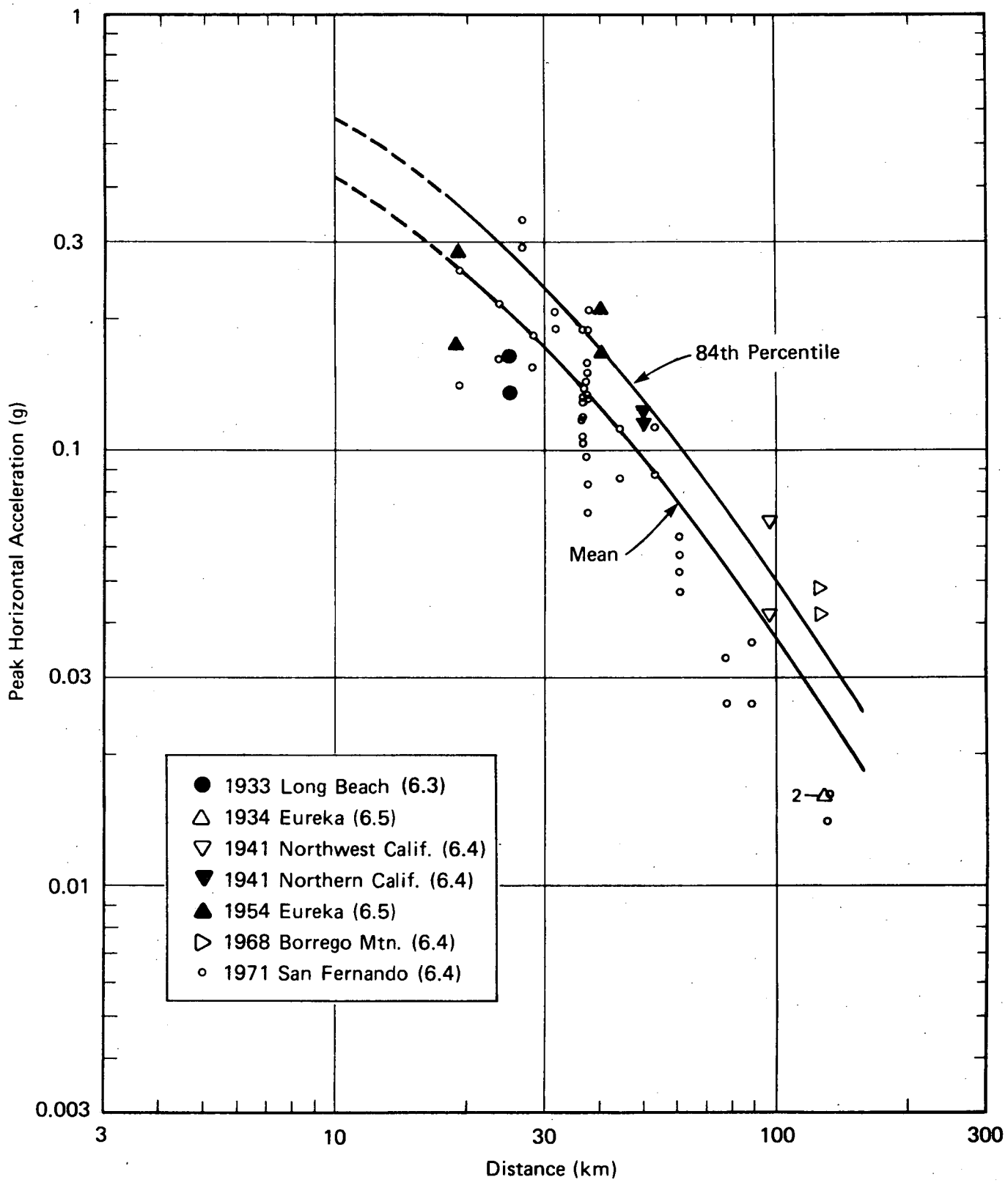

RESULTS OF SITE-SPECIFIC REGRESSION ANALYSIS FOR PEAK ACCELERATION – MAGNITUDE ≈ 6.5
SONGS 2 & 3

Project No. 41100I
Woodward-Clyde Consultants

Figure J-1

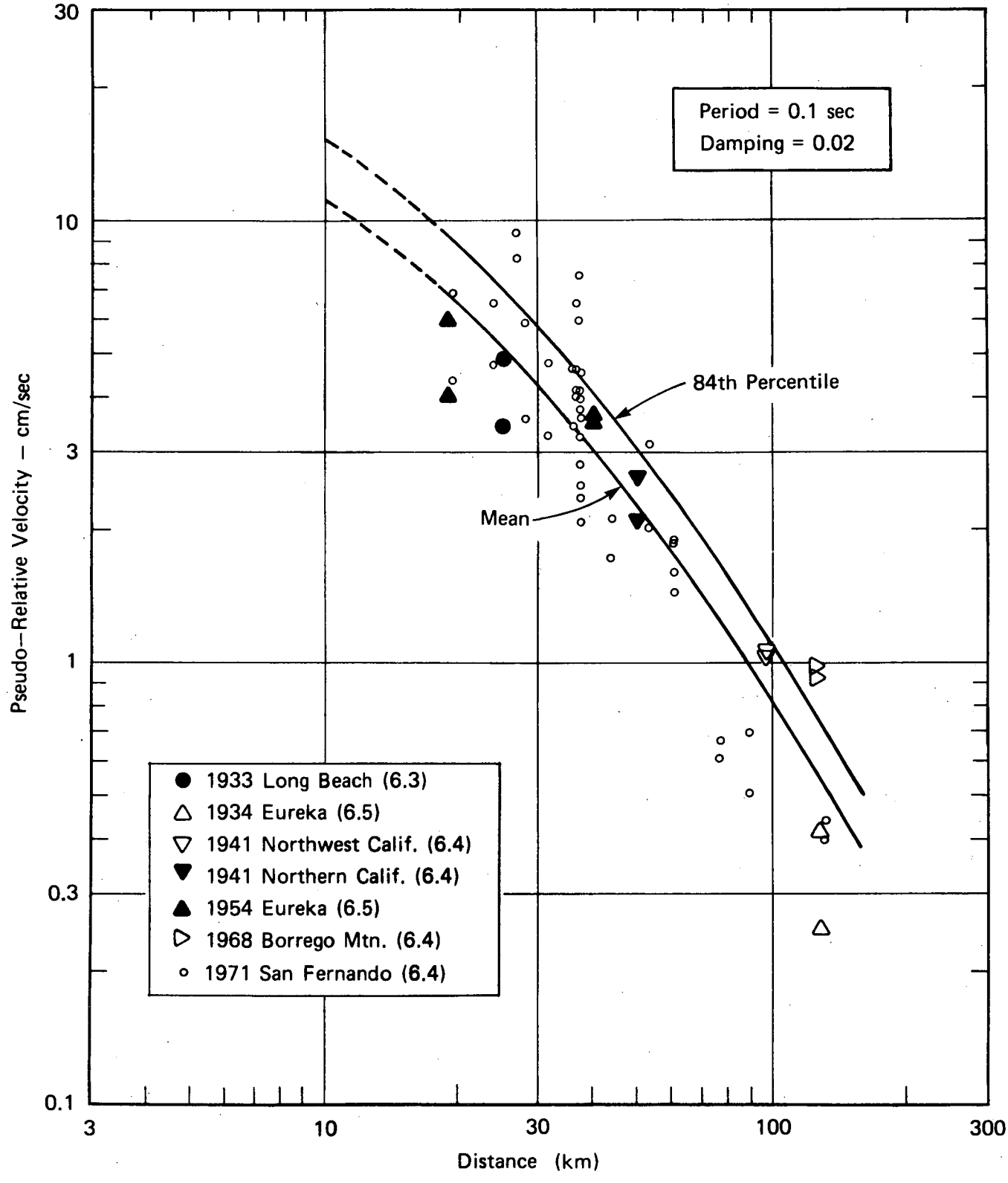

RESULTS OF SITE-SPECIFIC REGRESSION ANALYSIS FOR SPECTRAL VELOCITY (T = 0.1 sec) – MAGNITUDE ≈ 6.5 SONGS 2 & 3

Project No. 411001
Woodward-Clyde Consultants

Figure J-2

REFERENCES

Abe, K., and Kanamori, H., 1979 (in press), Magnitudes of great shallow earthquakes from 1973 to 1977: Submitted to Tectonophysics.

Addicott, W.O., 1968, Mid-Tertiary zoogeographic and paleogeographic discontinuities across the San Andreas fault, California: Proceedings of conference on geologic problems of San Andreas fault system, Stanford University, September 14-16, 1967, Stanford University Publications, v. 11, p. 144-165.

Albee, A.L., and Smith, J.L., 1966, Earthquake characteristics and fault activity in Southern California: Engineering Geology in Southern California, Special Publication, Association of Engineering Geologists, p. 9-33.

Allen, C.R., St. Amand, P., Richter, C.F., and Nordquist, J.M., 1965, Relationship between seismicity and geologic structure in the southern California region: Bulletin of the Seismological Society of America, v. 55, p. 753-797, Cited in Albee, A.L., and Smith, J.L., 1966, Earthquake characteristics and fault activity in southern California, in Lung, R., and Proctor, R., eds., Engineering geology in southern California: Association of Engineering Geologists Special Publication.

Allen, D.R., and Hazenbush, G.C., 1957, Sunset Beach oil field: California Division of Oil and Gas, Summary of Operations, California Oil Fields, v. 43, n. 2, p.47-50.

Ambraseys, N.N., 1970, Some characteristic features of the Anatolian fault zone: Tectonophysics, v. 9, p. 143-165.

Anderson, J.G., 1979, Estimating the seismicity from geological structure for seismic-risk studies: Bulletin of the Seismological Society of America, v. 69, n. 1, p. 135-158.

Artim, E.R., and Pinckney, C.J., 1973, La Nacion fault system, San Diego, California: Geological Society of America Bulletin, v. 84, p. 1075-1080.

Babcock, E.A., 1974, Geology of the northeast margin of the Salton trough, Salton Sea, California: Geological Society of America Bulletin, v. 85, p. 321-332.

Barnes, R.M., and Bowes, G.H., 1930, Seal Beach oil field: California Division of Oil and Gas, Summary of Operations, California Oil Fields, v. 16, n. 2.

Barrows, A.G., 1974, A review of the geology and earthquake history of the Newport-Inglewood structural zone, southern California: California Division of Mines and Geology Special Report 114, 115p.

Barrows, A.G., Kahle, J.E., and Beeby, D.J., 1976, Geology of the fault activity of the Palmdale segment of the San Andreas fault zone, Los Angeles County, California: California Division of Mines and Geology, Open File Report 76-6, 30p.

Benioff, H., 1938, The determination of the extent of faulting with application to the Long Beach earthquake: Bulletin of the Seismological Society of America, v. 28, p. 77-84.

Ben-Menahem, A., Nur, A., and Vered, M., 1976, Tectonics, seismicity and structure of the Afro-Eurasian junction - The breaking of an incoherent plate: Physics of the Earth and Planetary Interiors, v. 12, p. 1-50.

Blume, J.A., 1977a, Allowable stresses and earthquake performance: Proceedings of the Sixth World Conference on Earthquake Engineering, New Delhi, India.

Blume, J.A., 1977b, The SAM procedure for site-acceleration-magnitude relatonships: Proceedings of the Sixth World Conference on Earthquake Engineering, New Delhi, India, v. 1, p. 416-422.

Blume, J.A., 1978, Instrumental versus effective acceleration: D-LL26, U.S. Nuclear Regulatory Commission.

Bolt, B.A., 1978, Incomplete formulations of the regression of earthquake magnitude with surface fault rupture length: Geology, v. 6, p. 233-235.

Bolt, B.A., and Miller, R.D., 1971, Seismicity of northern and central California, 1965-1969: Bulletin of the Seismological Society of America, v. 61, n. 6, p. 1831-1847.

Boore, D.M., Oliver, A.A., Page, R.A., and Johner, W.B., 1978, Estimation of ground motion parameters: United States Department of the Interior, Geological Survey, open-file report 78-509.

Bowes, G.H., 1943, Seal Beach oil field, in Chapter VIII, Los Angeles Basin and southernmost California, in Geologic formations and economic development of the oil and gas fields of California: California Division of Mines and Geology Bulletin 118, p. 325-328.

Brune, J.N., 1968, Seismic moment, seismicity, and rate of slip along major fault zones: Journal of Geophysical Research, v. 73, n. 2, p. 777-784.

Buffington, E.C., 1963, Structural control and precision bathymetry of La Jolla submarine canyon, California: Marine Geoloy, v. 1, p. 44-58.

Burke, D.B., and Helley, E.J., 1973, Map showing evidence for recent fault activity in the vicinity of Antioch, Contra Costa County, California: U.S. Geological Survey Miscellaneous Field Studies Map MF-533, Scale 1:24,000.

Burke, D.B., Hite, J.S., Hedel, C.W., Clark, M.M., and Rust, D.J., 1979, Log of a trench in the Garlock fault zone, Fremont Valley, California: U.S. Geological Survey, Miscellaneous Field Studies Map MF-1028.

California Department of Water Resources, 1964a, Crustal strain and fault movement investigation: California Department of Water Resources Bulletin 116-2, 96p., cited in Albee, A.L., and Smith, J.L., 1966, Earthquake characteristics and fault activity in southern California, in Lung, R. and Proctor, R., eds., Engineering geology in southern California: Association of Engineering Geologists Special Publication.

California Department of Water Resources, 1966, Santa Ana gap salinity barrier, Orange County, Bulletin 147-1.

California Department of Water Resources, 1968, Sea water intrusion: Bolsa-Sunset area, California, Bulletin 63-2, 167p.

California Division of Oil and Gas, 1974, California oil and gas fields, v. 2, South, central, coastal and offshore California, report no. TR12.

California Institute of Technology, 1971-1975, Strong motion earthquake accelerograms, digitized and plotted data, Vol. I - uncorrected accelerograms: Pasadena, California.

California Institute of Technology, 1971-1975, Strong motion earthquake accelerograms, digitized and plotted data, Vol. II - corrected accelerograms and integrated ground velocity and displacement curves: Pasadena, California.

Caputo, M., 1976, The Nector Terrace in the Del Mar and Encinitas quadrangles, San Diego, County, California: San Diego State University, Geology Department, unpublished senior research paper.

Carriel, J.T., 1942, Huntington Beach oil field, oil field portion: California Division of Oil and Gas, Summary of Operation, California Oil Fields, v. 28, n 1.

Castle, R.O., and Yerke, R.F., 1976, Recent surface movements in the Baldwin Hills, Los Angeles County, California: U.S. Geological Survey Professional Paper 882, 125p.

Castle, R.O., 1960, Geologic map of the Baldwin Hills area, California: U.S. Geological Survey Open File Report, Scale 1;24,000.

Castle, R.O., 1966, Preliminary study of the geology at two proposed sites for a nuclear-powered desalting plant near Sunset Beach and Pelican Point, Orange County, California: U.S. Geological Survey Open File Report, 73p.

Chinnery, M.A., 1979, Investigations of the seismological input to the safety design of nuclear power reactors in New England: Annual report to the Nuclear Regulatory Commission, NUREG/CR-0563 RA, MIT, available from NTIS.

Christoffel, D.A., 1971, Motion at the New Zealand Alpine fault deduced from the pattern of sea-floor spreading - recent crustal movements: Royal Society of New Zealand Bulletin, p. 25-30.

Clark, M.M., Grantz, A., and Rubin, M., 1972, Holocene activity of the Coyote Creek fault as recorded in sediments of Lake Cahuilla, in The Borrego Mountain Earthquake of April 9, 1968: U.S. Geological Survey Professional Paper 787, p. 112-130.

Clark, R.H., and Wellman, H.W., 1959, The Alpine fault from Lake McKerrow to Milford Sound: New Zealand Journal of Geology and Geophysics, v. 2, p. 590-601, cited in Scholz, C.H., Rynn, J.M., Weed, R.W., and Frohlich, C., 1973, Detailed seismicity of the Alpine fault zone and Fiordland region, New Zealand: Geological Society of America Bulletin, v. 84, p. 3297-3316.

Clarke, S.H., Jr., and Nilsen, T.H., 1973, Displacement of Eocene strata and implications for the history of offset along the San Andreas fault, central and northern California: Proceedings of the conference on tectonic problems of the San Andreas fault system, Stanford University, June 20-23, 1973, Stanford University Publications, v. 13, p. 358-367.

Clayton, L., 1966, Tectonic depressions along the Hope fault, a transcurrent fault in North Canterbury, New Zealand: New Zealand Journal of Geology and Geophysics, v. 9, p. 95-104, cited in, Scholz, C.H., Rynn, J.M., Weed, R.W., and

Frohlich, C., 1973, Detailed seismicity of the Alpine fault zone and Fiordland region, New Zealand: Geological Society of America Bulletin, v. 84, p. 3297-3316.

Cleveland, G.B., 1960, Geology of the Otay clay deposit, San Diego County, California: California Division of Mines Special Report 64, 16p.

Clifton, H.E., 1968, Possible influence of the San Andreas fault on middle and probable late Miocene sedimentation, southeastern Caliente Range: Proceedings of conference on geologic problems of San Andreas fault system, Stanford University, September 14-16, 1967, Stanford University Publications, v. 11, p. 183-190.

Cluff, L.S., and Hansen, W., 1969, Seismicity and seismic geology of northwestern Venezuela: Woodward-Clyde Consultants report to Shell Oil Company of Venezuela, v. 2, 77p.

Cluff, L.S., 1978, Geologic considerations for seismic microzonation, in Proceedings of the second international conference on microzonation, v. I, San Francisco, California, November 26-December 1, 1978, p. 135-152.

Copp, W.W., and Bowes, G.H., 1927, Seal Beach oil field: California Division of Oil and Gas, Summary of Operations, California Oil Fields, v. 13, n. 3.

Corey, W.H., 1954, Tertiary basins of southern California, in Geology of southern California: California Division of Mines and Geology Bulletin 170, Chap. 3, p. 73-83.

Corwin, C.H., 1946, West Newport oil field: California Division of Oil and Gas, Summary of Operations, California Oil Fields, v. 32, n. 2, p. 8-14.

Crittenden, M.D., Jr., 1951, Geology of the San Jose-Mount Hamilton area, California: California Division of Mines and Geology Bulletin 157, 74p.

Crowell, J.C., 1962, Displacements along the San Andreas fault, California: Geological Society of America Special Paper 71, 61p.

Crowell, J.C., 1973, Problems concerning the San Andreas fault system in southern California: Proceedings of the conference on tectonic problems of the San Andreas fault system, Stanford University, June 20-23, 1973, Stanford University Publications, v. 13, p. 125-135.

Crowell, J.C., 1975, The San Andreas fault in southern California: California Division of Mines and Geology Special Report 118, 271p.

Cummings, J.C., 1968, The Santa Clara formation and possible post-Pliocene slip on the San Andreas fault in central California: Proceedings of conference on geologic problems of San Andreas fault system, Stanford Univeristy, September 14-16, 1967, Stanford University Publications, v. 11, p. 191-207.

Department of Water Resources, 1964, Investigation of failure - Baldwin Hills Reservoir: State of California Resources Agency, 64p.

Dewey, J.W., 1972, Seismicity and tectonics of Western Venezula: Bulletin of the Seismological Society of America, v. 62, n. 6, p. 1711-1751.

Dewey, J.W., 1978 personal communication, National Earthquake Information Center, Golden, Colorado, 303/234-3994.

Dibblee, T.W., Jr., 1975, Tectonics of the western Mojave Desert near the Sn Andreas fault, in San Andreas fault in southern California: California Division of Mines and Geology Special Report 118, p. 155-161.

Dickert, P.F., 1968, Phosphatic facies across the San Andreas fault: Proceedings of conference on geologic problems of the San Andreas fault system, Stanford University, September 14-16, 1967, Stanford University Publications, v. 11, p. 181-182.

Dodd, H.V., 1926, Dominguez oil field: California Division of Oil and Gas, Summary of Operations, California Oil Fields, v. 12, n. 4.

Donovan, N.C., and Bornstein, A.E., 1978, Uncertainties in seismic risk procedures: Journal of the Geotechnical Engineering Division, American Society of Civil Engineers, v. 104, n. GT7, July, p. 869-887.

Driver, H.L., 1943, Inglewood oil field, in Chapter VIII, Los Angeles Basin and southernmost California, in Geologic formations and economic development of the oil and gas fields of California: California Division of Mines and Geology Bulletin 118, p. 306-309.

Dudley, P.H., 1954, Geology of the Long Beach oil field, Los Angeles County: California Division of Mines and Geology Bulletin 170, Map Sheet 34.

Durham, D.L., and Yerkes, R.F., 1964, Geology and oil resources of the eastern Puente Hills area, southern California: U.S. Geological Survey Professional Paper 420-B, 62p.

Ehlig, P.L., 1975, Basement rocks of the San Gabriel Mountains, south of the San Andreas fault, in San Andreas fault in southern California: California Division of Mines and Geology Special Report 118, p. 177-186.

Ehlig, P.L., Ehlert, K.W., and Crowe, B.M., 1975, Offset of the upper Miocene Caliente and Mint Canyon formations along the San Gabriel and San Andreas faults, in San Andreas fault in southern California: California Division of Mines and Geology Special Report 118, p. 83-92.

Elders, W.A., Rex, R.W., Meidav, T., and Robinson, P.T., 1970, Crustal spreading in southern California: The Institute of Geophysics and Planetary Physics, University of California, Riverside, September 1, 1970, 12p.

Elliott, W., 1974, Seismicity of the San Diego region: in Recent geological and hydrologic studies, eastern San Diego County and adjacent areas, Guidebook for the 1974 field trip, San Diego Association of Geologists, p. 61-70.

Emery, K.O., 1960, The sea off southern California: John Wiley and Sons, New York, 366p., cited in Albee, A.L., and Smith, J.L., 1966, Earthquake characteristics and fault activity in southern California, in Lung, R. and Proctor, R., eds, Engineering geology in southern California: Association of Engineering Geologists Special Publication.

Esteva, L., 1970, Seismic risk and seismic design decision: in Hansen, R.J., ed., Seismic design for nuclear power plant: MIT Press, Cambridge, Mass.

Euge, K.M., and Miller, D.S., 1973, Evidence for a possible onshore extension of the Rose Canyon fault in the vicinity of Oceanside, California: Geological Society of America, abstracts with programs, v. 5, n. 1, 39p.

Foster, J.F., 1954, Rosecrans and south Rosecrans oil fields: California Division of Oil and Gas, Summary of Operations, California Oil Fields, v. 40, n. 2.

Freund, R., 1971, The Hope fault: A strike-slip fault in New Zealand: New Zealand Geological Survey Bulletin, n. 5, 86, 49p., cited in Scholz, C.H., Rynn, J.M., Weed, R.W., and Frohlich, C., 1973, Detailed seismicity of the Alpine fault zone and Fiordland region, New Zealand: Geological Society of America Bulletin, v. 84, p. 3297-3316.

Freund, R., Garfunkel, Z., Zak, I., Goldberg, M., Weissbrod, T., and Derin, B., 1970, The shear along the Dead Sea rift: Philosophical Transactions, Royal Society of London, Series A, v. 267, p. 107-130, cited in Ben-Menahem, A., Nur,

A., and Vered, M., 1976, Tectonics, seismicity and structure of the Afro-Eurasian junction - The breaking of an incoherent plate: Physics of the Earth and Planetary Interiors, v. 12, p. 1-50.

Fugro, 1978, High resolution reflection profiles offshore from SONGS site: Report to Southern California Edison.

Futterman, W.I., 1962, Dispersive body waves: Journal of Geophysical Research, v. 67, p. 5279-5291.

Gastil, R.G., Phillips, R.P., and Allison, E.C., 1973, Reconnaissance geologic map of the state of Baja California, Mexico: Geological Society of America Memoir 140.

Geller, R.J., 1976, Scaling relations for earthquake source parameters and magnitude: Bulletin of the Seismological Society of America, v. 66, p. 1501.

Geller, R.J., and Kanamori, H., 1977, Magnitudes of great shallow earthquakes from 1904 to 1952: Bulletin of the Seismological Society of America, v. 67, n. 3, p. 587-598.

Girdler, R.W., 1958, The relationship of the Red Sea to the East Africa rift system: Quarterly Journal of the Geological Society of London, v. 114, p. 79-115, cited in Ben-Menahem, A., Nur, A., and Vered, M., 1976, Tectonics, seismicity and structure of the Afro-Eurasian junction - The breaking of an incoherent plate: Physics of the Earth and Planetary Interiors, v. 12, p. 1-50.

Graves, D.T., 1954, Geology of the Dominguez oil field, Los Angeles County: California Division of Mines and Geology Bulletin 170, Map Sheet 32.

Greene, H.G., Lee, W.H.K., McCulloch, D.S., and Brabb, E.E., 1973, Faults and earthquakes in the Monterey Bay region, California: U.S. Geological Survey Miscellaneous Field Studies Map MF-518, 14p. Scale 1:200,000.

Grindley, G.W., 1963, Structure of the Alpine schists of South Westland, Southern Alps, New Zealand: New Zealand Journal of Geology and Geophysics, v. 6, p. 872-930, cited in Scholz, C.H., Rynn, J.M., Weed, R.W., and Frohlich, C., 1973, Detailed seismicity of the Alpine fault zone and Fiordland region, New Zealand: Geological Society of America Bulletin, v. 84, p. 3297-3316.

Greensfelder, S., 1943, Dominguez oil field, in Chapter VIII, Los Angeles Basin and southernmost California, in Geologic formations and economic development of the oil and gas fields of California: California Division of Mines and Geology Bulletin 118, p. 318-319.

Gutenberg, B., 1955, Wave velocities in the earth's crust: Geological Society of America Special Paper G2, p. 19-34.

Gutenberg, B., and Richter, C.F., 1954, Seismicity of the earth and associated phenomena: Hafner Publishing Company, New York and London, reprinted 1965, 310p.

Gutenberg, B., and Richter, C.F., 1956, Earthquake magnitude, intensity, energy and acceleration (second paper): Bulletin of the Seismological Society of America, v. 46, n. 2, April, p. 143-145.

Hadley, D.M., and Kanamori, H., 1978, Geophysical investigations of the structure and tectonics of southern California: PhD thesis, California Institute of Technology, 167p.

Hanna, M.A., 1926, Geology of the La Jolla quadrangle, California: University of California publications, Geological Sciences, v. 16, p. 118-247.

Hanks, T.C., and Johnson, D.A., 1976, Geophysical assessment of peak accelerations: Bulletin of the Seismological Society of America, v. 66, n. 3, June, p. 959-968.

Harding, T.P., 1973, Newport-Inglewood trend, California - an example of wrench style deformation: American Association of Petroleum Geologists Bulletin, v. 57, n. 1, p. 97-116.

Harding, T.P., 1974, Petroleum traps associated with wrench faults: Association of Petroleum Geologists Bulletin, v. 58, n. 7, p. 1290-1304.

Harrison, J.C., Van Huene, R.E., and Corbato, C.E., 1966, Bouguer gravity anomalies and magnetic anomalies off the coast of southern California: Journal of Geophysical Research, v. 71, p. 4921-4941.

Haskell, N., 1964, Total energy and energy spectral density of elastic wave radiation from propagating faults: Bulletin of the Seismological Society of America, v. 56, p. 1811-1842.

Haxel, G., and Dillon, J., 1973, The San Andreas fault system in southeasternmost California: Proceedings of the conference on tectonic problems of the San Andreas fault system, Stanford University, June 20-23, 1973, Stanford University Publications, v. 13, p. 332-333.

Hazenbush, G.C., and Allen, D.R., 1958, Huntington Beach oil field: California Division of Oil and Gas, Summary of Operations, California Oil Fields, v. 44, n. 1, p. 13-25.

Heath, E.G., 1954, Geology along the Whittier fault north of Horseshoe Bend, Santa Ana Canyon, California: Master's thesis, Claremont Graduate School, 84p.

Herd, D.G., 1978, Neotectonic framework of central coastal California and its implications to microzonation of the San Francisco Bay region, in Proceedings of the second international conference on microzonation for safer construction - research and application: v. 1, p. 231-240.

Hertlein, L.G., and Grant, U.S., IV, 1944, The geology and paleontology of the marine Pliocene of San Diego, California, pt. 1, Geology: San Diego Society of Natural History Memoirs, v. 2, p. 1-72.

Hertlein, L.G., and Grant, U.S., IV, 1939, Geology and oil possibilities of southwestern San Diego County: California Journal of Mines, v. 35, p. 57-78.

Hileman, J.A., Allen, C.R., and Nordquist, J.M., 1973, Seismicity of the southern California region, 1 January 1932 to 31 December 1972: Seismological Laboratory, California Institute of Technology, 481p.

Hill, M.L., 1954, Tectonics of faulting in southern California, in Jahns, R.H., ed., Geology of southern California: California Division of Mines and Geology Bulletin 170, p. 5-13.

Hill, M.L., and Hobson, H.D., 1968, Possible post Cretaceous slip on the San Andreas fault zone: in Dickinson, W.R., and Grantz, A., eds., Proceedings of the conference on geologic problems of San Andreas fault system: Stanford Univeristy Publication, Geological Sciences, v. 11, p. 123-129.

Hill, L., 1971, Newport-Inglewood zone and Mesozoic subduction, California: Geological Society of America Bulletin, v. 82, p. 2957-2962.

Howell, D.G., 1975, Early and middle Eocene shoreline offset by the San Andreas fault, southern California, in San Andreas fault in southern California: California Division of Mines and Geology Special Report 118, p. 69-74.

Howell, D.G., 1976, A model to accommodate 1000 kilometers of right-slip, Neogene, displacement in the southern California area, in Howell, D.G., eds., Aspects of the geologic history of the California continental borderland: American Association of Petroleum Geologists, Special Publication 24.

Huffman, O.F., 1972, Lateral displacement of upper Miocene rocks and the Neogene history of offset along the San Andreas fault in central California: Geological Society of America Bulletin, v. 83, n. 10, p. 2913-2946.

Huffman, O.F., Turner, D.L., and Jack, R.N., 1973, Offset of late Oligocene-early Miocene volcanic rocks along the San Andreas fault in central California: Proceedings of the conference on tectonic problems of the San Andreas fault system, Stanford University, June 20-23, 1973, Stanford University Publications, v. 13, p. 368-373.

Hugguenin, E., 1926, Inglewood oil field: California Division of Oil and Gas, Summary of Operations, California Oil Fields, v. 11, n. 12, p. 5-15.

Hunter, A.L., and Allen, D.R., 1956, Recent developments in west Newport oil field: California Division of Oil and Gas, Summary of Operations, California Oil Fields, v. 42, n. 2, p. 11-18.

Hunter, A.L., Bradford, W.C., and Allen, D.R., 1955, Huntington Beach oil field, southeast extension of townlot area: California Division of Oil and Gas, Summary of Operations, California Oil Fields, v. 41, n. 1, p. 61-68.

Idriss, I.M., 1978, Characteristics of earthquake ground motions: State-of-the-art paper presented at American Society of Civil Engineers Specialty Conference on Earthquake Engineering and Soil Dynamics, Pasadena, California, June 19-21.

Idriss, I.M., and Power, M.S., 1978, Peak horizontal accelerations, velocities and displacements on rock and stiff soil sites for moderately strong earthquakes: Submitted for possible publication in the Bulletin of the Seismological Society of America.

Ingram, W.L., 1966a, North block-east extension of Seal Beach oil field: California Division of Oil and Gas, Summary of Operations, California Oil Fields, v. 52, n. 1, p. 63-67.

Ingram, W.L., 1966b, Recreation park area of Long Beach oil field: California Division of Oil and Gas, Summary of Operations, California Oil Fields, v. 52, n. 2, pt. 2, p. 67-71.

Ingram, W.L., 1968 Long Beach oil field: California Division of Oil and Gas, Summary of Operations, California Oil Fields, v. 54, n. 1, p. 5-16.

Jahns, R.H., 1969, Long-term behavior of some major faults in southern California: American Geophysical Union Transactions, v. 50, p. 382-384.

Jennings, C.W., 1975, Fault map of California with locations of volcanics, thermal springs and thermal wells: California Division of Mines and Geology, California Geologic Data Map Series, Map No. 1, Scale 1:750,000.

Johnson, R.A., 1961, East area of Potrero oil field: California Division of Oil and Gas, Summary of Operations, California Oil Fields, v. 47, n. 2, p. 65-74.

Junger, A., and others, 1976, Tectonics of the southern California borderland, in Aspects of the geologic history of the southern California borderland: Howell, D.G., ed, American Association of Petroleum Geologists Miscellaneous Publication 24, p. 486-498.

Kanamori, H., and Jannings, P.C., 1978, Determination of local magnitude, M_l, from strong motion accelerograms: Bulletin of the Seismological Society of America, v. 68, n. 2, p. 471-485.

Kanamori, H., and Anderson, D.L., 1975, Theoretical basis of some empirical relations in seismology: Bulletin of the Seismological Society of America, v. 65, p. 1073-1095.

Kanamori, H., and Hadley, D.M., 1975, Crustal structure and temporal velocity change in southern California: Pure and Applied Geophysics 113, p. 257-280.

Katili, J.A., and Hehuwat, F., 1967, On the occurrence of large transcurrent faults in Sumatra, Indonesia: Journal of Geoscience, Osaka City University, 10, art. 1-1, p. 5-17, cited in, Tjia, H.D., 1973, Displacement patterns of strike-slip faults in Malaysia-Indonesia-Philippines: Geologie en Mijnbouw (Journal of the Royal Geological and Mining Society of the Netherlands), v. 52, n. 1, p. 21-30.

Kennedy, G.L., 1973, A marine invertebrate fanule from the Lindavista formation, San Diego, California: San Diego Society of Natural History, Transactions, v. 17, n. 10, p. 119-128.

Kennedy, M.P., 1975, Del Mar, La Jolla and Point Loma Quadrangles, western San Diego metropolitan area, California: California Division of Mines and Geology Bulletin 200A, p. 9-39.

Kennedy, M.P., 1977, Recency and character of faulting along the Elsinore fault zone in southern Riverside County,

California: California Division of Mines and Geology Special Report 131, 12p.

Kennedy, M.P., Bailey, K.A., Greene, H.G., and Clarke, S.H., 1978, Recency and character of faulting offshore from metropolitan San Diego, California: California Division of Mines and Geology Final Technical report.

Kennedy, M.P., and Moore, G.W., 1971, Stratigraphic relationship of upper Cretaceous and Eocene formations, San Diego coastal area, California: American Association of Petroleum Geologistis Bulletin, v. 55, n. 5, p. 709-722.

Kennedy, M.P., Tan, S.S., 1977, Geology of the National City, Imperial Beach, and Otay Mesa quadrangles, southern San Diego metropolitan area, California: California Division of Mines and Geology, Map Sheet 29.

Kennedy, M.P., Tan, S.S., Chapman, R.H., and Chase, G.W., 1975, Character and recency of faulting, San Diego metropolitan area, California: California Division of Mines and Geology Special Report 123.

Kennedy, M.P., Welday, E.E., Borchard, G., Chase, G.W., and Chapman, R.H., 1977, Studies of surface faulting and liquefaction as potential earthquake hazards in urban San Diego, California: California Division of Mines and Geology final technical report.

Kern, J.P., 1971, Paleoenvironmental analysis of a late Pleistocene estuary in southern California: Journal of Paleontology, v. 45, n. 5, p. 810-823.

Kern, J.P., Stump, T.E., and Dowlen, R.J., 1971, An upper Pleistocene marine fauna from Mission Bay, San Diego, California: San Diego Society of Natural History, Transactions, v. 16, n. 15, p. 329-338.

Kern, J.P., 1973a, Late Quaternary deformation of the Nestor Terrace on the east side of Point Loma, San Diego, California: in Ross, A., and Dowlen, R.J., eds, Studies on the geology and geologic hazards of the greater San Diego area, California, Guidebook of the San Diego Association of Geologists and the Association of Engineering Geologists, May 1973, p. 43-45.

Kern, J.P., 1973b, Origin and history of two upper Pleistocene marine terraces at San Diego, California: Geological Society of America Bulletin, v. 88, p. 1553-1566.

King, P.B., 1969, The tectonics of North America: U.S. Geological Survey Professional Ppaer 628, 94p.

Knapp, R.R., Traxler, J.D., Newbill, T.J., Laughlin, D.J., Stewart, R.D., Heath, E.G., Stark, H.E., Wissler, S.G., and Holman, W.H., 1962, Cenozoic correlation section across Loss Angeles basin from Beverly Hills to Newport, California: American Association of Petroleum Geologists, Pacific Section.

Knuepfer, P.L., 1977, Geomorphic investigations of the Vaca and Antioch fault systems, Solano and Contra Costa Counties, California: Master's thesis, Stanford University, 53p.

Ku, T., and Kern, J.P., 1974, Uranium-series age of the upper Pleistocene Nestor Terrace, San Diego, California: Geological Society of America Bulletin, v. 85, p. 1713-1716.

Kuno, H., 1936, On the displacement of the Tanna fault since Pleistocene: University of Tokyo, Earthquake Research Institute Bulletin, v. 14, p. 619-631.

Lamar, D.L., Merifield, P.M., and Proctor, R.J., 1973, Earthquake recurrence intervals on major faults in southern California, in Moran, D.E., Slosson, J.E., Stone, R.O., and Yelverton, C.A., eds, Geology, Seismicity, and Environmental Impact: Association of Engineering Geologists Special Publication, p. 265-276.

Lang, H.R., and Dreessen, R.S., 1975, Subsurface structure of the northwestern Los Angeles basin, in California Division of Oil and Gas Technical Papers: California Division of Oil and Gas Report TP01, p. 15-21.

Langston, C.A., and Helmberger, D.V., 1975, A procedure for modelling shallow dislocation sources: Geophysical Journal of the Royal Astrological Society, v. 42, p. 117-130.

Lee, W.H.K., Yerkes, R.F., and Simirenko, M., 1979, Recent earthquake activity and focal mechanisms in the western Transverse Ranges, California: U.S. Geological Survey Circular 799a.

Leighton and Associates, 1978, Preliminary review of fault locations and activity, proposed marine redevelopment project, City of San Diego, California.

Lensen, G.J., 1975, Earth-deformation studies in New Zealand: Tectonophysics, v. 29, p. 541-551.

Lensen, G.J., and Vella, P., 1971, The Waiohine faulted terrace sequence; recent crustal movements: Royal Society of New Zealand, Bulletin 9, p. 117-119.

Liem, T.J., 1977, Late Pleistocene maximum age of faulting, southeast Mission Bay area, San Diego, California: in Farrand, G.T., ed, Geology of southwestern San Diego County, California and northwestern Baja California: San Diego Association of Geologists, Guidebook, p. 61-64.

Malfait, B.T., and Dinkelman, M.G., 1972, Circum-Caribbean tectonic and igneous activity and the evaluation of the Caribbean Plate: Geological Society of America, v. 83, n. 2, p. 251-271.

Mandel, D.J., Jr., 1973, Latest Pliocene foraminifera in the upper part of the San Diego formation, California: in Ross, A., and Dowlen, R.J., eds, Studies on the geology and geologic hazards of the greater San Diego area, California; Guidebook of the San Diego Association of Geologists and the Association of Engineering Geologists, May, p. 33-36.

Maresch, W.V., 1974, Plate tectonic origin of the Caribbean mountain system of northern South America, discussion and proposal: Geological Society of America Bulletin, v. 85, n. 5, p. 669-682.

Masters, P.M., and Bada, J.L., 1977, Recemization of isoleucine in fossile molluses from Indian middens and interglacial terraces in southern California: Earth and Planetary Sciences Letters, v. 37, p. 173-183.

Matsuta, T., 1976, Empirical rules on sense and rate of recent crustal movement: Journal of Geodetic Society of Japan, v. 22, n. 4, p. 252-263.

McComb, H.E., and West, C.J., 1931, List of seismological stations of the world: National Academy of Sciences, Washington, D.C., p. 119.

McEuen, R.B., and Pinckney, C.J., 1972, Seismic risk in San Diego: Transactions of the San Diego Society of Natural History, v. 17, n. 4, 62p.

McEvilly, T.V., and Casaday, K.B., 1967, The earthquake sequence of September 1965 near Antioch, California: Seismological Society of America Bulletin, v. 57, n. 1, p. 113-124.

McGuire, R.K., 1978, Seismic ground motion parameter relations: Journal of the Geotechnical Engineering Division, American Society of Civil Engineers, v. 104, n. GT4, April, p. 481-490.

McGuire, R.K., and Barnhard, J.A., 1977, Magnitude, distance and intensity data for C.I.T. strong motion records: Journal of Research of the U.S. Geological Survey, v. 5, n. 4, July-August, p. 437-444.

McLaughlin, P.R., 1977, A chemical analysis of thermal waters at Agua Caliente State Park and Warner Resort with emphasis on the relationship of chemistry to rock weathering, geothermometry, and location of springs associated with faults: San Diego State University, Geology Department, unpublished senior research paper.

Metz, H.L., 1968, Geology of the El Pilar fault zone, State of Sucre, Venezuela: Fourth Caribbean Geology conference, transactions, Port-of-Spain, Trinidad, West Indies, 1965, p. 293-298.

Milow, E.D., and Ennis, D.B., 1961, Guide to geologic field trip of southwestern San Diego County: in Thomes, B.E., ed, Guidebook for field trips, 57th Annual Meeting Cordilleran Section, Geological Society of America, p. 23-43.

Minch, A., 1967, Stratigraphy and structure of the Tijuana-Rosarito Beach area, northwestern Baja California, Mexico: Geological Society of America Bulletin, v. 78, p. 1155-1178.

Molnar, P., 1979, Earthquake recurrence intervals and plate tectonics: Bulletin of the Seismological Society of America, v. 69, n. 1, p. 115-133.

Moody, J.D., and Hill, M.J., 1956, Wrench-fault tectonics: Geological Society of America Bulletin, v. 67, p. 1207-1246.

Moore, G.W., 1972, Offshore extension of the Rose Canyon fault, San Diego, California: U.S. Geological Survey Professional Paper 800-C, p. 113-116.

Moore, G.W., and Kennedy, M.P., 1975, Quaternary faults at San Diego Bay, California: Journal of Research of the U.S. Geological Survey, v. 3, n. 5, p. 589-595.

Nardin, T.R., and Henyey, T.L., 1978, Pliocene-Pleistocene diastrophism of Santa Monica and San Pedro shelves, California continental borderland: American Association of Petroleum Geologists Bulletin, v. 62, n. 2, p. 247-272.

Newmark, N.M., 1975, Seismic design criteria for structures and facilities, Trans-Alaska pipeline system: Proceedings of U.S. National Conference on Earthquake Engineering, Ann Arbor, Michigan, June 19-20, p. 94-103

Newmark, N.M., 1977, Design spectra for Diablo Canyon Reactor Facility: A report to the U.S. Nuclear Regulatory Commission.

Newmark, N.M., and Hall, W.J., 1978, Development of criteria for seismic review of selected nuclear power plants: Report NUREG-CR 0098 by the U.S. Nuclear Regulatory Commission.

Nowroozi, A.A., 1971, Seismo-tectonics of the Persian Plateau, Eastern Turkey, Caucasus, and Hindu-Kush regions: Bulletin of the Seismological Society of America, v. 61, n. 2, p. 317-341.

Patwardhan, A., Sadigh, K., Idriss, I.M., and Youngs, R., 1978, Attenuation of strong ground motion -- effect of site conditions, transmission path characteristics, and focal depths (in press): to be submitted to the Bulletin of the Seismological Soceity of America for possible publication.

Pavoni, N., 1961, Die Nordanatolische horizontalvershiebung: Ged. Rundschau, 51, p. 1-16.

Pechmann, J.C., 1979, Tectonic implications of small earthquakes in the central Transverse Ranges, California: California Institute of Technology, Pasadena, in press.

Peterson, G.L., 1970a, Quaternary deformation of the San Diego area, southwestern California: Geological Guidebook Pacific Sections AAPG, SEPM, SEG, p. 120-126.

Peterson, G.L., 1970b, Pleistocene deformation of the Lindavists Terrace near San Diego, California: Geological Society of America, abstracts with programs, v. 2, n. 2, 131p.

Peterson, M.S., 1975, Geology of the Coachella fanglomerate, in San Andreas fault in southern California: California Division of Mines and Geology Special Report 118, p. 119-126.

Plafker G., 1976, Tectonic aspects of the Guatamalan earthquake of February 4, 1976: Science, v. 193, p. 1201-1208.

Plafker, G., Hudson, T., and Bruns, T., 1978, Late Quaternary offsets along the Fairweather fault and crustal plate interactions in Southern Alaska: Canadian Journal of Earth Science, v. 15, p. 805-816.

Poland, J.F., 1959, Hydrology of the Long Beach-Santa Ana area, California: U.S. Geological Survey Water-Supply Paper 1471.

Poland, J.F., Garrett, A.A., and Sinnott, A., 1959, Geology, hydrology and chemical character of ground waters in the Torrance-Santa Monica area, California: U.S. Geological Survey Water-Supply Paper 1461, 425p.

Poland, J.F., Piper, A.M., and others, 1956, Ground water geology of the coastal zone Long Beach-Santa Ana area, California: U.S. Geological Survey Water-Supply Paper 1109.

Proctor, R.J., 1968, Geology of the Desert Hot Springs-upper Coachella Valley area, California: California Division of Mines and Geology Special Report 94, 50p.

Prowell, D.C., 1974, Geology of selected Tertiary volcanics in the central coast range mountains of California and their bearing on the Calaveras and Hayward fault problems: University of California Santa Cruz, unpublished PhD thesis, 182p.

Quennell, A.M., 1958, The structure and geomorphic evolution of the Dea Sea rift: Quarterly Journal of the Geological Society of London, v. 114, pt. 1, p. 1-24.

Real, C.R., Toppozada, T.R., and Parke, D.L., 1978, Earthquake catalog of California, Jan. 1, 1900 - Dec. 31, 1974: California Division of Mines and Geology, Special Publication 52, 15p.

Reyes, A., Brune, J., Barker, T., 1975, A microearthquake survey of the San Miguel fault zone, Baja California, Mexico: American Geophysical Union, Geophysical research letters, v. 2, n. 2, p. 56-59.

Richter, C.F., 1958, Elementary seismology: W.H. Freeman, San Francisco and London, 768p.

Richter, D.H., and Matson, N.A., Jr., 1971, Quaternary faulting in the eastern Alaska Range: Geological Society of America Bulletin, v. 82, n. 6, p. 1529-1539.

Rod, E., 1956, Strike-slip faults of northern Venezuela: American Association of Petroleum Geologists, v. 40, n. 3, p. 457-476.

Rogers, T.H., and Williams, J.W., 1974, Potential seismic hazards in Santa Clara County, California: California Division of Mines and Geology Special Report 107, 39p.

Rynn, J.M.W., and Scholz, C.H., 1978, Seismotectonics of the Arthur's Pass region, South Island, New Zealand: Geological Society of America Bulletin, v. 89, n. 5, p. 1373-1388.

Sadigh, K., Idriss, I.M., and Patwardhan, A.S., 1978, Effect of site conditions on attenuation of ground motions for shallow earthquakes: Paper presented at the 1978 Annual Meeting of the Seismological Society of America, Sparks, Nevada, April.

Sadigh, K., Power, M.S., and Youngs, R., 1978, Peak horizontal and vertical accelerations, velocities and displacements on deep soil sites for moderately strong earthquakes: Proceedings, Second International Conference on Microzonation, San Francisco, November.

Sage, O., 1973, Paleocene geography of the Los Angeles region, in Kovach, R.L., and Nur, A., eds, Proceedings of the conference on tectonic problems of the San Andreas fault system: Stanford University Publications in Geological Sciences, v. 13, p. 348-357.

SanFilipo, J., 1978, A magnetic survey of the Rose Canyon fault zone: San Diego State University, Geology Department, unpublished senior research paper.

Saul, R.B., 1967, The Calaveras fault zone in Contra Costa County, California: Mineral Information Service, v. 20, n. 3, p. 35-37.

Schnabel, P.B., and Seed, H.B., 1973, Accelerations in rock for earthquakes in the western United States: Bulletin of the Seismological Society of America, v. 63, n. 2, April, p. 501-516.

Scholz, C.H., 1973, A comparison of the San Andreas fault with the Alpine fault, in Kovach, R.L., and Nur, A., eds., Proceedings of the conference on tectonic problems of the San Andreas fault system: Stanford University Publications, Geological Sciences, v. 13, p. 186-191.

Scholz, C.H., Rynn, J.M., Weed, R.W., Frohlich, C., 1973, Detailed seismicity of the Alpine fault zone and Fiordland region, New Zealand: Geological Society of America Bulletin, v. 84, n. 10, p. 3279-3316.

Schubert, C., and Sifontes, R.S., 1970, Bocono fault, Venezuelan Andes, evidence of postglacial movement: Science, v. 170, p. 66-69.

Schwartz, D., Cluff, L.S., and Donnelly T., 1979, Quaternary faulting along the Caribbean and North American plate boundary: Tectonophysics, v. 52 (in press).

Seed, H.B., Murarka, R., Lysmer, J., and Idriss, I.M., 1976, Relationships of maximum accelerations, maximum velocity,

distance from source and local site conditions for moderately strong earthquakes: Bulletin of the Seismological Society of America, v. 66, n. 4, August, p. 1323-1342.

Shannon & Wilson, and Agbabian Associates, 1978a, Verification of subsurface conditions at selected 'rock' accelerograph stations in California: NUREG/CR-0055, prepared for the U.S. Nuclear Regulatory Commission, May.

Shannon & Wilson, and Agbabian Associates, 1978b, Date from selected accelerograph stations at Wilshire Boulevard, Century City and Ventura Boulevard, Los Angeles, California: NUREG/CR-0074, prepared for the U.S. Nuclear Regulatory Commission, June.

Shannon & Wilson, and Agbabian Associates, 1978c, Geotechnical and strong motion earthquake data from U.S. accelerograph stations: NUREG-0029, v. 2, prepared for the U.S. Nuclear Regulatory Commission, June.

Sharp, R.V., 1967, San Jacinto fault zone in the Peninsular Ranges of southern California: Geological Society of America Bulletin, v. 78, n. 6, p. 705-730.

Sharp, R.V., 1975, En echelon fault patterns of the San Jacinto fault zone, in San Andreas fault in southern California: California Division of Mines and Geology Special Report 118, p. 147-152.

Sharp, R.V., 1978, Salton trough tectonics: in Summaries of Technical Reports: U.S. Geological Survey, National Earthquake Hazards Reduction Program, v. VII, p. 34-35.

Shor, G.G., 1955, Deep reflections from southern California blasts: Transactions of the American Geophysical Union, v. 36, p. 133-138.

Sieh, K.E., 1977, A study of Holocene displacement history along the south-central reach of the San Andreas fault: PhD thesis, Stanford University, 219p.

Sieh, K.E., 1978, Prehistoric large earthquakes produced by slip on the San Andreas fault at Pallett Creek, California: Journal of Geophysical Research, v. 83, n. B8, p. 3907-3939.

Sieh, K.E., 1978, Slip along the San Andreas fault associated with the great 1857 earthquake: Bulletin of the Seismological Society of America (in press).

Simons, R.S., 1977, Seismicity of San Diego, 1934-1974: Bulletin of the Seismological Society of America, v. 67, n. 3, p. 809-826.

Slemmons, D.B., 1977, State-of-the-art for assessing earthquake hazards in the United States, Report 6: Faults and earthquake magnitude: U.S. Army Corps of Engineers Miscellaneous Paper S-73-1, 129p.

Smith, S.W., 1976, Determination of maximum earthquake magnitude: Geophysical Research Letters, v. 3, n. 6, p. 351.

Southern California Edison, 1976, Geotechnical studies, southern Orange County: In-house study.

Southern California Edison and San Diego Gas and Electric Company, 1977, Final Safety Analysis Report, San Onofre Nuclear Generating Station, Units 2 and 3, v. 3.

Southern California Edison and San Diego Gas and Electric Company, 1970, Preliminary Safety Analysis Report, San Onofre Nuclear Generating Station, Units 2 and 3, v. 2 and 3.

Stolz, H.P., 1943, Long Beach oil field, in Chapter VIII, Los Angeles Basin and southernmost California, in Geologic formations and economic development of the oil and gas fields of California: California Division of Mines and Geology Bulletin 118, p. 320-324.

Suggate, R.P., 1963, The Alpine fault: Transactions of the Royal Society of New Zealand, v. 2, n. 7, p.105-129.

Suggate, R. P., and Lensen, G.J., Rate of horizontal fault displacement in New Zealand: Nature, v. 242, 815p., cited in Walcott, R.I., 1978, Present tectonics and late Cenozoic evolution of New Zealand: Geophysical Journal, Royal Astronomical Society, London, v. 52, p. 137-164.

Sugimura, A., and Matsuda, T., 1965, Atera fault and its displacement vectors: Geological Society of America Bulletin, v. 76, p. 509-522.

Sykes, L.R., and Ewing, M., 1965, The seismicity of the Caribbean Region: Journal of Geophysical Research, v. 70, n. 20, p. 5065-5074.

Tchalenko, J.S., and Berbrian, M., 1975, Dasht-e Bayaz fault, Iran: Earthquake and earlier related structures in bedrock: Geological Society of America Bulletin, v. 86, n. 5, p. 703-709.

Teasley, J.F., 1978, Gravity traverses on portions of the Rose Canyon fault: San Diego State University, Geology Department, unpublished senior research paper.

Teng, T., and Manov, D., 1975, Microearthquake monitoring in the City of Long Beach area: Univerisity of Southern California Geophysical Laboratory, Technical Report 76-1, Department of Geological Sciences.

Thatcher, W., Hileman, J.A., and Hanks, T.C., 1975, Seismic slip distribution along the San Jacinto fault zone, southern California, and its implications: Geological Society of America Bulletin, v. 86, n. 8, p. 1140-1146.

Threet, R.L., 1973, Birth and death of a fault in Mission Valley, San Diego, California: in Ross, A., and Dowlen, R.J., eds, Studies on the geology and geologic hazards of the greater San Diego area, California, Guidebook of the San Diego Association of Geologists and the Association of Engineering Geologists, p. 105-110.

Tjia, H.D., 1968, The Lembang fault, West Java: Geologie en Mijnbouw (Journal of the Royal Geological and Mining Society of the Netherlands), v. 47, n. 2, p. 126-130.

Tjia, H.D., 1973, Displacement patterns of strike-slip faults in Malaysia-Indonesia-Philippines: Geologie en Mijnbouw (Journal of the Royal Geological and Mining Society of the Netherlands), v. 52, n. 1, p. 21-30.

Toppozada, T.R., Parke, D.L., and Higgins, C.T., 1978, Seismicity of Calfornia, 1900-1931: California Division of Mines and Geology Special Report 135, 39p.

Townley, D., and Allen, M.W., 1939, Description catalog of earthquakes of the Pacific Coast of the United States 1769 to 1928: Bulletin of the Seismological Society of America, 297p.

Trifonov, V.G., 1971, The pulse-like character of tectonic movements in regions of most recent mountain-building (Kopef Dagh and southeast Caucasus): Geotectonics, USSR Accademy of Sciences, Geological Institute, n. 1, p. 234-235.

Trifonov, V.G., 1978, Late Quaternary tectonic movements of western and central Asia: Geological Society of America Bulletin, v. 89, n 7, p. 1059-1072.

Trifunac, M.D., 1976, Preliminary analysis of the peaks of strong earthquake ground motion - dependence of peaks on earthquake magnitude, epicentral distance, and recording site conditions: Bulletin of the Seismological Society of America, v. 66, n. 1, February, p. 189-220.

Trifunac, M.D., and Brady, A.G., 1976, Correlation of peak acceleration, velocity and displacement with earthquake magnitude, distance and site conditions: International Journal of Earthquake Engineering and Structural Dynamics, v. 4, n. 5, July-September, p. 455-472.

Trifunac, M.D., and Anderson, J.G., 1977, Preliminary empirical models for scaling absolute acceleration spectra: Report CE 77-03, Department of Civil Engineer, University of Southern California, Los Angeles, August.

United States Atomic Energy Commission, 1972, Safety evaluation report for San Onofre Nuclear Generating Station: Atomic Energy Commission, Docket n. 50-361 and 50-362, 112p.

Vedder, J.G., 1975, Juxtaposed Tertiary strata along the San Andreas fault in the Temblor and Caliente Ranges, California, in San Andreas fault in southern California: California Division of Mines and Geology Special Report 118, p. 234-240.

Vedder, J.G., Beyer, L.A., Junger, A., Moore, G.W., Roberts, A.E., Taylor, J.C., and Wagner, H.C., 1974, Preliminary report on the geology of the continental borderland of southern California: U.S. Geological Survey Miscellaneous Field Map MF-624.

Walcott, R.I., 1978, Present tectonics and late Cenozoic evolution of New Zealand: Geophysical Journal, Royal Astronomical Society of London, v. 52, p. 137-164.

Wallace, R.E., 1975, The San Andreas fault in the Carrizo Plain - Temblor Range region, California, in San Andreas fault in southern California: California Division of Mines and Geology Special Report 118, p. 241-250.

Weber, F.H., Jr., 1977a, Total right lateral offset along the Elsinore fault zone, southern California: Geological Society of America Abstracts with Programs, v. 9, n. 4, p. 523-524.

Weber, F.H., Jr., 1977b, Seismic hazards related to geologic factors, Elsinore and Chino fault zones, northwestern Riverside County, California: California Division of Mines and Geology Open-File Report 77-4LA.

Weber, G.E., and Lajoie, K.R., 1977, Late Pleistocene and Holocene tectonics of the San Gregorio fault zone between Moss Beach and Point Ano Nuevo, San Mateo County, California: Geological Society of America Abstracts with Programs, v. 9, n. 4, p. 524.

Wellman, H.W., 1955, The geology between Bruce Bay and Haast River, South Westland: New Zealand Geological Survey Bulletin, n.s. 48, 46p., cited in Scholz, C.H., Rynn, J.M., Weed, R.W., and Frohlich, C., 1973, Detailed seismicity of the Alpine fault zone and Fiordland region, New Zealand: Geological Society of America Bulletin, v. 84, p. 3297-3316.1

Wellman, H.W., 1964, Age of the Alpine fault, New Zealand: Proceedings of Section 4, Rock deformation and tectonics, Sundaram, R.K., ed., International Geological Congress, India, p. 148-162, cited in Walcott, R.I., 1978, Present tectonics and late Cenozoic evolution of New Zealand: Geophysical Journal, Royal Astronomical Society of London, v. 52, p. 137-164.

Wellman, H.W., 1965, Active wrench faults of Iran, Afghanistan, and Pakistan: geological Rundschau, 55, p. 716-773.

Wellman, H.W., 1969, Wrench (transcurrent) fault systems: American Geophysical Union Monograph 13.

Wellman, H.W., 1972, Rate of horizontal fault displacement in New Zealand: Nature, v. 237, p. 275-277, cited in Walcott, R.I., 1978, Present tectonics and late Cenozoic evolution of New Zealand: Geophysical Journal, Royal Astronomical Society of London, v. 52, p. 137-164.

Wellman, H.W., and Cooper, A., 1971, Potassium-Argon age of some New Zealand lamprophere dikes near the Alpine fault: New Zealand Journal of Geology and Geophysics, v. 15, p. 22-32, cited in Scholz, C.H., Rynn, J.M., Weed, R.W., and Frohlich, C., 1973, Detailed seismicity of the Alpine fault zone and Fiordland region, New Zealand, Geological Society of America Bulletin, v. 84, p. 3297-3316.

Wellman, H.W., and Wilson, A.T., 1964, Notes on the geology and archeology of the Martins Bay District, New Zealand, Journal of Geology and Geophysical, v. 7, p. 702-721.

Wentworth, C.M., 1968, Upper Cretaceous and lower Tertiary strata near Gualala, California, and inferred large right slip on the San Andreas fault: Proceedings of conference on geologic problems of San Andreas fault system, Stanford University, September 14-16, Stanford University Publications, v. 11, p. 130-143.

Wesson, R.L., Helley, E.J., Lajoie, K.R., and Wentworth, C.M., 1975, Faults and future earthquakes, in Borcherdt, R.D., ed, Studies for seismic zonation of the San Francisco Bay region: U.S. Geological Survey Professional paper 941-A, p. A5-A30.

Western Geophysical Comapny, 1972, San Onofre offshore investigations: Final report to Southern California Edison and San Diego Gas and Electric companies.

Whitcomb, J.H., 1973, The 1971 San Fernando earthquake series focal mechanisms and tectonics: PhD thesis (Part II), California Institute of Technology.

Wicander, E.R., 1970, Planktonic foraminifera of the San Diego formation: in Pacific scope geology of northern Baja California and adjacent Alta California; Geologic Guidebook for the 1970 Fall field trip of the Pacific Sections AAPG, SEPM, and SEG, p. 105-117

Wiegand, W., 1970, Evidence of a San Diego Bay-Tijuana fault: Association of Engineering Geologists Bulletin, v. 7 n. 2, p. 107-121.

Willis, R., and Ballantyne, R.S., Jr., 1943, Potrero oil field: California Division of Mines and Geology Bulletin 118, pt. 3, p. 310-317.

Winslow, M.A., 1976, Active transcurrent shear zones in southern Chile as landward expressions of transform plate boundaries: Geological Society of America, Abstracts with programs, v. 8, n. 6, p. 1173-1174

Winslow, M.A., 1978 personal communication, Lamont-Doherty Geological Observatory of Columbia University, 914/359-2900.

Wood, H.O., 1933, Preliminary report on the Long Beach earthquake: Bulletin of the Seismological Society of America, v. 23, 43p.

Woodford, A.O., Schoellhamer, J.E., Vedder, J.G., and Yerkes, R.F., 1954, Geology of the Los Angeles basin: Geology of Southern California, California Division of Mines Bulletin 170, Chap. II, p.65-81.

Woodward-Clyde Consultants, 1978, Geotechnical evaluation of potential island and offshore California LNG terminal sites: Report to the California Coastal Commission.

Wright, T.L., Parker, S., and Erikson, R.C., 1973, Stratigraphic evidence for the timing and nature of late Cenozoic deformation in the Los Angeles basin: Paper presented at National American Association of Petroleum Geologists convention, Anaheim, California, May, 1973.

Wyss, M., 1979, Estimating maximum expectable magnitude of earthquakes from fault dimensions: Bulletin of the

Seismological Society of America, in press.

Yeates, R.S., 1973, Newport-Inglewood fault zone, Los Angeles basin, California: American Association of Petroleum Geologists Bulletin, v. 57, n. 1, p. 117-135.

Yerkes, R.F., 1972 Geology and oil resources of the western Puente Hills area, southern California: U.S. Geological Survey Professional Paper 420-C, 63p.

Yerkes, R.F., McCulloh, T.H., Schoellhamer, J.E., and Vedder, J.G., 1965, Geology of the Los Angeles basin - an introduction: U.S. Geological Survey Professional Paper 420-A, 57p.

Zak, I., and Freund, R., 1966, Recent strike slip movements along the Dead Sea rift: Israel Journal of Earth Sciences, v. 15, p. 33-37.

Ziony, J.I., 1973, Recency of faulting in the greater San Diego area, California, in Ross, A., and Dowlen, R.J., eds, Studies on the geology and geologic hazards of the greater San Diego area, California: 1973 Guidebook, San Diego Association of Geologists and Assocation of Engineering Geologists, p. 68-75.

Ziony, J.I., and Buchanan, J.M., 1972, Preliminary report on recency of faulting in the greater San Diego area, California: U.S. Geological Survey Open File report.

Ziony, J.I., Wentworth, C.M., Buchanan-Banks, J.M., and Wagner, H.C., 1974, Preliminary map showing recency of faulting in coastal southern California: U.S. Geological Survey, Miscellaneous Field Studies Map MF-585.